HYDROCARBON REDUCTION OF MANGANESE ORES.

Amit Bhalla

A thesis submitted to the Faculty of Engineering and the Built Environment, University of the Witwatersrand, Johannesburg, in fulfilment of the requirements for the degree of Doctor of Philosophy.

Johannesburg, March, 2018

DECLARATION

I declare that this thesis is my own unaided work. It is being submitted to the Degree of Doctor of Philosophy to the University of the Witwatersrand, Johannesburg. It has not been submitted before for any degree or examination to any other University.

Amit Bhalla

15th day of March 2018.

ABSTRACT

Reduction behavior of South African Mamatwan manganese ore using methane-argon-hydrogen gas mixture was investigated experimentally in the temperature range of 1050°C to 1250°C. The effect of changing gas mixture composition, time and temperature was studied using a vertical tube furnace. After each test, three representative samples were prepared; one was analyzed by chemical analysis to obtain metallization results as a function of each reducing condition for each time interval over the total reduction period of two hours. Second sample was analyzed by X-ray diffraction to determine the progress of phase changes; the third sample was mounted, polished and submitted for SEM-EDAX in order to examine the morphology of the ore and its changes in the course of reduction. It was seen that CH_4 was an effective reductant as it cracked, supplying the reaction site with hydrogen gas and very fine solid carbon. The excess carbon from cracking of methane ensures regeneration of reductants CO and H_2 from reaction product gases of CO_2 and H_2O ensuring low partial pressure of oxygen at the reaction site. Hydrogen gas may also be involved in the reduction of iron oxide components of the ore. Moreover, depending upon temperature and CH_4/H_2 ratio in the gas phase the activity of carbon in the system reaches values much higher than unity, shifting the reduction reaction by carbon to lower temperatures. It was observed that bulk of the metallization occurred in the first thirty to forty minutes and the metallization reached some kind of a reduction maximum at 73% metallization. The Mn/Fe ratios in the resulting alloy were higher than those in ordinary carbothermic solid-state reduction, indicating the simultaneous reduction of Fe and Mn at these low reducing temperatures due to a low oxygen potential set up by the methane bearing gas mixtures. It was seen that metallization of Mamatwan ore proceed in two stages. First, reduction of the higher oxides to MnO and metallic iron. Second, reduction of any remaining oxides and MnO to mixed carbide of iron and manganese. During first stage values of effective CO-CO_2 diffusivities generated by the model were found to lie in the range from $1.45 * 10^{-6}$ cm^2sec^{-1} to $8.43*10^{-6}$ cm^2sec^{-1} at 1100°C. Apparent activation energy for first stage calculated in the temperature range of 1050°C to 1250°C varied from 1.47 kJ/mol to 24.72 kJ/mol indicating possibility of diffusional control. For the second stage the experimental curves could be duplicated with the mathematical model reasonably well with a maximum difference between the experimental and predicted values being about 5 percent. Rate of metallization values during the second stage (Ms) changed between $1.83*10^{-8}$ $mol.sec^{-1}.cm^{-2}$ and $8.55*10^{-8}$ $mol.sec^{-1}.cm^{-2}$. Specific rate constant values (k_s) for the second stage, varied from $5.53*10^{-6}$ cm/sec to $3.16*10^{-5}$ cm/sec which are much smaller than specific rate constant for the first stage of reduction (k_f), which varied from $1.64*10^{-4}$ cm/sec to $1.15*10^{-4}$ cm/sec, as the rate of second stage of the reduction is much slower than the rate of the first stage. X ray analysis revealed that manganese ore was reduced primarily to carbide Mn_7C_3 at lower temperature range of the experiments, but at 1200°C the dominant reaction product was

Mn_5C_2 in both mixtures of methane-argon and methane-hydrogen. The S.E.M images revealed that the product metallic phase occurred all throughout the surface, with globular formation in case of reduction where hydrogen was the carrier gas.

DEDICATION

Dedicated to my parents Dr T.N BHALLA and Mrs M.BHALLA for their ever lasting love.

ACKNOWLEDGEMENTS

I wish to express my deep appreciation to my supervisor Prof R.H Eric for his guidance, insight supervision and advice throughout the study, it was due to his advice which made research work contained in this thesis possible. The author would also like to thank Prof C.S Kucukkaragoz for his guidance and support which was invaluable to this study.The author wishes to express his gratefulness to Prof R.H Eric for busary grant and financial support for the project. Recognition is also due to BHP-Billiton for providing the Manganese ore and Initial analysis.The author wishes to express sincere gratitude to Prof J.H Potieger, Head of Department of Chemical and Metallurgical Engineering for the encouragement. Sincere appreciation is extended to Alan of Scooby's laboratory for Chemical Analysis, Dr Dave Billing X-RD lab of Chemistry Department and Brayner Nelwalani for assistance in Scanning Electron Microscopy. Thanks are also due to staff of workshop for their help during the course of project.

Lastly but not the least , I wish to acknowledge the love of my parents, brothers Dr Pankaj Bhalla and Dr Mohit Bhalla for their moral understanding and unparalleled support during this period of absence from home.

The Author obtained his B.Tech degree from Department of Materials and Metallurgical Engineering, Indian Institute of Technology, Kanpur, India and M.S from Department of Chemical and Metallurgical Engineering, University of the Witwatersrand, Johannesburg, South Africa.

Table of contents **Page**

LIST OF FIGURES

LIST OF TABLES

LIST OF SYMBOLS

Concentration of solid reactant in the reaction zone	C_s
Initial concentration of solid reactant	C_{so}
Concentration of solid reactant at the outer surface	C_{ss}
Concentration of gas reactant at the outer surface of particle.	C_{gs}
Concentration of gas reactant in the reaction zone.	C_{gr}
Concentration of gas reactant at the boundary between reaction zone and product layer.	C_{gm}
Particle radius.	r_p
Distance from the center of particle to reaction surface.	r
Distance from the center of the particle to the boundary between reaction zone and product layer.	r_m
Flux of diffusing species.	N
Flux of diffusing species at radius (r).	N_r
Flux of diffusing species at radius (r+Δr).	$N_r + \Delta r$
Rate of chemical reaction.	R_{chem}
Mole fraction of CO.	X_{co}
Bulk concentration of CO.	$X_{co, b}$
Bulk concentration of CO_2.	$Xco_{2,b}$
Mole fraction of carbon monoxide at surface.	$X_{co,s}$
Mole fraction of carbon monoxide at reacting interface(r_m).	$X_{co,m}$
Effective diffusivity of (CO) and (CO_2) in the oxide particle.	D_{ef}
Total gas concentration.	C_g
Rate constant	k

Pore surface area.	S
Density of particle.	ρ
Equilibrium constant	K_e
Variable which is function of (r).	e
Dimensionless radius.	δ
Kinetic–diffusion modulus (Thiele modulus).	$\emptyset_f$
Total rate of reaction.	M_f
Total number of moles of gas.	N
Total volume of gas.	V
Total gas pressure.	P
Surface area available for reaction per cubic metre of ore.	A_s
Total initial concentration of oxygen available for reaction with carbon.	C_{oxy}
Molecular diffusion coefficient for gas (1) diffusing in gas (2).	D_{12}
Molecular masses of the two gasses.	M_1, M_2
Collision integral.	Ω_D
Force constant.	δ_{12}
Effectiveness factor.	ε
Film diffusional resistance around the particle.	γ
Sherwood number for mass transfer through gas layer.	N_{sh}
Fractional of the solid reactant at the end of the first stage.	F_f
Rate of metallization between MnO and the carbide.	M_s
Concentration of MnO after reduction of Mn_3O_4 to MnO completely.	Cs_2
Dimensionless time for the first stage of the metallization.	θ_f
Fractional conversion second stage.	F_s

CHAPTER 1

INTRODUCTION

1.1 Manganese ore in South Africa

World manganese production shows that South Africa is the largest producer of manganese ore followed by Australia (Table 1.1).

The most significant manganese ore deposits in South Africa are located in the Northern Cape Province. A gap of 55 km separates them into the southern field and northern field which are continuous from the Mamatwan mine in South to the Wessel mine in the North. Wessel mine is Kalahari's largest underground mine (Table1.2).

The Wessel type ore is hydrothermally upgraded, carbonate poor ore with manganese percent up to 44 %. The Mamatwan ore is composed chiefly of braunite [10,15] with smaller amount of manganite, hausmannite and hematite (Table 1.3). Its gangue material consists mostly of calcium carbonate and magnesium carbonate. The Mamatwan ore has less than 40 percent manganese content (Table 1.4).

Table 1.1: Manganese ore: world production (tons) in 2016[79].

Country	Tons
South Africa	6,200,000
Australia	3,000,000
China	2,900,000
Gabon	1,800,000
Brazil	1,000,000
India	950,000
Malaysia	400,000
Ukraine	390,000
Kazakhstan	390,000-
Ghana	390,000
Mexico	240,000
Myanmar	100,000

Table 1.2: Estimate of reserve in the Kalahari Manganese Deposit [111].

Wessel Grade (Mt)	Mamatwan Grade (Mt)
+44 % Mn (60% (Mn+Fe)) =330 Mt	38-40 % Mn =982 Mt
40-44 % Mn (60% (Mn+Fe)) =30Mt	30-38% Mn = 6284Mt
36-40 % Mn (60% (Mn +Fe)) =18 Mt	20-30% Mn =5938 Mt
30-40 % (5-10% Fe) =31 Mt	
Subtotal=409Mt	Subtotal=13204 Mt
Total Reserve = 13613 Mt	

Table1.3: The more important properties of the major Manganese Minerals found in the Kalahari [35].

Mineral	Colour	Hardness	Relative Density	Other Properties
Braunite	Brownish -black	6.0	4.8	Non-magnetic
Braunite II	Brownish-black	6.0	4.8	Non- magnetic
Hausmannite	Grey-black	5.5	4.8	Non- magnetic
Bixbyite	Dull- black	6.5	4.9-5.0	Non- magnetic
Cryptomelane	Dull-black	N.A	4.3	Non- magnetic
Jacobsite	Iron-black	6.0	4.8	Magnetic

Table 1.4: Typical chemical analysis of manganese ore from the Kalahari deposit (in weight percent)[18].

	Mamatwan-Type	Wessel-type
Total Mn	35.6-37.4	52.2-56.9
Total Fe	3.8-6.8	6.0-15.3
CaO	13.7-17.0	2.6-3.0
SiO_2	2.40-5.5	1.0-9.1
MgO	2.8-3.6	0.1-0.6
Al_2O_3	0.1-0.5	0.5-1.5
CO_2	16.3-19.3	0.5-1.5
H_2O	3.5-5.0	0.1-0.7

Besides being versatile additive in steel industry manganese has the added advantage of low cost and easy availability. A major use of manganese is as an alloy additive to steel, where it acts as a desulphurizer and deoxidizer, providing improved strength and hardenability by suppressing the hardening transformation of steel on quenching. Manganese can be added as an ore during iron making or as silico-manganese and ferromanganese in the steel making stage. Various types and grades of SiMn and FeMn, mostly containing from 70 to 90 percent manganese, are produced in large submerged arc furnaces.

In chemical industry, manganese is used as an oxidizing agent in chemical processes and for the production of chemical compounds. It is also added to silver, aluminum, copper, magnesium, nickel, titanium, and zinc alloys, where special properties, such as high damping capacity, high permanent magnet characteristics, low expansion and high electrical resistivity are developed.

About 93 percent of all manganese produced is in the form of manganese ferroalloys. The various FeMn grades are very low carbon (VLC), low carbon (LC), medium carbon (MC) and high-carbon (HC). The SiMn grades are low carbon (LC) and medium carbon (MC). The steel industry is one of the consumers of these FeMn and SiMn alloys. As a deoxidizer, and an alloy additive, silicon manganese and ferromanganese play an important role in improving the quality of steel and its properties. The research on production and market of ferromanganese and silicon manganese is important for overall development of the industry. To cover the need for manganese, the steelmaker has the choice of HCFeMn and SiMn in a proportion, governed by specifications on carbon, silicon and manganese. Commonly, a mixture of FeSi75 (Ferro silicon alloy with silicon % greater than 75) and HCFeMn is used, but an increased use of SiMn is seen at the expense of the HCFeMn and FeSi75. The SiMn production is integrated with the manufacture of HCFeMn so that the slag from the HCFeMn production is again processed in the production of silicon manganese. In this way a very high total yield of manganese is achieved. The other direct production of SiMn are more difficult then FeMn as they require higher temperature.

1.2 Manganese raw material

Manganese ore reserves are diminishing especially the high grade manganese ore. Furthermore environmental issues and energy problems are additional complexities, therefore the ferroalloy industry have to use the manganese raw material and energy more rationally [17,21,25,26,40,66,79,100,111].To achieve that following can be done: further development of reserves, producing the alloys by using a blend of both high and low grade manganese raw material and production of alloy with the lowest possible energy consumption. Various factors which are important in this process from quality point of view are metallurgical value of various raw material used, material cost, delivery cost and condition of supply. Manganese ore from different countries [72,76] are of different quality and some may require more elaborate processing, especially high

phosphorous containing ores. Manganese from tailings, slag, and dust have content value and should be used after pretreatment and estimation of metallurgical value.

Choice of ore depends on the physical and chemical properties as well as on economic factors. Metallurgical grade ore contains between 40% to 50% manganese. Ratio of manganese to iron is an important parameter. Typically Mn/Fe = 7.4 ratio is required for production of ferromanganese alloy with 77 % Mn which is the standard ferroalloy used. Ore with more than 11% SiO_2 are suitable for use in SiMn product, so silicon content need to be regulated as excessive slag formation in furnace increase the electrical energy requirement. As most part of phosphorus in the ore remains in the finished product, the phosphorus content is an important parameter in selection of manganese ore. Manganese ores from South Africa have low phosphorous content, other chemical and physical properties are also important such as level of volatiles. Table 1.5 given below shows difference in Chemical composition of various ores.

Table 1.5: Chemical composition of various ores 2007[90].

Manganese ore	Mn/Fe	Mn	MnO	MnO_2	Fe_2O_3	FeO	SiO_2	Al_2O_3	MgO	CaO	P
Comilog Sinter	16.7	58.5	59.6	19.7	-	4.5	7.0	6.5	0.0	0.1	0.12
Asman 48	5.1	51.3	37.9	34.7	14.3	-	5.5	0.4	0.7	4.3	0.04
Amapa Sinter	5.1	49.1	45.7	18.6	-	12.5	7.6	7.6	0.5	0.8	0.10
Mamatwan	8.2	37.8	29.8	23.4	6.6	-	4.0	0.5	3.5	14.7	0.02
Gloria	7.8	39.1	31.3	23.6	7.2	-	5.7	0.3	3.8	12.7	0.02
Groote Eylandt	11.6	48.8	2.6	73.9	6.0	-	6.9	4.2	0.1	0.1	0.09
CVRD lump	9.6	45.0	-	-	6.7	-	2.6	8.6	0.2	0.2	0.09
Wessel 50%	5.0	50.2	36.1	35.2	14.5	-	3.6	0.4	1.0	5.6	0.04
Nikopol	23.6	48.0	-	-	2.9	-	9.1	1.8	1.0	2.4	0.19

1.3 Agglomeration of manganese ores

Manganese ore fines [73,85] from mines are crushed and then screened into various size fractions from fines (< 5mm) to lump (<76mm). Various methods are used to upgrade screened ore to produce concentrates, like high intensity magnetic separation, separation by gravity concentration. Fines in the raw material often results in high power consumption per ton alloy, low productivity, fumes and dust losses.

Alloy producers generally prefer agglomerated ore, Sinter process at mines is used to agglomerate the fines. Travel grate technology is used to produce manganese sinter. Pelletizing

and briquetting are other process which can be used. Pelletizing is more difficult and costly as it requires firing the manganese ore pellet at high temperature. Briquetting requires less capital than sinter and pelletizing.

1.4 Manganese pre-reduction

For the production of ferromanganese and manganese metal, high grade manganese ore in South Africa such as Wessel and Hotazel deposits have been used. However, the ores are becoming depleted with time and hence it is important that large reserves of low grade manganese ore like Mamatwan ore be utilized to a larger extent even with alternative techniques. Pre-reduction of manganese ore by carbon is one such technique with the potential of lowering electrical energy requirement in arc furnaces. Few studies were done to determine the nature and extent of the reactions - occurring during the reduction of Mamatwan manganese ore by solid carbon. The degree and mechanism of reduction of Mamatwan manganese ore with graphite was studied at laboratory scale by W.D Grimsley[32] details of which will be discussed in chapter 2 section 2.3.1. The pre-reduction of manganese using carbon was not very efficient, which leads to the exploration of using alternative reductants that are effective but potentially operate at lower reducing temperatures.

1.5 Manganese Ferro Alloy Production

Electric smelting and blast furnaces processes are used for production of Manganese ferroalloys by carbothermic reduction of manganese oxide ores(Table 1.6). In submerged arc furnace coke serve as both reducing agent and electrical resistance element and heat requirement is supplied as electrical energy. In blast furnace coke supplies energy by burning and also serves as reductant. Electrical furnace have many advantages such as high yield of Mn from the ore, less carbon consumption, lower quality of reducing agents and greater flexibility in providing different grades of alloys. Electrical furnaces can be used for production of both HCFeMn (energy consumption around 2400kwh/ton) and SiMn (energy consumption around 3500-4500 Kwh/ton), therefore they provide more flexibility according to requirement in producing different grade of alloys, while Blast furnace smelting has serious disadvantages such as high coke consumption and high loss of Manganese in slag.

Table 1.6: Compositions of Ferromanganese alloys [35].

Alloy	Composition (%)			
	Mn	Fe	Si	C
High carbon	74-80	12.2-19.9	0.1-0.8	6-7
Medium carbon	80-85	11-18	1-2	1-2
Low carbon	80-85	13.5-18.5	1.0	0.5

1.6 Motivation and Scope of this study

In manganese alloys production in electric or blast furnaces, MnO is reduced from slag by carbon to manganese carbide at temperatures above 1500^{o}C. Hence reduction of manganese ore at lower temperatures in the solid state by carbon, carbon monoxide or hydrogen does not go beyond MnO. For temperatures at which manganese ore is solid, very low oxygen partial pressure is needed for reduction of MnO to metallic manganese or manganese carbides which cannot be achieved using solid carbon, hydrogen or carbon monoxide. On the other hand when methane-hydrogen gas mixture is used, methane cracks at temperatures above 550^{o}C into hydrogen gas and very fine particles of carbon. Depending upon temperature and CH_4/H_2 ratio of the gas phase activity of carbon much higher than 1.0, (relative to graphite) can be achieved which has the potential to reduce manganese oxide to manganese carbide at temperatures when manganese ore is solid. Solid carbon with high activity from CH_4- H_2- (Ar) gas is the main driving force for reduction of manganese oxide to manganese carbides. The activity of carbon from the CH_4-H_2 gas increases with CH_4/H_2 ratio of the gas and temperature, which in turn has the potential to kinetically enhance the reduction process at solid state temperatures.

In principle this particular alternative, hydrocarbon reduction, if successful should result in significantly lower energy requirements and lower carbon emissions. Most of the reduction to metallic state for both manganese and iron units is expected to take place at solid state reduction temperatures which would in principle require only a final smelting stage to complete the reduction and to separate the valuable metallic ferroalloy phase from the slag. The basis of this favorable discussion emerged from another study conducted on chromite reduction using hydrocarbon gas by Decampos[131] at the Pyrometallurgy Research group at the University of the Witwatersrand. It is well known that the ordinary carbothermic solid state reduction behavior of chrome and manganese ores are very different and such differences are also expected for the hydrocarbon reduction. Thus, it is essential to conduct kinetic studies on manganese ores to reveal the mechanism of hydrocarbon reduction and also establish the rate determining steps leading to process parameters.

The purpose and objective of this thesis was to attempt to answer following questions:

- To determine the rate and mechanism of reduction/metallization of Mamatwan manganese ore with the use of CH_4 containing gas mixture between 1050 ^oC and 1250 ^oC.
- To evaluate the rate determining step(s) during reduction.

This study did not describe the mechanism of hydrocarbon cracking and the mechanism of the possible reforming reactions over possible catalysts during the reduction process.

This study explored the use of different concentrations of methane gas in argon and in hydrogen as the reducing gas mixture for a better understanding of the reduction behavior of the manganese ore at different isothermal reducing temperatures.

For this study, a stagnant, loose particle bed of minimum depth of the commercially significant manganese ore was exposed to pre-set reducing gas mixture at known isothermal temperature settings and allowed to reduce. The tests were stopped at pre-determined reduction times and the partially reduced particles were analyzed for metallic manganese and iron.The particle morphology was studied microscopically and product phases were also analyzed by x-ray diffraction.

Ultimately, this study would contribute toward the continued development of practical and economic methods for pre-reducing manganese ore that maximizes efficiency and recovery rates, hence maximizing iron and manganese recovery.

This thesis is organized in six chapters. This first chapter entitled “Introduction” reviews the manganese ores, prereduction and ferromanganese production. The following chapter with the title “Background” discusses the findings of previous work on the pre-reduction of manganese ore and other studies which contribute to the current state of understanding on the pre-reduction behavior of manganese ore due to presence of a hydrocarbon gas. Chapter 3 entitled “Experimental” presents a description of the apparatus, experiments and analyses undertaken for this study. Chapter 4 gives the results and relevant discussions. Chapter 5 entitled “Mathematical modelling, analysis and discussion” describe a mathematical model for metallization of Mamatwan ore, analysis and discussion related to the model, this chapter also provide a proposal of the reduction mechanism and rate limiting steps when manganese is exposed to a methane gas mixture. Chapter 6 is the concluding chapter, summarizing the contributions made by this thesis. The final section presents the references cited in the thesis and Appendices A-E.

CHAPTER 2
BACKGROUND

The amount of research carried on reduction of manganese ores and Mamatwan manganese ore in particular is very limited. This chapter reviews information that has contributed to the present state of knowledge on manganese ore behavior. The following pages in this chapter will also assist in understanding the possible reductions reactions at the different reducing temperatures with carbon and hydrocarbon gases.

2.1 Manganese Oxides and Production of Manganese Alloys

In this section production of manganese containing ferroalloys will be discussed [90,126]. Manganese is only produced commercially from blends of ore in which manganese exists as oxide [16, 18]. Knowledge of the thermodynamics of the reduction of these oxides is therefore essential to the understanding of the production of alloys from manganese ores.

2.1.1 Manganese –Oxygen System

Of the known oxides of manganese (Mn_2O_7, MnO_2, Mn_5O_8, Mn_2O_3, Mn_3O_4 and MnO), the oxides found naturally in Manganese ores are MnO_2, Mn_2O_3, Mn_3O_4 and MnO [14,36,71]. Under normal conditions, manganese dioxide occurs as stable β-MnO_2. Mn_2O_3 is cubic for temperatures above 20^{o}C. Trimanganese tetra oxide (Mn_3O_4) exists at atmospheric pressure in the tetragonal modification and changes to the cubic form at 1170^{o}C. Manganese oxide (MnO) in normal conditions exists in only one modification. This oxide is, however, nonstoichiometric and is more accurately described as $Mn_{1-x}O$, with x=0-0.25. The complete phase diagram of the manganese–oxygen system [33] above 1000^{o}C is given in Figure 2.1.

The equations [126] for the thermal dissociation of the important Manganese oxides and corresponding enthalpy values[126] are as follows:

$$4MnO_2 \rightarrow 2\ Mn_2O_3 + O_2 \quad (2.1)$$

$$\Delta H_{298} = 166.0\ kJ \quad (2.2)$$

$$6\ Mn_2O_3 \rightarrow 4\ Mn_3O_4 + O_2 \quad (2.3)$$

$$\Delta H_{298} = 64.8\ kJ \quad (2.4)$$

$$2\ Mn_3O_4 \rightarrow 6\ MnO + O_2 \quad (2.5)$$

ΔH_{298} = 450.5 kJ (2.5a)

$2\ MnO \rightarrow 2Mn + O_2$ (2.6)

ΔH_{298} = 384 kJ (2.6a)

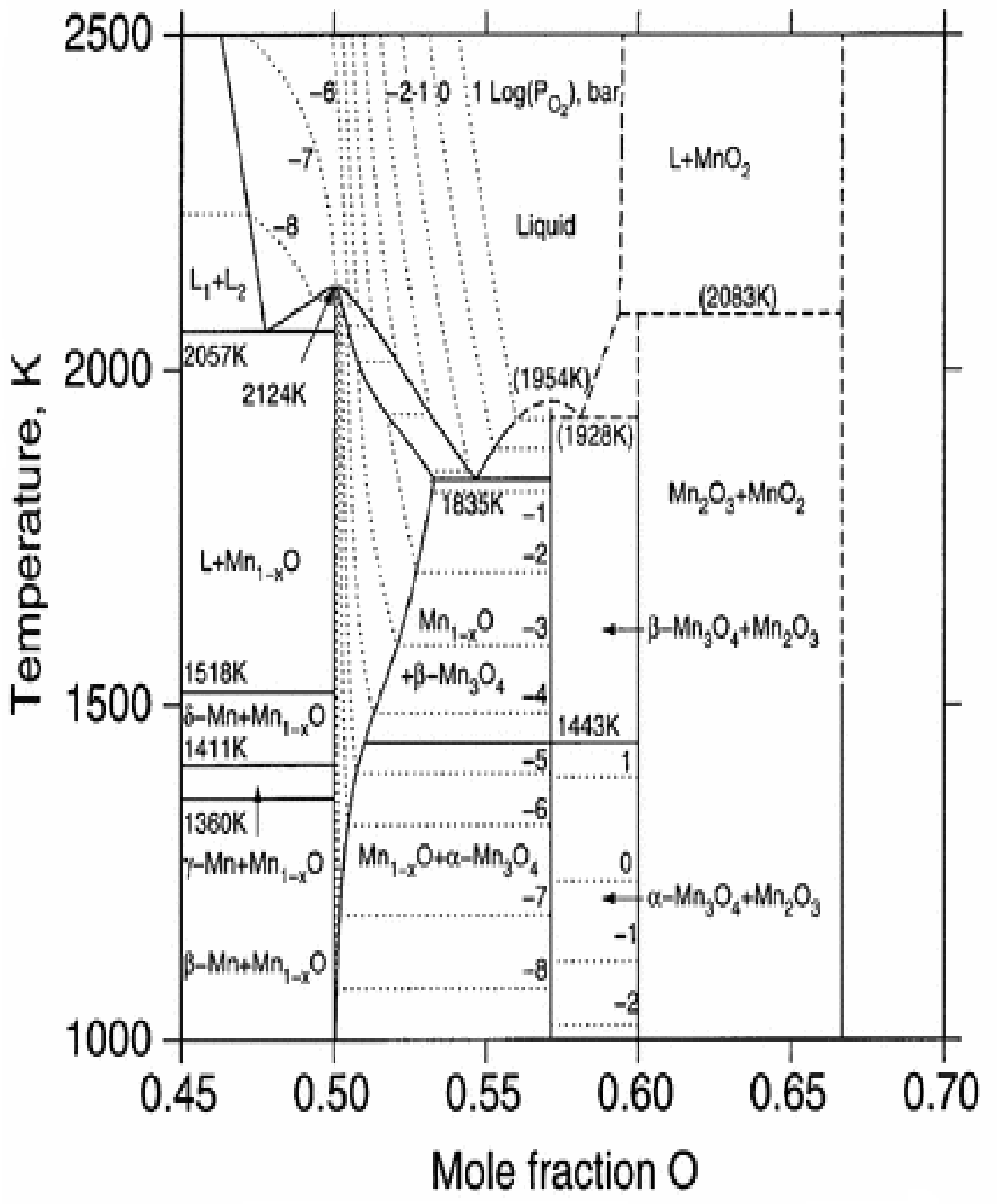

Figure 2.1 Mn-O Phase Diagram above 1000°C [33]

The oxygen partial pressures exerted by these reactions are given as a function of the temperature in Figure 2.2. According to the thermodynamics data the decomposition temperature at 1.013 bar for reaction (2.1) is 500°C and for reaction (2.3), 980°C. For reaction (2.5) to occur at atmospheric pressure a reductant is necessary. Reaction (2.6) requires a high reducing potential. It is important, therefore, to consider the reduction of the oxides of manganese in the presence of carbon monoxide, hydrogen, and carbon. These are the reactions that usually take place in the blast furnace and electric furnaces used to produce manganese alloys [126].

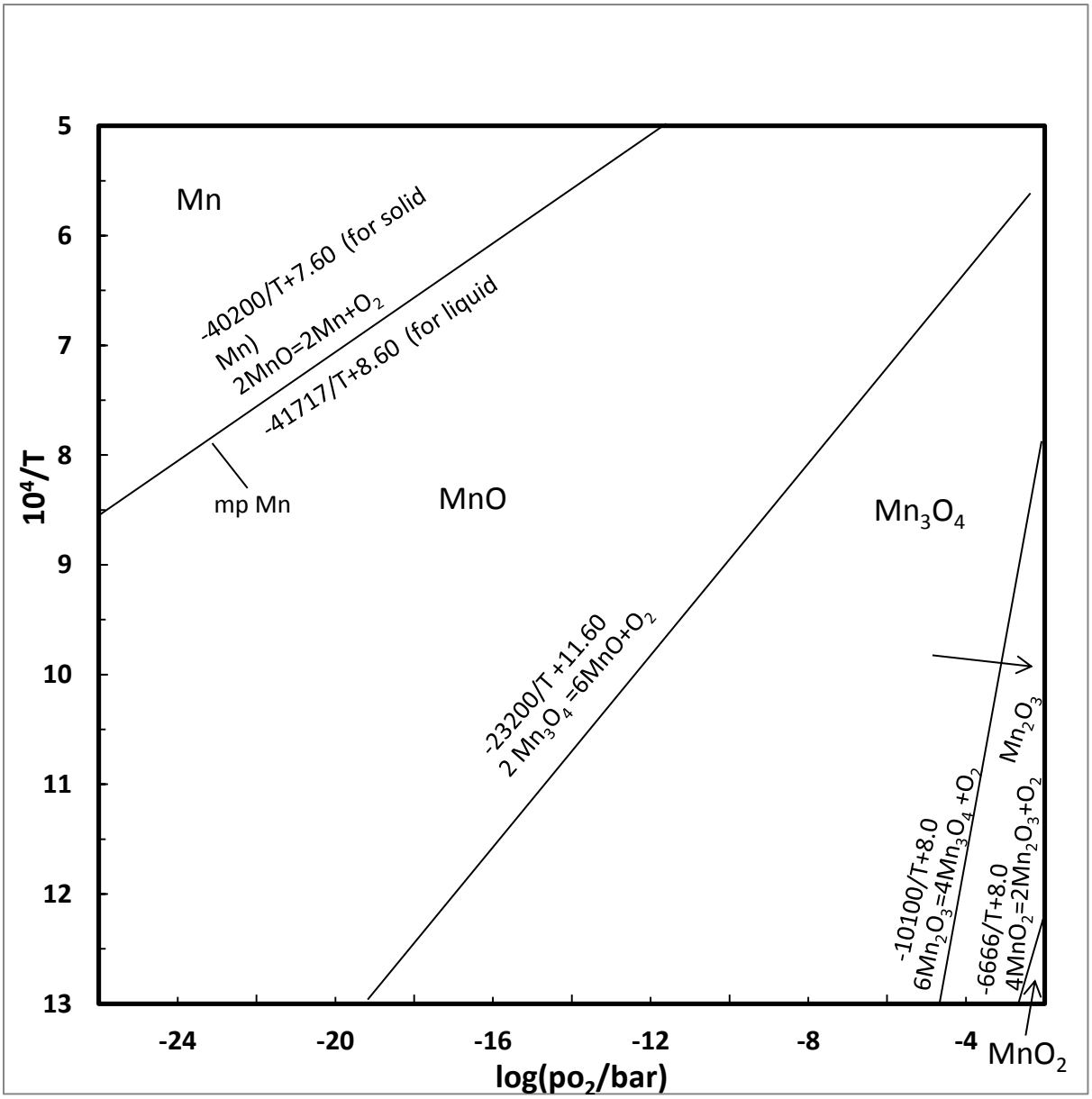

Figure 2.2 Variation of oxygen partial pressure in the Mn – O System with temperature. [126]

2.1.2 Reduction of Manganese oxides with Carbon Monoxide, Hydrogen, and Carbon

The reduction of MnO_2 to Mn occurs in four main steps[3,46,48,55,56] (See Eqs.2.1,2.3,2.5 and 2.6).The reduction is strongly exothermic in the presence of carbon, methane and carbon monoxide. The following equations and enthalpy apply[58,68,77,95,126]

$$MnO_2 + ¼\ C \rightarrow 1/2\ Mn_2O_3 + 1/4\ CO_2 \quad (2.7)$$

$$\Delta H_{298} = -56.8\ kJ \quad (2.8)$$

$$MnO_2 + 1/8\ CH_4 \rightarrow ½\ Mn_2O_3 + ¼\ H_2O + 1/8\ CO_2 \quad (2.9)$$

$$\Delta H_{298} = -56.8\ kJ \quad (2.10)$$

$$MnO_2 + ½\ H_2 \rightarrow 1/2\ Mn_2O_3 + 1/2\ H_2O \quad (2.11)$$

$$\Delta H_{298} = -79.5\ kJ \quad (2.12)$$

$$MnO_2 + ½\ CO \rightarrow ½\ Mn_2O_3 + ½\ CO_2 \quad (2.13)$$

$$\Delta H_{298} = -99.6\ kJ \quad (2.14)$$

The reduction reactions of Mn_2O_3 in the presence of the same reducing agents are also exothermic. The following equations and enthalpy[126] apply:

$$½\ Mn_2O_3 + 1/12\ C \rightarrow 1/3\ Mn_3O_4 + 1/12\ CO_2 \quad (2.15)$$

$$\Delta H_{298} = -16.3\ kJ \quad (2.16)$$

$$½\ Mn_2O_3 + 1/24\ CH_4 \rightarrow 1/3\ Mn_3O_4 + 1/24\ CO_2 + 1/12\ H_2O \quad (2.17)$$

$$\Delta H_{298} = -17.2\ kJ \quad (2.18)$$

$$½\ Mn_2O_3 + 1/6\ H_2 \rightarrow 1/3\ Mn_3O_4 + 1/6\ H_2O \quad (2.19)$$

$$\Delta H_{298} = -24.3\ kJ \quad (2.20)$$

$$½\ Mn_2O_3 + 1/6\ CO \rightarrow 1/3\ Mn_3O_4 + 1/6\ CO_2 \quad (2.21)$$

$$\Delta H_{298} = -31.0\ kJ \quad (2.22)$$

The third step is the reduction of Mn_3O_4, which is endothermic with carbon or methane and exothermic with hydrogen or carbon monoxide.

$1/3\ Mn_3O_4 + 1/6\ C \rightarrow MnO + 1/6\ CO_2$ (2.23)

$\Delta H_{298} = +11.8\ kJ$ (2.24)

$1/3\ Mn_3O_4 + 1/12\ CH_4 \rightarrow MnO + 1/12\ CO_2 + 1/6\ H_2O$ (2.25)

$\Delta H_{298} = +10.5\ kJ$ (2.26)

$1/3\ Mn_3O_4 + 1/3\ H_2 \rightarrow MnO + 1/3\ H_2O$ (2.27)

$\Delta H_{298} = -3.3\ kJ$ (2.28)

$1/3\ Mn_3O_4 + 1/3\ CO \rightarrow MnO + 1/3\ CO_2$ (2.29)

$\Delta H_{298} = -17.2\ kJ$ (2.30)

The last step, the reduction of MnO, is more difficult and requires a high reducing potential. The presence of carbon is therefore necessary, and at a carbon monoxide partial pressure of 101.3 kPa a temperature of 1420^{o}C is necessary for the reaction to proceed. The following, highly endothermic overall reaction and enthalpy[126] applies:

$MnO + C \rightarrow Mn + CO$ (2.31)

$\Delta H_{298} = +274.5\ kJ$ (2.32)

This reaction can be broken down into

$MnO + CO \rightarrow Mn + CO_2$ (2.33)

and the reaction of CO_2 with C to produce CO

$CO_2 + C \rightarrow 2CO$ (2.34)

which ensures that a high reducing potential is maintained.

Due to the importance of both carbon monoxide and carbon as reducing agents in the commercial production of manganese containing alloys, these are discussed in more detail. It is possible to predict the ratio CO/CO_2 that will reduce the individual manganese oxides by considering the relationship between the oxygen partial pressure and the equilibrium constants for reactions (2.1, 2.3, 2.5 and 2.6).

$$K_P = p_{O2} \quad (2.35)$$

Assuming that the activities of the solid phase are unity and the equilibrium constant of the reaction

$$2CO + O_2 \rightarrow 2CO_2 \quad (2.36)$$

which is

$$1/ K_P = p^2_{CO} . p_{O2} / p^2_{CO2} \quad (2.37)$$

and the relationships

$$\Delta G^o = -RT \ln Kp \quad (2.38)$$

and

$$\Delta G^o = -RT \ln p_{O2} \quad (2.39)$$

The oxygen potentials of the individual reactions at various temperatures can be calculated. This is shown graphically in the Ellingham diagram[62] (see Fig 2.3) which is illustrated again to show greater detail and the shift of the CO line as a function of carbon monoxide partial pressure. The same applies to the use of hydrogen as a reductant. Although the reduction of MnO_2, Mn_2O_3, and Mn_3O_4 takes place at low partial pressure of CO (see Eqs.2. 13, 2.21 and 2.29), the presence of carbon is necessary for the reduction of MnO (seen Eqs 2.31, 2.33 and 2.40). In this case the following reaction is important:

$$2C + O_2 \rightarrow 2CO \quad (2.40)$$

for which

$$\text{Log } p_{O2} = - 11672/T - 9.16, [126] \quad (2.41)$$

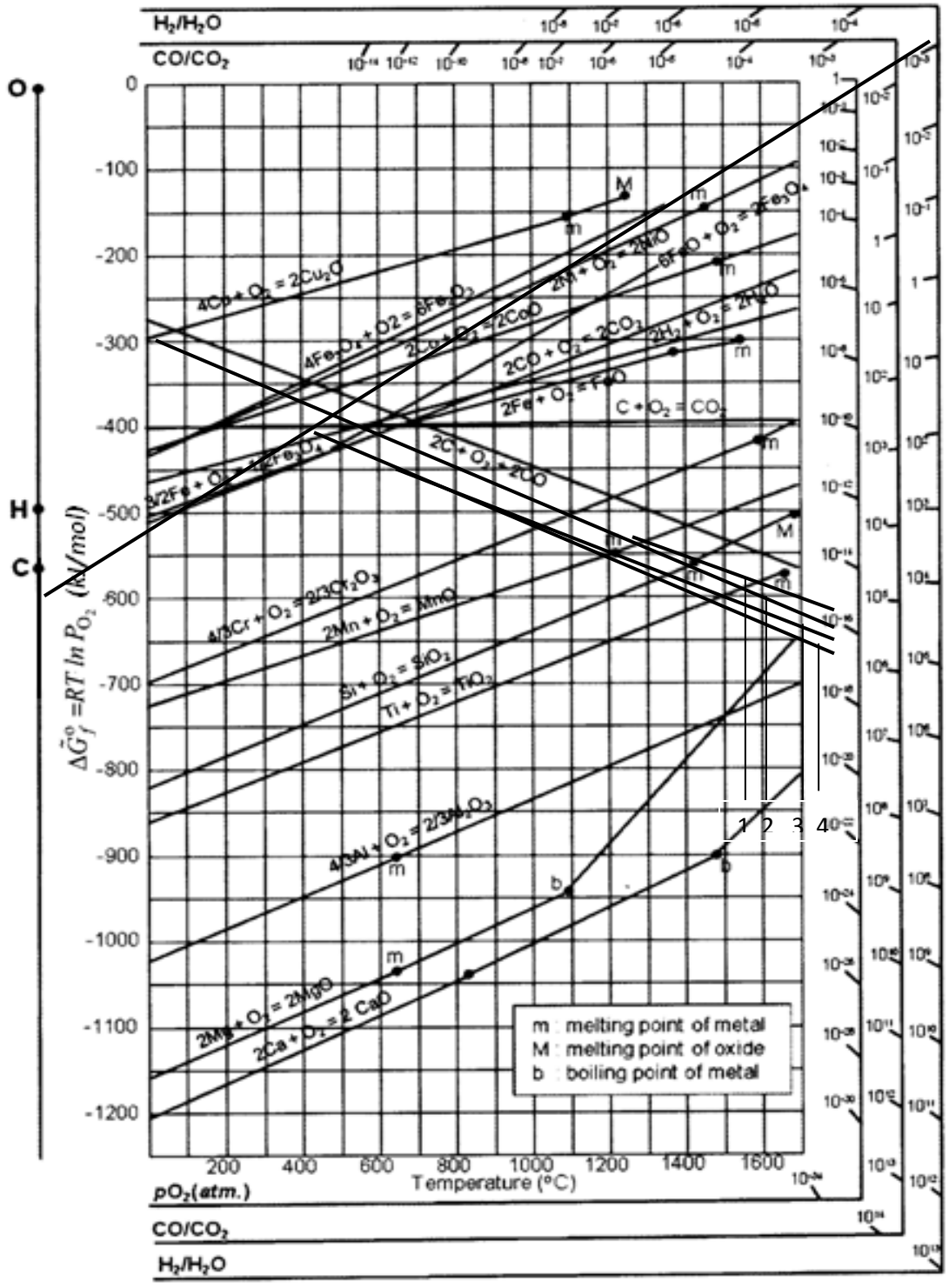

Figure 2.3 Temperature dependence and oxygen potentials of selected oxide systems. [62] 1: $2C+0_2 = 2CO$ (3.0 bar), 2: $2C+0_2 = 2CO$ (1.2 bar), 3: $2C+0_2 = 2CO$ (0.5 bar), 4: $2C+0_2 = 2CO$ (0.3 bar).

This reaction (2.40) is pressure dependent due to the change in the number of moles of gas and again the Ellingham diagram can be used to predict under which conditions the reduction of MnO will occur (see Eqs. 2.31,2.33 and 2.34). However, manganese carbides may be formed during the reduction of MnO with carbon, and this tends to lower slightly the temperatures at which the reaction occurs.Mixed carbide formation reduces the thermodynamic activity of reduced metals and hence promotes the reduction reaction to go forward despite the fact that melting point of carbides may be higher than individual metals. The products produced in this process always contain carbon. The phase diagram for the manganese –carbon system is shown in Figure 2.4. The melting point increases with increasing carbon content. Commercial ferromanganese (76% Mn, 16 % Fe) contains 7% carbon. The solubility of carbon decreases with increasing silicon content.

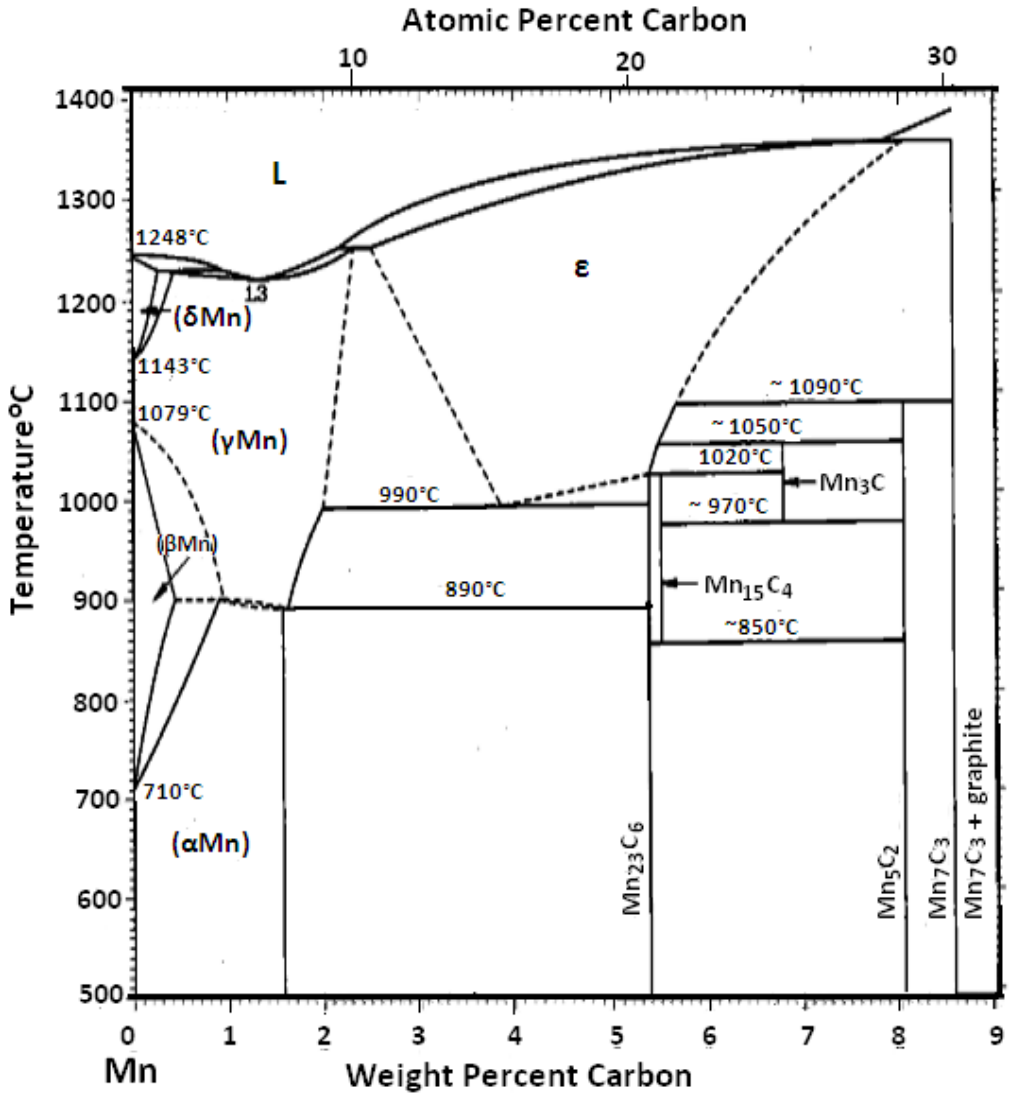

Figure 2.4 Phase diagram for the Mn-C system. [68,126]

2.1.3 Reduction of Mixed Oxides and Minerals Containing Manganese Oxides

In the discussion of the reduction of manganese oxides it has been assumed that the activity of the solid phase is unity. However, this is usually not true in practice because in some manganese ores the manganese oxides may be combined with iron oxides, silicates, aluminum oxides, calcium oxides, and phosphorous oxides [27,28,29,52,62,64,126].

The oxides FeO and P_2O_5 are reduced at lower temperature than MnO whereas SiO_2 needs slightly higher temperature (see Fig 2.3). Any iron oxide and oxides of phosphorous occurring in the ore, fluxes, and reductants used in commercial processes are reduced together with the manganese oxides and report to the product. A judicious choice of ores and raw material is therefore necessary to limit the amount of these elements which report to the metal' [69,92,93,94,105,106,122]. The silica contained in the ores can also be reduced, and in the production of silicomanganese this is desirable. Quartz or quartzite is therefore an important raw material for the production of silicomanganese.

When the presence of other oxides in the ores reduces the activity of the manganese oxide this must be compensated for by increasing the reducing potential by increasing the CO/CO_2 ratio of the gas mixture. Alternatively, the reduction temperature must be increased if the reaction is carried out with carbon.

2.1.4 Reduction of Manganese oxide by Silicon

Reduction of manganese (II) oxide by silicon is also possible [62,69,91,96] :

$$2MnO+Si \rightarrow SiO_2 +2Mn \qquad (2.42)$$

For which

$$K=a_{SiO2}.a^2_{Mn}/a^2_{MnO}.a_{Si} \qquad (2.43)$$

This reaction is the basis of the Frisch process for the production of low carbon ferromanganese and manganese metal from silicomanganese. The silicon content of the metal is restricted by using a basic slag that reduces the activity of SiO_2 by reaction with CaO, displacing reaction (2.42) as far to the right as possible.

2.1.5 Reduction of Manganese Oxide by Aluminum

It is easier to reduce Manganese (II) oxide with aluminum than with silicon because the difference in the oxygen potential of the dissociation equilibrium of MnO and Al_2O_3 are greater than for MnO and SiO_2 [62, 69] (see Fig 2.3). As in the case of carbon and silicon, the higher oxides

of manganese are also reduced if present in the ore. The aluminothermic process is used in the production of Manganese metal.

2.1.6 Production of Manganese Containing Ferroalloys

A number of manganese containing ferroalloys are manufactured which are used largely in the mild steel, foundry, and stainless steel industries. The names and typical compositions of these alloys are given in Table 2.1, and the international standards for the most commonly used alloys, namely high carbon ferromanganese HC-FeMn and silicomanganese FeSiMn, are given in Table 2.2.

Table 2.1 Types of ferromanganese and their general compositions* [126]

Alloy	Composition %		
	Manganese	Carbon	Silicon.
High carbon ferromanganese (carburé)	72-80	7.5	<1.25
Medium carbon ferromanganese (affiné)	75-85	< 2.0	
Low carbon ferromanganese (surraffiné)	76-92	0.5-0.75	
Silicomanganese	65-75	< 2.5	15-25
Ferromanganese silicon	58-72	0.08	23-35
Spiegeleisen	16-28	< 6.5	11-45

* balance is Fe

Generally, high carbon ferromanganese and silicomanganese are produced from a blend of manganese containing ores, and in the case of silicomanganese, slags and silica are added. Ferromanganese can be produced in either electric submerged furnaces or blast furnaces, although only few blast producers exist in the world, whereas silicomanganese is largely produced in submerged arc furnaces [41, 51, 75, 106,119, 126]. High carbon ferromanganese can be converted to medium carbon manganese by an oxygen blowing process, and silicon manganese can be further refined into medium or low carbon ferromanganese as well as manganese metal (See Fig 2.5(a),(b)).

Table 2.2 Ferromanganese standards [126]

Alloy	Country or Organization	Standard	Reference
FeMn	International Standards Organization	DIS	5446
	France	AFNOR NF	A-15-020
	Japan	JIS	G2301
	United States	ASTM	A99-66
	Former Soviet Union	GOST	4755-70
	Federal Republic of Germany	DIN	17564
FeSiMn	International Standards Organization	DIS	5447
	France	AFNOR NF	A-13-030
	Japan	JIS	G2304
	United States	ASTM	A701
	Former Soviet Union	GOST	4756-70
	Federal Republic of Germany	DIN	17564

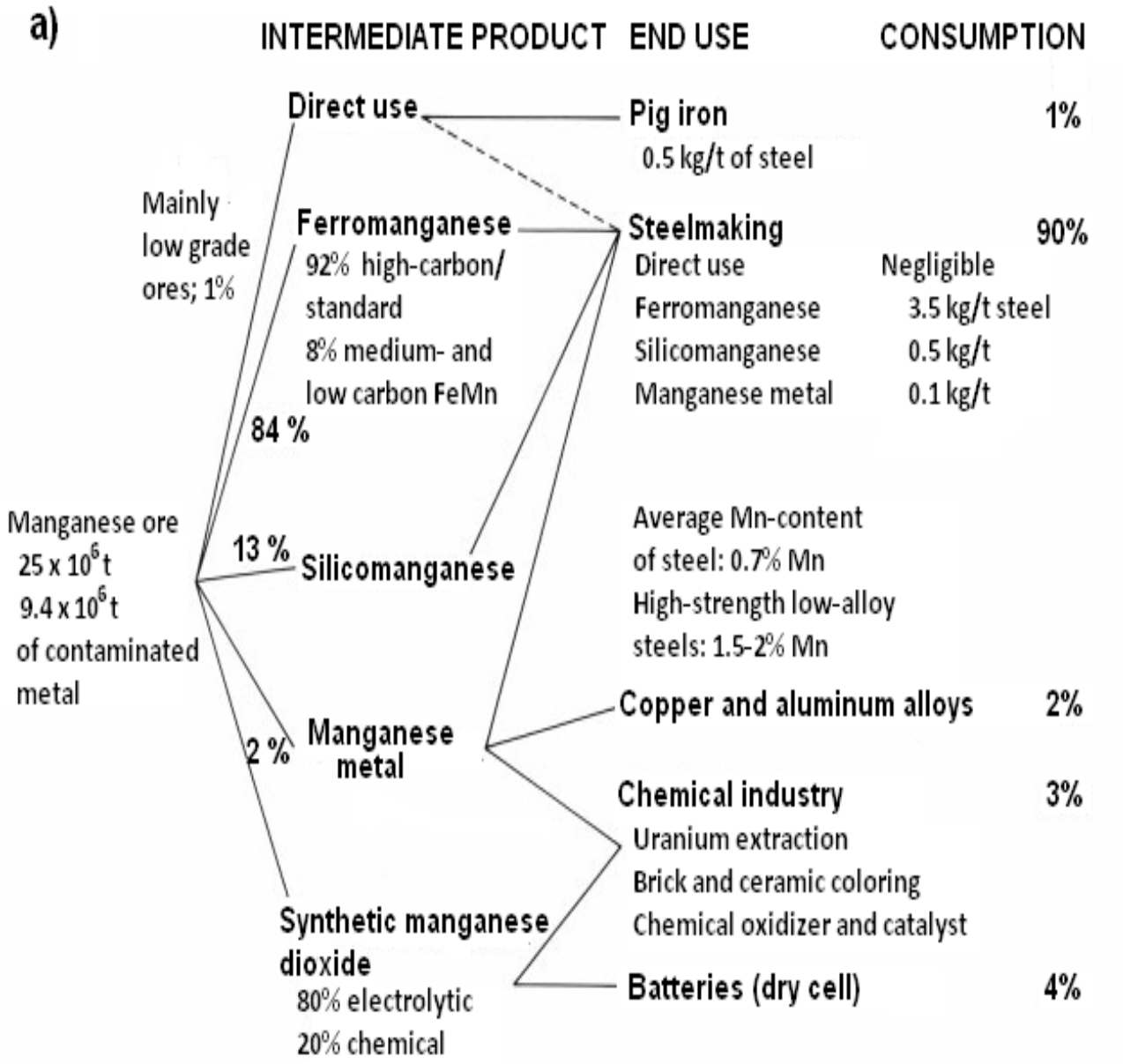

Figure 2.5 (a) Manganese intermediate products and end uses.[126]

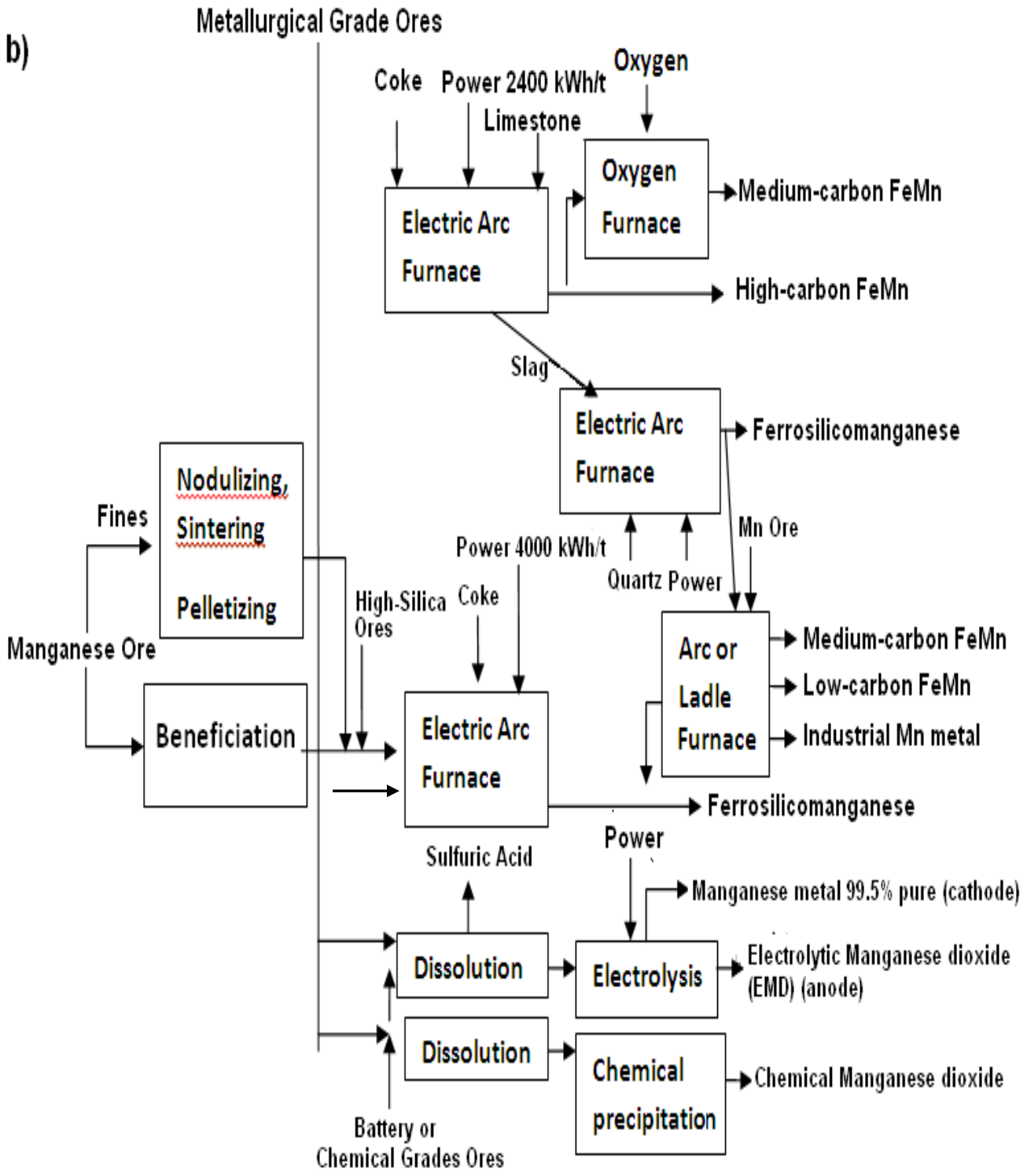

Figure 2.5 (b) Summary of Process routes. [126]

2.1.7 Production of Ferromanganese in Electric Arc Furnaces

The majority of producers of ferromanganese in the world use submerged arc electric furnaces [41,119, 126.].Although electric furnaces have lower capacities than blast furnaces they have the advantage that the heat requirement is provided by electricity, and coke and coal are added to the feed only as reductant. Consequently the coke consumption is lower in electric furnaces than in blast furnaces, which is a considerable advantage in the light of dramatically increasing coke prices. An additional advantage is that the process is not entirely dependent on high-strength coke unlike blast furnaces, and a portion of the carbon requirement can be supplied in the form of coal. In South Africa, where coking coal is in short supply, up to 70% of the carbon for the production of ferro- and silicomanganese is supplied in the form of bituminous coal.

Originally electric furnaces were small (3-8MVA); however, furnaces have grown progressively larger with time. More recently built electric furnaces have capacities of 75-90 MVA. Smaller furnaces are still popular with producers because they offer flexibility in that they can be switched more easily between different products than their larger counterparts. The larger size and more stable operation of modern electric furnaces, due largely to computer control, have resulted in lower electricity consumption. Electric furnaces used in the production of manganese alloys are generally circular and have three electrodes, each coupled to a separate electric phase (see Fig2.6). The diameters of these furnaces range from 2 to 20 m (see Table 2.3).

In modern electric arc furnaces the raw material is usually fed by gravity from bunkers above the furnace. Fresh burden therefore automatically enters the furnace as the raw materials are melted and slag and metal are removed from the system. In older furnaces charging cars are still used to introduce raw materials to the top of the units.

As the raw materials move down the furnace, the higher oxides of manganese are reduced to MnO by the gas leaving the furnace. The reduction of manganese (II) oxide occurs by the contact of carbon with the molten oxide in the slag phase. The overall reaction is:

$$MnO + 10/7C \rightarrow 1/7\ Mn_7C_3 + CO \qquad (2.44)$$

for which

$$\Delta G^{O} = 265.7 - 0.18T\ kJ, [126] \qquad (2.45)$$

The heat required for this endothermic reaction, for heating the burden, and to compensate for heat losses is supplied by the electrical input to the furnace. Heating takes place by the flow of electricity from the tips of the electrode, which are submerged in the burden, through the burden and slag to the metal, as well as through the flow of electricity between the electrodes.

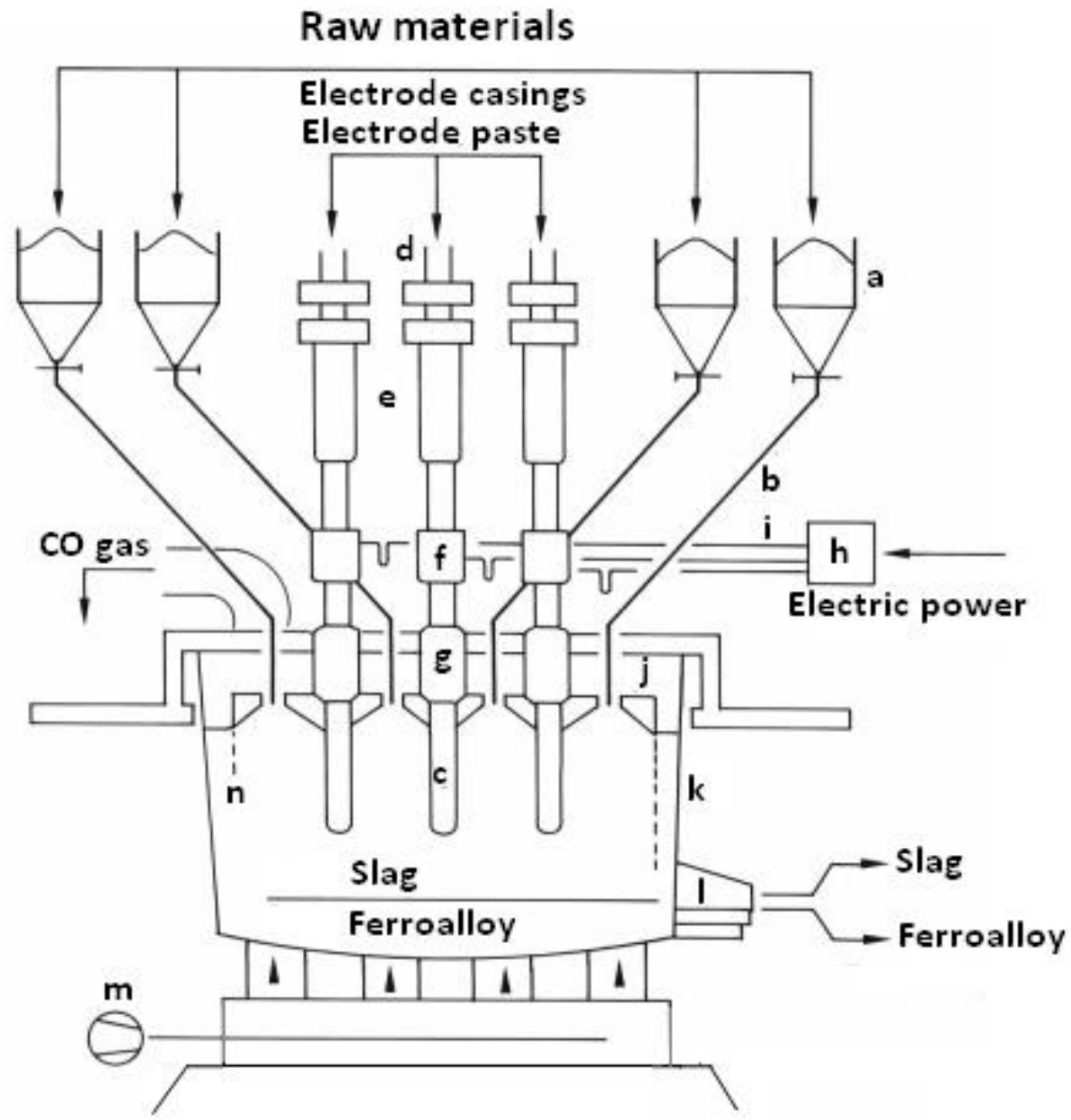

Figure 2.6 Layout of an electric arc furnace.[126] (a) Charging bins (b) Charging Tubes (c) Electrodes (d) Electrodes slipping device (e) Electrode positioning devices (f) Current Transmission to electrodes (g) electrode Scaling (h) Furnace transformer (i) Current bus bar system (j) Furnace cover (k) Furnace shell (l) Tap-hole (m) Furnace bottom cooling (n) Refractory material.

Table 2.3 Furnace design parameters. [126]

	Elkem Beauharious	Elkem Sauda	Tempco Belbay	Samancor Mayerton M10	Samancor Mayerton M4	Former Soviet Union Pro 2.5	Former Soviet Union Pkz33
Inside shell diameter(m)	15.1	12.5	10.0	16.0	9.8	2.7	8.7
Shell Height(m)	8.8	6.0	5.2	8.0	5.7	1.2	3.0
Electrode diameter(m)	1.90	1.90	1.4	1.9	1.2	0.30	1.5
Tap hole	2 Metal, 2 Slag	2Metal, 1Slag	2Metal, 1Slag	2Metal, 1Slag	2Metal, 1Slag	-	-
Megawatt rating	4.5	30	13	46	20	2.5	33

2.1.8 Production of Silicomanganese

Unlike ferromanganese, silicomanganese is only produced in electric arc furnaces [119, 126], most of which can be used interchangeably to produce either of the manganese containing alloys. Silicomanganese is used either as a substitute for ferromanganese and ferrosilicon in steel making or as a raw material for the production of medium and low carbon ferromanganese and industrial manganese metal. Although silicomanganese generally contains 14-19% Si, grades containing up to 35% are produced for the production of extremely low carbon alloys.

There are three general routes for the production of silicomanganese:

1) Reduction of manganese ores and silica with coke and coal.
2) Reduction of MnO rich slags from ferromanganese production and quartzite with coke and coal.
3) Reaction of standard ferromanganese and quartzite with coke.

The first two processes are used for the production of alloys containing 15-25% Si and can be carried out in the same furnaces used for ferromanganese production. The third method is used to produce alloys containing 30-35% Si and is generally performed in smaller furnaces.

2.1.9 Production of Medium-Carbon Ferromanganese

Medium- carbon ferromanganese contains 1-1.5% carbon and has a manganese content of 75-85%. Medium –carbon ferromanganese can be produced either by refining high carbon ferromanganese with oxygen or by the silicothermic route, whereby the silicon in silicomanganese is used to reduce additional MnO added as ore or slag[41, 119, 126]. The former process has considerable advantage like lower energy consumption, lower production cost and is used by most producers.

2.1.10 Production of Low Carbon Ferromanganese

Low carbon ferromanganese contains 76-92% Mn and 0.5-0.75% C. The production of low carbon silicomanganese is not possible by the decarburization of high carbon ferromanganese without incurring extremely high losses of manganese. Therefore silicothermic reduction process is used.

The process is similar to that used in the silicothermic production of medium carbon ferromanganese[119, 126]. High purity ores are used and in particular ores containing iron and phosphorus should be avoided. An artificial manganese ore produced as a high grade slag is particularly suitable because of its low impurity level and because all the manganese is present as MnO. The reduction of the higher oxides of manganese is therefore unnecessary.

The operating figures for 1 t of ferromanganese containing 85 -92% Mn, 0.1 % C, and 1 % Si with a manganese recovery of 75% are:

Calcined manganese ore	1250-1350 kg
Silicomanganese (32-33%Si)	800 -850 kg
Burnt lime	1000-1100 kg
Electrodes	10-12 kg
Electricity	1800-2500 kWh.

Since the required silicon content of the metal is low, a slag high in MnO is necessary. The MnO content of the slag is reduced by use of a two-stage refining operation. In the first stage, an excess of silicomanganese is maintained and a slag containing 6-8 % Mn is teemed and discarded. The second refining stage with manganese ore and lime results in a slag containing 10-14% Mn, which is returned to the silicomanganese furnace. After reviewing (section 2.1)

information that has contributed to the present state of knowledge on manganese ore behavior , next section 2.2 studies reduction of manganese oxide by use of methane / hydrogen gas mixture which is to contribute to present knowledge.

2.2 Reduction of manganese oxide

2.2.1 Reduction by the use of methane/hydrogen mixture

Reduction of manganese ore in the solid state by solid carbon, hydrogen or carbon monoxide does not go beyond MnO [87]. This is seen from the 1200°C Mn-O-C stability diagram [20] in Fig 2.7 below. At temperatures when manganese ore is solid such as 1000°C, extremely low oxygen partial pressure is needed for reduction of MnO to metallic manganese or manganese carbides which cannot be achieved (in practical sense) using solid carbon, hydrogen or carbon monoxide.

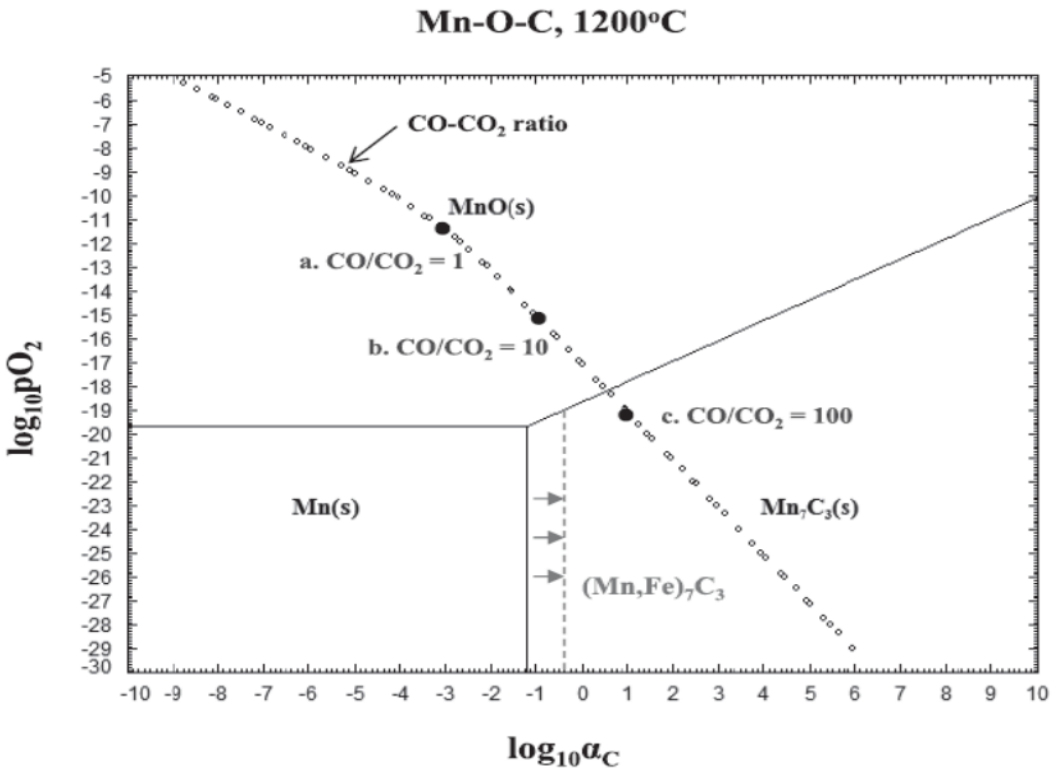

Figure 2.7 Stability Diagram for the Mn-O-C system at 1200°C as a function of oxygen partial pressure (atm) and the activity of carbon. [20]

However, it can be achieved by using methane-hydrogen [31,34,38] gas mixture with appropriate CH_4/H_2 partial pressure ratio at which activity of carbon is above unity (relative to graphite). Reduction of manganese oxide by methane to manganese carbide occurs in accordance with the following overall reaction (Ostrovski et al [87]):

$$MnO + 10/7\ CH_4 = 1/7\ Mn_7C_3 + CO + 20/7\ H_2 \quad (2.46)$$

$$\Delta G^o = 377{,}682 - 314.44\ T\ J/mol, [87] \quad (2.47)$$

At standard conditions, overall reaction (46) proceeds spontaneously at temperatures above 928^{o}C , while carbothermic reduction of MnO; reaction (2.48), starts at 1340^{o}C (Ostrovski et al [87]).

$$MnO + 10/7\ C = 1/7\ Mn_7C_3 + CO \quad (2.48)$$

The equilibrium constant for reaction (46) is equal to 8.5 at 1000^{o}C, 114 at 1100^{o}C and 1075 at 1200^{o}C. This indicates that MnO reduction to manganese carbide may have a high extent at 1000^o-1200^{o}C using an appropriate gas composition. This thermodynamic analysis shows that manganese oxide can be reduced by methane-containing gas to manganese carbide at temperatures below 1200^{0}C when manganese ore is solid. In the non-isothermal reduction by CH_4-H_2-Ar gas, MnO_2 was reduced to Mn_3O_4 and further to MnO by hydrogen and methane at temperatures very close to the reduction by H_2-Argon gas. The reduction of MnO to manganese carbide started at 760^{o}C and was completed at about 1200^{o}C (O. Ostrovski et al [87]). In the process of MnO reduction to manganese carbide, only CO was detected in the gas phase (O. Ostrovski et al [87]).

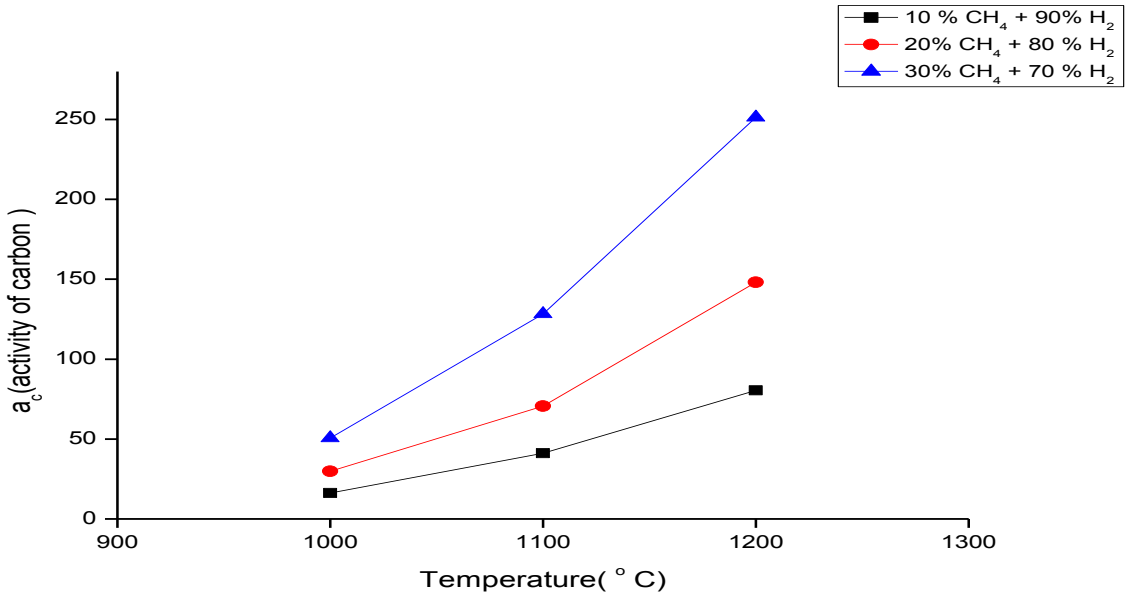

Figure 2.8 Plot showing activity of carbon versus temperature for 10% methane, 20% methane and 30% methane containing methane/hydrogen gas mixture from 1000ºC to1200ºC.

Figure 2.8 illustrates the variation of activity of carbon with change in percentage of methane and hydrogen as a function of temperature (drawn based on Eqation 2.49 and 2.50). At constant temperature activity of carbon increases as the methane percentage increases and for fixed methane percentage it increases as temperature increases. Variation of activity was calculated from the reaction.

$$C(s) + 2H_2(g) = CH_4(g) \quad (2.49)$$

$$\Delta G^o = -16{,}520 + 12.25\ T \log T - 15.62T \text{ cal/mol, [59]} \quad (2.50)$$

Reduction/metallization of Mamatwan manganese ore through the use of methane gas [88, 89] is principally a carbothermic reduction possibly assisted by hydrogen gas. This is due to cracking of methane into very fine sized particles of very high activity carbon and hydrogen gas at temperatures above approximately 550 ^oC in the presence of a solid phase. Although hydrogen is kinetically a fast reductant, thermodynamically hydrogen gas cannot reduce MnO to metal but can reduce iron oxide components and higher manganese oxides into MnO. However due to very high thermodynamic activity of carbon, it dominates the reduction and is potentially assisted by hydrogen in the early stages in the reduction of iron oxides and higher manganese oxides.

2.2.2 Reduction mechanism of manganese oxide

Depending on temperature, the nature of the oxide, reductant and furnace atmosphere reduction of metal oxide can take place by more than one mechanism. Although the process that is most likely to occur under a given set of conditions can be determined from thermodynamic considerations, the kinetics of the process may be unfavorable and different processes may occur. Kolchin[53] stated that the reduction process cannot be explained by a universal mechanism and that reduction by carbon for example may occur by various mechanisms depending on the system and conditions.

One of the ways of lowering the consumption of electric power and raising the productivity in production of manganese alloys is by pre-reduction of the charge before the final smelting. Manganese is present in manganese ores as higher oxides and silicate, and during the early stages of reduction these are reduced to MnO by reducing atmosphere in the furnace. Most of the investigations[4,5,6,7,19,86,97,102,114,122] carried out until recently on the reduction behavior of manganese ores involved carbon reduction of manganese oxide. Koursaris et al[50] found that the early stages of reduction of Mamatwan ore with carbon in temperature range between 1200 ^oC and 1600^oC involve complex mineralogical changes as given below :

1) Breakdown of braunite and gangue minerals.
2) The reduction of higher manganese oxide to MnO and hematite to metallic iron.
3) Formation of slag as a result of reaction between gangue and manganous oxide.

Koursaris[50] also stated that further reduction of the ore involved the carburization of the metallic phase and the reduction of the solid MnO, or liquid MnO dissolved in the slag, by solid carbon or carbon dissolved in the metal. They proposed a reduction sequence which can be represented as follows:

$$\text{Manganese ore} \longrightarrow Mn_3O_4 + \text{slag} \longrightarrow Mn_{1-X}O \longrightarrow MnO_{(\text{stoichiometric})} \longrightarrow Mn_{\text{carbides}}$$

2.3 Literature review

Manganese is only produced from blends of ore in which manganese exists as oxide [22,49,74,80,82,83,98,105,118,127,129].Knowledge of the thermodynamics of the reduction of these oxides is essential in the production of alloys from manganese ores [8,24,45,30,60,61,70,81,99,108,109,110,122].This section will assist in understanding the possible reductions reactions at different reducing temperatures and the characteristic behavior that the manganese ore displays when pre-reduced with a hydrocarbon gas.

2.3.1 The carbothermic and gaseous reduction studies of manganese.

Grimsley[32] studied the degree and mechanism of reduction of Mamatwan manganese ore with graphite at temperatures ranging from 1000°C to 1300°C, the reduction being carried out in a resistance furnace in argon or carbon monoxide atmospheres. The reduction of Mamatwan manganese ore by carbon at temperatures in the range 1000°C to 1300°C occurs in two stages: (i) reduction of the higher oxides of manganese to MnO by carbon and carbon monoxide with concurrent formation of $CaMn_2O_4$ and (ii) reduction of $CaMn_2O_4$ and MnO to carbide by carbon dissolved in the ferromanganese phase. At 1000°C and 1100°C, very little reaction occurs during the second stage and the products of reaction are $CaMn_2O_4$ and MnO. At 1200°C, the second stage accounts for up to one-half of the total reduction, at 1300°C, if sufficient carbon is present, most of the reduction occurs during the second stage, the product probably being $(Fe, Mn)_7C_3$. The rate and overall degree of reduction at 1300°C increase as the carbon addition is increased up to 30 per cent (by mass) or 2.4 times the stoichiometric amount of carbon required to reduce the iron and manganese oxides to their metals. Further increases in the amount of carbon added have no apparent effect on the rate and overall degree of reduction.

G. Akdogan[35] investigated reduction of manganese ore from Wessel mine of South Africa in the temperature range 1100°C to 1350°C with pure graphite as the reductant under argon

atmosphere. He concluded that the rate and degree of reduction increased with increasing temperature and decreasing particle sizes of both the ore and the graphite. Akdogan[35] studied effect of chemical composition of the manganese ores on the reduction degree and the rate by varying Mn_2O_3 content of the manganese samples from 50.78% to 75.09%, Mn/Fe ratios varied from 1.86 to 5.82 and Fe_2O_3 content changed from 12.86 % to 27.02 %. Their results showed that the reduction rate increased with decreasing the Mn: Fe ratio of the ore and increasing the Fe_20_3 content. Akdogan[35] came to significant conclusions that reduction was found to occur in two stages: during the first stage rapid reduction of higher oxides of manganese and iron to MnO and FeO occurred. The rate control appears to be mixed; both inward diffusion of CO and outward diffusion of CO_2 across the porous product layer, and the reaction of carbon monoxide on the pore walls of the oxide phase play important roles. The second stage is slower during which MnO and FeO are reduced to mixed carbide of iron and manganese. The chemical reaction between the manganous oxide and carbon dissolved in the metal phase or metal carbide seems to be the rate-controlling process. Also during the first stage they found that the rate and degree of reduction of the WH, W1, and W4 type Wessel (these designated WH, W1 and W4 ore were from Wessel mine in the Kalahari field supplied by Samancor with different Mn_2O_3 content and different Fe_20_3 content mainly.) manganese ores increase with increasing temperature and decreasing particle sizes of both ore and graphite, markedly, at temperatures 1300^{o}C and 1350 ^{o}C under argon atmosphere.

Akdogan[35] modelled their results mathematically. He found that for the first stage, the mathematical treatment gave the values of effective CO-CO_2 diffusivities as 2.25* 10^{-5}, 5.10 *10^{-5}, and 6.17*10^{-5} $cm^2.s^{-1}$ for WH, W1, and W4 ores, respectively, at 1300 ^{o}C and as reduction proceed relative contribution of chemical resistance increased while that of the diffusional resistance decreased. Apparent activation energies calculated from the reduction rate data corresponding to the first stage of the reduction were 81.3, 87.0, and 94.6 kJ/ mol for W4, W1, and WH ores, respectively. He concluded that after about 6 minutes, the second slower stage started with nucleation of iron from wustite. The chemical reaction between manganous oxide and carbon dissolved in the metal or metal carbide seemed to be the rate-controlling process. The rate of chemical reaction between MnO and carbide was found to lie in the range from 1.53*10^{-8} to 1.32*10^{-7} $mol.s^{-1}.cm^{-2}$. Apparent activation energies calculated were 102.1, 107.8, and 141.7 kJ/mol for W4, W1, and WH ores, respectively. During this stage, the reaction was localized at the oxide/carbide interface and proceeds as a shrinking core. For the two stages a detailed kinetic model was developed, taking into account the chemical and diffusional factors affecting the process.

Burucu, E [9] studied kinetics of reduction of the manganese ore from the Mamatwan mine using TGA analysis, X-RD, optical microscopy, and energy dispersive analysis of x – rays (EDAX) between 1100 ^{o}C and 1350 ^{o}C with pure graphite under argon atmosphere. It was observed that

the rate and degree of reduction increased with increasing temperature and decreasing particle size. The effect of the different reaction atmosphere has also been investigated by replacing argon atmosphere with carbon monoxide and carbon dioxide. The results clarified importance of some reactions in the reduction mechanism of the ore. In early stage of reduction, up to about 4 minutes of reaction time, carbothermic reduction of higher oxides of manganese and iron (Mn_2O_3 and Fe_2O_3) to manganous oxide (MnO) and metallic iron respectively was observed which was controlled by diffusional process across the boundary layer between the solid phases. Apparent activation energy is calculated as 61.03 kJ for this stage which corresponds to about 30 % reduction. Metallization started as random nucleation of iron rich carbides around MnO grains inside the particle. After 30 percent reduction the formation of a silicate phase was observed. Up to 70 percent reduction at 1350^{o}C, reduction rate was controlled by chemical reaction between oxide phase and gaseous phase with apparent activation energy of 153.32 kJ. The later part of the reduction proceeded by the reduction of MnO covered by either the carbide or silicate phase by carbon dissolved in carbide phase $(Mn, Fe)_5C_2$. Diffusion of Mn^{2+} ions in oxide phase was the most likely rate determining step for this stage. Apparent activation energy was found to be as 310.40 kJ.

Cem Akil and Ahmet Geveci[12] carried out a study on optimization of conditions to produce manganese and iron carbides from Denizli-Tavas manganese ore of Turkey by solid state reduction. The ore was calcined and then mixed with active carbon and CaO. Experiments were performed in a horizontal tube furnace that can be heated up to 1700 $^{\circ}$C with $MoSi_2$ heating elements. The optimized parameters were: temperature, time, carbon percentage, and CaO percentage. After each experiment, weight loss data were obtained and converted to percentage reduction. Akil and Geveci[12] subsequently concluded from the experimental results that to obtain a high reduction percentage, temperature should be as high as possible to a point at which partial melting of the charge starts to occur. Akil and Geveci[12] showed utilizing 1250°C as the reduction temperature was advantageous since it ensured a high reduction percentage, and kept the charge completely at solid state. It was also noted by them that from the energy consumption and high reduction percentage points of view, 4 hours of reduction time was found to be advantageous since further increment in duration does not provide a significant change in reduction percentage. Akil and Geveci[12] confirmed that in order to obtain satisfactory reduction percentage, it was not necessary to utilize active carbon in excess of the stoichiometric amount. Amounts higher than 100% of the stoichiometric amount of active carbon decreased the reduction percentage values. Akil and Geveci[12] also found that presence of calcium oxide in the charge was beneficial for the reduction and helps as a binder up to 5 wt. %, but it prevented carbide formation and decreased the reduction percentage above that value. Akil and Geveci[12] thus argued that prereduction of the manganese ore prior to smelting offers several advantages over direct smelting such as increased manganese recovery, less

carbon requirement for smelting, and also the overall operation are easily controlled ,more oxygen and volatile matter are removed prior to smelting. Hence they concluded that the manganese content of the ore product increased under the optimum conditions, the product obtained in this study could be used for ferromanganese production.

Gökhan Çil and Kenan Yıldız[30] investigated the carbothermic reduction of calcined and mechanically activated manganese carbonate ore with graphite under an argon atmosphere at temperatures between 1100°C and 1300°C and the effects of mechanical activation (performed in a planetary mono mill) on the ore structure (due to structural disordering) were analyzed by X-ray diffraction, scanning electron microscopy and particle size analysis. They found that the activation procedure led to amorphization in the ore and accelerated the degree of reduction in the mixture of the calcined ore and graphite. They showed that the non-activated and activated manganese ore were reduced at temperatures between 1100 and 1300°C in the presence of graphite. It was concluded from their investigation that high energy ball milling is effective for the reduction of manganese ore with graphite and usage of the mechanical activation process increased the degrees of reduction and metallization in the ore due to structural disordering in the ore structure. The reduction degrees of activated ore were higher than those of non-activated ore at the same reduction temperatures and times.

Çardaklı, İsmail Seckin et al[13] studied the production of high carbon ferromanganese by smelting a manganese ore located in Erzincan, Turkey. Time, charge basicity, fluorspar addition and coke to ore weight ratio were used as experimental variables. After characterization of the ore, they took a mixture of 100 grams of manganese ore and carefully weighed amounts of coke powder, lime, fluorspar and scrap iron which were put into a conical graphite crucible. The graphite crucible with its contents was covered with a graphite lid and placed in an electronically controlled muffle furnace. The furnace was heated to 1600°C and held at this temperature for a predetermined time and cooled to room temperature. The crucible was taken out of the furnace and the metal and slag phases formed were removed from the crucible by breaking the crucible and carefully weighed. Finally, the metal and slag phases were subjected to chemical analysis. From the experimental results they confirmed that Erzincan manganese ore can be used in the production of high carbon ferromanganese. Effect of time on experiments was investigated in the range 1 to 5 hours. It was found that almost all of the iron oxides in the charge were reduced into metal in less than 1 hour whereas reductions of MnO and SiO_2 were still not complete at the end of 5 hours. The results indicated that metal Mn and Si contents and Mn and Si recoveries from the charge increased with time. Slag SiO_2 content was found to remain almost constant whereas slag MnO content was found to decrease with time. Çardaklı, İsmail et al[13] noted that Erzincan manganese ore is not a self – fluxing ore, $\%CaO/\%SiO_2 < 1$. CaO was added to the charge to study the effect of basicity on smelting. Experiments were conducted with charge basicity of 1, 1.25 and 1.5. Results showed that

manganese metal – slag distribution ratio increased and silicon metal – slag distribution ratio decreased with increasing charge basicity. Mn recovery was found to increase with increasing charge basicity whereas Si recovery decreased with increase in the charge basicity. Fluorspar was added into the charge in amounts of 2.5% and 5% of the weight of CaF_2 free charge. Fluorspar addition resulted in good slag – metal separation. Manganese metal – slag distribution ratio increased and silicon metal - slag distribution ratio decreased with increase in CaF_2 addition. Mn recovery from the charge increased whereas Si recovery from the charge decreased with the addition of fluorspar into charge. Çardaklı, İsmail Seckin et al[13] also investigated the effect of graphite to ore weight ratio by conducting experiments with graphite to ore weight ratios of 0.05, 0.10 and 0.15. They concluded that increase in graphite to ore weight ratio increased manganese and silicon metal – slag distribution ratios and manganese and silicon recoveries from the charge. Their experimental results showed that it is possible to produce high carbon ferromanganese with above 75% manganese content close to chemical composition specified by ASTM standards by smelting Erzincan manganese ore. Manganese recovery during the smelting experiments was about 60 – 80 percent.

K.S. Abdel Halim[37] studied reduction of compacts of pure and 2% MnO doped iron oxide isothermally at 800°C–1100 °C by solid carbon. The reduction behavior was investigated using advanced quadrupole mass spectrometer. XRD and SEM analysis were used to characterize the reduced samples. The aim of this work was to clarify the reduction behavior of Fe_2O_3/MnO composite materials with solid carbon. The influence of reduction conditions on the structural characteristics of the products was extensively studied to get clear comprehension of reduction process. It was found that the reduction rate increases with temperature and decreases with the presence of MnO. Halim**[37]** used the experimental measurements to elucidate the carbothermic reduction mechanism of iron oxide doped with MnO. The reactions proceeded in a stepwise manner and Boudouard reaction was the rate controlling step. The calculated values of activation energy revealed that solid state diffusion mechanism had a significant role in the reduction process. Pure Fe_2O_3/C and Fe_2O_3/C doped with 2% MnO compacts were prepared and isothermally reduced using two different techniques, thermo-gravimetric technique was used to measure the weight loss as a function of time while effluent gas analysis method was applied to follow the outlet gases. At lower reduction temperatures (800–900°C), pure and doped compacts show low weight loss percentages (50–85%) which can be attributed to the formation of dense metallic iron and hardly reducible phases which can be reduced only at higher temperatures. The presence of MnO in the iron oxide compacts decreased the rate of reduction due to the internal microstructure changes occurred during reduction. Halim[37] examined the variation of gas composition CO and CO_2 in the product gas to clarify the kinetics and mechanism of the reduction with solid carbon. The reactions proceeded in a stepwise manner and the reduction process takes place by gaseous reduction mechanism and Boudouard

reaction is the rate controlling step. The calculated values of activation energy revealed that solid state diffusion mechanism had a significant role in the reduction process similar to the suggestion by other authors (Akdogan and Eric[35]).

N. A. El-Hussiny et al[42] studied low-grade ores of Egypt because of intensive mining of high grade manganese ores for a long time while leaving behind the low-grade ores, the utilization of the latter has become necessary. He noted that there are several physicochemical differences among the components in manganese ores, which can be used for the enrichment of manganese. In particular, the abundant low-grade manganese ores, which contain iron oxide, may be upgraded by pre-reduction and magnetic separation. They investigated pre reduction of ferruginous low-grade manganese ore with coke breeze as source of carbon, which converted iron oxide to Fe_3O_4, while manganese ore was reduced to Jacobsite ($MnFe_2O_4$) and iron manganese oxide compounds which can be separated later. The reduction in the temperature up to 950^oC was controlled either by chemical controlling mechanism with energy of activation of 10 kJ/mole or solid diffusion process with energy of activation of 29.26 kJ/mole. They observed the following: 1.The pressing pressure load in the briquetting process of low grade manganese ore with coke breeze powder increased both the drop damage resistance and compressive strength. 2. The degree of reduction of low grade manganese ore with coke breeze at constant temperature increased as the percentage of coke breeze increased. 3. The reduction rate of low grade manganese ore with coke breeze under a constant amount of coke breeze as reducing agent increased with increasing temperature. 4. The reduction process was controlled either by contracting volume model $(1-(1-R)^{1/2}=kt)$ with energy of activation of 10 kJ/mole or solid diffusion model $(R+(1-R)\ln(1-R)=kt)$ with energy of activation of 29.26 kJ/mole. (Where k is rate constant, R is fraction of reduction and t, time in minutes).

Bo Zhang and Zheng-Liang Xue[130] investigated reduction of manganese ore pellets containing carbon using high temperature carbon tube furnace. The reaction was divided into two stages. They found that, the reaction rate in the earlier stage was controlled by the chemical reactions between FeO, MnO and carbon reductant, and the activation energy was 28.85 kJ/mol. In the later stage, as the carbon reductant replaced by CO, the reaction rate was controlled by CO-diffusing in solid products, and the corresponding activation energy was 86.56 kJ/mol. Reaction rate of the later stage was less than the earlier one.

Manoj Kumar et al[65] studied the reducibility of three different manganese ores with coke. The three groups of manganese ores studied (siliceous, carbonate, oxide) reacted differentially upon heating. Coke used in these studies contained 80.11% fixed carbon; 14.94% ash and 3.85% volatile matter. They took 10 grams of the ore and mixed with coke stoichiometrically sufficient to reduce all the iron and manganese in the ore. The three ores were reduced to different

extents under the same experimental conditions. The investigations showed that in the temperature range of 900°C-1000°C, Fe_2O_3 in the ore was reduced to metallic iron. MnO_2 was reduced to Mn_3O_4 in all cases except one in which it was reduced to Mn_2O_3. The kinetics of reduction was controlled by different mechanisms in the different ores. Temperature had a significant influence on the reducibility of the ores. Manoj Kumar et al[65] found that degree of reduction was dependent on the nature of the ore and temperature. It was concluded that the process was controlled by diffusion when reduction was restricted to the stage of formation of Mn_3O_4. When the stage of reduction extended up to the formation of MnO, the rate was controlled by chemical reaction. At 900°C and 1000°C, manganese metal was not formed. When the flow rate of argon over the reaction site increased, reduction proceeded up to the stage of the formation of manganese metal, because when the rate of flow of argon gas in the reaction chamber is varied, the following reaction plays an important role in controlling the rate of reduction $2C + O_2 = 2CO$. (The reduction was controlled by chemical reaction).

Tor Lindstad and Lars-Arne Stalheim[63] investigated the reduction of Mn_3O_4 to MnO in a thermo balance apparatus. The charge was composed of Mn_30_4 and coke, in about the same proportion as in an industrial scale reduction furnace. Argon supplied only at the start before heating to reaction temperature, no extra gas was furnished. The reaction between the two solids proceeded through CO and $C0_2$ as gaseous intermediates. The reaction was described by the shrinking core model for the manganese oxide, and seemed to be rate-controlled by chemical reaction at the reaction front or a mixed resistance of chemical reaction and gaseous diffusion through the product layer. They mentioned that their experiments could not be directly compared with the industrial process, but by performing reduction experiments in laboratory scale at different conditions; with and without feed gas, with different ores and cokes, varying coke/ore ratios, size ranges and temperatures, they hoped to obtain more general reduction rate parameters. The present results showed that the chemical reaction in the ore to a great extent controlled the total reaction rate for the reduction of Mn_30_4 to MnO.

R. Kononov, O. Ostrovski and S. Ganguly[54] studied carbothermic reduction of manganese oxides and manganese ores in hydrogen, helium and argon at different temperatures, ore compositions and carbon to manganese oxide ratios. Wessel ore (South Africa) and two grades of the Groote Eylandt ore (Australia) with different level of impurities were examined. They characterized the ore by XRD, X-ray fluorescence, optical microscopy and scanning electron microscopy. Isothermal and temperature programmed carbothermic reduction experiments were conducted in a fixed bed reactor in a vertical tube furnace, with on-line monitoring of gas composition by the CO-CO_2 infrared sensor. The reduced samples were characterized by XRD, SEM and LECO analyses. Extent of reduction was calculated using data on the off-gas composition, and LECO analyzed carbon and oxygen contents in the reduced sample.

Manganese oxides in the ore were reduced to α-Mn and carbides $Mn_{23}C_6$ and Mn_7C_3 depending on the carbon to ore ratio. They observed that reduction rate of manganese ores in hydrogen was higher than in helium and argon. They found that carbothermic reduction of manganese oxide and manganese ores were strongly affected by the reduction temperature and gas atmosphere. It was observed by them that reduction of MnO in hydrogen was close to completion at 1200 ^oC in about two hours (final product was dependent on MnO/C ratio), while in helium and argon reduction of MnO was not completed during this reaction time at temperatures below 1300 ^oC. They concluded that carbothermic reduction of MnO and manganese ores at constant temperature was the fastest in hydrogen and slowest in argon, rate and extent of reduction of Wessel ore was higher in comparison with Groote Eylandt ores. Composition of phases formed in the reduction process depended on the manganese oxide to carbon ratio, and was independent of the gas composition.

O. Ostrovski, N. Anacleto, and S. Ganguly[87] studied the reduction of Groote Eylandt (Australia) and Wessel (South Africa) manganese ores using CH_4-H_2-Ar gas mixture in a fixed bed laboratory reactor in the temperature range 1000–1200°C. The extent and kinetics of manganese ore reduction as a function of gas composition and temperature was determined by on-line off-gas analysis using mass-spectrometer and dew point sensor. Morphology of ores and their change in the course of reduction was examined by optical and scanning electron microscopy. Phases of raw materials and reduced samples were analyzed by XRD and EPMA.

O. Ostrovski, N. Anacleto, and S. Ganguly[87] found that manganese oxides were reduced to carbide Mn_7C_3. High extent and rate of reduction by methane-containing gas in comparison with carbothermic reduction were attributed to high carbon activity in the reducing gas, which was in the range 15 - 50 (relative to graphite). They found that reduction rate of Wessel manganese ore increased with increasing temperature. Reduction rate and extent of Groote Eylandt manganese ore achieved maximum at 1050°C. The decrease in rate and extent of reduction of Groote Eylandt ore at higher temperatures, particularly at 1150^oC-1200°C, was due to sintering and formation of semi-liquid silicate slag. From the investigation they established the optimum conditions for the reduction of manganese ores as follows: a) temperature: 1150^oC-1200°C for Wessel and 1050^oC-1100°C for Groote Eylandt ores, b) methane concentration: 10-15 vol%, c) hydrogen concentration: above 30 vol%, (d) size: 1-3 mm. An addition of lime (10-15 wt% CaO) to the Groote Eylandt manganese ore increased melting temperature of slag and significantly increased the rate and extent of reduction at elevated temperatures. They found that in the reduction of pure MnO and manganese ores by CH_4-H_2-Ar gas, manganese oxides are reduced to manganese carbide by the overall reaction: $MnO + 10/7\ CH_4 = 1/7\ Mn_7C_3 + CO + 20/7\ H_2$.

It was observed that at 1200^oC, reduction of Wessel ore by CH_4- H_2-Ar gas containing 10 vol% CH_4 and 50 vol% H_2 was close to completion in less than 50 min. The rate of reduction of pure

manganese oxide and Wessel ore increased with increasing temperature in the range 950-1200°C and methane content up to 10-15 vol% CH_4. Further increase in methane content above 15 vol% had a slight effect on the rate of reduction. Increasing hydrogen content above 20 vol% favored the reduction process. It was also noted that addition of CO to the gas phase strongly retarded the reduction process. Solid carbon deposited as a result of the methane cracking, blocked access of the reducing gas to the oxide, and retarded MnO reduction. Significantly methane cracking was enhanced by an increase in reduction temperature and methane content in reducing gas, and with iron addition.

In Department of Ferrous Metallurgy (IEHK); Martins K.O and Senk.Dieter[67] of RWTH Aachen University conducted studies on direct reduction of different combination of blends of manganese ore, iron ore and coal. A mixture of iron and manganese ore in a ratio of 75/25 was a good raw material for steelmaking of high Mn-alloyed grades. The experimental studies of reduction of (a) fine material and (b) agglomerated material (briquettes) were carried out in the temperature range of 1000°C to 1400°C. The behavior of combined reduction of manganese ore and iron ore and the employment in the direct reduction on a coal and gas basis for production of steels with high Mn content were investigated. Martins K.O and Senk.Dieter[67] found that a high metallization degree for Mn can be reached at 1000°C with the reduction of manganese ore by hydrogen-containing gas. Addition of carbon monoxide to the reducing gas retarded the reduction process which was also observed by O. Ostrovski, N. Anacleto, and S. Ganguly [2, 87]**.** The addition of coal to manganese ore and iron ore blends increased the degree of reduction. The results of carbothermic reduction of briquettes consisting of a mixture of manganese ore and iron ore combined with coal as reducing agent showed that a high temperature, a low Mn/Fe ratio and a high Fe_2O_3 content had a favorable effect on the degree of reduction. In order to obtain a high degree of metallization, the temperature should be higher than 1200°C. The reduction of briquettes at higher temperatures (up 1300°C) has shown a molten phase and the separation of slag and metal.

Tetsuo Yagihashi[121] et al studied manganese ore reduction with CO gas or CO-CO_2 gas mixture by the method of thermal balance analysis, and then discussed its reducibility with mineral composition. The findings were:
(1) Reducibility decreased in the order: i.e. MnO_2 ore, burnt ore of $MnCO_3$ (manganese oxide ores such as Mn_2O_3 or Mn_3O_4 etc.) and manganese silicate ore. It was plain enough that every ore was reduced to MnO with CO gas.
(2) There was no real difference in reducibility with CO gas among all MnO_2 phases i.e. cryptomelane, pyrolusite, γ-MnO_2 and birnessite. MnO_2 transformed to reduced state (till Mn_3O_4) through thermal decomposition simultaneously with reduction by CO gas. Therefore,

authors supported the general reasoning that easily thermal-decomposable and incomplete crystalline γ-MnO_2 was most reactive.
(3) At low temperature reduction, the obtained MnO was unstable in air after cooling in CO gas flow. It was also shown that through reduction above 700°C, the obtained MnO was rather stable in the air after cooling.
(4) During manganese ore reduction with CO gas, carbon deposition was observed on certain ores; especially in high iron-content ores and this tendency was remarkable.

Rodney Ishak [43] studied the reduction of Mn_30_4 to MnO in a thermobalance apparatus. The charge was composed of manganese ore (decomposed by heating/calcination or pre-reduction to mainly Mn_30_4) and coke. The material was charged into a crucible, which was suspended to the balance. CO-gas was distributed through a grid in the bottom of the crucible. Ore sizes used were; 2.4-4.8 mm and 6.7-9.5 mm whereas Coke particles were in the size range 4.8-6.7 mm. Experiments were conducted in the 900°C-1100°C temperature range. The composition of the product gas was monitored continuously. External mass transport between bulk gas and particle surface did not seem to limit the rate of reduction. It was assumed that both diffusion through product layer and chemical reaction at the interface between MnO and Mn_30_4 were rate controlling. The grain model gave the best physical description of the process. With this model the effective diffusivity was calculated to be in the 1.5-6.0*10^{-5} m^2 /s range. The pore size was mainly between 0.1 and O.11μm. It was also found[43] that with no alkali additions simulating the effect of alkalis accumulating in the furnace, the Boudouard reaction did not take place at the experimental conditions in question. Thus the reduction of Mn_30_4 to MnO took place by "indirect reduction" with CO (g), and not by the energy and coke consuming "direct reduction" with C(s). In light of these observations[43] it would be advantageous for ferromanganese producers to use raw materials with as low alkali contents as possible so as to reduce the extent of the Boudouard reaction in the process of ferromanganese production, thus reducing both the coke and the electric energy consumption. Obviously based on experimental results, decreasing the particle size of the manganese ore material in the charge would be preferable in trying to achieve total reduction of Mn_30_4 to MnO before the Boudouard reaction starts. However other effects have to be taken into consideration, such as the fact that reducing the size of the manganese ore particles would make the charge less permeable which is a very important issue in shaft furnace ferromanganese processes. However the reaction mechanism deduced in this present study[43] may only be valid for the specific type of ore used in these experiments, the Comilog ore. Other types of manganese ores with a different mineralogy may display different reaction mechanisms from the ones found for Comilog ore. In applying the conclusions of this study[43] to the actual industrial process it should also be kept in mind that the manganese ore material was most likely not thermally decomposed (calcined) to Mn_30_4 in an industrial furnace, but rather pre-reduced. Hence it

would be interesting for future investigations to repeat some of the experimental work done with calcined manganese ore.

Hala H. Abd El-Gawad et al [23] studied reduction of low grade manganese ore fine (Egyptian ore) briquetted with different amounts of molasses under different pressure, in the temperature range of 800°C-950°C with hydrogen gas. In this study[23], the characterization of raw materials was done by X-ray and chemical analyses. The results of briquetting showed that as the pressing pressure load increased both the drop damage resistance and crushing strength increased and the optimum amount of molasses added was 2% and the pressing pressure was 217 MPa. The produced briquettes were reduced under different flow rates of hydrogen at different temperatures, and the reduction kinetics was determined. The results indicated that: 1) The reduction rates by hydrogen increased with increasing temperature of the reduction; 2) Increased hydrogen flow rate at constant temperature of reduction led to increased rate of reduction; 3) The zeroth order chemical reaction controlled the rate up to 5 minutes of reaction, from 5 to 20 min the gaseous diffusion was controlling the rate and from 20 to 60 min the reduction was controlled by nucleation and growth. There were several physicochemical property differences among the components in manganese ores, which could be used for the enrichment of manganese ores. In particular the abundant low-grade manganese ores, which contain iron oxide, may be upgraded by prereduction and magnetic separation.

Theresa Coetsee[11] et al's work showed that manganese ore reduction rates were strongly influenced by the extent of slag phase formation. In their work, the effect of ore composition on slag formation during manganese oxide reduction was predicted using thermochemical calculations. FactSage was used to calculate the equilibrium phase relations in the oxide system MnO–SiO_2–CaO–MgO– Al_2O_3.Observed differences in ore composition, even within the same orebody, were predicted to cause significant differences in slag formation during reduction with large differences in ore reducibility. It was found that: 1) The extent of slag formation determined the reduction rate and MnO recovery level that could be achieved in a furnace at a specific reaction temperature. Slag formation slowed reduction by forming diffusion barriers at the reaction interfaces. 2) FactSage thermochemical software could be used to calculate phase equilibria for manganese ore (including slag formation) to aid interpretation of differences in ore reduction behavior. 3) Ore bulk chemical composition (total manganese and iron content) was likely to be a poor indicator of ore reducibility. Phase equilibria, and specifically slag formation should be considered to predict the relative reduction rates of manganese ores. 4) Additions made to the ore to manipulate chemical composition to limit liquid silicate formation would be expected to be effective in reaction systems such as pellets in which close proximity of reactants promote homogenization. This would not be the case in mixtures of fine ore and reductant in a packed bed; in such a mixture the ore would likely react according to its inherent chemical composition and not respond to additives. 5) An increase in temperature might not always remedy the problem of slow reaction rates. In some

cases, the reduction rate might even decrease upon increasing temperature, due to excessive slagging.

Davood Moradkhani et al[78] studied a three-stage methane gas (CH_4) reduction of manganese ore. Methane gas reduction was carried out at 850°C, 875°C, 900°C, 925°C, and 950 °C for 120 min. The morphology and particle size of the products were determined from scanning electron microscope (SEM) images and X-ray diffraction (XRD) patterns. Reduction results indicated that MnO-rich phase was significantly formed at 950 °C as MnO_2 phase disappeared.

Sorensen and Ostrovski[103] studied the phase compositions of Wessel, Groote Eylandt, CVRD (Brazil ore) and Gabonese manganese ores and their change in the process of calcination in different gas atmospheres. Wessel and Groote Eylandt manganese ores were examined using XRD, optical microscopy, SEM and EPMA analyses; CVRD ore, Gabonese ores were studied using quantitative XRD analysis. The manganese ores had significant differences in chemistry and mineralogy. Equilibrium phases in ores at temperatures of 800°C, 1000°C and 1200°C in different gas atmospheres was predicted by using FactSage software. The calculated phase composition was in agreement with quantitative XRD analysis. In the process of calcination (in the temperature range of 1000°C-1200°C) of manganese ores in air, MnO_2 was reduced to Mn_2O_3 and Mn_3O_4, while during calcination in reducing atmosphere manganese oxides were reduced to MnO and iron oxides to metallic iron. Formation of a liquid slag in ores at equilibrium was predicted for Wessel, Groote Eylandt and Gabonese ores at 1200 °C in air and 1000°C–1200 °C in a reducing atmosphere. No liquid slag was predicted for equilibrium phases in CVRD ore.

2.4 SUMMARY

Although solid state reduction showed the particle morphology resulting from carbothermic reduction, and gaseous studies propose reduction behavior of manganese in presence of a methane gas, the studies provide little data on characteristic morphologies.

This study will present the characteristic morphologies, provide kinetic data on the reduction of manganese in a methane gas mixture.

CHAPTER 3

EXPERIMENTAL

The experimental technique and analyses used to investigate the effect of methane gas mixture on reduction of a manganese ore particle in the temperature range 1050 ^{o}C to 1250 ^{o}C have been described in detail in this chapter.

3.1 Experimental Aims

The aim of the experimental work is to describe the behavior of a naturally occurring manganese ore particle in hydrocarbon gas-reducing atmosphere with temperature ranging from 1050 ^{o}C to 1250^{o}C. In order to define characteristic changes taking place particles in the reducing bed must behave more or less in an identical manner. The results of the experiments must reflect only the characteristics of the reducing particle in the given reducing conditions and not be dependent on the geometry of the particle bed nor on the features of the apparatus as a whole. Hence investigations on the kinetics of reduction were carried out on crushed and screened powder ore. It is the aim of the present work to characterize the reduction behavior and identify the structures formed in a single particle of manganese under known methane containing gas composition. For this, the preparation of sample was done in such a way that each manganese particle in the reducing bed was in as narrow a size range as possible. Gas flow rates had to be measured and maintained constant to allow close control of the reducing atmosphere in the reduction furnace operating isothermally in the temperature range of 1050 ^{o}C to 1250 ^{o}C. It is necessary that the reducing gas prevailing at the reaction interface have a composition as close as possible to the composition of the bulk gas stream and that the gas composition is kept uniform in composition throughout the particle bed. The manganese ore chosen for the experimental program was the naturally occurring manganese ore used in the industry. Methane gas is principal constituent of natural gas; and the methane gas used in the experiments was supplied by Afrox. With these objectives in mind, the apparatus and experimental procedure are described below.

3.2 Experimental set up

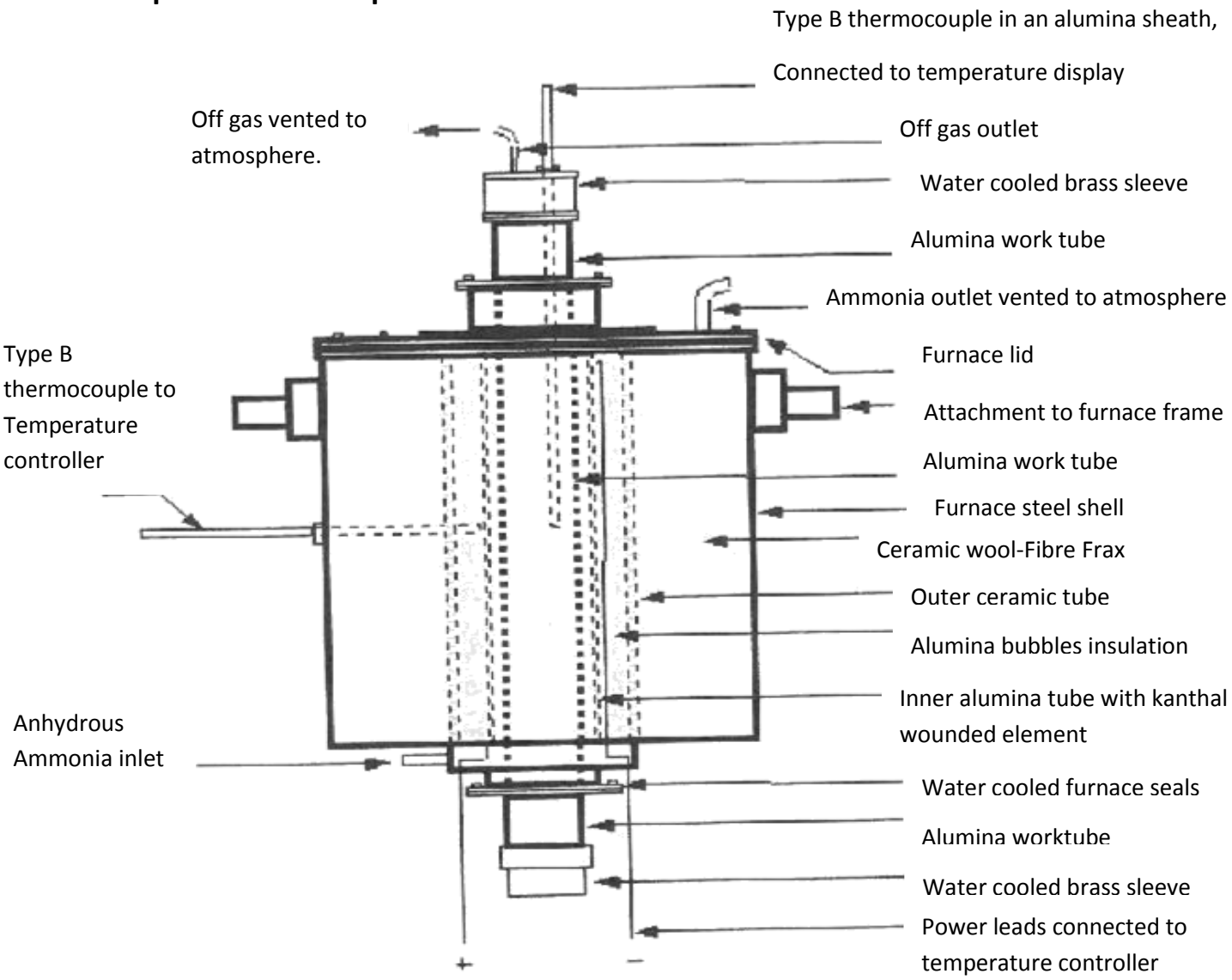

Figure 3.1 The furnace proper.

A vertical tube (TGA) furnace was used to perform reduction reactions. The furnace was designed with heating element made up of kanthal wire 0.8 mm in diameter and measured resistance of 12.76 ohms wound around alumina tube. For protection of the tube alumina cement was applied on it. The tube was surrounded by 1-2mm diameter bubble alumina (between the outer tube and heating element). The gap between the outer tube and steel was filled with refractory wool. The work tube used was a nonporous recrystallized alumina tube with dimensions 900mm in length, 54 mm inner diameter and 60mm outer diameter. The furnace easily reached and maintained temperature 1050 ^{o}C to above 1250 ^{o}C which is required for isothermal reduction tests in the hot zone of the work tube. Temperature was controlled [104]

by a B type thermocouple inserted perpendicular to the work tube around the hot zone of the furnace and which was connected to the Eurotherm thyristor fired electronic temperature control system. A separate B type thermocouple suspended from the top of the work tube reaching the hot zone of the furnace next to the sample crucible measured the actual reduction/metallization temperature.

For this vertical tube furnace, a thermogravimetric analysis (TGA) set up was also available for continuous measurement of mass change as a function of time with the charge material maintained at constant temperature under a selected atmosphere. Initial pure hydrogen gas experiments were done by monitoring continuous change of mass with time in order to understand the effect of hydrogen reducing gas on reduction of the ore continuously and directly. A balance was contained in a sealed perplex box and placed beneath the work tube onto an up and down moving platform. A rubber bellows was used to connect the Perplex box to the bottom of the furnace work-tube. A pedestal with sample crucible rested on the balance. The pedestal was an alumina rod with an inverted crucible cemented to the top tip. During the runs the sample in a crucible sitting on the pedestal could be easily raised to, and lowered from, the hot zone of the furnace. The rubber bellows was tightened on the bottom end of the work tube and the system was sealed during the runs. After sealing, a known mixture of gases was passed through the balance box, the rubber bellows, up the work tube and out of the top of the work tube. The balance chosen for this set up was an Oahu's 410, it was connected by cable from its port to a PC. A program was written to convert mass loss data recorded by the PC from the balance into reduction percentage. The balance was tared at the start of reduction and logged the mass measurements and converted them to reduction percentages as a function of time and saved. As mentioned above this TGA setup illustrated in Figure 3.2 was used only for pure hydrogen runs. However this TGA method of measuring the progress of reduction with time was not appropriate for methane runs where the mass loss resulting from reduction was accompanied by mass gain due to carbon deposition from cracking of methane at temperatures above 550^{o}C into solid carbon and hydrogen gas and it was not possible to distinguish and separate the opposing phenomena.

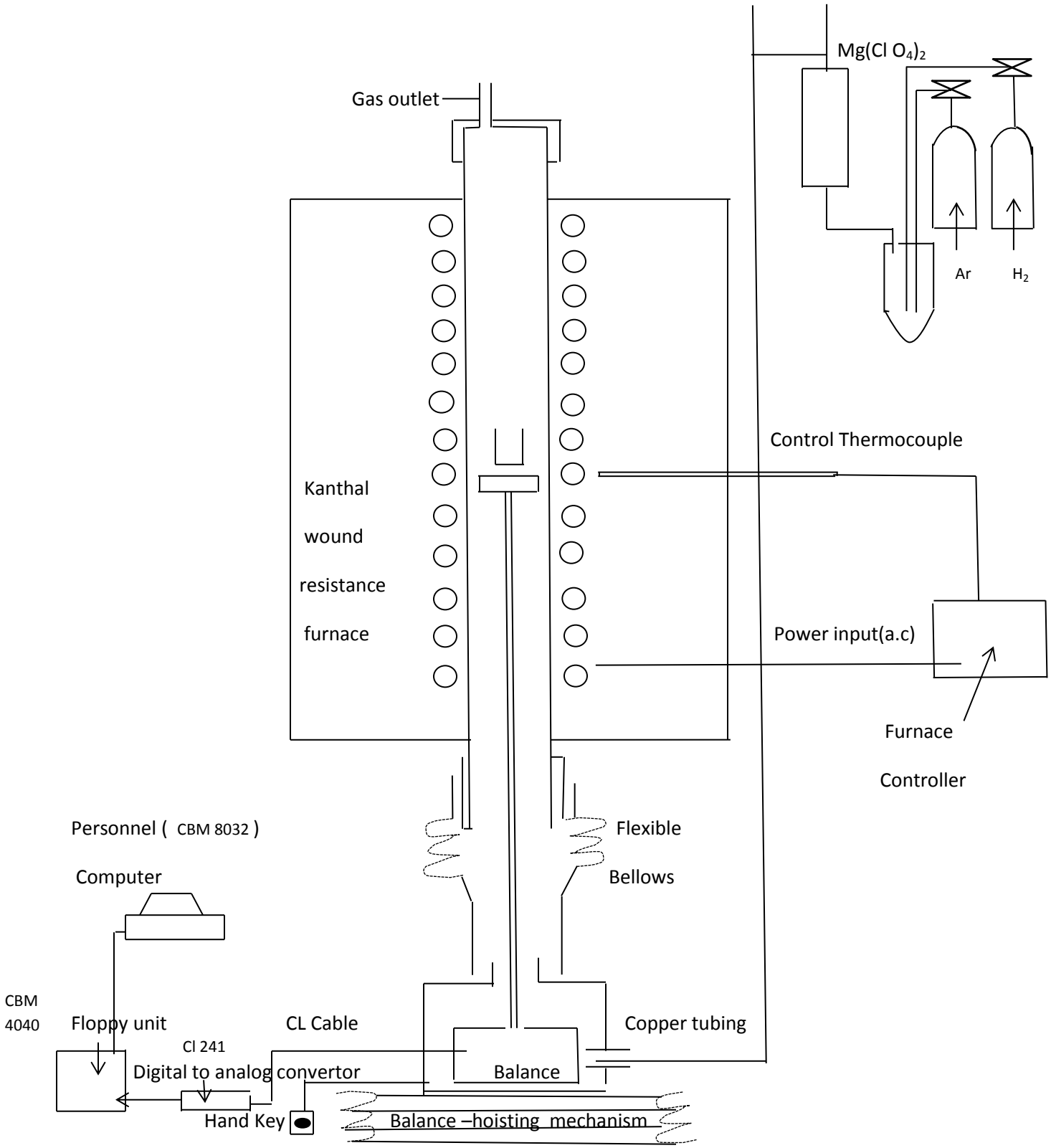

Figure 3.2 Schematic illustration of the TGA set up.

Although TGA was abandoned in favor of analytically determining the metallization of products in the partially reduced material, the set-up itself remained unchanged and was used without the mass loss recording and conversion function. From the point of view of the crucible position and gas movement; the sample crucible sat in a uniform temperature zone (reduction zone) and the reducing gas of known composition, which flowed up the furnace tube. The upward flow of the gas somewhat helped to reduce unnecessary settling of carbon on the particle bed by sweeping the very fine carbon particles away with the bulk gas flow direction. This sweeping away action of the carbon from the particle bed prevented the immediate and complete clogging of the porous bed of particles with carbon deposition and does not affect the activity of solid carbon on reduction at reaction site.

The progress of reduction as a function of time was instead measured by stopping the experiment at predetermined time intervals and analyzing the partially reduced material by wet chemistry methods for metallic Fe and metallic Mn. This was done by lowering the pedestal from the reduction zone as fast as possible, while preventing the thermal shock, and cooling the sample in a stream of argon gas. The stream of argon gas simultaneously purges the furnace of gases which may explosively react with the atmosphere when the furnace was opened to retrieve the sample.

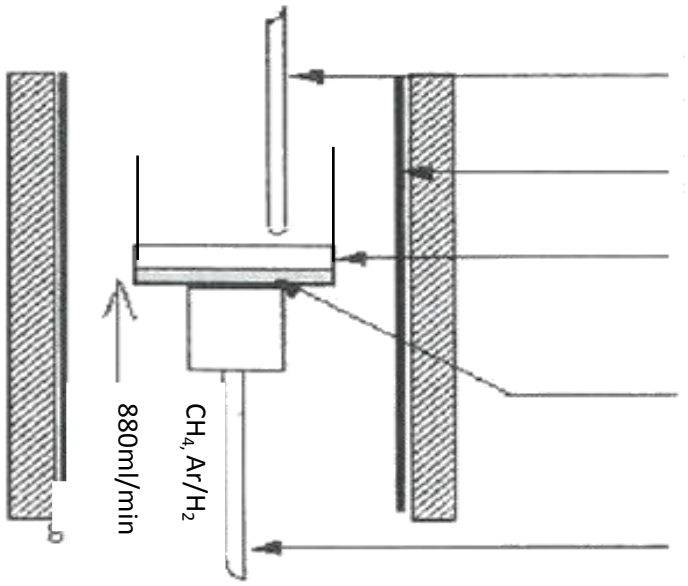

Figure 3.3 Sample crucible in the reduction zone of the furnace.

Recrystallized alumina crucibles of 34mm height, 19mm internal diameter and 24 mm outer diameter were used. The crucible with sample sits on pedestal which itself rest on the balance and at start of runs it was pushed to hot zone for pure hydrogen runs. For methane mixture runs the crucible rests on pedestal which itself rest on a step made inside the perplex box avoiding mass change measurements. The shape of crucible and hence the particle bed surface area exposed to the reducing gases were the important design parameters. It was important that the particle bed depth is minimized so that each particle is exposed to the same bulk composition of the reducing gas. That is the gas composition at the reduction interface is the same as that in the bulk gas stream.

3.3 Manganese ore

The manganese feed chosen was industrially significant Mamatwan manganese ore of size -150µm +106µm. The aim was to understand and quantify behavior of a representative Mamatwan particle. The size -150µm +106µm was chosen for following reasons:

-The particles of this size range were small enough for rapid reactions kinetics to be measured in a reasonable time period.

-They were large enough to maintain a porous particle bed for even gas penetration and large enough for clear metallographic preparation and examination.

-Close particle size range was chosen so that each particle behaved as ideally as possible.

The sample mass used in each reduction test had to be kept to a minimum to fulfill the objectives of the experimental programme. That is based on the crucible size and on the minimum requirement for product analysis, each particle must be exposed to the same initial reducing gas composition, and there must be minimum resistance to product gas removal and hence producing metallization data that more closely quantifies the metallization of each individual particle in the bed. For pure hydrogen runs 2 gram sample was used wherelse for methane mixture runs 4-5 gram samples were employed so that wet chemical, XRD and SEM analyses could be performed. The composition of Mamatwan manganese ore is given in the Table 3.1.

Table 3.1 Mineralogical composition of manganese ore.

Mamatwan	Mn_2O_3	FeO	SiO_2	CaO	MgO	Al_2O_3	P
%	77.84	4.75	3.24	11.61	2.37	0.176	0.014

Table 3.2 Mineralogical analysis of mamatwan ore detected from X-ray diffraction patterns

Mineral	Composition
Braunite	$Mn^{2+}(Mn,Fe)^{3+}_6\ SiO_{12}$
Calcite	$CaCO_3$
Kutnahorite	$Ca_{0.97}Mn_{0.5}Mg_{0.5}Fe_{0.03}(CO_3)_2$
Hausmannite	Mn_3O_4
Manganite	Y -MnOOH
Hematite	Fe_2O_3

All the mineral phases are listed in the Table (3.2) from the most abundant one (topmost in the table) to the least abundant (mineral at the bottom of the table).

3.4 Gases

Argon (99.9%), Methane (99.7%), ultra-high purity hydrogen gas 99.9%) was used. Argon and hydrogen also acted as carrier gases for methane. The relative concentration of methane in argon and hydrogen was changed for different tests. The gas flow rate was 880ml/min at ambient pressure. The flow rate was adjusted for correct volumetric flow rate using calibrated rotameter placed after gas cleaning systems. Argon gas was cleaned through a column filled with magnesium perchlorate to remove water vapor whereas methane gas was treated in columns of magnesium perchlorate and ascarite to remove water vapor and carbon dioxide.Hydrogen gas was also treated in the column of magnesium perchlorate to remove water vapor.The gases after cleaning were passed through a calibarated rotameter to a junction design with knobs to mix the required combination of gasses to achieve the required ratio to be passed to the furnace (The concentration of methane in both argon/methane and hydrogen/methane gas mixtures was changed from 10% to 20% and then to 30% (all volume percentages) at a total flow rate of 880ml/min.). This chosen flow rate was determined by the need to maximize the flow rate and hence maximizing the product gas removal and gas penetration into the sample bed as well as avoiding the blowing away of fine particle sized carbon from the reaction bed.

3.5 Experimental Method

The reduction behavior of manganese particles exposed to methane containing gas was assessed on the percent metallization results for the reducible components Mn and Fe. The experimental procedure was as follows. Reduction tests were run for 10, 20, 30, 60, 90 and 120 minutes. The experimental variables were time, concentration of methane in argon and concentration of methane in hydrogen gases and temperature.

The ore was first calcined at 1000^{o}C for 12 hours and the calcined ore was kept in desiccators. The mineralogical analysis of the calcined ore was also determined by XRD and is given in the Table (3.3). All the mineral phases are listed in the table from the most abundant one (topmost in the Table 3.3) to the least abundant (mineral at the bottom of the table).

Table 3.3 Mineralogical analysis of calcined ore

Mineral	Composition
Braunite	$Mn^{2+}(Mn,Fe)^{3+}{}_6SiO_{12}$
Hausmannite	Mn_3O_4
Manganosite	MnO
Jacopsite	$MnFe_2O_4$
Lime	CaO

Initially for pure hydrogen test, the crucible containing 2.0 grams of ore placed on the pedestal was pushed in the work tube sealed with the flexible bellow which was attached to the box with the balance. The reduction test was conducted for 120 minutes to monitor loss of weight due to reduction by pure hydrogen. For methane containing gas runs 4-5 gram of ore samples were loaded into the crucibles which were then placed on the pedestal sitting on the step in the perspex box. The whole system was sealed using the flexible rubber bellows. Argon was introduced into the work tube and sample was pushed slowly inside the work tube reaching the hot zone in 30 minutes and then was allowed to stay in the hot zone for another 30 minutes while argon gas continued flowing. Thereafter, a predetermined mixture of methane-argon or methane hydrogen gas mixture was introduced into the system while stopping the primary argon gas flow. The reducing gas mixture was introduced in the right proportion at a total flow rate of 880ml/min which was regulated using a flowmeter at room temperature of 25^{o}C and atmospheric pressure over a period of 10, 20, 30, 60 ,90 and 120 minutes individually and the reduction time was recorded. After the predetermined time interval the sample was quickly

brought down to the cooler part of the work tube, the flow of methane containing reducing gas mixture was stopped and system was flushed with argon gas for another 15 minutes before bellows was removed and the sample retrieved(see Figure 3.4).

After, each methane containing gas test sample was split into three portions; one was taken for wet chemical analysis for metallization values. The other two were prepared for scanning electron microscopy (SEM) and XRD. Further details of the sample series performed under the experimental variables are mentioned below.

The effect of the hydrogen as the reductant was investigated by running tests at 1100 ^{o}C and 1200 ^{o}C using 100 % (v/v) H_2 at 880 ml /min on the 2 gram manganese ore sample. The loss of mass was measured using the TGA system. It was observed that reduction occurred in H_2 with maximum loss of mass within the first 30-40 minutes. Due to explosive nature of the hydrogen gas, in all the experiments high level of precautions were taken to insure no build of gas takes place in the sealed system (balance, work tube and outlet tube).

The effect of relative concentration of methane in argon/methane and in hydrogen/methane gas mixtures on the metallization/reduction behaviour of the manganese ore particle was measured in two separate test series. The concentration of methane in both argon/methane and hydrogen/methane gas mixtures was changed from 10% to 20% and then to 30% (all volume percentages) at a total flow rate of 880ml/min. The experiments were conducted at temperatures of 1050^{o}C, 1100^{o}C, 1200^{o}C and 1250^{o}C. The reasons and effectiveness of using two type of mixture of gases is discussed in the following chapter.

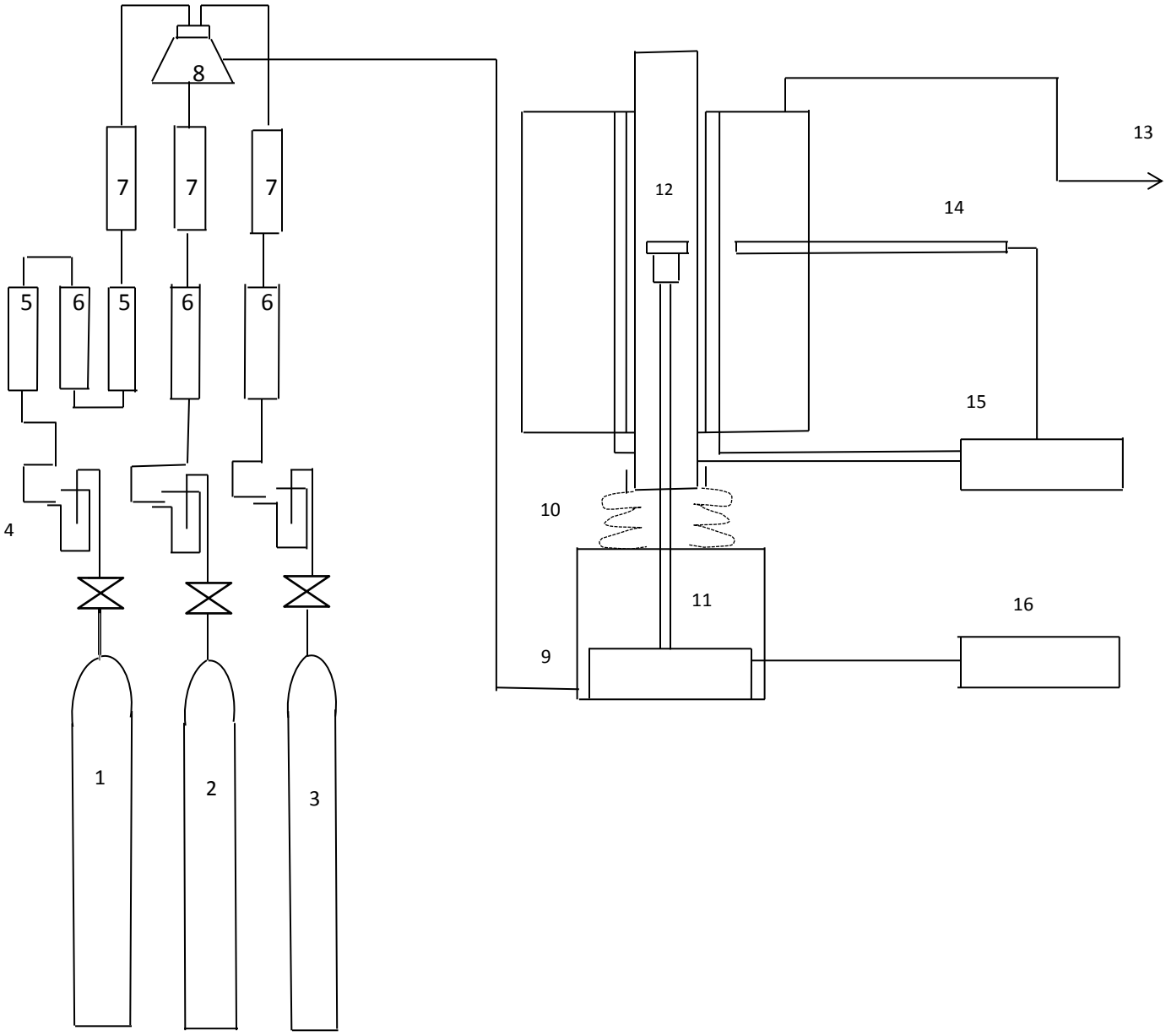

Figure 3.4. Layout of furnace and ancillaries.

1. Methane 5. Ascarite 9 Gas mixture in pre set 13 off -gases

2. Argon 6. Magnesium Perchlorate 10 Flexible bellows 14 Thermocouple

3. Hydrogen 7. Flowmeter 11 Alumina pedestal 15 Temperature controller

4. Gas Bubbler. 8. Gas mixture 12 Crucible with manganese ore. 16 Data logger

3.6 Product analyses

3.6.1 Metallization measurements

The extent of reduction/metallization of manganese and iron from the ore was determined by wet chemical analysis technique. All chemical analysis were performed at Scrooby's laboratories (SANAS accreditation (ISO 17025)) of South Africa. The reacted samples were analyzed for total Mn and total Fe as well as for metallic Mn and metallic Fe. The degree of carburization does not affect the metallization calculated through the equations described below. Inductively coupled plasma spectroscopy (ICP) was used to analyze all samples. Manganese ion was determined volumetrically by using 5ml Bromine and 95ml methanol solution, a magnet stirrer and 25ml Teflon follower with 250ml Erlenmeyer flask with fitted cooling condenser were used as apparatus. It was expected that all metals and carbide present in reduced material reacted with sulphuric acid and some hydrochloric acid and nitric acid in reflux and reported to the filtrate. This is an empirical method so there are no references for comparing results, the only comparison that can be made is with duplicate made of the same sample. Ferrous ion (Fe^{2+}) was determined by adding 1g sodium carbonate, 20ml hydrochloric acid and two to three drops hydrofluoric to 1g of sample and titrating with N/10 potassium dichromate.Details of the work procedure for manganese ion and ferrous ion are given in Appendix (E). Percent Metallization is defined as:

$Met_{Mn\,(\%)} = (Mn^0 / Mn_{Total}) * 100$

$Met_{Fe\,(\%)} = (Fe^0 / Fe_{Total}) * 100$

$Met_{Total\,(\%)} = (Mn^0 + Fe^0) / (Mn_{Total} + Fe_{Total}) * 100$

Where Mn_{Total} and Fe_{Total} represent total Mn and Fe in the product expressed as a percent of the total product mass, Mn^0 and Fe^0 represent metalized Mn and Fe in the product expressed as percent of the total product mass, and Met_{Mn} , Met_{Fe} , Met_{Total} represents manganese, iron and total percent metallization respectively.

3.6.2 Product phase analysis

The product phases on the reduced particle were determined using X-ray diffraction; XRD and Scanning Electron Microscopy; SEM. XRD analysis was used to qualitatively determine phases present. Bruker d-2 phaser was used for X-ray diffraction analysis. The d-2 phaser is desktop diffractometer for all X-ray diffraction applications. It is equipped with an integrated flat screen monitor, an integrated Pc window 8.1. Sample was placed in the cavity of sample holder and it was then pushed into the d-2 phaser. It was observed, due to nature of pattern of the reduced manganese ore that one hour of run on d2 phaser was necessary on each sample. After

collection of pattern, peak identification was performed using the latest version of the “Diffract Suite” software.

3.6.3 Product morphology Analysis

For scanning electron microscopy analysis samples were prepared by mounting them with poly fast and using polisher of sizes 1200 µm and 200 µm. The polished sample produced by this technique was mounted on the base, 2 samples at a time and was placed in SEM for analysis. The sample was analyzed at magnification level of around 1000 times with 20 KV. These samples were also analyzed quantitatively for elemental composition under SEM using energy dispersive technique (EDX). The EDX analysis was made on a specific point in representative particle. From the results the phases present at different points in the particle may be reconstituted and their effect on the reaction kinetics discussed. The SEM results from hydrogen, methane/argon and methane/hydrogen runs are further discussed in the next chapter on results and discussion.

3.6.4 Experimental precaution:

1. Due to the nature of gases used a lot of precaution (monitoring of continuous flow of gases out of the system) were taken especially during pure hydrogen runs which can be explosive otherwise.

CHAPTER 4

RESULTS AND DISCUSSION

The previous chapter detailed the experimental method , apparatus and conditions used in the investigation of manganese reduction using methane as the hydrocarbon gas, at the reducing temperatures of 1050^{o}C to 1250^{o}C. This chapter describes the results and discusses the findings and interpretations of the experimental analyses. These findings are explained in order to be able to elucidate the reduction behavior as completely as possible with the experimental techniques used. The discussions made herein are summarized in the following in order to assemble the reduction mechanisms, where the behavior of Mamatwan ore in the methane containing gas mixture is presented.

The metallization values for each of the different conditions are presented first, this is followed by findings of the X-ray diffraction and finally the results of S.E.M particle morphology investigation. In the back scattered images, the white areas represent metallic phases and the grey areas represent partially and also unreduced oxide phases. A series of hypotheses are discussed from the evidence of the combined experimental results.

4.1 The Kinetics Results

The reduction results are presented, primarily, in the form of metallization versus time plots at different temperatures and gas mixtures employed. For each and all of the reduction test series described in the previous chapter the results are collected in Appendix (A & B) both in tabular and graphical form.

4.1.1 Gaseous reduction using methane in Argon (% CH_4 in Ar)

When reducing gas mixture, containing CH_4 was introduced into the reaction zone of the furnace, there was the instant presence and a considerable amount of the fine carbon mist throughout the reaction zone. This was visually noted by standing above the furnace alumina tube, looking through a peephole and observing the cloud of carbon that formed with the introduction of CH_4 into the reaction zone of the furnace. This is consistent with the thermodynamics of the system and the finding of similar investigations[87] where CH_4 was introduced into the furnace at high temperature.

From this visual observation, it can be inferred that CH_4 cracking may have occurred on the alumina tube wall, which is a suitable nucleation site for carbon formation. Carbon deposition was seen to occur at all times throughout the reduction period where deposition was present

on the furnace tube walls, the crucible and pedestal, and throughout the sample[87]. The carbon tended to clump in large black spongy deposits on the sample pedestal and on the sample surface.

The manganese ore sample was introduced into the reduction zone that already had a significant cloud of carbon present.

It was mentioned in previous chapter 3 that it was difficult to discriminate between the changes in weight of the reducing manganese due to either oxygen removal or the carbon deposited when both occurred simultaneously. For this reason, the progress of the reduction was mapped as the percent metallization which was determined by wet chemistry. Sample were withdrawn to the cold end of the furnace and hence quenching it under a flow of cold argon gas, virtually stopping the reaction at predetermined time intervals.

Mapping the progress of the reduction in short time intervals such as a few minutes was not appropriate here since this would lead to inaccurate results that did not reflect the reducing conditions. This is because the introduction of the sample crucible resulted in a drop in the reduction zone temperature and it was practically very difficult due to the continuous cracking of methane. The time it took the sample to reach isothermal conditions and hence represent the appropriate reduction temperature reported was approximately 20 minutes. This said however, it appeared from metallization curves that bulk of the metallization occurred within the first thirty minutes and the metallization reached some kind of a reduction maximum.

Figures 4.1 to 4.11 at the end of this section summaries the metallization results. Generally, an increase in the concentration of CH_4 in the input gas, at a constant temperature, increases the percent total metallization. An increase in temperature also causes an increase in the reduction extent. A closer look at the reduction curves showed some distinct patterns, and several exceptions of these are discussed below purely from the visual observation of the kinetic metallization versus time curves.

The 30 % CH_4 in Ar at 1050^{o}C appeared to have much lower metallization levels relative to the 30% CH_4 in Ar and CH_4 in H_2 for the other reduction temperatures. A distinct gap between the metallization values at 1050^{o}C and those at the higher temperatures appeared after 30 minutes. This temperature effect was much larger than that expected for simple thermal activation in term of higher metallization values achieved for small change in temperatures(from 1050 ^{o}C to 1250 ^{o}C, see Figures 4.6 ,4.10). This observation was quite distinct in the Fe metallization curve as a function of time, where the Fe metallization extent is not considerable with reduction time after the first 30 minutes. The cause for metallization reaching some kind of a reducing ceiling for both Fe and Mn is not clear from the kinetic data. This is especially interesting from a Fe reduction point of view, which kinetically should not be

ceasing altogether. The iron component should be able to reduce completely within the time given; this observation is discussed further with the study of the particle morphologies later.

Total metallization value achieved after a two hour reduction test ranged from 28.2% for what was considered the lowest reducing potential of 10% CH_4 in Ar at 1050 ^oC, to 73% for 10% CH_4 in Ar at 1200^oC. The associated Mn/Fe metallization ratio was 0.24 and 0.85 all much higher than those achieved as 0.20 with ordinary carbothermic solid state [57] reduction.

4.1.2 Gaseous reduction using methane in hydrogen (% CH_4 in H_2).

As with the Ar carrier gas, as soon as CH_4 was introduced into the reduction zone there was also an instant presence of the fine carbon mist occurring throughout the reaction zone of the furnace. Carbon deposition was observed throughout the sample, the crucible and pedestal. An important difference between this form of carbon deposited and described in previous section was that it visibly appeared to be significantly more lustrous, appearing almost metallic in nature[87]. Thermodynamically, in a H_2 carrier gas, CH_4 cracking is stifled to a certain extent, showing slightly less carbon deposition at equilibrium.

In H_2, the effect of CH_4 concentration and temperature did not have a simple direct relationship with rate and extent of metallization. Metallization extent is considerably low after first 20 or 30 minutes for all the CH_4 concentrations in H_2 reaching a very distinctive reduction ceiling for both Fe and Mn components.

The metallization curves as a function of time for 10% CH_4 in H_2 indicated higher metallization values than for 30% CH_4 in H_2 under certain conditions and is explained later with reference to the particle morphologies.

Distinct gap existed between all the metallization curves for the low temperature experiments (1050^oC, 1100^oC) and those for the high temperature (1200^oC, 1250^oC) experiments as noted from curves of metallization as a function of time. This gap appeared more distinct at the higher CH_4 concentrations.

The Fe metallization curves at 1050^oC and 1100^oC indicated that reduction more or less reached a maximum after the first thirty minutes.

At higher reduction temperatures of 1200^oC and 1250^oC, the Fe seems to reach complete metallization and the Mn metallization curves appeared to reach a maximum level of around 70%.The reasons for this observed asymptotic behavior for both Fe and Mn at 1050^oC and 1100^oC could not be explained from the kinetic data alone and needed further discussion with reference to the particle morphology.

From the metallization versus temperature plots in Figures 4.1 to 4.3, a few distinct observations could be made. Firstly, for 30% CH_4 in H_2 approximately the same metallization level was achieved across the temperatures range from 1050°C to 1250°C with increase in time from 30 minutes to two hours. Secondly, for first hour of reduction at 1100°C and 1200°C, the 10% concentration of CH_4 in H_2 showed significantly higher metallization than 30% CH_4 in H_2. The product morphologies studied that are presented later were able to explain this difference.

The total metallization values achieved after two hours of reduction ranged from 45% for what was the lower concentration of CH_4 of 10% CH_4 in H_2 at lower temperature 1050°C, to 54% for the higher temperature 1200°C for 10% CH_4 in H_2.

4.1.3 Comparing the characteristics of the kinetic data between two carrier gases; H_2 and Ar

The most distinct difference in the kinetic data between the two carrier gases, H_2 and Ar, are discussed herein. The initial rate of reduction was higher for 10% CH_4 in H_2 than the test using 10% CH_4 in Ar. This observation emphasized the role that H_2 played in the system, as it is kinetically the more rapid reductant and is able to instantly take part in the reduction reaction[87].

For the 30 % CH_4 concentration in the two carrier gas – the two curves for the highest reduction temperature, 1250°C, yielded high metallization levels with 30% CH_4 in Ar having higher metallization value. This is followed in magnitude by the two metallization curves at 1200°C, which also had difference between metallization levels for the two carrier gases, again 30% CH_4 in Ar had higher metallization value. The lowest metallization rate and progress of metallization occurred at 1100°C with hydrogen being the carrier gas. The reason for this is not clear from the kinetic data and is again discussed in section 4.3.5 with reference to the particle morphology.

The differences observed for 10% to 30% CH_4 in H_2 emphasized the specific importance and significant role of CH_4 in the system. A general observation showed that more carbon was present in the samples reduced by CH_4 in H_2 carrier gas where the samples exposed to 30% CH_4 in H_2 contained the highest total carbon.

The Mn and Fe metallization curves as a function of time were not far from linear behaviour. This feature appeared to be indicating a gas mass transfer limitation to the particle surface. Generally, according to Fick's law of diffusion, the rate of metallization is directly proportional to the concentration difference of the reducing gas[87]. Where the concentration difference between the bulk gas and the gas at particle surface is a constant, the rate of metallization is a constant, so that the extent of metallization with time appears as a straight-line relationship, which is similar to the present case.

It is also seen that the results of 10% CH_4 in Ar have the steepest curve, indicating that Mn component gradually increased its metallization level over time relative to Fe. This occurred at a relatively lower rate than for the other reducing gas mixtures, which were again in line with the proposal that gas mass transfer control[87] was potentially rate controlling throughout the reduction time for 10% CH_4 in Ar. For the other gas mixtures, the profiles were flat indicating simultaneous reduction of the Fe and Mn after the original burst of metallization that occurred within the first 30 minutes.

The hydrogen carrier gases had higher Mn/Fe metallization ratios due to the more rapid reduction rate that occurred in the first 30 minutes.

Up to 30 minutes, the gas mixture with H_2 as the carrier gas appeared from the graphs to show higher reducing potential, allowing significant reduction of the thermodynamically and kinetically more difficult to reduce Mn. In the first 30 minutes, 10%CH_4 in H_2 showed the highest apparent reducing potential at low temperatures.

Although an optimization study of the reduction was not part of the scope of this study, it was possible from the above kinetic results to observe some trends and propose conditions for an optimum pre-reduction condition prior to a smelting process.

If the objective of a pre-reduction process is to achieve the highest possible reduction in the shortest time interval, say within 30 minutes, the reduction temperature should be at least 1200^{o}C with H_2 as the carrier gas. At 1200^{o}C and 1250^{o}C, the CH_4 concentration did not appear to significantly influence the Fe metallization rate and only slightly influenced the Mn reduction rate over the first 30 minutes.

If the objective is to operate with the lowest possible reduction temperature, then after 30 minutes, the lower CH_4 concentration in H_2 or the higher concentration in Ar is the more effective reductant. H_2 carrier gas appeared to contribute to the reduction of the Mn component at a higher rate in the first 30 minutes. If longer reduction times are permitted, 30% CH_4 in Ar may be the most effective gas mixture, followed by 10% CH_4 in H_2. If residence time of reduction is two hours, 30 % CH_4 in Ar appeared to be the most effective gas mixture. Where the residence time fluctuates with temperatures, it would appear that 30% CH_4 in Ar is consistently the most aggressive reductant towards Manganese.

If residence time fluctuates, and a choice may be made for the optimum temperature of reduction, the most effective reducing condition would be a high CH_4 concentration with Ar as the carrier gas, at temperatures at or above 1200^{o}C.

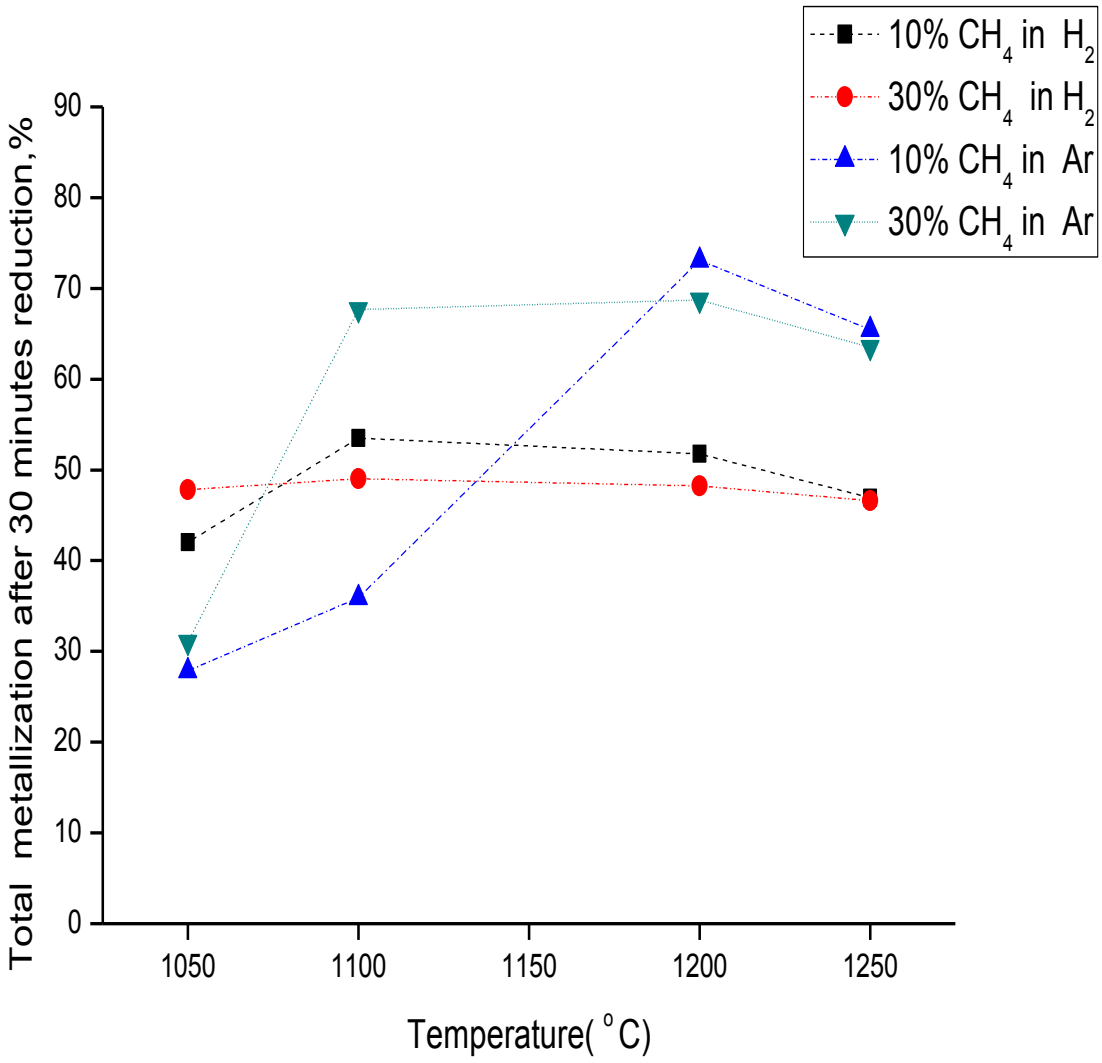

Figure 4.1 Total percent metallization as a function of temperature for 30 minutes reduction time.

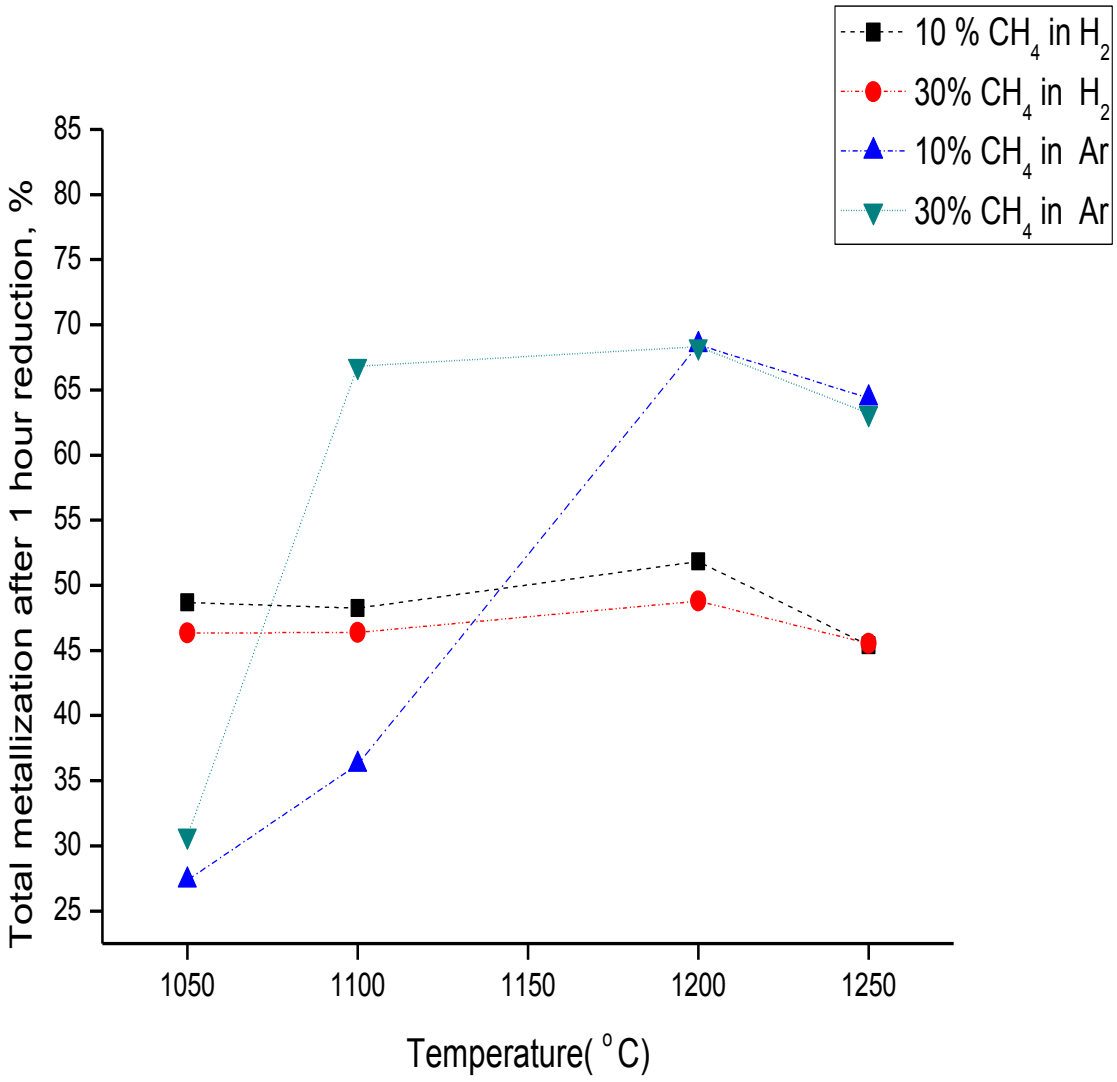

Figure 4.2 Total percent metallization as a function of temperature for 1 hour reduction time.

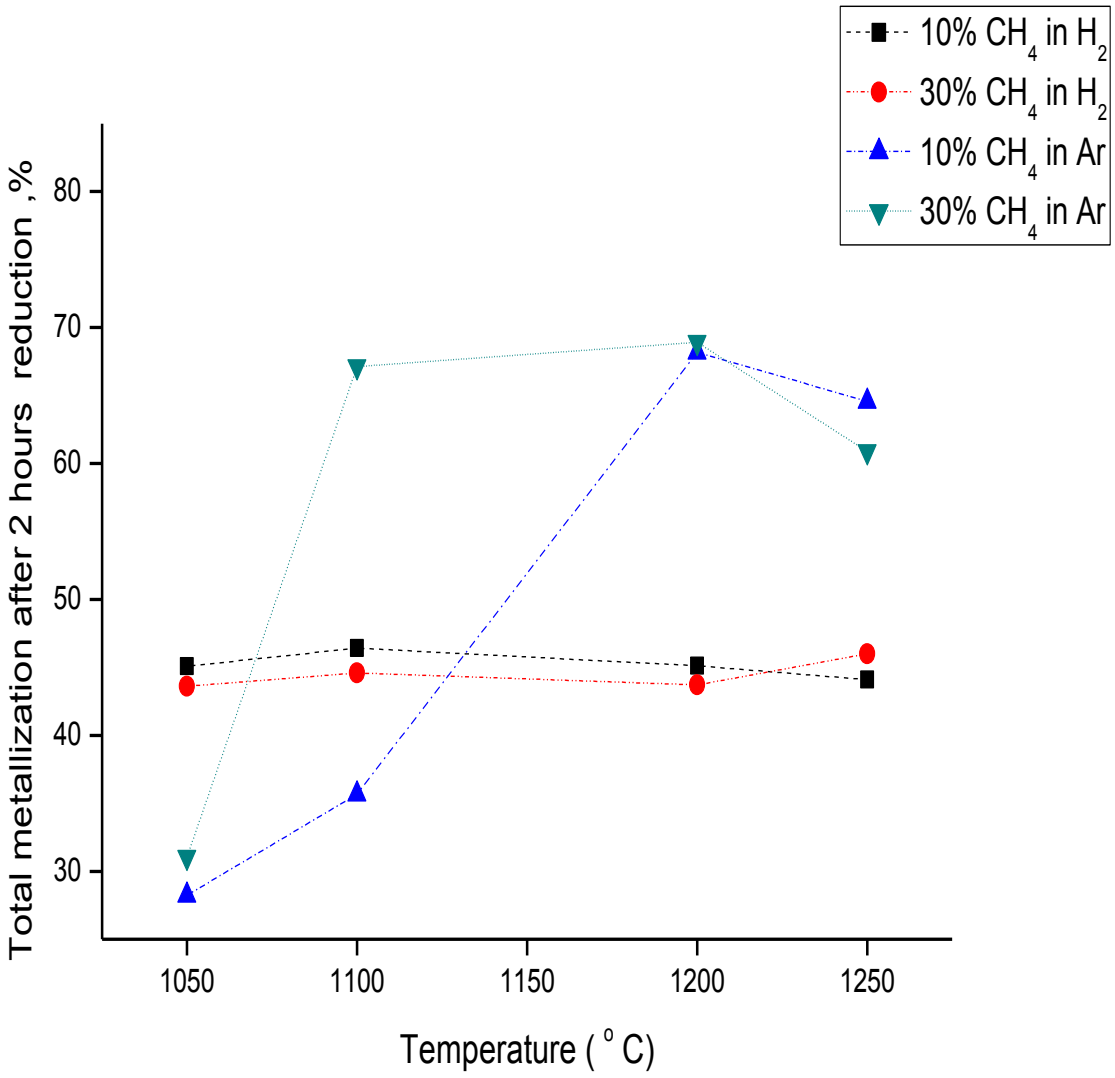

Figure 4.3 Total percent metallization as a function of temperature for 2 hours reduction time.

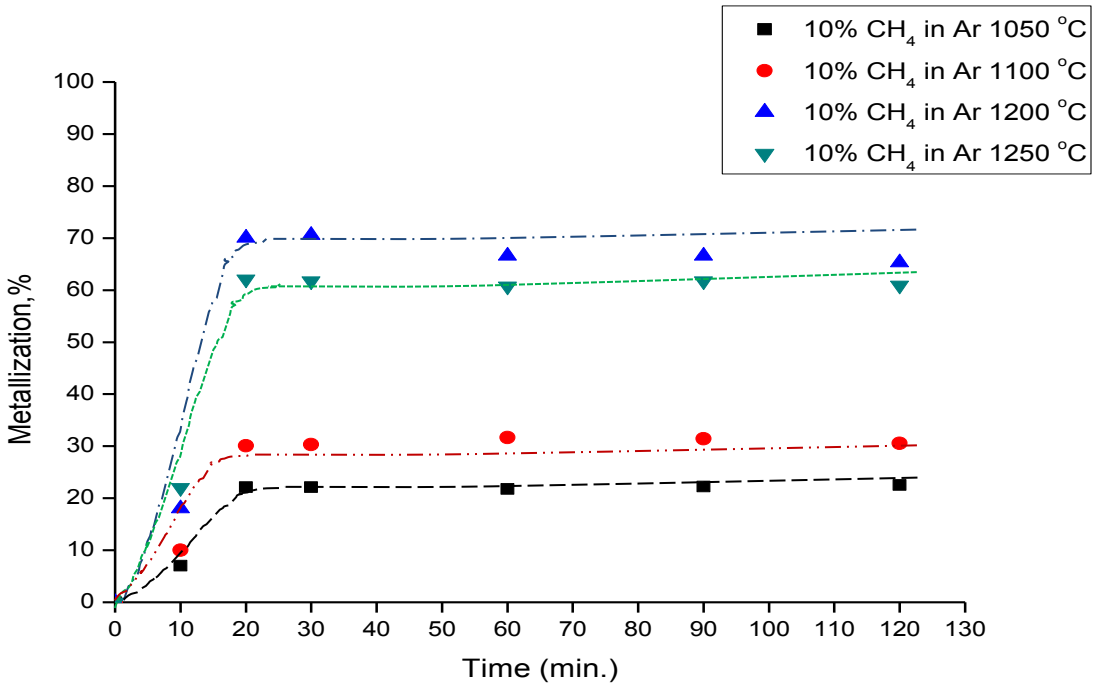

Figure 4.4 % Mn metallization in 10% CH_4 in Ar as a function of time at different temperatures.

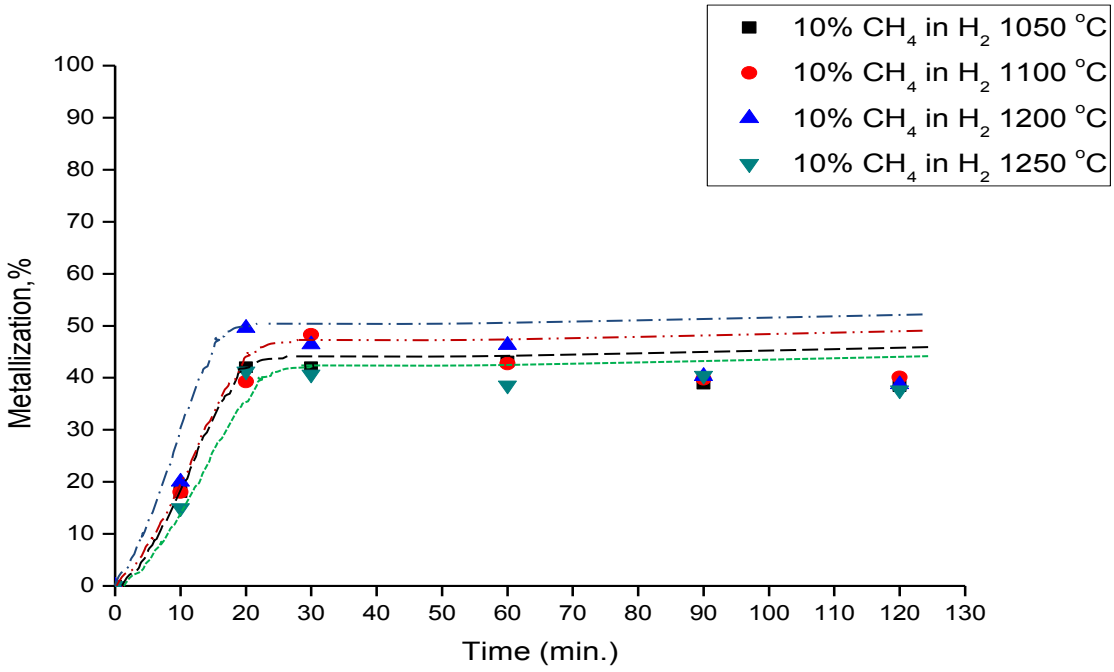

Figure 4.5 % Mn metallization in 10% CH_4 in H_2 as a function of time at different temperatures.

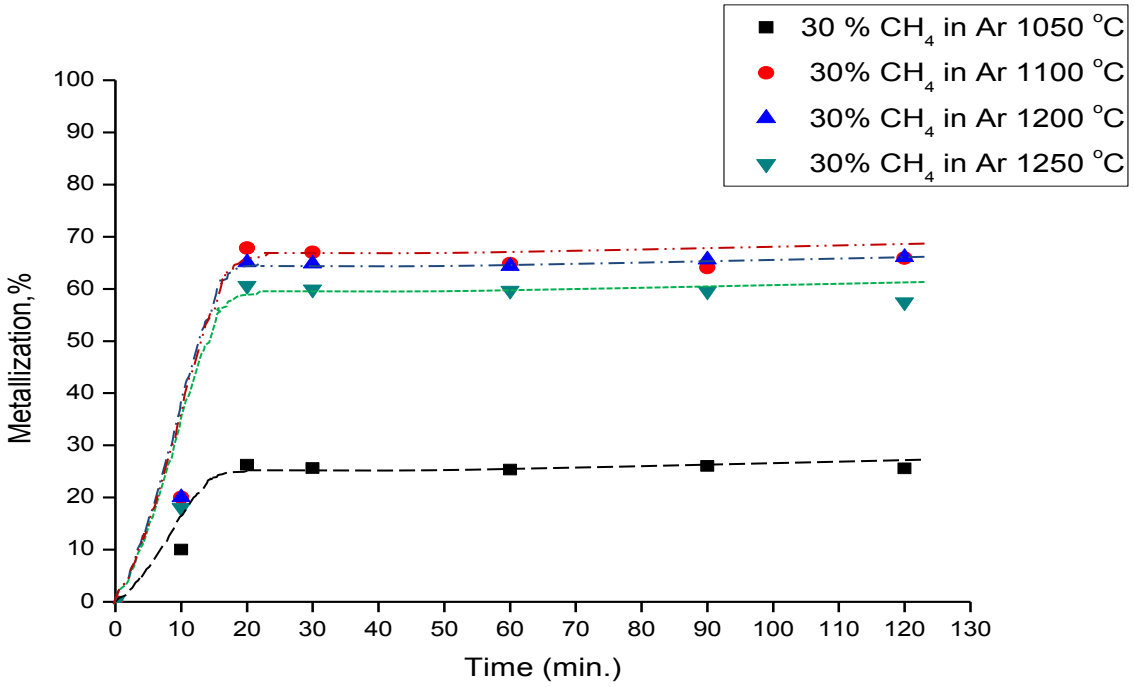

Figure 4.6 % Mn metallization in 30 % CH_4 in Ar as a function of time at different temperatures.

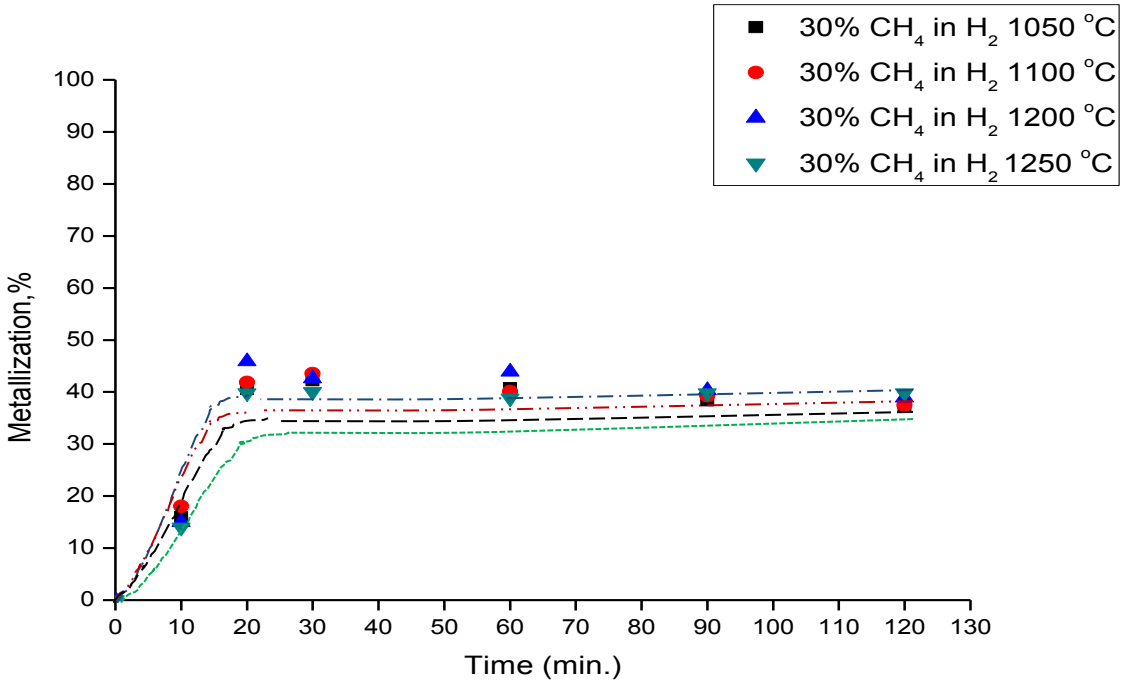

Figure 4.7 % Mn metallization in 30 % CH_4 in H_2 as a function of time at different temperatures.

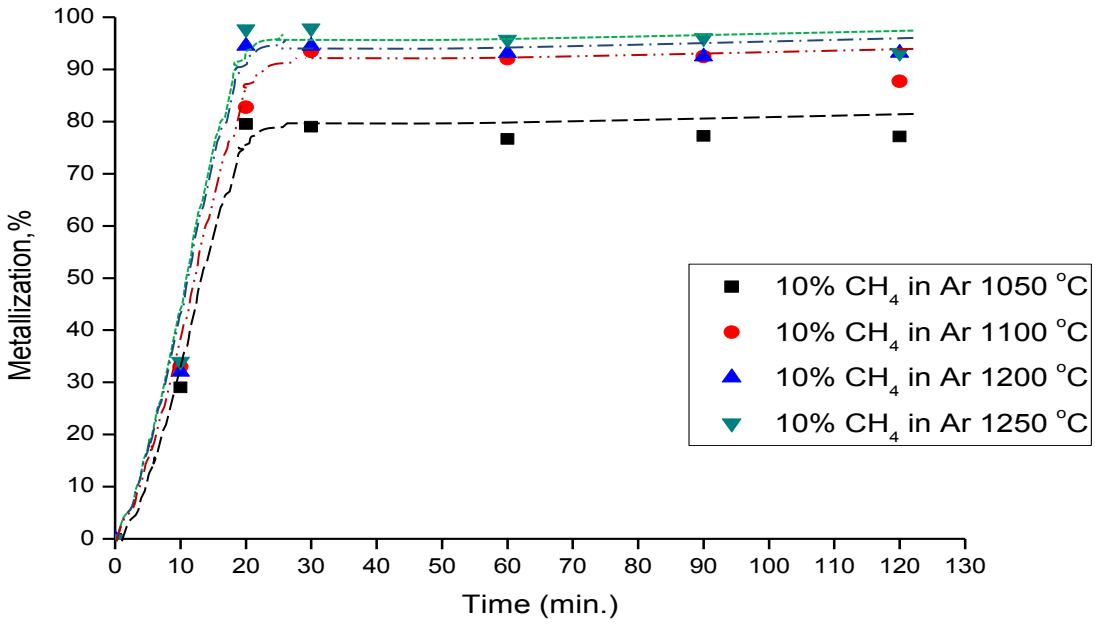

Figure 4.8 % Fe metallization in 10% CH_4 in Ar as a function of time at different temperatures.

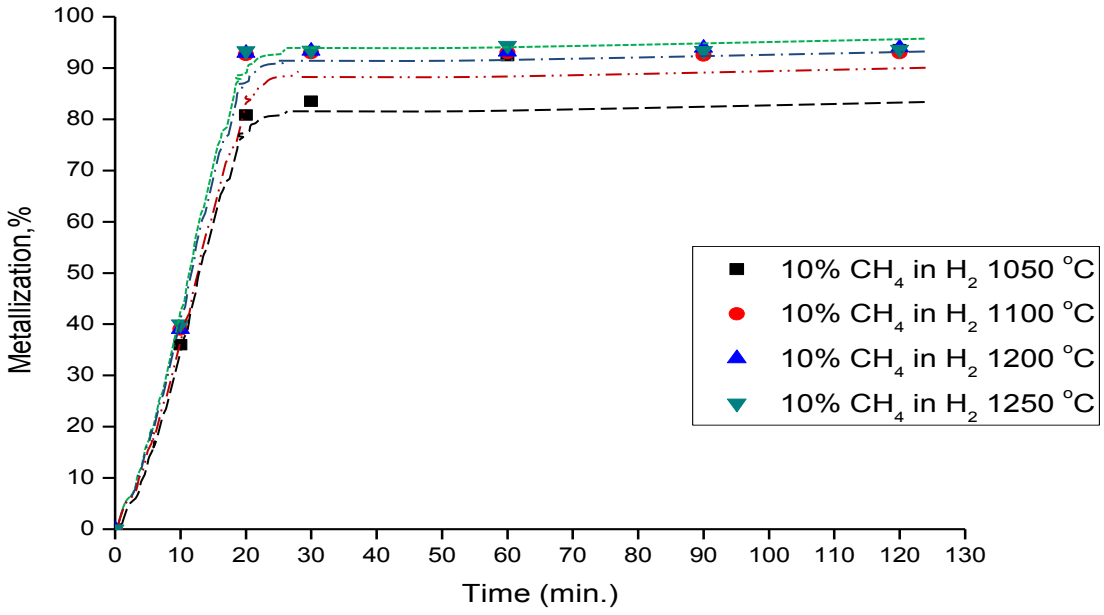

Figure 4.9 % Fe metallization in 10% CH_4 in H_2 as a function of time at different temperatures.

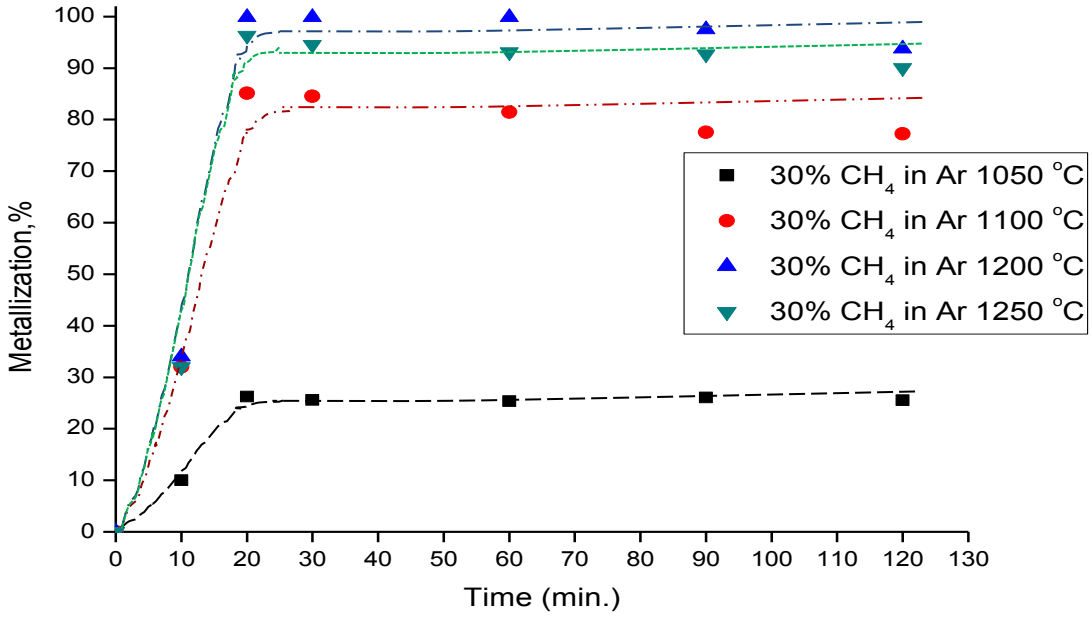

Figure 4.10 % Fe metallization in 30% CH_4 in Ar as a function of time at different temperatures.

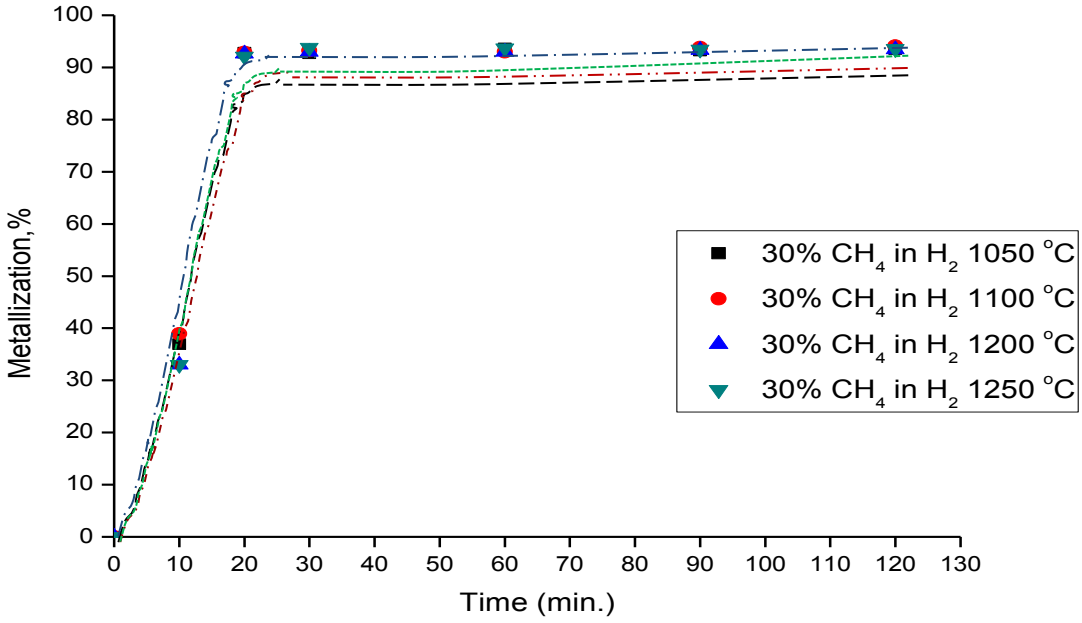

Figure 4.11 % Fe metallization in 30% CH_4 in H_2 as a function of time at different temperatures.

4.2 The product phases

4.2.1 Methane-argon runs

The phases formed in the partially reduced manganese ore under different reducing conditions were determined by X-ray powder diffraction. Tables B1, B2 and B3 in Appendix B present a summary of X-ray powder diffraction results showing the phases present with progress of reduction time and reducing conditions for all the tests performed during this investigation. Any phases present with concentrations less than 5% could not be detected. The XRD findings are summarized below:

- After calcination the dominant oxide feed material analyzed was in the form of $CaMn_20_4$ with some $MnFe_2O_4$.

- The following phases appeared under most conditions: Mn_7C_3, Fe_7C_3 and $CaMn_20_4$.

- Specifically, with the progress of metallization, the concentration of the original oxide phase decreased with reduction time and new oxide phases; Ca_2FeMnO_5 and $Mn_2Fe\ (CO)_{14}$ emerged.
- Under least aggressive reduction conditions (10% CH_4 in Ar at 1050 ^oC) where less carbon was deposited, metallic iron was also detected. Mostly the metallic phase occurred consisting primarily of Fe with dissolved C and Mn.
- The Fe_7C_3 appeared as the dominant iron carbide phase early in the reduction test but with progress of metallization, this phase disappeared and was replaced by increasing amounts of Fe_3C.
- Generally, the higher the concentration of methane in the reducing gas, the sooner the Fe_3C appeared potentially due to the higher amount of carbon availability from the decomposition of more CH_4.
- Manganese ore was reduced primarily to carbide Mn_7C_3 at lower temperature range of the experiments, but at 1200^oC the dominant reaction product was Mn_5C_2.
The extent of reduction required for each phase to appear was dependent on the reaction time and hence on the percent metallization the sample had undergone, and on the reducing gas composition, temperature and hence the amount of carbon deposited.

4.2.2 Methane-hydrogen runs

Results for methane hydrogen runs revealed that manganese ore was reduced primarily to carbide Mn_7C_3 at lowest temperature of 1050^oC of the experiments, but at higher temperatures of 1100^oC, 1200^oC and 1250^oC the dominant reaction product was Mn_5C_2. Most of the results are similar to those mentioned above for methane-argon runs.

- After calcination the dominant oxide feed material analyzed was in the form of $CaMn_20_4$ with some $MnFe_2O_4$. .
- The following phases appeared under initial (1050^oC) conditions: Mn_7C_3, $Mn_{15}C_4$, Fe_7C_3 and $CaMn_20_4$.

- The following phases appeared under later (1100 ^{o}C and above) conditions: Mn_5C_2, Fe_3C and oxides Ca_2FeMnO_5 and $Mn_2Fe(CO)_{14}$.
- Specifically, with the progress of metallization the concentration of the original oxide phase decreased with reduction time and new oxide phases appeared: Ca_2FeMnO_5 and $Mn_2Fe(CO)_{14}$.
- Under all reducing conditions as carbon was deposited, iron was detected consisting primarily of Fe but with dissolved C and Mn.
- The Fe_7C_3 appeared as the dominant iron carbide phase early in the reduction test but with progress of metallization, this phase disappeared and was replaced by increasing amounts of Fe_3C.
- Generally, the higher the concentration of methane in the reducing gas, the sooner the Fe_3C appeared potentially due to the higher amount of carbon availability from the decomposition of more CH_4.
- Manganese ore was reduced primarily to carbide Mn_7C_3, $Mn_{15}C_4$ at lower temperature range of the experiments, but at 1100^{o}C and above the dominant reaction product was Mn_5C_2.

The extent of reduction required for each phase to appear was obviously dependent on the reaction time and hence on the percent metallization the sample had undergone and on the reducing gas composition, temperature and hence the amount of carbon deposited.

The above findings are also consistent with the findings of work on the carbothermic reduction of manganese [52]. The phase detected with the progress of reduction using methane gas may be summarized in three very general steps as shown in the illustration below.

$$CaMn_2O_4$$

$$\downarrow$$

$$Ca_2Fe\ MnO_5,\ MnFe\ (CO)_{14},\ Fe_7C_3,\ Mn_7C_3,\ Mn_{15}C_4$$

$$\downarrow$$

$$Ca_2FeMnO_5,\ MnFe\ (CO)_{14},\ Fe_3C,\ Mn_5C_2$$

These three steps are grouped as: the starting material; moving to the intermediate phases detected that occur at the initial stages of the reduction; and the final phases that are present at the end of the two-hour reduction period. The extent of reduction required for each phase to appear was dependent on the reduction time and hence on the percent metallization the sample had undergone and on the reducing gas composition, temperature and hence the amount of carbon deposited. With the identity of the product phases confirmed, the overall reactions can be derived. However, for a comprehensive understanding of the rate changes observed in the kinetic curves and hence the mechanisms of reduction, the particle morphology was studied.

4.3 The Particle Morphologies

This section describes the typical particle morphologies that were observed and possible rate controlling step(s) as a result of the different reducing conditions. The implications of these observations on the mechanism and kinetics are discussed.

The photomicrographs of the back scatter images under the SEM as well as results of the electron dispersion of x rays analyses of the cross-sections of particles under the different reducing conditions are presented in summary tables in each section below, but for clarity of the different features, the text in these section also refer to the photomicrographs collected in Appendix C.

4.3.1 General characteristics of the particle morphologies

This section has been placed first in order to assist the reader with identification of the typical features. Obviously, it is rather difficult to draw generalizations because -as will be noted below- temperatures, extent of metallization and the reducing potential of the gas appear to produce different product morphologies but the basic features proposed are recognizable. When analyzing the particle morphologies certain general appearances point to different possible rate determining steps in the reduction of the particle. The particle morphologies proved to be most informative in elucidating the rate controlling steps in the reduction of manganese particle. These recognizable features were deduced mainly from comparison of this work with the solid-state reduction work by previous worker [9] as well as with the established mathematical kinetic models. The initial rapid metal nucleation was common in all the CH_4 gas concentrations (in both carrier gases) and across all the temperatures of reduction, where obviously the only difference was the length of time over which this initial structure persisted. From this common initial partially reduced particle structure, the particle was further altered to uniquely different morphologies by the different gaseous reducing conditions described in the following.

4.3.2 Morphological features of the particles in 10% CH_4 in Ar runs

In the Ar carrier gas, using 10% CH_4, at each of the temperature of the reduction experiments the product morphologies that developed are discussed herein. From the illustrations below it is seen that with the increase of time of reduction for the same temperature, while the percentage of reduction increases, the reduction takes place at the surface. There are no indications of formation of pores, cracks or fissures. Comparison of micrograph in the figures in Table 4.1 (magnification 1000X) together with metallization data reveal the following at 1100^{o}C. Product morphologies of particle reacted under 10% CH_4 in Ar showed that the extent of metallization was around 20-30% for periods below 60 minutes but increased to above 50% for 90 minutes and 120 minutes and at higher temperature of 1200^{o}C the extent of metallization was higher for the same gas mixture. At the highest temperature of 1250^{o}C the extent of metallization was

highest for a given time and there are indications of metallic nuclei that formed at surface converting into globular shapes.

Table 4.1 Summary morphologies for 10% CH_4 in Ar(Magnification 1000X).

Time	**10% CH_4 in Ar**		
	T=1100 °C	**T= 1200 °C**	**T =1250 °C**
30 min	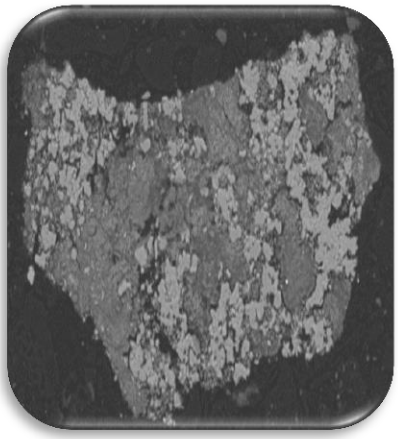		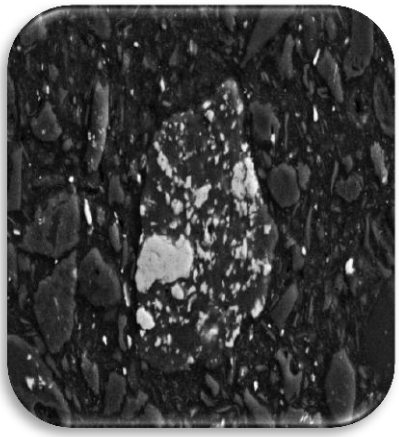
1 hr	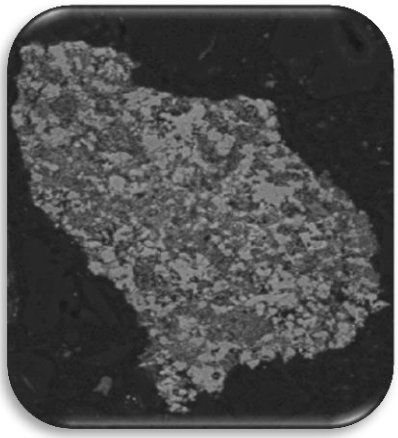		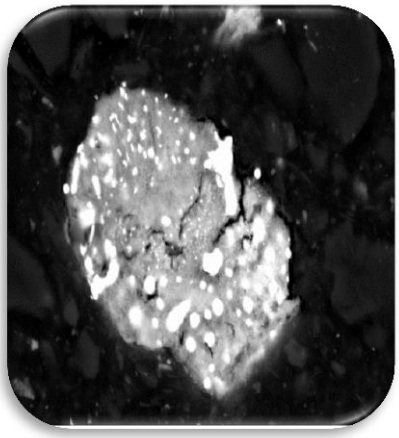
2 hr	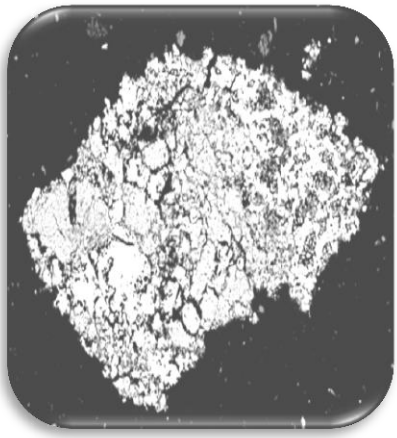	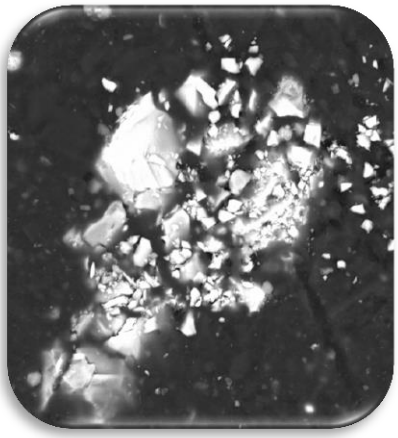	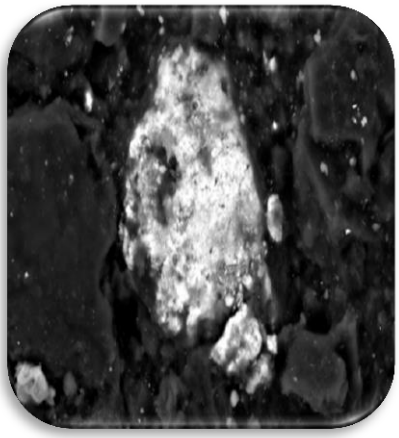

Metallic phase was observed with samples having higher than 20-30 percent reduction levels. As reduction time increases carburization of metallic phases occur (which was quatitatively determined), thereafter initial carbide might have played a role in reduction of manganous oxide. The oxide was found to be in the form of rounded grains that consisted of manganous oxide with magnesium oxide as main impurity (Mg was observed in EDAX analysis). With increases in retention times, growth of small white metallic nuclei on the edge of grey MnO grains occurred. At higher temperature of 1250^{o}C after 1 hour partial melting of these white nuclei seems to be taking place.

Initially oxide phases observed by EDAX consisted mainly of manganous oxide and calcium manganese oxide and as reduction proceeded with time and with increase of temperature calcium, iron, manganese and magnesium containing oxide phases were detected along with iron manganese carbide phase.

4.3.3 Morphological features of the particles in 30% CH_4 in Ar runs

From the figures of Table 4.2 (magnification 1000X) shown below it can be seen that the percentage of reduction increases with increase in time for the same temperatures. Also for the same time it increases with increase in temperature.

Interpretations of micrograph in the below figures are performed together with metallization data. It can be seen that at 1100^{o}C under 30% CH_4 in Ar the extent of metallization was around 50-60% for periods below 60 minutes but increased to above 70% for 90 minutes and at 120 minutes and also at 1200^{o}C the extent of metallization was higher than 75%. At 1250^{o}C it is seen that the metallic globules colluded and formed larger metallic phases and the extent of metallization was well over 81%. Hence, at temperature of 1250^{o}C the extent of metallization was highest.

At 1050^{o}C, the photomicrographs illustrated metallization occurring on the surfaces. At 1100^{o}C, there was a finer metallic product on the surface within the first 30 minutes. This appeared common to low temperature reduction behavior. There is still the initial dense product layer formation enveloping the particle surface. At 1100^{o}C, it was seen that there was diffusion of the Mn and Fe to the surface resulting in the fine metal phase on the surface.

As the reduction time increases carburization of metallic phase occurs and thereafter the carbide might have played a role in reduction of manganous oxide and oxide was found to be in the form of rounded grains that consisted of manganous oxide with magnesium oxide as the main impurity (Mg was observed in EDAX analysis). With increase in retention time, growth of small white nuclei on the edge of grey MnO grains occurred. At 1250^{o}C partial melting of these white nuclei seems to be taking place. Again, initial oxide phases observed by EDAX consisted

mainly of manganous oxide and calcium manganese oxide and as reduction proceeded with time (and also with increase of temperature) calcium, iron manganese and magnesium containing oxide phases were detected along with iron manganese carbide phase.

Table 4.2 Summary morphologies for 30% CH_4 in Ar(Magnification 1000X).

Time	**30% CH_4 in Ar**		
	T=1100 °C	**T= 1200 °C**	**T =1250 °C**
30 min	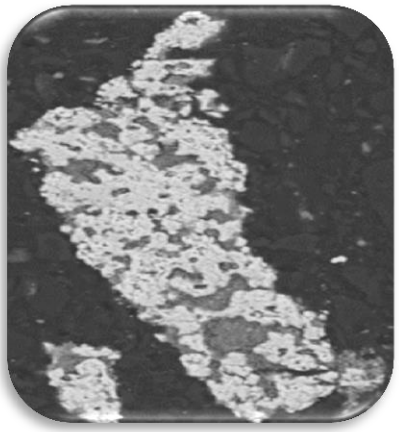	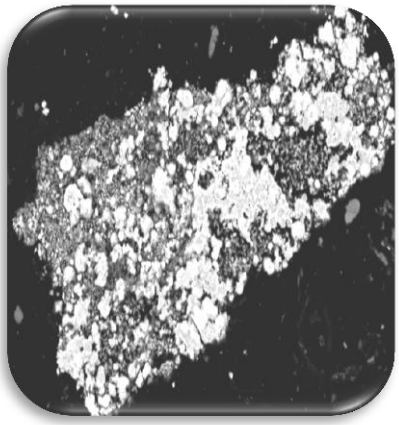	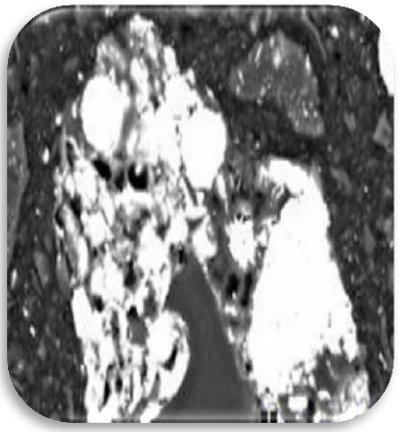
1 hr	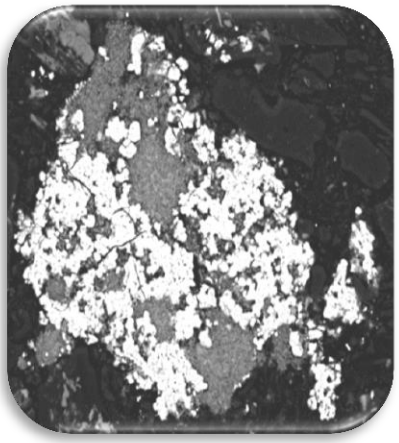	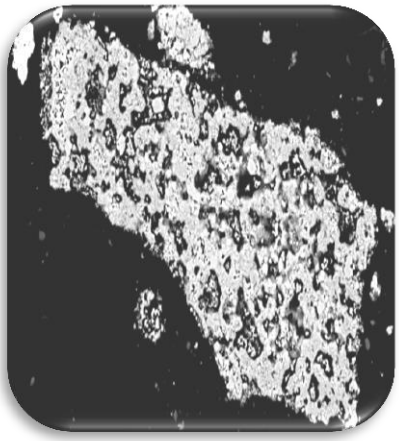	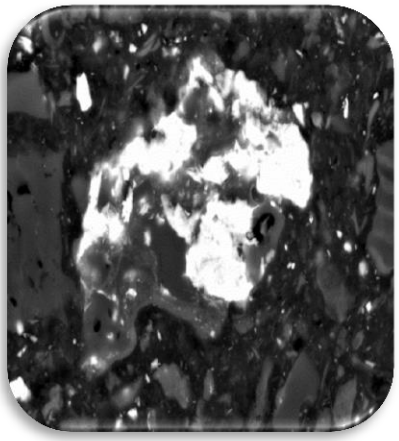
2 hr	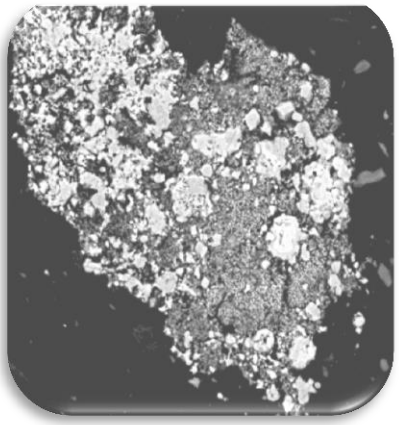	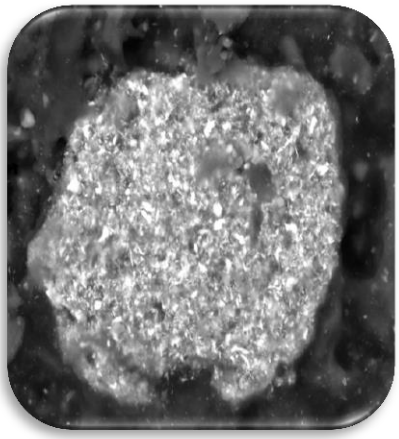	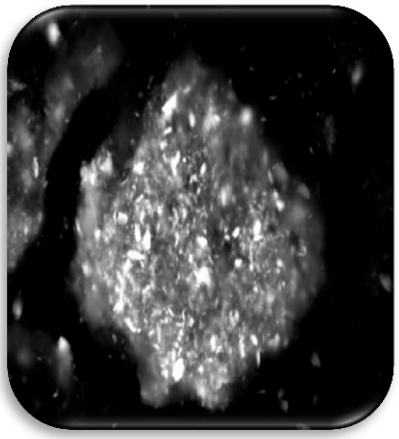

4.3.4 Morphological features of the particles in 10% CH_4 in H_2 runs

From the figures of Table 4.3 (magnification 4.5KX) below it can be seen that with increase in time for the same temperature the percentage of reduction increases and for fixed time the percentage of reduction is higher at higher temperature. Metallic nuclei was seen on the surface, there were no indications of cracks or fissures. At 1100^{o}C under 10% CH_4 in H_2, 20-30% metallization occurred for period below 60 minutes and metallic deposition was in form of small globules in a concentrated area where reduction took place on the particle surface. It was also observed that for 90 and 120 minutes, the extent of metallization was higher around 50-60% level and the metallic nuclei in globular form coalesced to form larger metallic phase. At 1100^{o}C, the morphologies indicated no change in the structure with time for periods longer than 30 minutes. At 1250^{o}C the extent of metallization was higher around 50-60% for periods less than 60 minutes and was above 80% for 90 and 120 minutes. Formation of metallic nuclei took place at localized areas, it was not uniformly spread. In the H_2 carrier gas, at this low concentration of 10% CH_4, the following features were characteristics of the particle exposed to this reducing gas.

When the reduction was conducted under 10% CH_4 in argon atmosphere, product morphology showed scattered metallic phase formation in contrast to this case of 10% CH_4 in H_2. This may indicate that different types of gas diffusion processes were taking place in these two cases one favoring scattered metal formation the other localized metal formation. The metallic product is a potential catalytic site for CH_4 cracking and metal nucleation and it may be possible that the presence of much larger amounts of hydrogen in the gas mixture when H_2 is the carrier gas facilitates the fast reduction of iron component of the ore enabling the metallic nuclei to form and grow faster resulting in localized formations which further enhance the process through its potential catalytic effects[87]. Precipitated fine carbon is also a suitable nucleation site for further precipitation from CH_4 cracking. Thus, up to 30 minutes time metallic globules were smaller, but at higher times of 1 hour and more metallic globules coalesced and grew in size and became even more localized and at higher temperatures, partial melting also took place.

On the other hand, unlike 10% CH_4 in Ar, in H_2 the kinetic curves showed that the reduction rate decreases after 30 minutes. The gap between the kinetic curves for the different temperatures as a function of time may indicate a change in the rate-controlling step. At low temperatures, the reduction stifling effect of carbon (precipitating from the gas) by covering the exposed surface of the ore particle may have a dominating effect in passivating the reduction process after the first 30 minutes. At higher temperatures, this effect might be happening after higher levels of reduction/metallization.

Table 4.3 Summary morphologies for 10% CH_4 in H_2(Magnification 4.5KX).

Time	10% CH_4 in H_2		
	T=1100 °C	T= 1200 °C	T =1250 °C
30 min	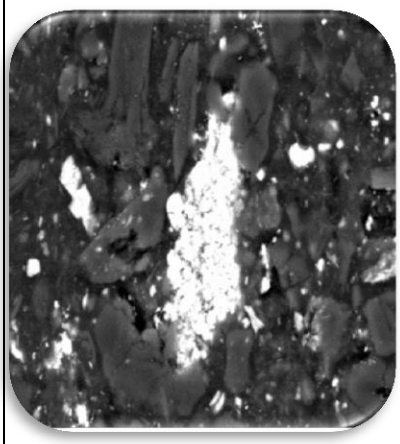	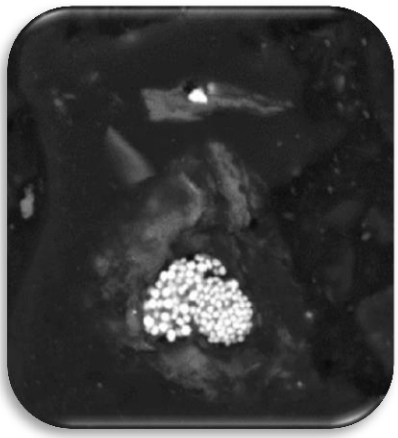	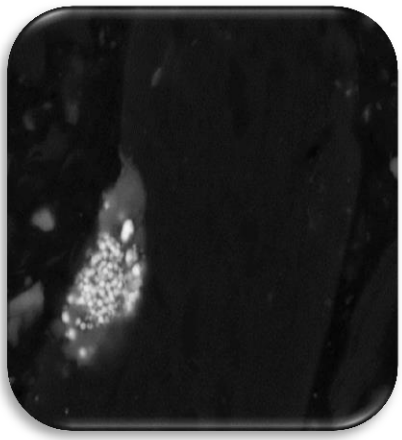
1 hr	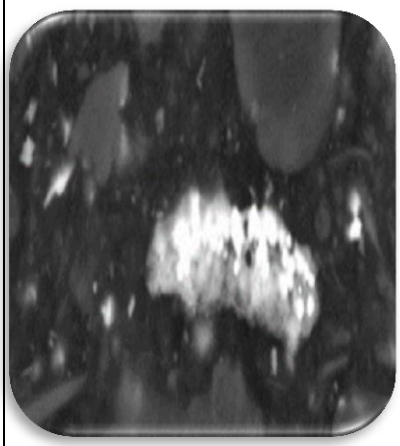	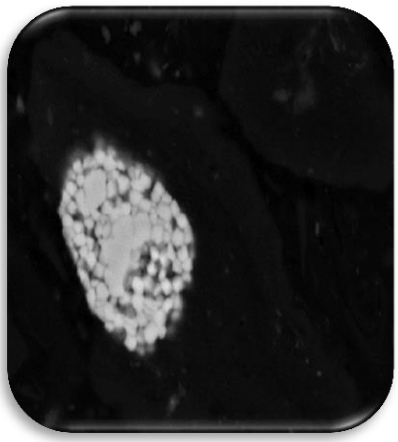	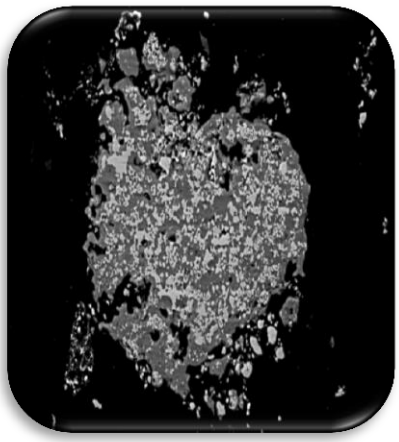
2 hr	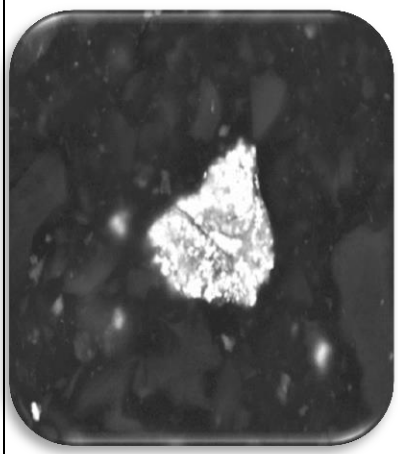	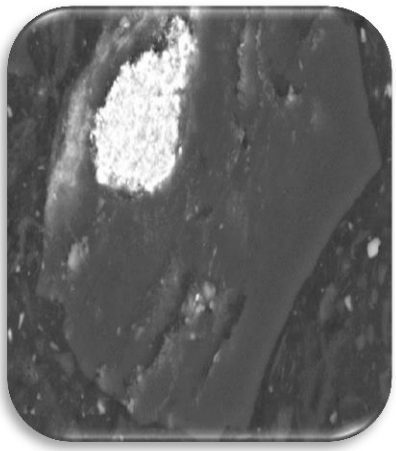	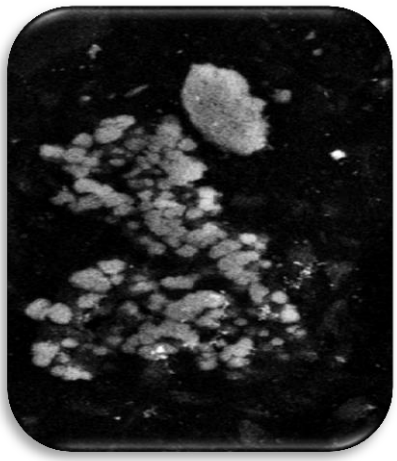

4.3.5 Morphological features of the particles in 30% CH_4 in H_2 runs

Table 4.4 Summary morphologies for 30% CH_4 in H_2(Magnification 4.5KX).

Time	30% CH_4 in H_2		
	T=1100 °C	T= 1200 °C	T =1250 °C
30 min	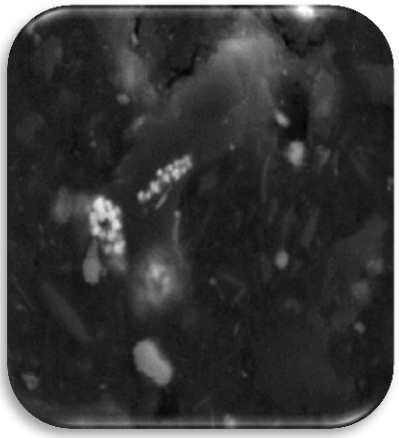	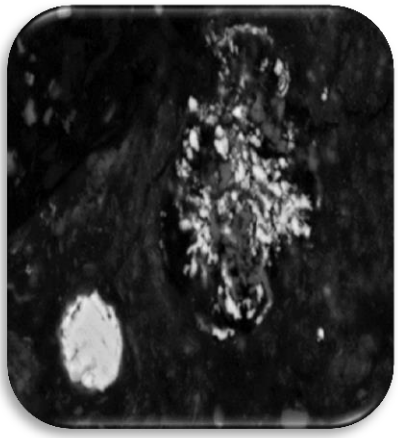	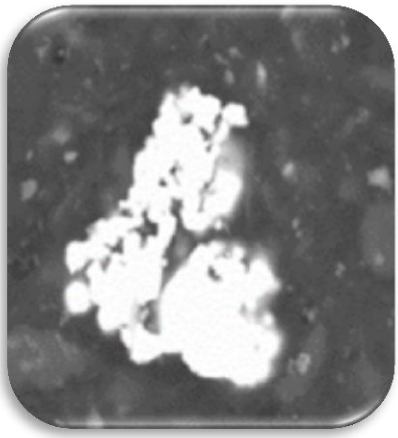
1 hr	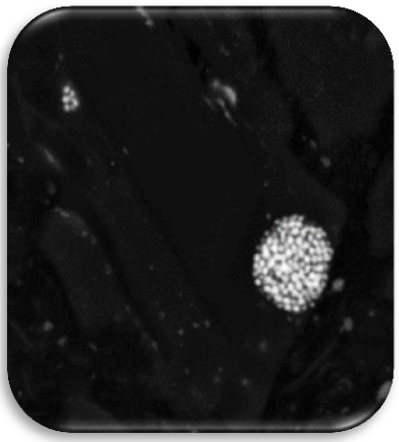	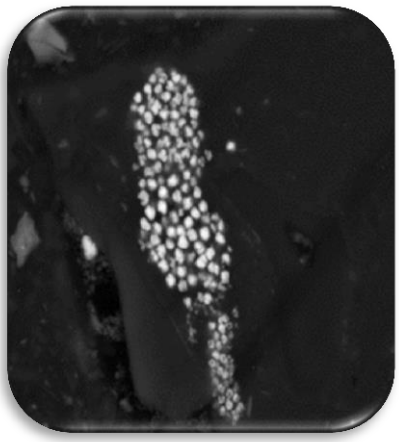	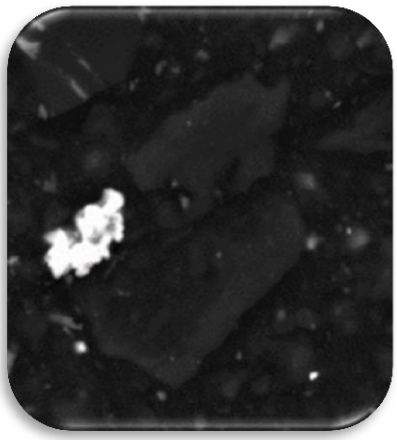
2 hr	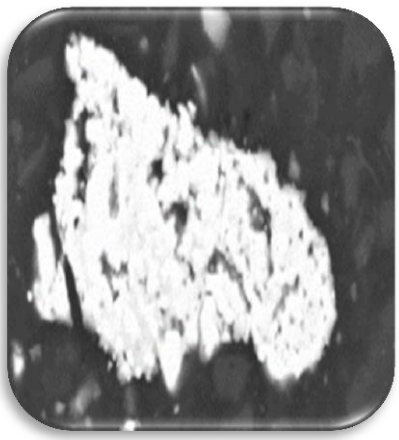	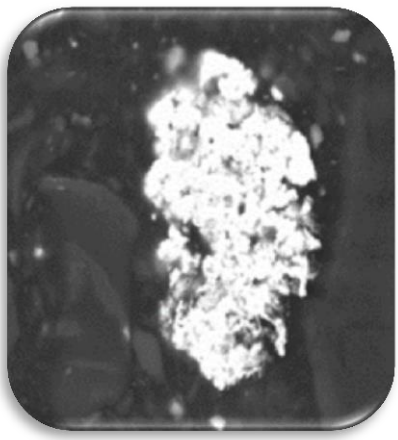	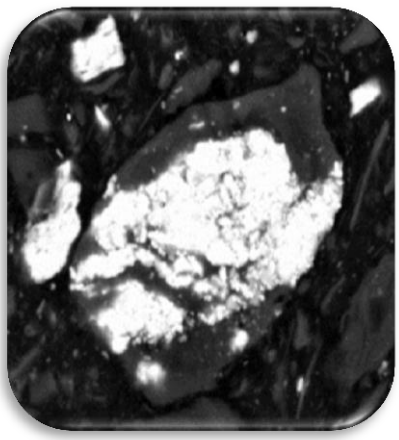

From Table 4.4 (magnification 4.5KX) it can again be observed that with increase in the time for the same temperature the percentage of reduction increases and also for fixed time the percentage of reduction is higher at higher temperature, highest being at 1250^{o}C.

The following observations can be made. At 1100^{o}C samples reacted under 30% CH_4 in H_2 showed 30-40% metallization for periods below 60 minutes and metal formation was in the form of very small metallic nuclei deposited in a concentrated area where reduction took place on the particle surface. It was also seen for 90 minutes and 120 minutes that the extent of metallization was higher around 60-70% and the small metallic nuclei in globular form coalesced to form a bigger metallic phase. At 1200^{o}C the extent of metallization was higher around 40-50% for times less than 60 minutes and was above 75% for 90 and 120 minutes. Again at higher time of 120 minutes small metallic nuclei globules colluded to form bigger metallic phase. At highest temperature of 1250^{o}C it was observed that extent of metallization was 50-60% for times less than 60 minutes and was above 80% for 90 and 120 minutes. It was also similarly seen that at times less than 60 minutes the metallic nuclei coalesced to form larger metallic phase that grew in size for longer times of 90 and 120 minutes.

The metallic formations were localized for lower temperatures and periods less than 1 hour (at 1100^{o}C and 1200^{o}C) but for 2 hours at these temperatures and at the highest temperature of 1250^{o}C they tend to coalesce and partially melt.

CHAPTER 5

MATHEMATICAL MODELLING, ANALYSIS AND DISCUSSION

This chapter discusses the overall gas-solid reaction systems and their rate control, as well as development of a mathematical model for metallization of Mamatwan manganese ore involving predicted stages of the metallization.Details of the derivation of the mathematical model equations, their application and limitations are also presented.

A brief discussion on the proposal of reduction behavior of Mamatwan ore with methane containing gas in temperature range of 1050^{o}C -1250^{o}C is given at the end of the chapter .

5.1 Introduction

Overall process in all gas-solid reaction systems may involve several intermediate steps. These steps generally involve the following:

(1) Gaseous diffusion (mass transfer) of reactants and products to and from the bulk of the gas phase to the reaction interface.
(2) Diffusion of gaseous reactants or gaseous products through the pores of a solid reaction product or through the pores of partially reacted solids.
(3) Adsorption of gaseous reactants on and desorption of reaction products from the solid surfaces.
(4) The chemical reaction between the adsorbed gas and the solid.

Slowest of the above steps which take place consecutively is the rate determining step. However, single step rate determining processes are limiting cases; the majority of gas solid reactions are influenced simultaneously by more than one step.
Wen[125] classified the heterogeneous non catalytic reactions according to the manner by which the reaction progresses: (1) Reactions in which solid contains enough voidage for the reactant and product gas, to pass freely and reactants are distributed homogenously throughout the solid phase. (2) Reactions during which the porosity of solid is small, so that the reactions occur at the surface of the solid or at the interface between the unreacted solid and the product layer.

Either of mechanism (1) or mechanism (2) does not completely describe gas–solid reactions. Intermediate of these two models are ones which describe majority of cases. The overall

process consists of chemical reaction at the interface, and the diffusion of gaseous reactants and products through the solid products layer and through the boundary layer at the external surface of the solid. The overall rate may be controlled by the rate of chemical reaction or by the rate of diffusion. In other cases, the rate of chemical reaction and diffusion may be present comparable resistances to the progress of reduction and may both influence the overall process. Most models proposed previously assume either of the first two extremes. This is not justified for many systems, nor is it necessary, because they are merely two asymptotes of the general case of both chemical reaction and diffusion determining the overall rate.

The following cases may be considered:

(1) When overall rate is controlled by chemical reaction at the interface, which is the principal resistance to the progress of reaction, then the rate equation can be expressed in terms of fraction reacted as follows:

$$kt = [1 - (1 - \mathrm{F})^{1/3}] \qquad 5.1$$

Where F=fraction reacted.

k = rate constant.

t= time.

Above equation was derived assuming that:

1. Reaction rate is controlled by a chemical process occurring at the phase boundary.
2. Reaction rate is proportional to the surface area of the fraction of unreacted material and such process may be referred to as topo chemical.
3. The nucleation step occurs virtually instantaneously so that the surface of each particle is covered with a product layer.

(2) When the chemical reaction at the interface presents less resistance to the progress of reaction compared with diffusion through the product layer, the overall rate is controlled by diffusion through the product layer.

Assuming that the rate of accumulation of diffusing species in the product layer is negligibly small compared to diffusive fluxes, the rate of reaction may be written in terms of fractional conversion as:

$$kt = [1 - 3(1 - F)^{\frac{2}{3}} + 2(1 - F)] \qquad 5.2$$

It is mostly seen that the rate of reaction is fairly high at the beginning and slows down as the reaction approaches completion revealing the contribution of more than one mechanism in the process. Mixed controlling factors involving both diffusional and surface chemical reaction have been postulated by many authors [39,107,123,124].

5.2 The reduction behavior

The previous sections discussed the reactions, morphologies resulting from the different gas mixtures, temperatures and reduction time. This part assembled these discussions into a proposal of the reduction behavior of Mamatwan manganese ore with the CH_4-containing gas mixture in temperature range of 1050°C -1250°C.

This study is limited to considering the following:

a) Gas mas transfer to and from the bulk gas to the particle surface – this is assumed to be fast due to the continuous flow of the gas and the observed rapid reaction rates especially during the early stages.
b) CH_4 cracking – the cracking of CH_4 is not proposed to be rate controlling. CH_4 is not thermodynamically stable at these reducing temperatures and starts to decompose at temperature as low as 550°C. When it is exposed to a suitable nucleation site, it promptly cracks, providing carbon, which is itself a suitable nucleation site for further carbon deposition. The other suitable nucleation site is oxide surface, metal phase and carbide.
c) Chemical reaction between reducing agents and the ore – gas (H_2 and CO) - solid oxide and solid (C) - solid oxide reaction, especially the initial H_2 gas reduction of the oxide is considered to be quite rapid relative to the gas mass transfer to the reaction surface.
d) Rate of regeneration reactions – these are gas (H_2)–gas (CO_2) and gas (CO_2)–solid (C) reactions which cannot not be rate limiting for the following reasons: carbon which precipitates from CH_4 cracking at the reduction site has very high thermodynamic activity and hence highly reactive. The metallic surfaces, carbon surfaces and carbide surfaces act as catalytic sites for these regeneration reactions.
e) Nucleation – the relative period of the duration of product/metal nucleation compared to the period required for the entire reduction reaction makes it unlikely for such a process to dominate the kinetics over any extended period of reaction.

The reaction sequence is postulated to have been as follows for -125 + 106 μm Mamatwan manganese ore reduction by CH_4 gas in Ar or H_2 mixture.

$$CH_4 \rightarrow C + 2\,H_2 \qquad 5.2a$$

This reaction provided both reductants; solid carbon and H_2 gas, reacting rapidly with the Mn and Fe oxides on the particle surface

$$3Fe_2O_3 + H_2 \longrightarrow 2Fe_3O_4 + H_2O \qquad 5.2b$$

$$Fe_3O_4 + H_2 \rightarrow 3FeO + H_2O \qquad 5.2c$$

$$FeO + H_2 \longrightarrow Fe + H_2O \qquad 5.2d$$

$MnO_2 + ½ H_2 \longrightarrow ½ Mn_2O_3 + ½ H_2O$ 5.2e

$3Mn_2O_3 + H_2 \longrightarrow 2Mn_3O_4 + H_2O$ 5.2f

$Mn_3O_4 + H_2 \longrightarrow 3MnO + H_2O$ 5.2g

Parallel to these, reaction sequence of Fe_2O_3 to Fe_3O_4 to FeO to Fe as well as the reaction sequence MnO_2 to Mn_2O_3 to Mn_3O_4 to MnO takes place by carbon precipitating from the gas phase as well as by CO formed. The metallic iron formed will also be carburized by reaction (5.2h).

$3Fe + C \rightarrow Fe_3C$ 5.2h

The reduction interface is defined as the reacting surface of the oxide. The CH_4 that diffused to the particle surface deposits C and H_2 at the reduction site allowing carbon to spread throughout the whole exposed solid surface of the ore. The carbon precipitating during CH_4 cracking has very high thermodynamic activity well above unity and also due to good solid-solid contact, the ore is also directly reduced. At the reaction site, regeneration of CO and H_2 from CO_2 and H_2O is also very effective again due to high activity of carbon and the reduction/metallization of the manganese ore then proceeds as solid oxide-gas (CO and H_2) reaction. It is supposed that in this way the reduction potential is significantly raised at the reaction site, bringing about a faster reduction rate and efficient utilization of the reducing gas.

MnO reduction to metallic state starts at the later stages of the first stage of reduction through

$MnO + C \rightarrow Mn + CO$ 5.2i

$MnO + CO \rightarrow Mn + CO_2$ 5.2j

$C + CO_2 \rightarrow 2CO$ 5.2k

followed immediately by carburization of Mn

$7Mn + 3C \rightarrow Mn_7C_3$ 5.2l

The rate of reduction for the first 20 or 30 minutes of reaction is likely to be controlled by gas diffusion. The higher the concentration of the methane in the gas mixture, the higher is the resulting reaction rate and reaction extent. The significant variables in the Mamatwan manganese ore reduction by CH_4 gas are: CH_4 concentration; carrier gas type; temperature and time. Generally CH_4 was an effective reductant because it supplied both high activity C and H_2 to the reduction site. Due to very high thermodynamic activity of carbon it dominates the reduction and is potentially assisted by hydrogen in the early stages in the reduction of iron

oxides and higher manganese oxides. A reduction maximum of 73% metallization was achieved in a methane/argon gas mixture at 1200°C in less than 2 hours.

5.3 Determination of rate controlling processes.

For the following presentations and discussions of this and later chapters "metallization" term refers both to reduction and actual metallization of the ore particles since for example at the very early stages while manganese oxides were reduced to lower oxides with no metallic manganese formation iron oxides were reduced to metallic state. In this work the experimental initial rate which corresponds to the first stage of reduction/metallization, were evaluated as slopes of experimental metallization versus time curves the logarithm of which were plotted with respect to inverse temperature. The activation energy obtained by this method in the temperature range of 1050 °C to 1250 °C varied from 1.47 kJ/mol to 24.72 kJ/mol for manganese (Figures 5.1 to 5.4) and from 0.29 kJ/mol to 14.80 kJ/mol for Fe (Figures 5.5 to 5.8) much lower than the ones reported by Akdogan [35] (1100 °C to 1350 °C) of 81.3 kJ/mol to 94.6 kJ/mol for ordinary solid-state carbothermic reduction of Wessel manganese ores. In his study on pre-reduction of manganese ore for ferromanganese smelting Mishra [75] reported an apparent activation energy value of 38 kJ/mol and attributed this value to the gaseous diffusion rate controlling mechanism. It can be seen from the present experimental and reported activation energy values that for the first stage it appears that metallization of Mamatwan ore is most likely diffusional controlled as suggested by lower value of activation energy (value less than 25kJ/mol).

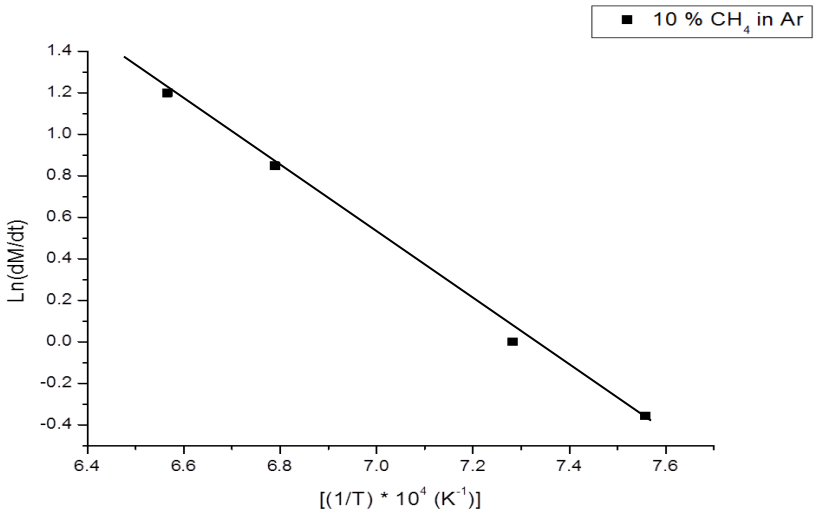

Figure 5.1 Determination of Activation Energy for Mn metallization with 10 % Methane + Argon (E_A =13.3024 kJ/mol).

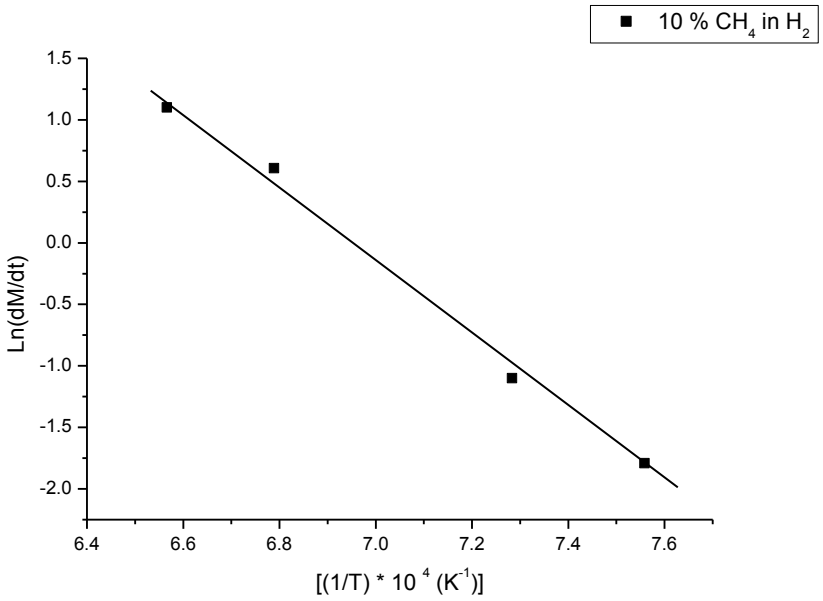

Figure 5.2 Determination of Activation Energy for Mn metallization with 10 % Methane + Hydrogen (E_A = 24.72 kJ/mol).

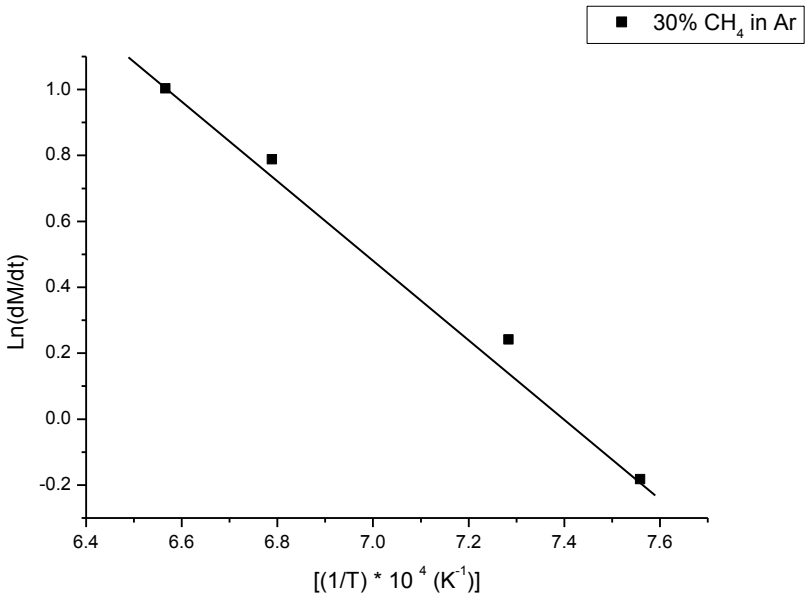

Figure 5.3 Determination of Activation Energy for Mn metallization with 30 % Methane + Argon (E_A =24.68 kJ/mol).

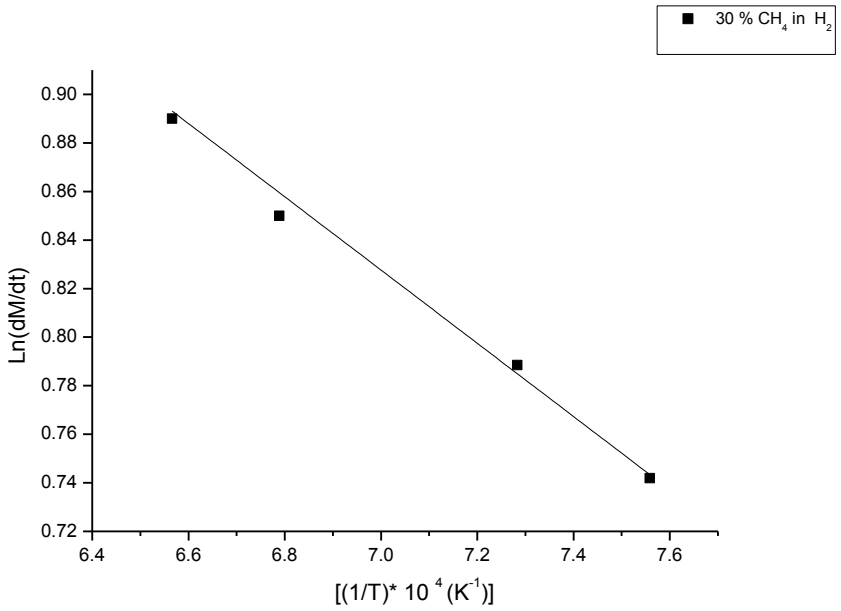

Figure 5.4 Determination of Activation Energy for Mn metallization with 30 % Methane + hydrogen (E_A =1.4639 kJ/mol).

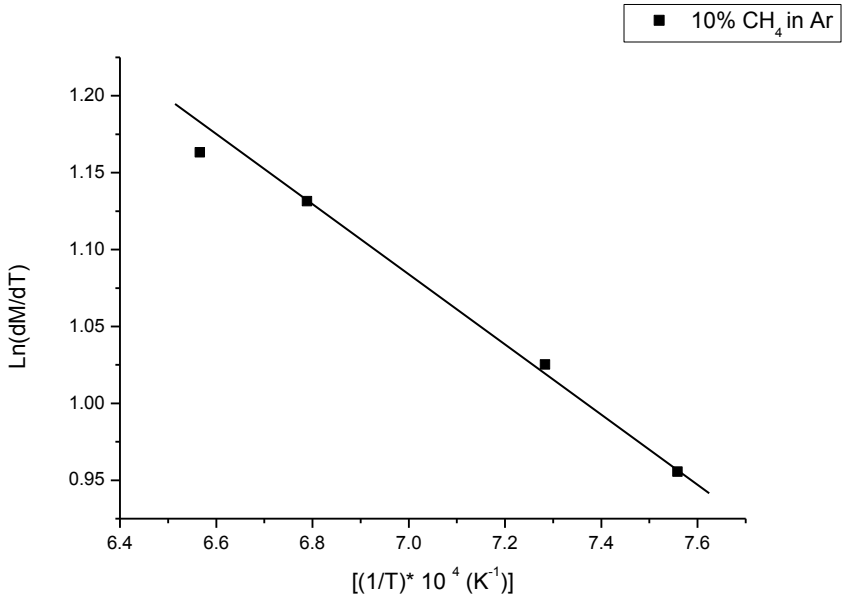

Figure 5.5 Determination of Activation Energy for Fe metallization with 10 % Methane + Argon (E_A = 1.9122 kJ/mol).

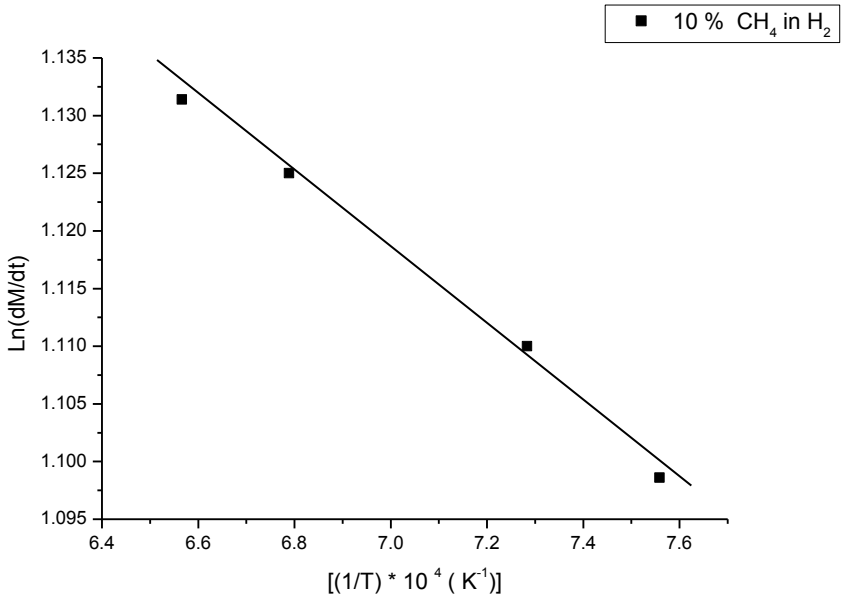

Figure 5.6 Determination of Activation Energy for Fe metallization with 10 % Methane + Hydrogen (E_A = 0.286833 kJ/mol).

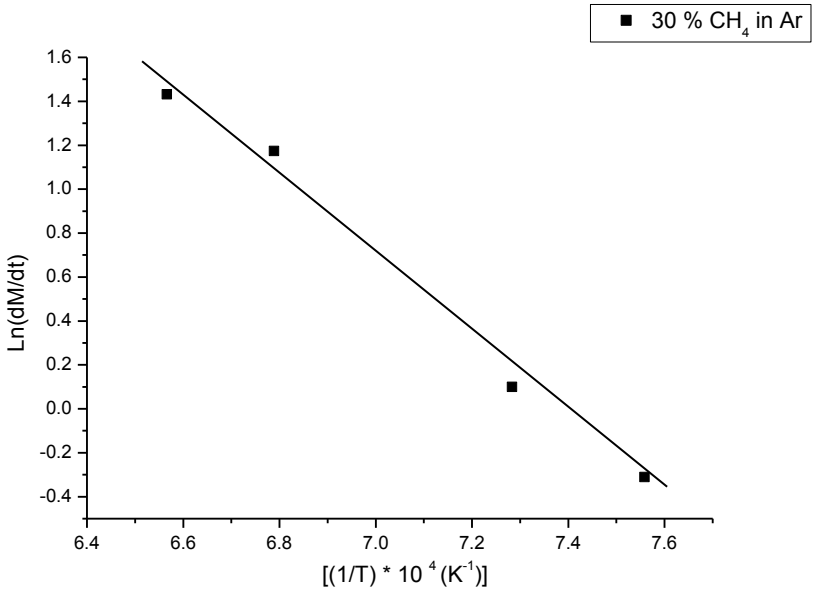

Figure 5.7 Determination of Activation Energy for Fe metallization with 30 % Methane + Argon (E_A =14.798 kJ/mol).

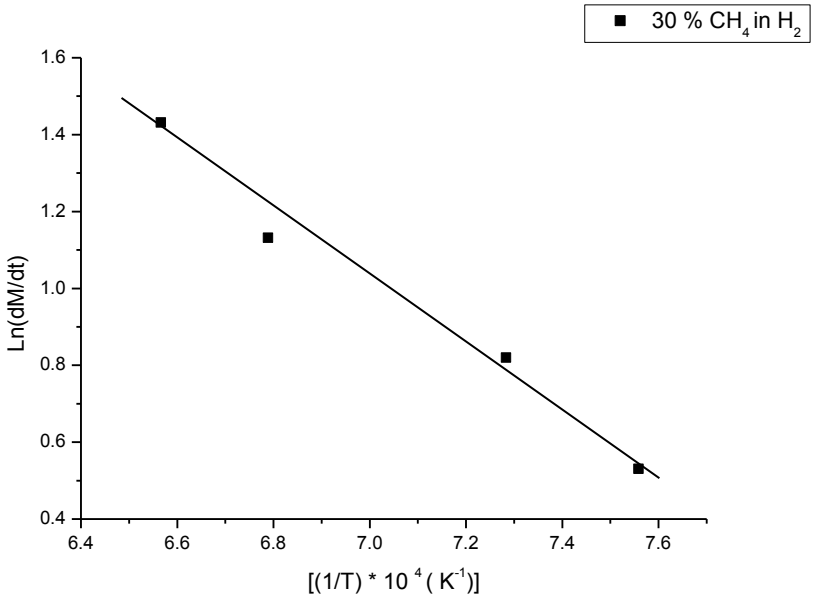

Figure 5.8 Determination of Activation Energy for Fe metallization with 30 % Methane + Hydrogen (E_A =7.483 kJ/mol).

5.4 Reduction stages and development of a Mathematical Model for the metallization of the Mamatwan manganese ore.

For this study a mathematical model was developed. It was seen that metallization of Mamatwan ore proceed in two stages as was deduced from examination of the partially reduced/metallized samples.

Stage 1: The reduction of the higher oxides to MnO, metallization of iron and start of metallization of manganese. This stage continues up to approximately 30 minutes of reaction time after which a drastic change in the slope of the kinetic curves is seen. Stage 1 potentially consists of two Sub stages: Sub-stage 1 and Sub-stage 2. The sub-stages could not be clearly identified from the metallization versus time kinetic curves (due to severe experimental difficulties more samples could not be obtained within the first 30 minutes etc.) since they did not show clear changes in slope within the first 30 minutes. However the data gathered by XRD provided the clues for the sub stages.

Sub-stage 1 up to about 20 minutes is the reduction of higher oxides of both iron and manganese to lower oxides (in the case of manganese Mn_2O_3 to first Mn_3O_4 and then to MnO) and also reduction of all iron oxide to metallic state by high activity carbon assisted with hydrogen gas. The XRD did not detect iron oxide in the samples after about 20 minutes, and

only several different iron carbides existed together with manganese oxides. Thus all the iron is reduced to metallic state within the first 20 minutes defining the end of sub-stage 1, thereafter sub-stage 2 commences.

Sub-stage 2 between approximately 20 and 30 minutes is the reduction of higher manganese oxides that still exists to MnO as well as the start of reduction of MnO to metallic state forming mixed iron-manganese carbides. These are carbothermic reductions by the high activity carbon precipitating from the gas phase. XRD illustrated that up to 30 minutes limited metallization of manganese is seen and mostly higher oxides of manganese are reduced to MnO with some or little Mn_2O_3 and Mn_3O_4 still remaining.

Stage 2: After about 30 minutes the kinetically slow and long stage 2 starts during which partial reduction of MnO and any remaining oxide to mixed carbide of iron and manganese occurs and growth of the carbide phase covering the surface of the partially reduced ore particles is seen. The rate of reduction/metallization during this stage is substantially slower compared to Stage 1 and the extent of reduction/metallization does not improve much reaching a maximum of 73% at 1200^{o}C. Potentially the reason for this is the extensive deposition of very fine sized carbon precipitating from the gas mixture on the partially reduced ore particles covering their surface and hence hindering the reduction/metallization by acting as a barrier to reducing CO gas. Moreover during this extended period beyond 30 minutes the deposited carbon particles on the surface of the partially reduced ore graphitize resulting in their thermodynamic activity dropping to around unity. Although fresh carbon particles of activity greater than 1.0 are continuously being precipitating from the flowing gas mixture, they are not anymore in contact with the partially reduced ore particles. Carbon with activity of 1.0 cannot reduce MnO to metal at 1200^{o}C or 1250^{o}C, thermodynamically[87] the minimum temperature for reduction of MnO to metal with carbon of activity equal to 1.0 is around 1420^{o}C. Thus Second stage is compromised both thermodynamically and kinetically displaying small increases in reduction/metallization extent as well as slow kinetics with diffusion of the gas being the most likely rate limiting step.

For mathematical analysis, the iron oxide in the ore is assumed to reduce very quickly to metallic iron as was evidenced by XRD and behave similarly to manganese oxide because of the chemical and physical similarities of the two elements, manganese and iron. In the next sections from 5.4.1 to 5.4.3 equations and derivations of the mathematical model for first stage of the metallization, for transition from first to second stage of the metallization and for second stage of the metallization are given and the use of model equations will be explained in section 5.4.4.

5.4.1 First stage of the metallization

As standard free energy change for reaction of carbon with Mn_2O_3 over temperature range considered is largely negative, Mn_2O_3 instantaneously reduces to Mn_3O_4 under the reducing conditions in the system:

$$3Mn_2O_3 + C = 2\,Mn_3O_4 + CO \qquad 5.3$$

Thereafter, the Mn_3O_4 is reduced by carbon monoxide by the following reaction:

$$Mn_3O_4 + CO = 3\,MnO + CO_2 \qquad 5.4$$

A mathematical analysis of metallization of manganese oxides is done on the basis of experimental findings, it was noted that the metallization process was affected collectively by the reaction on the pore walls of oxides and gas diffusion in the porous oxide.

In this study for the first stage of the metallization, the core and product layer formed are porous. Because of the porous nature of the product layer and the core, the total pressure within the particle is assumed to be constant and essentially the same as that in the gas stream. Since the metallization of manganese ore proceeds carbothermically by the action of high activity carbon particles continuously precipitating from the CH_4 -H_2 and CH_4-Ar gas mixture the mathematical analysis is done for a binary gas mixture of CO-CO_2 for which the diffusivity is independent of gas composition. The effect of pure CO was investigated in an earlier study[9].The effect of the other gaseous species in the gas phase were neglected.This assumption can be justified due to the fact that hydrogen in the gas phase, thermodynamically cannot reduce MnO and the fact that iron oxides are reduced to metallic form very quickly by high activity carbon (and to a limited extent by hydrogen). Furthermore, because of the relative high thermal conductivity of the metal oxides heat transfer can be dismissed as possible rate controlling process. With these justified implications, the mathematical formulation is based on the assumptions:

1. As the reaction on the pore walls of oxide is accompanied by gas diffusion depending on the porosity and gas diffusivity therein, there will be partial internal metallization slightly ahead of nominal product/oxide interface resulting in a rather diffuse interface.
2. Quasi–stationary conditions prevail for a first order type reaction involving CO and CO_2 in a spherical porous particle.
3. The resistance to the film diffusion around the particle is negligibly small.
4. Isothermal and isobaric conditions exist.

The mathematical development for this stage is based on the principle given by Ishida and Wen [44] for the single step porous core reaction. A Schematic diagram of the reacting particle during

the first stage is shown in figure 5.9, and material balance of a section of the reacting particle is given in figure 5.10.

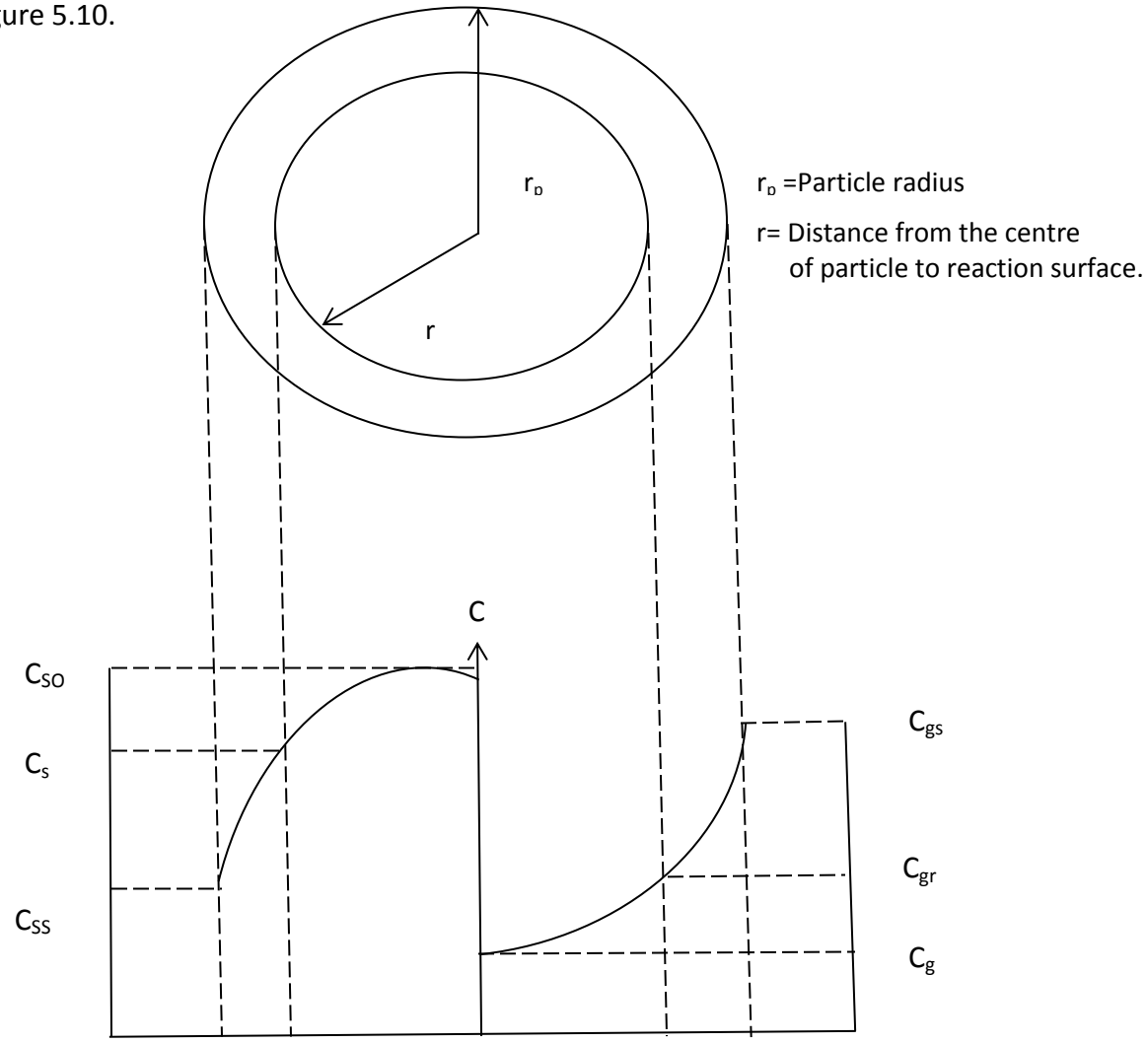

C_{SO} = Initial concentration of solid reactant

C_{SS}= Concentration of solid reactant at the outer surface

C_s = Concentration of solid reactant in the reaction zone

C_{gs} = Concentration of gas reactant at the outer surface of particle

C_{gr} = Concentration of gas reactant in the reaction zone

C_g = Equilibrium concentration of reactant gas

Figure 5.9 Schematic diagram for concentration profiles during the first stage of the metallization[44].

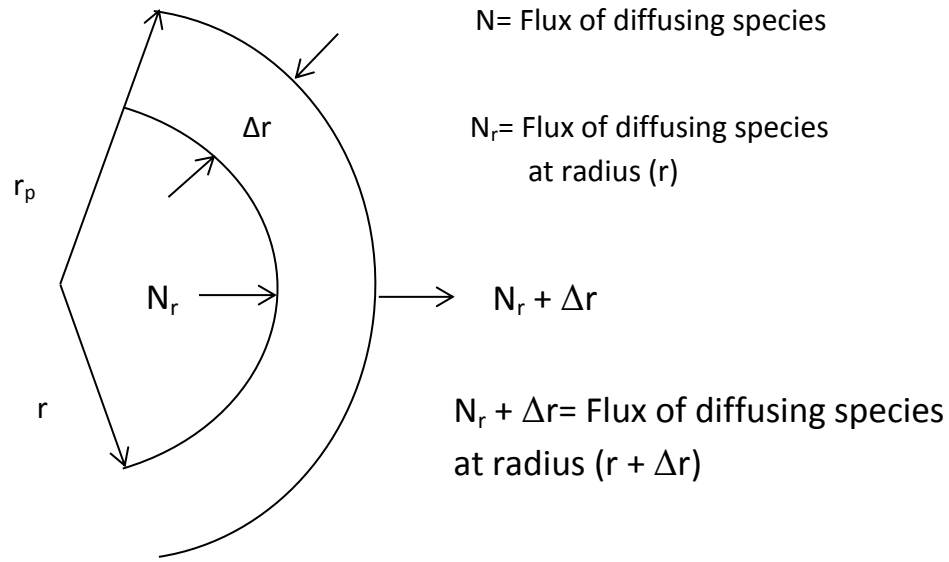

Figure 5.10 Section of the reacting particle.

Under quasi–stationary assumption a material balance for reactant gas and solid reactant for a spherical particle can be written as:

$$4\,\pi\,r^2\,N_r = 4\,\pi\,r^2\,(N_r + \Delta r) + k_c C_g\,4\,\pi\,r^2\,\Delta r \qquad 5.5$$

$$(r^2(N_r + \Delta r) - r^2 N_r\,)/\Delta r = -k_c C_g\ r^2 \qquad 5.6$$

Above equation can be written in general differential form as follows:

For CO: $$\frac{d}{dr}(r^2\,N_{CO}\,) = -r^2\,R_{chem} \qquad 5.7$$

and

For CO_2: $$\frac{d}{dr}\left(r^2\,N_{CO_2}\,\right) = -r^2\,R_{chem} \qquad 5.8$$

Where R_{chem} is the rate of chemical reaction.

Using Fick's law:

$$N_{CO} = -D_{ef}\ C_g\,dX_{CO}\,/dr \qquad 5.9$$

Where D_{ef} is the effective diffusivity of (CO) and (CO_2) in the oxide particle, C_g is total gas concentration and X_{CO} is the mole fraction of CO, and together, with Equation (5.7) results in the following:

$$-D_{ef}\ C_g\ \frac{d}{dr}(r^2)dX_{CO}/dr = -r^2\ kS\rho C_g\ (\ X_{CO}\ - X_{CO_2}\ )/(K_e\ ) \qquad 5.10$$

Where, S is pore surface area; ρ is density of particle, k is rate constant; and K_e is equilibrium constant. A new variable, e which is a function of (r) can be defined as:

$$X_{CO} = e_1\ /\mathrm{r} \text{ and } X_{CO_2}\ = e_2\ /\mathrm{r} \qquad 5.11$$

Then differentiating the above for CO with respect to (r) results in:

$$dX_{CO}\ /dr = (1/r)(de_1/dr) - e_1/r^2 \qquad 5.12$$

Multiplying both sides of the above equation by $r^{2:}$

$$r^2 dX_{CO}\ /dr = r(de_1/dr) - e_1 \qquad 5.13$$

Differentiating the above with respect to (r) again and rearranging the terms results in the following:

$$d/dr(r^2 dX_{CO}\ /dr) = r(d^2e_1/dr^2) + de_1/dr - de_1/dr \qquad 5.14$$

$$D_{ef}\ C_g\ r\frac{d^2e}{dr^2} = rkS\rho C_g\ (e_1 - e_2/K_e) \qquad 5.15$$

Assuming that outward diffusion of carbon dioxide and inward diffusion of carbon monoxide proceed at the same rate and since

$X_{CO}\ + X_{CO_2} = 1$ and $e_1 + e_2 = r$

Then equation (5.15) is simplified to:

$$D_{ef}\ \frac{d^2e}{dr^2} = [kS\rho(e_1 - \frac{r-e_1}{K_e}] \qquad 5.16$$

$$=\ e_1(kS\rho + kS\rho/K_e) - kS\rho r/K_e \qquad 5.17$$

$$= e_1\frac{kS\rho(K_e+1)}{K_e} - kS\rho r/K_e \qquad 5.18$$

Further rearranging the above relation:

$$\frac{d^2e}{dr^2} = e_1\left[\frac{kS\rho\left(\frac{(K_e+1)}{K_e}\right)}{D_{ef}}\right] - \left(\frac{kS\rho r}{D_{ef}\ K_e}\right) \quad 5.19$$

$$\frac{d^2e}{dr^2} - \tau e_1 = -\beta r \quad 5.20$$

Where, $\tau = \frac{kS\rho\left(\frac{(K_e+1)}{K_e}\right)}{D_{ef}}$ and $\beta = \frac{kS\rho}{D_{ef}\ K_e}$

The solution to the above differential equation (Equation 5.20) is as follows:

$$e_1 = Q_1\ \cosh(\sqrt{\tau}\mathrm{r}) + Q_2\ \sinh\sqrt{\tau}\,\mathrm{r}) + \left(\frac{\beta}{\tau}\right)\mathrm{r} \quad 5.21$$

Where Q_1 and Q_2 are constants and hence;

$$X_{CO} = Q_1\ /r\ (\cosh(\sqrt{\tau}\quad r) + Q_2/r(\ \sinh\sqrt{\tau}\ r) + \left(\frac{\beta}{\tau}\right) \quad 5.22$$

Together with the following boundary conditions:

b.c 1) at r = r_p, X_{CO} =1

b.c 2) at r=0, dX_{CO} /dr = 0

From boundary conditions. 2 Q_1 = 0, and

From boundary condition. 1

$$1 = Q_2/r_p(\ \sinh\sqrt{\tau}\ r_p) + \left(\frac{\beta}{\tau}\right) \quad 5.23$$

$$Q_2 = (r_p - \left(\frac{\beta}{\tau}\right)r_p)/(sinh\sqrt{\tau}\ r_p) \quad 5.24$$

Therefore, during first stage carbon monoxide concentration profile at a radial position (r) in the particle is given by:

$$X_{CO,r} = \frac{r_p\left(\frac{K_e}{K_e+1}\right)}{r}(\sinh(\sqrt{\tau}\,\mathrm{r})/sinh(\sqrt{\tau}\ r_p)) + 1/(K_e+1) \quad 5.25$$

Where K_e is the equilibrium constant of the reduction reaction (5.4) and r/ r_p =1.

At 1100 ^oC K_e =2.5 *10 ^{4}

When, Ke $_{>>}$1 the equation 5.25 can be simplified to:

$$X_{CO,r} = \frac{r_p}{r}(\sinh(\sqrt{\tau}\,\mathrm{r})/sinh(\sqrt{\tau}\ r_p)) \quad 5.26$$

Two new dimensionless parameters are defined as follows;

$\delta = (\frac{r}{r_p})$ Where, δ is dimensionless radius and $\emptyset_f = (\frac{kS\rho\left(\frac{(K_e+1)}{K_e}\right)}{D_{ef}})^{\frac{1}{2}}.r_p$

Where,$\emptyset_f$, is kinetic–diffusion modulus.

Hence, equation (5.26) can be rewritten as:

$X_{CO,r} = sinh(\emptyset_f\delta)/\delta\, sinh(\emptyset_f)$ 5.27

$\emptyset_f$, is kinetic–diffusion modulus also known as Thiele modulus. $\emptyset_f$ is used in the study of reactions on catalyst to show the effect of gas diffusion on the reaction rates on catalyst pore walls. The Thiele modulus was defined based on the following assumptions:

1. Reactants gas is transported into and within the porous structure of a particle by a diffusive flux through a concentration gradient.
2. The pores are interconnected, uniform in cross sections and surface area remains unchanged throughout the process.

The rapid rate of reduction of Mn_2O_3 above 1000°C with the following initial reaction;

$3\ Mn_2O_3 + C = 2\ Mn_3O_4 + CO$ 5.3

makes it necessary to assume that the total rate of metallization in the first stage depends mostly on the rate at which carbon monoxide diffuses into the Mn_3O_4 layer. If the carbon monoxide produced by reduction of Mn_2O_3 reacts with Mn_3O_4 according to the reaction below:

$Mn_3O_4 + CO = 3\ MnO + CO_2$ 5.4

Then each mole of carbon monoxide produced reacts with one mole of Mn_3O_4. Thus the total rate of reaction, M_f, can be written as:

$M_f = 4\pi {r_p}^2\ D_{ef}\ C_g\ (\frac{dX_{CO,r}}{dr})$ 5.28

Differentiating quasi –stationary carbon monoxide concentration profile at $r = r_p$

$\left(\frac{dX_{CO,r}}{dr}\right)_{r=r_p} = \frac{r_p}{\sinh(\emptyset_f)}[(1/r(\sinh\sqrt{\tau}\,\mathrm{r})]$ 5.29

$= \frac{r_p}{\sinh(\emptyset_f)}[\frac{\sqrt{\tau}(\cosh(\sqrt{\tau}\ r)}{r} - (\sinh\sqrt{\tau}\,\mathrm{r})/r^2]$ 5.30

Rearranging the terms:

$\left(\frac{dX_{CO,r}}{dr}\right)_{r=r_p} = [[\frac{r_p\sqrt{\tau}(\cosh(\sqrt{\tau}\ r)}{r\ \sinh(\emptyset_f)} - r_p\ (\sinh\sqrt{\tau}\ r/r^2\ \sinh(\emptyset_f))]$ 5.31

$= [\ \emptyset_f \cosh\emptyset_f)/(\ r_p \sinh\emptyset_f) - r_p \sinh\emptyset_f\ /({r_p}^2\ \sinh\emptyset_f)]$ 5.32

$\left(\frac{dX_{CO,r}}{dr}\right)_{r=r_p} = [(\emptyset_f \cot\mathrm{h}\,\emptyset_f - 1)/r_p]$ 5.33

$$M_f = 4\pi {r_p}^2 D_{ef} C_g [(\emptyset_f \coth \emptyset_f - 1)/r_p)] \quad 5.34$$

Further rearrangement of the terms for Equation (5.34) results in the following equation for M_f

$$M_f(mole/_{sec}) = 4\pi {r_p}^2 C_g (kS\rho D_{ef})^{\frac{1}{2}}[(\emptyset_f \coth \emptyset_f - 1)/ \emptyset_f] \quad 5.35$$

Equation 5.35 is similar to the one defined by Tien and Turkdogan[113] for the rate of reduction of iron oxides, which was controlled jointly by gas diffusion in the pores of wustite and reaction on the pore walls of the wustite.

When $\emptyset_f$ is large, e.g. $\emptyset_f$ >2, with decreasing (D_{ef}), the dimensionless parameter in the square parenthesis in equation (5.35) approaches to unity and equation (5.35) simplifies to:

$$M_f = 4\pi {r_p}^2 C_g (kS\rho D_{ef})^{\frac{1}{2}} \quad 5.36$$

The total gas concentration, C_g, can also be expressed as

$$C_g = N/V = P/RT \quad 5.37$$

Where N =total number of moles of gas

V= total volume of gas

P= total gas pressure

R= universal gas constant

T= temperature (K)

Hence, equation (5.36) may be written as:

$$M_f = 4\pi {r_p}^2 (D_{ef} \sqrt{\tau}) P/RT \quad 5.38$$

In equation 5.4 if all carbon monoxide reacts with Mn_3O_4, then each mole of carbon monoxide produced reacts with one mole of Mn_3O_4. Thus, Equation 5.38 becomes the rate of reaction in the moles Mn_3O_4 reduced. For every mole of Mn_3O_4 reduced, half a mole of oxygen is removed and thus the above equation becomes:

$$M_f = 4\pi {r_p}^2 (D_{ef} \sqrt{\tau}) P/2RT \quad 5.38\ a$$

Using the surface area available for reaction per cubic meter of ore, A_s and the total initial concentration of oxygen available for reaction with carbon,(C_{oxy}), the above equation become:

$$M_f = A_s (D_{ef} \sqrt{\tau}) \frac{P}{2RT}.1/(C_{oxy}) \quad 5.39$$

The rate of metallization can be obtained from the slopes of the straight line portions of the first stage of metallization of corresponding Metallization versus time (M_f versus time) curves, as given in Figures 4.4 to 4.11. Total initial concentration of oxygen available for reaction is calculated in Appendix D. The only unknown in the equation is $(D_{ef}\ \sqrt{\tau})$ and when the other terms of equation 5.39 are known, $(D_{ef}\ \sqrt{\tau}\ )$ can be easily calculated (discussed further in detail in section 5.4.4).

To estimate the molecular carbon monoxide–carbon dioxide diffusivities the method used is derived by the theoretical equation based on the modern kinetic theory and Lennard-Jones expression for intermolecular forces [101]; this is:

$$D_{12} = \frac{0.00185T^{3/2}}{P\ \delta^2{}_{12}\ \Omega_D}\left[\ (M_1 + M_2)/\ (M_1.M_2)\right]^{1/2} \qquad 5.40$$

Where;

D_{12} = Molecular diffusion coefficient for gas (1) diffusing in gas (2)

T = Absolute temperature (K)

M_1, M_2 = Molecular masses of the two gases.

P = Total Pressure in atmospheres.

Ω_D = Collision integral.

δ_{12} = Force constant.

Equation (5.40) was evaluated for CO diffusing in CO/CO_2 mixtures using data listed in Satterfield and Sherwood[101]. The calculated molecular diffusivity of CO in CO/CO_2 mixtures are given in Table D1 of Appendix D, The details of the calculation procedure are also summarized in Appendix D.

Effect of diffusion on the metallization rate during first stage can be examined by effectiveness factor,ε defined as the ratio of actual rate of the reaction,M_f, in the spherical particle to the reaction rate in the particle at the bulk phase concentration of the reacting gas , M_b.

$$M_f = 4\pi {r_p}^2\ D_{ef}\ C_g\ \left(\frac{dX_{CO,r}}{dr}\right) \qquad 5.41$$

$$M_b = \ (\tfrac{4}{3})\pi {r_p}^3(\ kS\rho)\ C_g\ (X_{CO,b} - X_{CO_2,b}\ /K_e) \qquad 5.42$$

Where $X_{CO,b}$ and $X_{CO_2,b}$ are the bulk concentration of respective gases. Thus, the effectiveness factor, ε , can be written as follows :

$$\varepsilon = 4\pi {r_p}^2 D_{ef} C_g \left(\frac{dX_{CO,r}}{dr}\right) / ((\frac{4}{3})\pi {r_p}^3 (kS\rho) C_g (X_{CO,b} - X_{CO_2,b}/K_e)).\, 1/\gamma \quad 5.43$$

Where, γ, accounts for film diffusional resistance around the particle. Assuming that Mn_2O_3 is instantaneously reduced to Mn_3O_4 and carbon monoxide diffuses into the Mn_3O_4 layer and the reaction given below occurs:

$Mn_3O_4 + CO = MnO + CO_2$ 5.44

For which equilibrium constant, $K_e >> 1$ over the temperature range 1050°C to 1250 °C, the term for the reverse reaction would be small enough to be neglected. And $X_{CO,b}$ is the mole fraction of carbon monoxide which prevails at the carbon-Mn_3O_4 interface during the first stage. The equilibrium partial pressure of carbon monoxide is very high (due to the large K_e value). Therefore the mole fraction of carbon monoxide can be assumed to be unity.

Then, the equation (5.43) reduces to

$$\varepsilon = 3\,((\emptyset_f \coth \emptyset_f - 1)/{\emptyset_f}^2))\,.\,1/\gamma \quad 5.45$$

And the film diffusion may be defined as:

$$\gamma = 1 + ((\emptyset_f \coth \emptyset_f - 1)\,/N_{sh}) \quad 5.46$$

Where N_{sh} is Sherwood number for mass transfer through gas layer.

The fraction of the solid reactant at the end of the first stage; F_f, can be given as :

$$F_f = \varepsilon.\gamma \quad 5.47$$

When the gas film diffusion resistance is negligibly small (i.e. N_{sh} is infinity), then γ becomes unity.

The time at the end of the first stage can be found by integration of the equation [44] below:

$$\frac{dC_S}{dt} = -kS\rho C_g\,((X_{CO,b} - X_{CO_2,b})/K_e) \quad 5.48$$

Where C_s is solid reactant concentration and C_g is not a function of time.

Integration of equation (5.48) when $X_{CO} = 1$ gives:

$$C_s = -kS\rho C_g\, t + Q_3 \quad 5.49$$

Initial condition; at t=0 $C_s = C_{so}$

Where

C_{so} is the initial concentration of solid reactant.

Then, $Q_3 = C_{so}$

Replacing Q_3 in equation (5.49) yields:

$$C_s = C_{so} - kS\rho C_g\, t \qquad 5.50$$

Let t_f be time at the end of the first stage, and

At t_f, $C_s = 0$

$$0 = C_{so} - kS\rho C_g\, t_f \qquad 5.51$$

$$t_f = C_{so}/\, kS\rho C_g \qquad 5.52$$

The unreacted solid concentration, C_{sf}, at the end of the first stage can be as follows:

$$C_{sf} = C_{so} - kS\rho C_g\, X_{CO,r}\, t_f \qquad 5.52a$$

Inserting equation 5.27 and 5.52 in equation 5.52a gives:

$$C_{sf} = C_{so} - kS\rho C_g\, C_{so}/\, kS\rho C_g\ [\sinh(\emptyset_f \delta)/\, \delta \sinh(\emptyset_f)] \qquad 5.53$$

And rearranging the terms gives:

$$C_{sf}=C_{so}\left[1 - \sinh(\emptyset_f \delta)/\, \delta \sinh(\emptyset_f)\right] \qquad 5.54$$

Section 5.4.4 discusses in detail the application of this model for the first stage of metallization data.

5.4.2 Mathematical Modelling of transition from first to second stage of the metallization

To predict from the metallization versus time curves, the transition from first to second stage is difficult and it should not be abrupt, hence in order to quantitatively model the second stage of the metallization, transition from the first to the second stage of metallization has been mathematically analyzed. Although the contribution of this transition to the overall metallization process is very small, following analysis has been performed for mathematical purpose [44].

As the metallization progresses two zones appear;

1. An outer porous zone in which solid reactant , Mn_3O_4 is completely converted to MnO , and

2. An inner zone where the first stage reaction still takes place. It is again assumed that the inner core is porous (as it is transitory stage where transition from first stage to second stage takes place) and diffuse interface develops.

This is shown in figure 5.11 which gives the concentration profile just before commencement of the second stage.

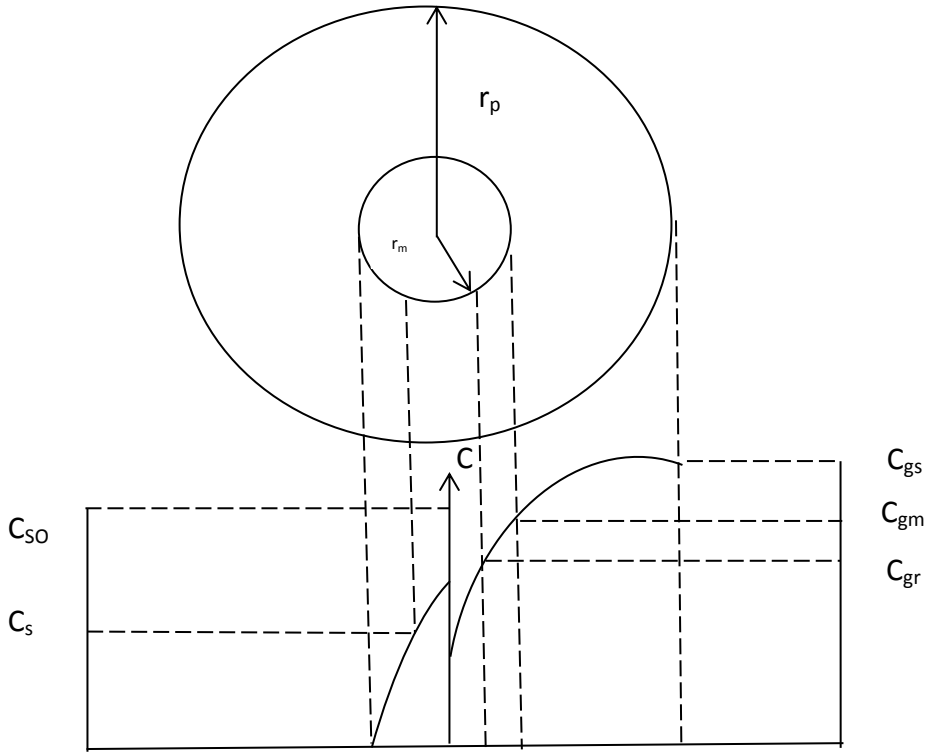

C_{SO} = Initial concentration of solid reactant

C_s = Concentration of solid reactant in the reaction zone

C_{gs} =Concentration of gas reactant at the outer surface of particle

C_{gr} = Concentration of gas reactant in the reaction zone

r_m = Distance from the centre of the particle to the boundary between reaction zone and product layer

C_{gm} =Concentration of gas reactant at the boundary between reaction zone and product layer

Figure 5.11 Schematic diagram of the concentration profiles just before commencement of the second stage.

The material balance equations and the initial conditions can be given as follows.

A differential mass balance in the product layer:

$$\frac{1}{r^2}\left(\frac{dr^2N_{CO}}{dr}\right) = 0 \qquad 5.55$$

Integration gives;

$$r^2N_{CO} = Q_4 \qquad 5.56$$

Inserting Fick's law results in:

$$-r^2D_{ef}\ C_g\left(\frac{dX_{CO,r}}{dr}\right) = Q_4 \qquad 5.57$$

Integration:

$$D_{ef}\ C_g\left(X_{CO,r}\right) = \frac{Q_4}{r} + Q_5 \qquad 5.58$$

Boundary conditions:

At $r = r_p\ X_{CO} = X_{CO,s}$

$r = r_m\ X_{CO} = X_{CO,m}$

Where $X_{CO,s}$ = mole fraction of carbon monoxide at the surface.

$X_{CO,m}$ = mole fraction of carbon monoxide at reacting interface (r_m)

Inserting the boundary conditions into equation 5.58 gives:

$$D_{ef}\ C_g\left(X_{CO,s}\right) = \frac{Q_4}{r_p} + Q_5 \qquad 5.59$$

$$D_{ef}\ C_g\left(X_{CO,m}\right) = \frac{Q_4}{r_m} + Q_5 \qquad 5.60$$

$$D_{ef}\ C_g\left(X_{CO,s} - X_{CO,m}\right) = Q_4\left(\frac{1}{r_p} - \frac{1}{r_m}\right) \qquad 5.61$$

$$Q_4 = \left(D_{ef}\ C_g\left(X_{CO,s} - X_{CO,m}\right)\right)/\left(\frac{1}{r_p} - \frac{1}{r_m}\right) \qquad 5.62$$

<u>In the inner core:</u>

Chemical reaction is still proceeding in the reaction zone and differential mass balance for diffusing species is:

$$\frac{1}{r^2}\left(\frac{d(r^2N)}{dr}\right) = -kS\rho C_g\left(X_{CO} - X_{CO_2}/K_e\right) \qquad 5.63$$

Inserting Fick's law results in:

$$-D_{ef}\ \frac{d(r^2C_g)\left(\frac{dX_{CO}}{dr}\right)}{dr} = -r^2kS\rho C_g\left(X_{CO} - X_{CO_2}/K_e\right) \qquad 5.64$$

Defining new variables:

$u_1 = rX_{CO}$ and $u_2 = rX_{CO_2}$

Differentiating and rearranging the terms yield:

$$\frac{d(r^2)\left(\frac{dX_{CO}}{dr}\right)}{dr} = rd^2u/dr^2 \qquad 5.65$$

Inserting equation (5.65) into (5.64) gives:

$$D_{ef}\ r\left(\frac{d^2u}{dr^2}\right) = \text{r}\ kS\rho(u_1 - u_2)/(K_e)) \qquad 5.66$$

Since

$X_{CO} + X_{CO_2} = 1$ and $u_1 + u_2 = r$

$$D_{ef}\ (\frac{d^2u}{dr^2}) = u_1(\frac{kS\rho}{D_{ef}})((K_e + 1)/(K_e)) - (\frac{kS\rho}{D_{ef}\ K_e})r \quad 5.67$$

And;

$$\frac{d^2u}{dr^2} - \tau u_1 = -\beta r \quad 5.68$$

Where, $\tau = \frac{kS\rho\left(\frac{(K_e+1)}{K_e}\right)}{D_{ef}}$ and $\beta = \frac{kS\rho}{D_{ef}\ K_e}$ Solving equation (5.68) results in:

$$u_1 = Q_6\ \cosh(\sqrt{\tau}\, r) + Q_7 \sinh(\sqrt{\tau}\, r) + \left(\frac{\beta}{\tau}\right) r \quad 5.69$$

And

$$X_{CO,r} = \frac{Q_6}{r} \cosh(\sqrt{\tau}\, r) + \frac{Q_7}{r} \sinh(\sqrt{\tau}\, r) + \left(\frac{\beta}{\tau}\right) \quad 5.70$$

Boundary conditions:

At r= r_m $X_{CO,r} = X_{CO,m}$

r=0 $d(X_{CO})/dr = 0$

From the second boundary condition

$$Q_6 = 0$$

And the first boundary condition

$$Q_7 = X_{CO,m} r_m - (\left(\frac{\beta}{\tau}\right) r_m)/ \sinh(\sqrt{\tau}\ r_m) \quad 5.71$$

Thus equation (5.70) can be rewritten as:

$$X_{CO,r} = (r_m/r) X_{CO,m} \sinh\left(\sqrt{\tau}\, r\right) / (\sinh(\sqrt{\tau}\ r_m) \quad 5.72$$

Rearranging the terms:

$$\frac{X_{CO,r}}{X_{CO,m}} = (\delta_m/\delta)(\sinh(\emptyset_f\, \delta)/(\sinh(\emptyset_f\, \delta_m)) \quad 5.73$$

Where

$$\delta_m = r_m/r_p$$

$X_{CO,m}$ is the molar fraction of carbon monoxide at the boundary of two zones at a radial position r=r_m in the particle.

Variation in the solid concentration in the reaction zone can be found by integration of the following equation:

$$\frac{dC_S}{dt} = -kS\rho C_g X_{CO,r} \quad 5.74$$

$$C_S = kS\rho C_g \int X_{CO,r}\, dt + Q_8 \quad 5.75$$

At t= t_f (end of first stage), $C_S = C_{sf}$; thus the integral vanishes and $Q_8 = C_{sf}$, then ;

$$C_S - C_{so} + C_{so}\ ((\sinh(\emptyset_f\ \delta)/(\delta\ \sinh(\emptyset_f) = -kS\rho \int_{t_f}^{t} X_{CO,m}(\ \delta_m/\delta)(\sinh(\emptyset_f\ \delta)/ \sinh(\emptyset_f\ \delta_m))\ dt \quad 5.76$$

and

And from equation (5.76) at $\delta = \delta_m$ and $C_{so} = 0$

$$\int_{t_f}^{t} X_{CO,m}((\ \delta_m)/(\sinh(\emptyset_f\ \delta_m))dt = C_{so}\delta_m/\ (\ kS\rho(\sinh(\emptyset_f\ \delta_m)) - C_{so}/(kS\rho(\sinh(\emptyset_f)) \quad 5.77$$

Substituting above equation into equation 5.76, the concentration distribution for solid reactant is obtained;

$$C_S = C_{so}[1 - \frac{\left(\frac{\delta_m}{\delta}\right)(\sinh(\emptyset_f\delta)}{\sinh(\emptyset_f\delta_m)}] \quad 5.78$$

Variation in the solid concentration is related to the variation in the core radius (r_m) as follows:

$$\frac{\Delta C_s}{\Delta t} = -kS\rho X_{CO,m} \quad 5.79$$

And

$$\frac{\Delta C_s}{\Delta r_m} = \frac{dC_s}{dr}\ |r = r_m \quad 5.80$$

From equation 5.79 and 5.80,

$$\frac{\Delta r_m}{\Delta t} = -kS\rho X_{CO,m}/\frac{dC_s}{dr}\ |r = r_m \quad 5.81$$

As Δt goes to zero, equation (5.81) becomes

$$\frac{dr_m}{dt} = -kS\rho X_{CO,m}/\frac{dC_s}{dr}\ |r = r_m \quad 5.82$$

Differentiation of equation (5.78) with respect to (r) gives:

$$\frac{dC_s}{dr}\ |r = r_m\ = C_{so}[1/r_m - \sqrt{\tau}\ \coth\sqrt{\tau}\ r_m) \quad 5.83$$

And inserting this into equation (5.82) yields:

$$\frac{dr_m}{dt} = -kS\rho X_{CO,m} r_m/(C_{so}[1\text{-}\sqrt{\tau}\, r_m \ \coth\sqrt{\tau}\ r_m) \quad 5.84$$

And using $\delta_m = \frac{r_m}{r_p}$ equation (5.84) can be rewritten as:

$$\frac{d\delta_m}{dt} = -kS\rho X_{CO,m} \delta_m/(C_{so}[1\text{-}\delta_m \emptyset_f \ \coth \emptyset_f\ \delta_m)) \quad 5.85$$

Contribution of this transition to the overall metallization process is very small, above analysis has been performed for mathematical purpose.

5.4.3 Mathematical analysis of the second stage of the metallization.

Mn_3O_4 has been completely reduced to manganous oxide once the inner interface reaches the center of the particle; the second stage starts at the outer interface at points of contact by the reaction:

$7MnO+10C=Mn_7C_3+7CO$ 5.86

The reaction is localized at the MnO/carbide interface as the solid carbon cannot diffuse in the oxide. The carbon is transported, either as carbide or as dissolved carbon to the reaction interface by diffusion through the molten or partially molten carbide layer. The carbide spreads over the particle surface and dissolves carbon, by which the metallization continues at the oxide/carbide interface.

Rewriting equation (5.85) for the second stage of the metallization at the outer interface;

$$\frac{d\delta_s}{dt} = -M_s/C_{S_2} r_p \quad 5.87$$

Where $\delta_s = r/r_p$

M_s , is the rate of Metallization between MnO and the carbide.

C_{S_2} , is the concentration of MnO after metallization of Mn_3O_4 to MnO completely.

From the stoichiometry of the reaction given below, one can deduce that C_{S_2} , is equal to $3C_{SO}$.

$Mn_3O_4 + CO = 3\ MnO + CO_2$ 5.4

Therefore;

$$\frac{d\delta_s}{dt} = -M_s/3C_{SO}\ r_p \quad 5.88$$

Integrating equation (5.88) gives:

$$\delta_s = -M_s / 3C_{SO}\, r_p \int dt \quad (5.89)$$

$$\delta_s = \frac{-M_s}{3C_{SO}\, r_p} t + Q_9 \quad (5.90)$$

And

$$\frac{r}{r_p} = \frac{-M_s}{3C_{SO}\, r_p} t + Q_9 \quad (5.91)$$

With initial condition t= t_f, r=r_p at start of second stage.

$$\frac{r}{r_p} = \frac{-M_s}{3C_{SO}\, r_p} t_f + Q_9 \quad (5.92)$$

$$Q_9 = 1 + \frac{M_s}{3C_{SO}\, r_p} \quad (5.93)$$

Substituting Q_9 into equation (5.90) and rearranging the terms:

$$\delta_s = 1 - \frac{M_s}{3C_{SO}\, r_p}(t - t_f) \quad (5.94)$$

Equation (5.94) gives the position of the outer interface during the second stage at time (t).

The time required for the reaction to complete both the first stage and the second stage, t_{tot}, can be found from equation (5.94) by letting δ_s=0, then

$$t_{tot} = t_f + (3C_{SO}\, r_p / M_s) \quad (5.95)$$

A dimensionless ratio of the time to complete the first stage to the time taken for complete metallization of MnO as a shrinking core can be defined as:

$$\theta_r = 3kS\rho C_g\, r_p / M_s \quad (5.96)$$

Where C_g is, already mentioned, total gas concentration. Letting the dimensionless time for the first stage of the metallization be θ_f, then equation (5.94) can be rewritten in dimensionless form:

$$\delta_s = 1 - ((\theta_r + 1)/(\theta_r))(\theta - \theta_f) \quad (5.97)$$

Where θ is dimensionless time and equal to (t/t_{tot}). The fractional conversion during the second stage, F_s, can be found from the following equation:

$$F_s = 1 + \delta^3{}_s\, F_f - \delta^3{}_s \quad (5.98)$$

Equation (5.98) is similar to that used by King and Brown [47] for impervious core reactions.

5.4.4 Application of mathematical model to the metallization data

For the first stage of metallization, parameters evaluated in Equation (5.39), are given in Appendix D. It can be seen that the only unknowns in the rate equation are $D_{ef}\ \sqrt{\tau}$ and M_f.

The value of M_f is best obtained from the slopes of the linear portions of the experimental metallization versus time curves. Table 5.1 and Table 5.2 summarize the slopes M_f, of the linear portions of each of the metallization versus time curves of manganese ore.

In Equation 5.39 with all other terms known, $D_{ef}\ \sqrt{\tau}$ can be calculated. The value of $D_{ef}\ \sqrt{\tau}$ was found to vary between $9.69 * 10^{-3}$ and $3.11 * 10^{-1}$ cm sec^{-1} in the temperature ranges from 1050°C to 1250 °C. To calculate effective CO - CO_2 diffusivities from the model equation using experimental data, it is needed to calculate $(\sqrt{\tau})$. To calculate $(\sqrt{\tau})$ the following procedure is followed:

$$\tau = (kS\rho/D_{ef}) \qquad 5.99$$

Multiplying both sides by $D_{ef}^{\ 2}$ and rearranging the terms gives:

$$\left(\frac{(D_{ef}\ \sqrt{\tau})^2}{kS\rho}\right) = D_{ef} \qquad 5.100$$

The term in numerator $(D_{ef}\ \sqrt{\tau})^2$ in equation (5.100) is evaluated from the rate equation (Equation 5.39) as mentioned above. The terms in the denominator of Equation (5.100) is calculated through the relationship by using Equation (5.52):

$$kS\rho = C_{so}/t_f C_g \qquad 5.101$$

Known values for C_{so}, C_g and t_f are inserted in equation 5.101 and the time at the end of the first stage which is determined as about 30 minutes from the kinetic curves, XRD and EDAX studies. The values of effective CO-CO_2 diffusivities generated by the model were found to lie in the range from $1.45*10^{-6}$ cm^2sec^{-1} to $8.43*10^{-6}$ cm^2sec^{-1} (Appendix D, Table D3 and Table D 4), which are much lower than the intermolecular diffusivities calculated by using the theoretical equation based on the kinetic theory and Lennard-Jones expression for intermolecular forces (TableD2 Appendix D). It can thus be deduced that in the present study Knudsen diffusivity is the predominant mode of diffusion, with molecular diffusion playing a very minor role. Diffusive flux occurs via two diffusional processes: molecular diffusion and Knudsen diffusion in porous media. In most of the cases reported by previous investigator [101], Knudsen diffusivities values were several orders lower than those of molecular diffusivity. Because the effective diffusivity values generated by the model are so much lower than the molecular diffusivity values, it can be assumed that in this case Knudsen diffusion is the predominant mode of

diffusion. The value of Knudsen diffusivity calculated for the present study is $2.76*10^{-6} cm^2 sec^{-1}$ at 1100°C(see Appendix D) which is in reasonable agreement (considering the temperature difference) with the value for Knudsen diffusivity calculated by Grimsley[32] for the ordinary carbothermic reduction of Mamatwan manganese ore at 1300°C which is $3.03*10^{-4}$ $cm^2 sec^{-1}$. Grimsley [32] also calculated the effective CO-CO_2 diffusivities which were in the range from $7.9*10^{-5}$ $cm^2 sec^{-1}$ to $1.59*10^{-4}$ $cm^2 sec^{-1}$. He attributed these values to the major role played by Knudsen diffusion. The values of effective diffusivities generated by the present model, which is already mentioned above, seem in line with the values calculated by Grimsley [32] which can also be attributed to the dominant role played by Knudsen diffusion during the first stage of the metallization. Moreover, it has been pointed out by Vinters and Turkdogan [117] that diffusivity ratio of D_{ef}/D_{12} is a property of a given porous material and characterizes the pore structure. The ratio of the effective CO-CO_2 diffusivity to molecular diffusivity may be used as a test to understand whether the process is being controlled by Knudsen diffusion or molecular diffusion. Where Knudsen predominates, values of D_{ef}/D_{12} will be low. In the present study, the ratio of the effective CO-CO_2 diffusivity to molecular diffusivity was found to be $2.40*10^{-5}$ and $1.25*10^{-4}$ at temperatures 1050 °C and 1250°C respectively. Vinters and Turkdogan [117] stated that as the reduction temperature decreases pore structure becomes much finer, presumably with many channels on connected capillaries. As the reduction temperatures decreases, the ratio becomes smaller which results in much finer pore structure, hence an indication of predominant Knudsen diffusion. On the other hand, the pore structure becomes coarser with an increase of reduction temperature bringing about easy passage through the pores, i.e. higher values of D_{ef}/D_{12}.

Effectiveness factor given in equation 5.45 for the first stage of the Metallization was calculated. Effectiveness factor is a measure for relative contributions of chemical reaction control. It is defined as the ratio of the chemical reaction resistance to the total resistance consisting of the diffusional resistance and chemical resistance. Calculated values of the effectiveness factor are in very good agreement with the experimentally determined metallization percentages for the first stage of the metallization of the Mamatwan ores, and in turn give fractional conversion at the end of the first stage by using Equation 5.47. Predicted and experimental metallization percentages at the end of the first stage were within 5 percent (Figure 5.12-5.15).

By studying the nature of the plots of metallization versus dimensionless time and applying experimental data for model prediction using equation 5.47 and equation 5.98 all experimental data reduces to a single line. These plots are given as Figure 5.12 to 5.15 for Mamatwan ore. From the plots we can see that first stage of metallization is between 0-63 percent metallization levels and there is slight difference between experimental and predicted curves which is probably due to inadequacy of the assumptions that the effective diffusivities of CO and CO_2

are equal and also constant at a given temperature. In addition to these in the definition of kinetic–diffusion modulus($\emptyset_f$), the pores are assumed to be uniform in cross sections and surface area remains unchanged throughout the process. These assumptions may have caused discrepancies between the model prediction and experimental data.

Using equation 5.98 model predictions of metallization percentages during the second stage of metallization, F_s, can be found. In order to determine F_s, one needs to determine the dimensionless radius during the second stage of metallization which is δ_s. In equation 5.47, F_f , is the fractional conversion at the end of the first stage which was predicted during the first stage of the metallization. In order to determine δ_s certain key parameters such as time to complete conversion ($t_{tot.}$) and dimensionless time taken for complete conversion of MnO as a shrinking core (θ_r) had to be estimated by using the experimental data of the metallization during the second stage. The time to complete conversion was estimated by using the experimental values for the degree of metallization during the second stage in equation 5.95 to get δ_s values which were later used in equation 5.97, where t_f is the time taken to complete the first stage which was taken as 30 minutes. These were then used to determine the rate of metallization during the second stage, (M_s). M_s value changed between $1.83*10^{-8}$ mol.sec^{-1}.cm^{-2} and $8.55*10^{-8}$ mol .sec^{-1}.cm^{-2}. Specific rate constant values for the second stage (k_s) varies from $5.53*10^{-6}$ cm/sec to $3.16*10^{-5}$ cm/sec which are much smaller than specific rate constant for the first sage of reduction (K_f), which varied from $1.64*10^{-4}$ cm/sec to $1.15*10^{-4}$ cm/sec, as the rate of second stage of the reduction is much slower than the rate of the first stage.

The value of M_s estimated was then used in equation 5.94 from which the time to complete conversion can be predicted. These values were later inserted in equation 5.96 and equation 5.97 to predict the parameter, θ_r and δ_s which were used to calculate the value of F_s. During the second stage, as can be seen from the Figures 5.12 - 5.15, it was felt that the shape of the experimental curves could be duplicated with a maximum difference between the experimental and predicted values being about 5 percent. This is probably due to inadequacies of the assumptions that the particle shape is spherical and from the inadequacy of their sizing. The following section summarizes the limitations of the developed model.

5.4.5 Limitations of the developed model.

While developing the model which would represent the experimental metallization data few assumption were made and also certain parameters were estimated by using some of the experimental observations. The main assumptions were the presence of two distinct stages in the metallization process, existence of isothermal conditions throughout the reactions, equality of the effective diffusivities of CO and CO_2 in the interior of the particle.

The parameters estimated were θ_r , dimensionless ratio for the reaction rates of the first and second stages and $\sqrt{\tau}\, D_{ef}$ which was calculated from the slope of the metallization versus time curves in the first stage of the metallization. In the mathematical analysis quasi-stationary approximation was also contained and Wen [125] examined the accuracy of the mathematical practicability of the quasi stationary approximation. He showed that except for systems with extremely high pressure and very low solid concentration, quasi-stationary approximations were a good assumption for most solid-gas reaction systems. Therefore, the quasi-stationary approximation is found to be appropriate for the model under discussion.

Although the theoretically derived metallization curves fit the experimental curves reasonably well, there are deviations which may have a number of explanations. A major cause for the lack of complete agreement between theoretical and experiment results may lie in the complex mineralogy of the ore as well as the rather complex gas mixture actually existing including not only CO and CO_2 but also hydrogen, methane and argon. Several basic assumptions were made regarding the effective diffusivities of CO and CO_2 which may have had much to do with the deviations from the model. Iron oxide in the ores was assumed to reduce very quickly to metallic state and for simplicity iron oxide was assumed to behave similarly to manganese oxide. On the other hand, the differences in metallization of these two oxides may have an effect. The effective diffusivities of CO and CO_2 were not only assumed to be equal, but also to be constant for a given temperature. These assumptions were necessary to keep the mathematics relatively uncomplicated. The assumption that the carbon in the metallized layer was uniformly distributed throughout the layer at all times, may also account for some of the differences between the experimental and theoretical curves. Thus there was assumed to be no depletion of carbon at the mixed carbide/MnO interface, but this is easily justifiable due to the continuous precipitation of high activity carbon from the gas phase, however replenishment of carbon after reaction at the interface would require diffusion of carbon through the metal to the interface. The model should therefore be regarded as a useful simplification for data analysis to describe the metallization mechanism of Mamatwan ore.

It was assumed in the development of the model that the particles are uniform in size and spherical. To prepare spherical particles in this system is impossible; so it was assumed that the

pulverized material was spherical, which might not be a good assumption since the particles are irregularly shaped. The initial surface area of sample of irregularly shaped particles will be larger than if the sample were made up of spheres. The model also assumes that the particles are of uniform particle size which might not be case always.

In the previous work done[1,112,114,115,116,120] on similar topic, in order to eliminate difficulties arising from dealing with the complex mineralogy of naturally occurring ores, most of the mathematical models describing the metallization of oxides have been developed for synthetically prepared pure oxides and most of the previous models developed were not successful in fitting the experimental data for high percentage of metallization. Therefore the aim of this mathematical analysis has been to describe the metallization kinetics of an actual single manganese oxide ore particle, taking into account, all resistances affecting the process as far as possible.

Further improvement on the model or, the possibility of alternate acceptable mechanisms is not precluded, although the present model shows a considerable improvement over previous work [1,112,114,115,120]. In future work testing of this mathematical analysis on synthetically prepared pure oxides is recommended.

5.5 Experimentally determined Metallization rate values for the first stage of the metallization

The value of M_f is obtained from the slopes of the linear portions of the experimental metallization versus time curves. Table 5.1 and Table 5.2 summarize the slopes M_f, of the linear portions of the metallization versus time curves of manganese ore.

Table 5.1 Experimentally determined Metallization rate values for the first stage under 10 % CH_4 in Ar and H_2 atmospheres.

M_f , % per minutes				
	1050 ^oC	1100 ^oC	1200 ^oC	1250 ^oC
10 % CH_4 in Ar	0.7	1.0	2.33	2.10
10 % CH_4 in H_2	2.1	1.5	1.83	1.33

Table 5.2 Experimentally determined Metallization rate values for the first stage under 30 % CH_4 in Ar and H_2 atmospheres.

M_f , % per minutes				
	1050 ^oC	1100 ^oC	1200 ^oC	1250 ^oC
30 % CH_4 in Ar	0.83	2.1	2.2	2.0
30 % CH_4 in H_2	1.73	1.83	1.43	1.3

In Equation 5.39 these value of M_f are used with all other terms known, $D_{ef}\sqrt{\tau}$ can be calculated. The value of $D_{ef}\sqrt{\tau}$ was found to vary between 9.69* 10^{-3} and 3.11 * 10^{-1} cm sec^{-1} in the temperature ranges from 1050^{o}C to 1250 ^{o}C(as discussed in section 5.4.4)

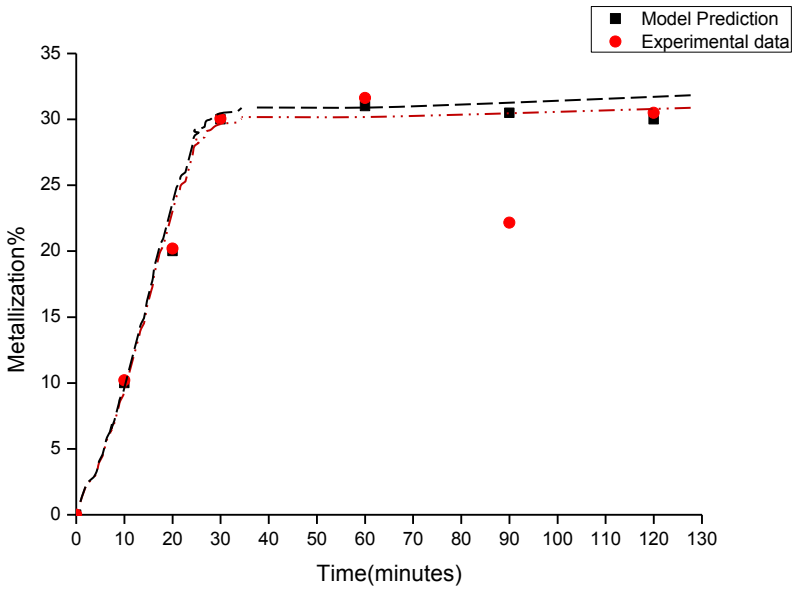

Figure 5.12 Model prediction compared with experimental data for 10 % CH_4 in Ar at 1100^{o}C

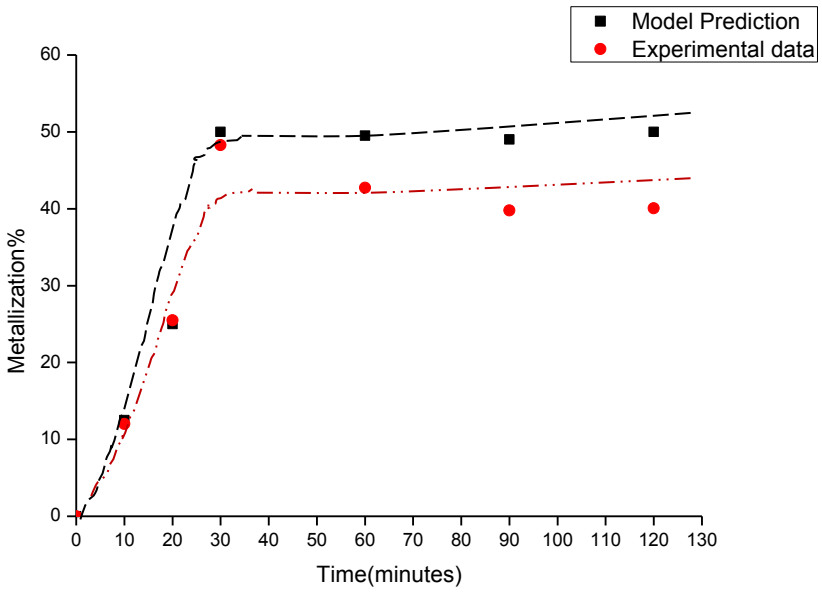

Figure 5.13 Model prediction compared with experimental data for 10 % CH_4 in H_2 at 1100^{o}C

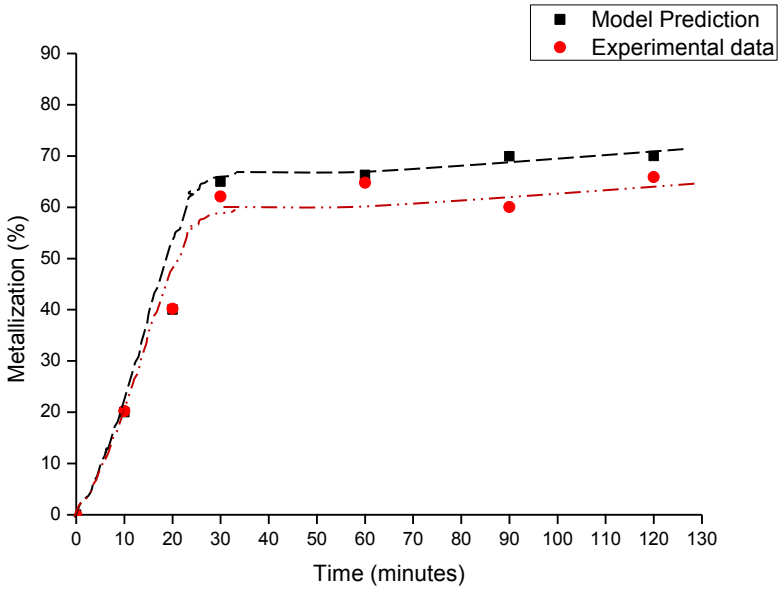

Figure 5.14 Model prediction compared with experimental data for 30 % CH_4 in Ar at 1100^{o}C

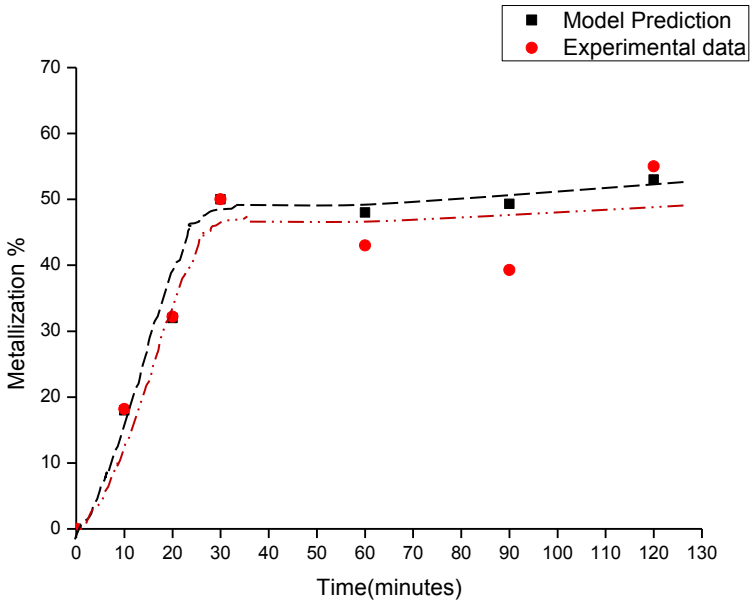

Figure 5.15 Model prediction compared with experimental data for 30 % CH_4 in H_2 at 1100^{o}C

CHAPTER 6

CONCLUSIONS

In this study hydrocarbon reduction of manganese ore was studied. Reduction mechanism and rate controlling steps were proposed. The summary and conclusions are outlined below.

6.1 SUMMARY

1. Methane is a better reductant as it can reduce manganese ore in the solid state at lower temperatures then ordinary carbothermic process resulting in energy savings and lower carbon footprints.
2. Methane gas cracked, precipitating high activity solid carbon and hydrogen gas promoting lower temperature reductions at a fast rate compared to ordinary carbothermic reduction.
3. (a) CH_4 (g) = C (s) + $2H_2$ (g) ΔH^o = -74.85 kJ, cracking of methane is exothermic while (b) CO_2 (g) +C(s) =2CO (g) ΔH^o = +172.47 kJ, Boudouard reaction maintaining reducing conditions in ordinary carbothermic processes is endothermic.
4. Solid carbon precipitating from the gas phase was discussed to have high thermodynamic activity in the form immediately after cracking of methane, restoring promptly the reducing gases CO and H_2 at the reaction site. Hence, from a thermodynamic point of view, the presence of the carbon ensures a very low oxygen potential at the reaction site.
5. Reduction/metallization of Mamatwan manganese ore through the use of methane gas is principally a carbothermic reduction possibly assisted by hydrogen gas. This is due to cracking of methane into very fine sized particles of very high activity carbon as well as hydrogen gas at temperatures above approximately 550^{o}C in the presence of a solid phase. Although hydrogen is kinetically a fast reductant, thermodynamically hydrogen gas cannot reduce MnO to metal but can reduce iron oxide components and higher manganese oxides into MnO. However due to very high thermodynamic activity of carbon it dominates the reduction and is potentially assisted by hydrogen in the early stages in the reduction of iron oxides and higher manganese oxides.
6. The bulk of the metallization occurred within the first 30 to 40 minutes and the reaction reached a reduction maximum at 73% metallization at 1200^{o}C.

7. The maximum 73% metallization was achieved in a methane/argon gas mixture at 1200°C in less than 2 hours. The extent of reduction as well as the Mn/Fe ratios in the resulting alloy were higher than those in ordinary carbothermic solid-state reduction at these temperatures, indicating the simultaneous reduction of Fe and Mn due to a low oxygen potential set up by the methane bearing gas mixtures.
8. CH_4 in Ar had somewhat higher reduction rate in most cases (Table 5.1 and 5.2).
9. From the morphological evidence of this current study, it appeared that the metallization was mostly on the surface of the particles and at high temperature some melting was observed.
10. The sequences of phase change detected by XRD when compared with other studies were found to be similar.
11. The S.E.M images revealed the product metallic phase occurring throughout the surface.
12. The changing of CH_4 concentration had limited effect on changing the kinetic rate and extent of reduction.
13. CH_4 is thermodynamically unstable at the temperatures of these experiments. This, and the catalytic effect that the presence of solid oxide phase and freshly formed carbide and metal has on CH_4 cracking at these temperatures make it highly unlikely that CH_4 would partake directly in the reduction of the oxide but rather would dissociate providing solid carbon and H_2 gas.

    a) CO and H_2 was regenerated due to the presence of high activity carbon deposited everywhere on the particle and crucible. The reduction reactions thus were mainly CO based since thermodynamically hydrogen cannot reduce MnO.

    b) Three important variables in Mamatwan ore reduction were CH_4 concentration (affecting the thermodynamic activity of carbon), type of carrier gas and temperature. Time was less important, after 30 minutes for most of the tests metallization leveled off.

    c) The study proposed a reduction sequence based on the observations of kinetics, XRD and S.E.M-E.D.S analyses.

    d) The proposed reduction mechanism is in line with the morphological and kinetic observations of this study.
14. For this study a mathematical model was developed. It was seen that metallization of Mamatwan ore proceed in two stages as was deduced from examination of the partially reduced/metallized samples.

    Stage 1: The reduction of the higher oxides to MnO, metallization of iron and start of metallization of manganese.

Stage 2: The slow, long and partial reduction of MnO and any remaining oxide to mixed carbide of iron and manganese and growth of the carbide phase covering the surface of the partially reduced ore particles.

15. The bulk of metallization occurs within approximately the first 30-40 minutes. For the described mechanism the first stage is confined to approximately 30 minutes due to the almost straight line behaviour of the kinetic plots for this period. The first stage is primarily the reduction of iron oxides to metallic state and reduction of higher manganese oxides to MnO mainly by high activity carbon and assisted by kinetically fast hydrogen, the second stage is the partial carbothermic reduction of MnO and any remaining oxide to mixed iron-manganese carbide by high activity carbon precipitating from the gas mixture. During this stage the carbide phase grows and eventually covers the surface of the partially reduced ore particles. Very fine sized particles of the precipitating high activity carbon eventually covers the partially reduced/metallized ore particles hindering the diffusion of reducing CO gas, and converts into unit activity graphite as a result of which reduction/metallization virtually comes to an end.
16. The experimental initial rate which corresponds to the first stage of metallization, were evaluated as slopes of metallization versus time curves the logarithm of which were plotted with respect to inverse temperature. The activation energy obtained by this method in the temperature range of 1050 ^{o}C to 1250 ^{o}C varied from 1.47 kJ/mol to 24.72 kJ/mol, indicating possibility of diffusional control.
17. The values of effective CO-CO_2 diffusivities generated by the model were found to lie in the range from $1.45*10^{-6}$ cm^2sec^{-1} to $8.43*10^{-6}$ cm^2sec^{-1} (Appendix D, Table D3 and Table D4), which are much lower than the intermolecular diffusivities calculated by using the theoretical equation based on the kinetic theory and Lennard-jones expression for intermolecular forces (Table D2 Appendix D).
18. The value of Knudsen diffusivity calculated for the present study is $2.76*10^{-6}$ cm^2 sec^{-1} at 1100^{o}C(see Appendix D) .
19. As the effective diffusivity values generated by the model are much lower than the molecular diffusivity values, it can be assumed that in this case Knudsen diffusion is the predominant mode of diffusion.
20. In the present study, the ratio of the effective CO-CO_2 diffusivity to molecular diffusivity was found to be $2.40*10^{-5}$ and $1.25*10^{-4}$ at temperatures 1050^{o}C and 1250^{o}C respectively.
21. During the second stage, as can be seen from the Figure 5.12 - 5.15, it was felt that the shape of the experimental curves could be duplicated reasonably well with a maximum difference between the experimental and predicted values being about 5

percent. This is probably due to inadequacies of the assumptions that the particle shape is spherical and from the inadequacy of their sizing.

22. The values of rate of metallization during the second stage, (Ms) changed between $1.83*10^{-8}$ mol.sec^{-1}.cm^{-2} and $8.55*10^{-8}$ mol.sec^{-1}.cm^{-2}.
23. Specific rate constant values for the second stage (ks), varied from $5.53*10^{-6}$ cm/sec to $3.16*10^{-5}$ cm/sec which are smaller than specific rate constant for the first stage of reduction (K_f), which varied from $1.64*10^{-4}$ cm/sec to $1.15*10^{-4}$ cm/sec, as the rate of second stage of the reduction is slower than the rate of the first stage.

6.2 CONCLUSIONS.

This study investigated the use of different concentrations of methane gas in hydrogen and in argon as the reducing gas mixture for a better understanding of the reduction behavior of manganese ore at different temperatures (1050^{o}C to 1250 ^{o}C).

This study has described the reduction mechanism and the rate controlling steps toward the development of practical and economic method for pre–reducing manganese ore that maximizes efficiency and recovery of Fe and manganese from Mamatwan ore.

Generally, CH_4 was an effective indirect reductant because it supplied both high activity solid carbon and H_2 gas to the reaction site. Methane gas is unstable at high temperatures especially in the presence of a solid phase and effortlessly cracks, and was an effective means of providing the reaction sites with fresh supply of reductants. In – situ formed carbon from CH_4 cracking, in its atomic form with thermodynamic activity well above unity (depending on temperature and CH_4/H_2 ratio of the gas phase), ensured the rapid regeneration of the reductants CO and H_2 from CO_2 and H_2O maintaining a low reduction potential in gas phase, promoting lower temperature reduction/metallization at a faster rate compared to ordinary solids state carbothermic reduction.

Diffusional rate control for the process is proposed from the values of activation energy calculated and from the experimentally determined kinetics values using mathematical model.

6.3 Recommended further work .

The optimisation of the reducing conditions using CH_4 in a gas mixture at several temperatures should be studied. It should be noted that the optimum gas mixture may also be a function of temperature. It is not expected that the same gas mixture applies

throughout the reducing temperatures, where a shift in temperature will cause a shift in reducing potential due to a change in the activity of carbon precipitating from the gas which may cause a change in the rate controlling step affecting the particle morphologies being setup and hence a significant change in metallization rate and extent. Moreover depending upon the nature and particle size of ore the potential type of reactor should be examined and hence the study can be extended to a small pilot scale test work using potentially a rotary kiln or a fluidized bed reactor for feasibility. Obviously a complete mass and energy balance is required.

REFERENCES.

[1] Antonov, V. K. and Chufarov, G. I. (1961) "Reduction of MnO by solid carbon", Tr. Inst. Met. Akad. Nauk SSSR, Uralsk. Filial, 7, pp. 101-105.

[2] Anacleto, N, Ostrovski, O. and Ganguly, S. (2004) "Solid state reduction of manganese oxides by methane -containing gas", ISIJ International, 144, pp. 1480-1487.

[3] Ashin, A.K, Rostovtsev, S.T. and Avdeev, V.F. (1964) "Kinetics and mechanism of the reduction of manganese oxides with Carbon .III. Reduction of manganous oxide", Izv. VYSSH. Uchen. Zavedenii, Chern .Met, vol.7, no.10, pp. 13-16.

[4] Alekseev, V.F, and Shvartsman, L.A. (1961) "The Free energy of formation of Manganese carbide $Mn_{23}C_6$", Dokl. akad. Nauk. SSSR. vol.141, no.2, pp. 346-348.

[5] Barmin, L.N. (1968) "Kinetics of manganese oxide reduction by carbon of Iron-Manganese –carbon melts", IZV.an, SSR, Metally, no.2, pp. 71-77.

[6] Barmin, L.N. (1968) "Kinetics of reduction of solid manganese II oxide by iron-manganese- carbon melts", Fiz. Khim. Osn. Proizvod. Stali, pp. 406-411.

[7] Benz, R, Elliot, J.F. and Chipman, J. (1973) "Thermodynamics of Solid phases of the Mn-C system", Met. Trans, vol.4, pp. 1449-1452.

[8] Benz, R. (1974) "Thermodynamics of the Fe-Mn-C from Solid state EMF Measurements", Met. Trans., vol.5, pp. 2217-2224.

[9] Burucu, E. and Eric, R. (1991) "Kinetics and mechanism of the reduction of mamatwan manganese ore fines by solid carbon", M.Sc. (dissertation), University of the Witwatersrand, Johannesburg.

[10] Bystrom, A. and Mason, B. (1943) "The crystal structure of braunite", Arkiv.kemi.Min.Geol, vol.16, pp. 133-146.

[11] Coetsee, T, Zietsman, J. and Pistorius, C. (2014) "Predicted effect of ore composition on slag formation in Manganese ore reduction". Mineral Processing and Extractive Metallurgy. Transaction of the Institutions of Mining and Metallurgy, vol.123, no.3, pp.141-147.

[12] Cem, A. and Ahmet, G. (2008) "Optimization of conditions to produce Manganese and iron carbides from Denizli-Tavas manganese ore by solid state reduction", Turkish Eng. Env. Si 32, pp. 125-131.

[13] Cardakli, I.S, Naci, S. and Tayfur, O. (2011) "Production of high carbon Ferro manganese from a manganese ore located in Erzincan", Turkish J. Eng. Env. Sci., 35, pp. 31-38.

[14] Davies, M.W. and Richardson, F.D. (1959) "Non–stoichiometry of manganous oxide", Trans. Farad. Soc, vol.55, pp. 604-610.

[15] De Villiers, J.P.R. (1975) "The crystal structure of braunite with references to its solid solution behavior", Am.Min, vol.60, pp. 1098 -1104.

[16] De Villiers, J.P.R. (1971) "The geology and mineralogy of the Kalahari Manganese field, north of sishen, Cape provinces". Geol .Survey Memoir, no.59, pp. 1-84.

[17] De Villiers, J.P.R. (1973) "A mineralogical investigation of natural and heated Mamatwan manganese ore, Johannesburg". NIM, technical memorandum, no.1, 12pp.

[18] DeVillers, J.P.R. (1977) "A mineralogical Investigation of Mamatwan and Wessel Manganese ores", NIM Report- No.1920, 10pp.

[19] Dewar, K. and See, J.B. (1978) “The influence of carboneous reducing agents on the rate of reduction of representative manganese and chromium ores”, NIM, Report- No .1968.
[20] Dong-Yuk Kim, Hyun-Soo Kim and Sung-Mo Jung. (2015) “Production of (Mn, Fe)-carbide containing low phosphorous by carbothermic reduction of Mn oxide and Fe oxide”, ISIJ International, vol.55, no.3, pp.504-512.
[21] Dressel, W.M. and Kenworthy, H. (1961) “Thermal behavior of manganese minerals in controlled atmosphere”, U.S Bureau of Mines, Report of investigation 5761, pp. 4-15.
[22] Dubois, P. (1934) “Hydrate et Varieties Allotropiques Duo Sesquioxyde de Manganese”, Comptes Roudus, vol.199, pp. 1416-1418.
[23] EL-Gawad, Hala H, Hussiny, N.A, Mohamed F.M. and Shalabi,M.E.H. (2015) “Reduction of low grade Egyptian Manganese ore via hydrogen at 750^{o}C-950^{o}C”, International Journal of Scientific and Engineering Research,no.5,vol.6.pp.339-346.
[24] Eric, R.H, Hejja, A.A. and Stange, W. (1991) “Liquidus temperature and Electrical Conductivities of synthetic Ferromanganese slags”, Minerals Engineering, vol.4, No.12, pp. 1315-1332.
[25] Featherstone, R.A. (1974) “Application of Mawatwan Manganese ore”, Infacon 1, Glen, H. (ed), Johannesburg, SAIMM, pp. 263 -273.
[26] Gericke, W.A. (1989) “The establishment of a 500.000 T/A sinter plant at Samancor’s Mawatwan manganese ore fines”,Proceedings.Infacon-5, vol1.1, 5th International Ferroalloy Congress, held at New Orleans, Louisiana, USA, April, 1989, pp. 24 -33.
[27] Glasser, F.P. (1958) “The system MnO-SiO_2”, Am. J. Sci., vol.256, pp. 398-412.
[28] Glasser, F.P. (1962) “The Ternary system CaO-MnO-SiO_2 ”, J. of Am. Ceramic. Soc. vol.45, no.5, pp. 242-249.
[29] Glasser, F. P. (1961) “The system Ca_2SiO_4-Mn_2SiO_4 ”, Am. J. Sci., vol.259, pp. 46-49.
[30] Gokhan, C. and Kenan, Y. (2014) “Carbothermal reduction of calcined and mechanically activated manganese carbonate ore”, Turkish Online Journal of Science & Technology.
[31] Gosh, D, Roy, A.K. and Ghosh, A. (1986) “Reduction of ferric oxide pellets with methane”, Transactions ISIJ, vol.26, pp. 186-193.
[32] Grimsley, W.D. (1977) “A study of the characteristics and mechanism of reduction of manganese ore by solid carbon”, M.Sc. Dissertation, University of the Witwatersrand.
[33] Grundy, A.N, Hallstead, B. and Gauckler, L.J. (2003) “Assessment of the Mn-O System”, Journal of Phase Equilibria, vol.24, no.1, pp. 21-38.
[34] Gudenau, H.W. (1980) “Investigations on Carbon deposition due to methane and carbon monoxide decomposition at high temperatures in direct reduction processes” (translation), Arch. Eisenhuttenwes, vol.51, no.12, pp. 493-499.
[35] Guven.A. (1992) “Kinetics and mechanism of the solid state carbothermic reduction of Wessel type Ferro manganese ores”, Ph.D. thesis, University of the Witwatersrand.
[36] Hahn, W. C. and Muan, A. (1960) “Studies in system Mn-O. The Mn_2O_3-Mn_3O_4 and MnO equilibria”, Am. J. Sci., vol.258 (1), pp. 66-78.
[37] Halim, K.S.A. (2007) “Isothermal reduction behavior of Fe_2O_3/MnO composite materials with solid carbon”, Materials Science and Engineering A 452-453, pp. 15-22.Ellsevier.
[38] Henderson, G. and Slatter, D. (1985) “Low- Temperature Pre – Reduction of Chromites Fines with Hydrocarbon Gases”, R & D. Report 12, Gencor Proceeds Research, S.A.
[39] Habashi, F. (1980) Principles of extractive Metallurgy, vol.1, pp 195-202.

[40] Hooper, R.T. (1975) “The Optimum Utilization of Raw materials in Manganese smelting”, Infacon 1, Johannesburg, South Africa, pp. 101-105.
[41] Hooper, R.T. (1967) “The production of Ferromanganese”, Electric furnace Proceedings .Met.soc. AMIE, vol.25, pp. 141-145.
[42] Hussiny, N.A.EL, Gawad .H, Marwa. A. and Shalabhi. M. (2015) “Reduction of low grade Egyptian Manganese ore by carbon of coke breeze in the briquette form”, Journal of multidisciplinary Engineering Science and Technology ISSN: 3159-0040, vol.2, Issue 1, pp. 77-82.
[43] Ishak, R. (2002) “Reaction kinetics for reduction of manganese ore with carbon monoxide in presence of carbon”, Ph.D. thesis, Norwegian University of Science and Technology, Faculty of Natural Science and technology, Department of Materials Technology.
[44] Ishida, M. and Wen, C.Y. (1968) “Comparison of Kinetic and diffusional models for Solid –Gas Reactions”, AICHE Journal, vol.14, no.2, pp. 311-317.
[45] Jones, R. and Meichack, K. (1990) “Thermo. Software for thermodynamic calculations”, Council for Mineral Technology, Pyro metallurgy Division.
[46] Kawasaki, E, Sanscrainte, J. and Walsh, T.J. (1962) “Kinetics of reduction of Iron oxide with Carbon Monoxide and Hydrogen”, AICHE.Journal, vol.8, no.1, pp. 48-52.
[47] King, R.P. and Brown, C.P. (1980) Met. Trans, vol.11b, pp. 585-592.
[48] Klingsberg, O.P. (1968) “The mechanism of reduction of metals from their oxides by carbon”, Mekh.Kinet. Vosstanov, Metal.Mater.SIMP. (Nim translation no.244), pp. 40-48.
[49] Klingsberg, C. and Roy, R. (1960) “Solid –Solid and Solid Vapour reactions and a new phase in the system Mn-O”, J. Am. Ceramic .Soc., vol.43, no.12, pp. 620-626.
[50] Kouraris, A, Kleyenstuber, A.S.E .and Finn, C.W.P. (1983) “A mineralogical investigation of the reduction of Mawatwan manganese ore with carbon”, Spec. publ. Min. Metal. Inst. S.A, 7, pp. 375-382.
[51] Koursaris, A. and See, J.B. (1975) “Reactions in production of high carbon ferromanganese from Mawatwan Manganese ore”, Nim. Report- No 1975.
[52] Kohl, H. K. and Engell, H.J (1963) “Uber die reduktien van wustit mit wasserstoff, Arch.Eisenhutenwes”, 34. pp 411-418.
[53] Kolchin, O.P. (1968) “The Mechanism of reduction of Metals from their Oxides by Carbon”,Mekhn. Kinet.Vosstanov, Meatl. Mater-Simp. (NIM translation No. 244), pp. 40-48.
[54] Kononov, R, Ostrovski, O. and Ganguly, S. (2008) “Carbothermal reduction of manganese oxide in different gas atmosphere”, Metallurgical and Materials Transactions B, 39B, pp. 662-668.
[55] Kononov, R, Ostrovski, O. and Ganguly, S. (2009) “Carbothermal solid state reduction of manganese ores: 1, Manganese ore characterization”, ISIJ International, 49(8), pp. 1099-1106.
[56] Kononov, R, Ostrovski, O. and Ganguly, S. (2009) “Carbothermal solid state reduction of manganese ores: 2. Non-isothermal and isothermal reduction in different gas atmosphere”, ISIJ International, 49(8), pp. 1107-1114.
[57] Kononov, R, Ostrovski, O. and Ganguly, S. (2009) “Carbothermal solid state reduction of manganese ores: 3, Phase Development”, ISIJ International, 49(8), pp. 1115-1122.

[58] Kor, G.J.W. (1978) "The Thermal decomposition of Mn_2O_3 and the reduction of Mn_3O_4 by C and CO", Metallurgical Trans., vol.9B, pp. 307-311.
[59] Kubaschewski, O, Evans, E, LL. and Alcock, C.B. (1974) "Metallurgical Thermochemistry", 4th ed. Pergamon Press, Oxford.
[60] Kuo, K. and Persson, L.E. (1954) "A contribution to the constitution of the ternary System Fe-Mn-C", J. Iron Steel Inst., vol.178, pp. 39-44.
[61] Kukhtin, B.A. (1969) "Kinetics of reduction of Manganese from Molten slags by solid carbon", Izv. Akad. Nauk. SSSR Metallii No. 1, pp. 119-124.
[62] Lee, Hae-Geon. (2012) "Materials Thermodynamics with Emphasis on Chemical Approach" World Scientific Publishing Co., pp.221.
[63] Linstad, T. and Stalheim, L. (2001) "Kinetics of gaseous reduction of manganese ores" Infacon IX, Quebec, Canada, pp. 223-229.
[64] Mah, A.D. (1960) "Thermodynamic properties of Manganese and its Compounds", Washington, U.S. Dept. of interior, Bureau of Mines.
[65] Manoj, K, Ranganathan, S. and Sinha, S.N. (2007) "Kinetics of reduction of different Manganese ores", Infacon XI, pp. 241-246.
[66] Maier, C.G. (1934) "Manganese, its occurrence, milling and metallurgy", U.S.B.M Info. Circ. No.6769, pp. 68.
[67] Martins, K.O. and Senk, D. (2008) "Direct reduction of mixtures of Manganese ore and Iron ore.", Steel Research International 79(11), pp. 811-816.
[68] Massalski, T.B. (1986) "Binary Alloy Phase Diagrams, American Society of Metals", vol.1, pp.558-575.
[69] Mehta, S.R. and Richardson, F.D. (1965) "Activities of Manganese Oxide and Mixing Relationships in silicate and aluminate melt", J.Iron and steel Inst., vol.203, pp. 524-528.
[70] McCabe, C.L. and Hudson, R.G. (1957) "Free Energy of Formation of Mn_7C_3 from Vapor Pressure Measurements", Trans. Met. Soc. Amie, vol.209, pp. 17-19.
[71] McMurdie, H.F. and Golovato, E. (1948) "Study of modifications of Manganese Dioxide", Nat.Bur.standards jour. Research, vol.41, pp. 589-600.
[72] McRae, B. L. (1981) "The Pre-reduction of Mamatwan-type ores", NIM. Report - No 2020, 11pp.
[73] McRae, B.L. (1977) "Proc. Of the Inst. Symp .on Agglom", 2nd, Atlanta, Ga, Mar.6-10, publ. Amie, vol.1, pp. 356-377.
[74] Millar, R.W. (1928) "The specific heats at low Temperatures of Manganous oxide, Manganous - manganic oxide and Manganese di oxide", Am. Chem. Soc. Jour., vol.50, pp. 1875 -1883.
[75] Mishra, V.N. (1990) "Pre-reduction of manganese ore for ferromanganese smelting", 14th Congress of the Council of Mining and metallurgical Instit. I.M.M, Scotland, Edinburg, pp. 39-47.22
[76] Mishra, V.N. and Khangaoukar, P.R. (1975) " Pre-reduction of Indian Manganese Ores", Jr. Instn of Engrs (India), vol.55 mm, no.283, pp. 59-63.
[77] Mishra, V.N., Sinvhal, R.C. and Khangaonkar, P.R. (1975) "Prereduction of Manganese ore pellets with Carbon Monoxide", Trans. Indian Inst. Of Metals, vol.28, no.3, pp. 268-369.

[78] Moradkhani, D, Malekzadeh, M. and Ahmadi, E. (2013) "Nano structured MnO_2 Synthesized via methane gas reduction of manganese ore and hydrothermal precipitation methods", Transactions of nonferrous metals society of China (23), pp. 134-139.
[79] Morral, F. R. (1984) Manganese – A Chronology and Bibliography, CIM bulletin, vol.77, no.86, pp. 72-75.
[80] Moore, T.E, Ellis, M. and Selwood, P.W. (1950) "Solid oxides and hydroxides of Manganese", Am. Chem. Soc. Jour., vol.71, pp. 856-866.
[81] Moatter, F. and Anderson. S. (1971) "Thermodynamics of the Manganese Carbides", Trans. Farad. Soc., vol.67, no.8, pp. 2303-2307.
[82] Meyer, R.J. and Rotgers, K. (1980) "Die dissociations Temperatures of Manganous oxide, Manganous- manganic oxide and Manganous Dioxide", Am. Chem. Soc. Jour., vol.50, pp. 1875-1883.
[83] Muan, A. (1959) "Phase equilibria in the system Manganese oxide -SiO_2 in air", Am. J. Sci., vol.257, pp. 297-315.
[84] Nabi, G. and Lu, W.K. (1968) "Reduction Kinetics of Hematite to magnetite in hydrogen – water vapour Mixture", TMS- AIME, vol.242. pp 2971-2977.
[85] Naruse, W. (1975) "Manganese alloy production by the Sintering process", Infacon 7, 4, Glen, (ed.), Johannesburg, S.A inst. Min. Metall., pp. 69-76.
[86] Nguyen, V.H. and Ryzhonkov, D.I. (1972) "An investigation of the reduction of a mixture of wustite and manganese oxide by carbon", Steel in USSR, vol.2, pp. 178-180.
[87] Ostrovski, O, Anacleto, N. and Ganguly, S. (2004) "Reduction of manganese ores by methane containing gas", Proceedings: Tenth International Ferroalloys Congress; 1- 4 February 2004, Infacon X, pp. 173-183, Cape Town, South Africa.
[88] Ostrovski, O, Jacobs, A, Anacleto, N. and McKenzie, G. (2000) "Reduction of chromium oxide by methane – containing gas", Infacon 9, Canada, pp. 138-140.
[89] Ostrovski, O. and Zang, G. (2006) "Reduction and carburization of metal oxides by methane containing gas", AICHE Journal, 52, pp. 300-310.
[90] Oslen, S. E, Tangstad, M. and Lindstad, T. (2007) "Production of manganese ferroalloys", pp. 43-110, Sintef and Tapir Academic Press, Trondheim.
[91] Oslen, S.E. and Tangstad, M. (2004) "Silico-Manganese production process understanding", Tenth Ferro-Alloy Congress, Infacon X, pp. 231-238, Cape Town, South Africa.
[92] Oates, W.A. and Trodd, D.D. (1962) "Kinetics of the reduction of oxides", J. Aust. Inst. MET., vol.7, pp. 109-114.
[93] Pentz, R. D. (1970) M.Sc. Dissertation, Potchefstroom University.
[94] Pilter, P. (1967) "The Reduction of metallic oxides with solid carbon", Kohasz. lapok, vol.11, pp. 303-308.
[95] Pilter, P. (1967) "The reduction of manganese oxides in solid state with carbon monoxides and hydrogen", Kohasz. Lapok, vol.11, pp. 492-500.
[96] Pomfret, R.J. and Grieveson, P. (1978) "Kinetics of fast Initial stage reduction of MnO from silicate slags by carbon in Molten Iron", Iron and steelmaking, No.5, pp. 191-197.
[97] Rankin, W.J. and Van Deventer, J.S.J. (1980) "The kinetics of the reduction of manganous oxides by graphite", Journal of SAIMM, pp. 239-247.

[98] Rebound, P.V. and Maun, A. (1963) "Melting relations of CaO – Manganese oxide and MgO-manganese oxide mixtures in air", J. Am .Ceramic. Soc., vol.46, no.1, pp. 33-36.
[99] Rao, Y. K. (1971) "The kinetics of reduction of Hematite by carbon", Met. Trans, vol.2B, pp. 1439-1447.
[100] Samancor (1979) "Brochure describing the manganese and iron ore interests of the Samancor Group of companies", Samancor, Johannesburg.
[101] Satterfield, C.N. and Sherwood, T.K. (1963) "The role of diffusion in catalysis", Addison-Wesley Co., Inc., pp. 5-16.
[102] Shantarin, V.D, Shestakovskii, O.F. and Suchilnikov, S.I. (1972) "Kinetics of the reduction of manganese concentrates with solid carbon", Communication.1. Steel in the USSR.pp.790-792.
[103] Sorensen, B, Gaal, S, Ringdalen, E, Tangstad, M, Konnov, R. and Ostrovoski, O. (2010) "Properties of manganese ores and their change in the process of calcination", International Journal of Mineral Processing, pp. 101-110.
[104] Soykan, O. and Eric, R.H. (1988) "The solid state reduction characteristics of the bushveld complex chromite", Ph.D. Thesis, University of the Witwatersrand.
[105] Southard, J.C. and Moore, G.E. (1942) "High temperature heat content of Mn_3O_4, $MnSiO_3$ and Mn_3C", Am. Chem. Soc. Jour., vol.64, pp. 1796-1770.
[106] Stukel, J.E and Cocubinsky, J. (1954) "Distribution of Manganese between slag and metal under reducing conditions", Trans .AIME, vol.203, pp. 524-528.
[107] Suguta, M. (1967) Nippon Kinzoku Gakkaishi, pp. 574-580.
[108] Tarby, S.K. and Philbrook, W.O. (1967) "The rate and mechanism of reduction of FeO and MnO from silicate and aluminate slags by carbon saturated Iron", Trans. Metal. Soc. Amie, vol.239, pp. 1005-1017.
[109] Tanaka, H. (1971) "Free energy of Formation of Mn_7C_3 by emf measurements", Nippon Kinzoku. Gakkaishi, vol.35, no.10, pp. 997-1000.
[110] Tanaka, H. (1973) "Thermodynamic study of the Manganese –carbon System by EMF Measurements", Nippon Kinzoku Gakkaishi, vol.37, no.5, pp. 568-570.
[111] Taljaardt, J. (1982) "Major manganese ore fields", Republic of South Africa, unpubl. REP. Samancor, Johannesburg, pp. 7.
[112] Tereyama, K. and Masao, I. (1985) "Study on reduction of manganese oxide with carbon by effluent gas analysis method", Transaction of the japan inst. Of metals, vol.26, no.2, pp. 104-108.
[113] Tein, R.H. and Turkodgan, E.T. (1972) "Gaseous reduction of Iron oxides", part IV, Met. Trans., vol.3, pp. 2039-2048.
[114] Tein, R.H. and Turkdogan, E.T. (1977) "Mathematical analysis of reactions in metal oxide /carbon mixtures", Metal. Trans, vol.8B, no.1, pp. 305-313.
[115] Tsylev, L.M. (1963) "The smelting of Ferroalloys in the blast Furnace Using Oxygen Enriched Blast", Pergamum Press, pp. 14.
[116] Turkdogan, E. T. (1980) "Physical chemistry of high temperature Technology", Academic Press, N.Y.
[117] Turkdogan, E.T. and Vinters, J.V. (1971) "Gaseous Reduction of Iron oxides: Part 1", Met. Trans., vol.2, pp. 3175-3188.

[118] Vanhook, H.J. and Keith, M.L. (1958) "The system Fe_3O_4-Mn_3O_4", Am. Mineral, vol.43, no.1, pp. 69-83.
[119] Van der Waltz. (1998) "Recent and anticipated developments of ferroalloys in SA", The proceedings of Infacon 8, Beijing, China, pp. 1-4.
[120] Vanhien, N. and Ryzhonkov, D.I. (1972) "An investigation of the reduction of a mixture of wustite and Manganese oxides by carbon", steel in the U.S.S.R., vol.2, pp. 178-180.
[121] Yagihashi, T, Asada, K, Atarashiya, K, Ichinose, S. and Hanada, H. (1963) "Properties and reduction of Manganese ores. II. Manganese ore reduction with CO gas or CO-CO_2 gas mixtures", Tetsu to hagane, vol.49, no.8, pp. 1059-1065.
[122] Yagi, T. and Ono, Y. (1970) "The rate of reduction of MnO from Molten slag by carbon saturated Iron", Iron and steel Inst. japan. Trans. vol.10, no.1, pp. 36-37.
[123] Warner, N.A. (1964) Proc. Australian Inst.Min.Metall.No.210, pp. 31-53.
[124] Warner, N.A. (1964) Trans. Am. Inst. Min. Engrs. 230, pp. 63-76
[125] Wen, C.Y. (1968) "Non catalytic Heterogeneous Solid Fluid Reaction Models", Ind. and Eng. chem., vol.60, no.9, pp. 34-54.
[126] Wellbeloved, D.B, Craven, P.M. and Waudby, J.W. (1990) "Manganese and Manganese Alloys" Wiley-VCH Verlag GmbH & Co. KGaA, Weinheim, pp.1-48.
[127] Wollocat, L. (1974) "The viscosity and Electrical conductivity of the system MnO-CaO-MgO-Al_2O_3-SiO_2", M.sc Thesis, University of the Witwatersrand, Johannesburg.
[128] Wheeler, A. (1951) "Advances in catalysis", III, Academic Press, New York.p 249.
[129] White, J, Howat, D.D. and Hay, R. (1934) "The Binary System: MnO-SiO_2", Royal Tech.Coll.Jour. (Glasgow), vol.3, pp. 230-240.
[130] Zhang, B. and Xue, Z.L. (2013) "Kinetic analyzing of direct reduction on manganese ore pellets containing carbon", International Journal of nonferrous metallurgy, 2, pp. 116-120.
[131] Decampos, M. (2003) "The reduction of chromite using a hydrocarbon gas", Ph.D. Thesis, University of the Witwatersrand.

APPENDIX A

METALLIZATION DATA TABLES

Table A1: Metallization at T=1050°C, 10 % CH_4 in Ar reducing gas.

Time (min.)	Mn_{tot}	Fe_{tot}	Mn^0	Fe^0	Metallization (%)			Mn^0/Fe^0	Mn_{met}/ Fe_{met}
					Mn_{met}	Fe_{met}	Total Met.		
0	0	0	0	0	0	0	0	0	0
10	46.0	5.14	3.22	1.490	7.00000	29.00000	9.19000	2.16107	0.24137
20	46.1	5.14	10.20	4.090	22.12581	79.57198	27.88837	2.49388	0.27806
30	46.2	5.18	10.21	4.091	22.09957	78.97683	27.83379	2.49572	0.27982
60	47.0	5.34	10.22	4.093	21.74468	76.64794	27.34620	2.49694	0.28369
90	46.0	5.30	10.24	4.094	22.26087	77.24528	27.94152	2.50122	0.28818
120	45.5	5.31	10.25	4.096	22.52747	77.13748	28.23460	2.50244	0.29204

Table A2: Metallization at T=1050°C, 30 % CH_4 in Ar reducing gas.

Time (min.)	Mn_{tot}	Fe_{tot}	Mn^0	Fe^0	Metallization (%)			Mn^0/Fe^0	Mn_{met}/ Fe_{met}
					Mn_{met}	Fe_{met}	Total Met.		
0	0	0	0	0	0	0	0	0	0
10	45.7	5.13	4.57	1.54	10.00000	15.00000	12.0200	2.9690	0.33333
20	45.7	5.13	12.01	4.10	26.26039	79.92203	31.6761	2.9293	0.32857
30	46.9	5.37	12.01	4.20	25.60768	78.21230	31.0121	2.8595	0.32741
60	47.5	5.43	12.03	4.25	25.32632	78.26880	30.7576	2.8306	0.32358
90	46.2	5.45	12.04	4.27	26.06061	78.34860	31.5779	2.8197	0.33262
120	47.2	5.42	12.06	4.28	25.55085	78.96680	31.0528	2.8177	0.32356

Table A3: Metallization at T=1100°C, 10 % CH_4 in Ar reducing gas.

Time (min.)	Mn_{tot}	Fe_{tot}	Mn^0	Fe^0	Metallization (%)			Mn^0/Fe^0	Mn_{met}/ Fe_{met}
					Mn_{met}	Fe_{met}	Total Met.		
0	0	0	0	0	0	0	0	0	0
10	44.1	4.76	4.4100	1.5700	10.00000	33.00000	12.23000	2.80890	0.30303
20	44.2	4.78	13.2861	3.9556	30.05929	82.75520	35.20164	3.35880	0.36323
30	44.0	4.27	13.3390	3.9900	30.31600	93.44270	35.90031	3.34310	0.32443
60	45.4	3.77	14.3597	3.4703	31.62940	92.05130	36.26190	4.64219	0.34360
90	39.8	3.61	12.5027	3.3378	31.41391	92.45930	36.49040	2.64332	0.33976
120	45.5	4.49	13.8908	3.9378	30.52920	87.70110	35.66430	3.52755	0.34810

Table A4: Metallization at T=1100°C, 20 % CH_4 in Ar reducing gas.

Time (min.)	Mn_{tot}	Fe_{tot}	Mn^0	Fe^0	Metallization (%)			Mn^0/Fe^0	Mn_{met}/ Fe_{met}
					Mn_{met}	Fe_{met}	Total Met.		
0	0	0	0	0	0	0	0	0	0
10	45.0	4.32	9.0000	1.7280	20.00000	40.0000	21.75182	5.20830	0.50000
20	45.0	4.32	23.9800	3.4878	53.28889	80.7356	55.69290	6.87539	0.66004
30	43.4	3.25	24.4977	2.6120	56.44640	80.3692	58.11290	9.37890	0.70233
60	42.5	3.90	20.1839	3.0678	47.49160	78.6609	50.11110	6.57927	0.60375
90	45.2	3.96	31.1023	2.5834	68.81040	65.2357	68.52240	12.03928	1.05479
120	45.6	3.78	31.6920	2.9556	69.49990	78.1893	70.16510	10.72269	0.88886

Table A5: Metallization at T=1100°C, 30 % CH_4 in Ar reducing gas.

Time (min.)	Mn_{tot}	Fe_{tot}	Mn^0	Fe^0	Metallization (%)			Mn^0/Fe^0	Mn_{met}/ Fe_{met}
					Mn_{met}	Fe_{met}	Total Met.		
0	0	0	0	0	0	0	0	0	0
10	45.2	3.76	9.0400	1.2032	20.00000	32.00000	20.92100	7.51330	0.62500
20	45.2	3.76	30.6598	3.2000	67.83140	85.10640	69.15800	9.58118	0.79701
30	44.2	4.37	29.6033	3.2578	66.97600	84.54870	67.65720	8.42507	0.79215
60	42.4	5.79	27.4805	4.7167	64.81240	81.46230	66.81280	5.82621	0.79561
90	39.4	4.28	25.2346	3.3195	64.04730	77.55870	65.37110	7.41373	0.82579
120	43.0	5.32	28.3334	4.1090	65.89150	77.23680	67.14060	6.89540	0.85311

Table A6: Metallization at T=1200 °C, 10 % CH_4 in Ar reducing gas.

Time (min.)	Mn_{tot}	Fe_{tot}	Mn^0	Fe^0	Metallization (%)			Mn^0/Fe^0	Mn_{met}/ Fe_{met}
					Mn_{met}	Fe_{met}	Total Met.		
0	0	0	0	0	0	0	0	0	0
10	43.5	4.55	7.8300	1.4560	18.00000	32.0000	19.3260	5.37700	0.56250
20	43.6	4.55	30.5287	4.2991	70.02000	94.4862	72.3319	7.10118	0.74106
30	43.0	4.97	30.3563	4.6978	70.59610	94.5227	73.0751	6.46182	0.74686
60	44.2	3.38	29.4340	3.1469	66.59280	93.1060	68.4760	9.35333	0.71520
90	48.4	5.65	32.2310	5.2231	66.59298	92.4443	69.2953	6.17085	0.72035
120	49.5	5.69	32.3210	5.3020	65.29495	93.1811	68.1699	6.09600	0.70073

Table A7: Metallization at T=1200°C, 20 % CH_4 in Ar reducing gas.

Time (min.)	Mn_{tot}	Fe_{tot}	Mn^0	Fe^0	Metallization (%)			Mn^0/Fe^0	Mn_{met}/ Fe_{met}
					Mn_{met}	Fe_{met}	Total Met.		
0	0	0	0	0	0	0	0	0	0
10	37.6	4.65	10.5280	2.0925	28.0000	45.0000	29.8710	5.03130	0.62222
20	37.6	4.65	23.7552	4.2900	63.1787	92.2580	60.8801	5.53734	0.68480
30	43.8	5.51	30.1448	5.5023	68.8238	99.8589	72.2917	5.47858	0.68921
60	43,4	5.30	3.8253	5.2923	62.7056	99.8533	64.7217	0.72280	0.62797
90	48.2	5.59	30.2130	5.3010	62.6825	94.8300	66.0234	5.69949	0.66099
120	51.2	5.85	30.2220	5.3110	59.2589	90.7863	62.5030	5.69045	0.65273

Table A8: Metallization at T=1200°C, 30 % CH_4 in Ar reducing gas.

Time (min.)	Mn_{tot}	Fe_{tot}	Mn^0	Fe^0	Metallization (%)			Mn^0/Fe^0	Mn_{met}/ Fe_{met}
					Mn_{met}	Fe_{met}	Total Met.		
0	0	0	0	0	0	0	0	0	0
10	43.8	5.30	8.7600	1.8020	20.00000	34.0000	21.5110	4.8620	0.58823
20	43.8	5.30	28.5011	5.2922	65.07112	99.8533	68.8256	5.3854	0.65166
30	43.7	5.43	28.3379	5.4222	64.84652	99.8568	68.7159	5.2262	0.64939
60	43.3	5.43	27.8747	5.4222	64.37578	99.8568	68.3294	5.1408	0.64468
90	49.4	5.57	32.4000	5.4300	65.58704	97.4865	68.8193	5.9668	0.67278
120	50.4	5.79	33.3000	5.4301	66.07143	93.7841	68.9270	6.1324	0.70450

Table A9: Metallization at T=1250°C, 10 % CH_4 in Ar reducing gas.

Time (min.)	Mn_{tot}	Fe_{tot}	Mn^0	Fe^0	Metallization (%)			Mn^0/Fe^0	Mn_{met}/ Fe_{met}
					Mn_{met}	Fe_{met}	Total Met.		
0	0	0	0	0	0	0	0	0	0
10	48.7	5.63	10.714	1.914	22.00000	34.00000	23.24000	5.59000	0.64700
20	48.7	5.63	30.230	5.500	62.07392	97.69094	65.76477	5.49636	0.63541
30	49.0	5.63	30.240	5.510	61.71429	97.86856	65.44023	5.48820	0.63058
60	49.8	5.75	30.250	5.500	60.74297	95.73913	64.36544	5.50000	0.63446
90	49.0	5.75	30.260	5.520	61.75510	96.00000	65.35160	5.48188	0.64328
120	49.7	5.74	30.270	5.510	60.90543	96.18467	64.55808	5.49364	0.63321

Table A10: Metallization at T=1250°C, 30 % CH_4 in Ar reducing gas.

Time (min.)	Mn_{tot}	Fe_{tot}	Mn^0	Fe^0	Metallization (%)			Mn^0/Fe^0	Mn_{met}/ Fe_{met}
					Mn_{met}	Fe_{met}	Total Met.		
0	0	0	0	0	0	0	0	0	0
10	50.0	5.74	9.000	1.83	18.0000	32.0000	18.6333	4.89998	0.56250
20	50.0	5.74	30.300	5.53	60.6000	96.3414	64.2805	5.47920	0.62901
30	50.6	5.85	30.310	5.51	59.9011	94.5471	63.4915	5.50090	0.63355
60	50.8	5.94	30.320	5.54	59.6850	93.1313	63.1864	5.47292	0.64086
90	50.9	5.97	30.330	5.53	59.5874	92.6800	63.0613	5.48462	0.64293
120	52.8	6.22	30.340	5.60	57.4621	90.0321	60.8946	5.41785	0.63824

Table A11: Metallization at T=1050°C, 10 % CH_4 in H_2 reducing gas.

Time (min.)	Mn_{tot}	Fe_{tot}	Mn^0	Fe^0	Metallization (%)			Mn^0/Fe^0	Mn_{met}/ Fe_{met}
					Mn_{met}	Fe_{met}	Total Met.		
0	0	0	0	0	0	0	0	0	0
10	47.6	5.63	8.5680	2.0268	18.0000	36.0000	19.9038	0.3835	0.50000
20	47.6	5.63	19.9920	4.5481	42.0000	80.7832	46.1020	1.0138	0.51991
30	48.8	5.61	20.4960	4.6847	42.0000	83.5073	46.2795	4.3750	0.50295
60	40.0	5.11	17.2414	4.7211	43.1035	92.3896	48.6865	3.6519	0.46654
90	42.6	5.53	16.5541	5.1411	38.8592	92.9676	45.0761	3.2199	0.41798
120	43.6	6.02	16.7321	5.6311	38.3766	93.5400	45.0691	2.9713	0.41026

Table A12: Metallization at T=1050°C, 20 % CH_4 in H_2 reducing gas.

Time (min.)	Mn_{tot}	Fe_{tot}	Mn^0	Fe^0	Metallization (%)			Mn^0/Fe^0	Mn_{met}/ Fe_{met}
					Mn_{met}	Fe_{met}	Total Met.		
0	0	0	0	0	0	0	0	0	0
10	48.5	5.49	3.8800	2.5800	8.0100	47.0000	11.7433	1.50575	0.17021
20	48.5	5.49	3.9500	4.8300	8.1443	87.9781	16.2622	0.81780	0.09257
30	41.6	4.96	17.5140	4.5700	42.1004	92.1595	47.4332	3.83230	0.45682
60	41.0	5.30	16.9770	4.9111	41.4073	92.6624	47.2745	3.45686	0.44686
90	44.6	5.98	17.8586	5.5911	40.0417	93.4968	46.3616	3.19411	0.42826
120	45.7	6.11	19.1483	5.7211	41.8999	93.6352	48.0011	3.34696	0.44748

Table A13: Metallization at T=1050°C, 30 % CH_4 in H_2 reducing gas.

Time (min.)	Mn_{tot}	Fe_{tot}	Mn^0	Fe^0	Metallization (%)			Mn^0/Fe^0	Mn_{met}/ Fe_{met}
					Mn_{met}	Fe_{met}	Total Met.		
0	0	0	0	0	0	0	0	0	0
10	42.9	5.40	6.8640	1.9938	16.0000	36.9233	18.3391	4.23700	0.43333
20	42.9	5.40	17.3597	5.0111	40.4656	92.7983	46.3165	3.46424	0.43605
30	41.9	5.30	17.6690	4.9111	42.1713	92.6624	47.8392	4.45108	0.46000
60	44.2	5.29	18.0275	4.9011	40.7864	92.6486	46.3299	3.67825	0.44022
90	45.3	5.78	17.3574	5.3911	38.3167	93.2718	44.5352	3.21963	0.41080
120	45.6	5.98	16.8989	5.5911	37.0588	93.4969	43.6021	3.02246	0.39636

Table A14: Metallization at T=1100°C, 10 % CH_4 in H_2 reducing gas.

Time (min.)	Mn_{tot}	Fe_{tot}	Mn^0	Fe^0	Metallization (%)			Mn^0/Fe^0	Mn_{met}/ Fe_{met}
					Mn_{met}	Fe_{met}	Total Met.		
0	0	0	0	0	0	0	0	0	0
10	43.8	5.27	7.8840	1.7391	18.0000	39.0000	20.2400	3.84580	0.46150
20	43.8	5.28	17.1856	4.8911	39.2353	92.6349	44.9799	3.51364	0.42354
30	41.3	5.52	19.9322	5.1311	48.2620	92.9549	53.5312	3.88458	0.51919
60	44.7	5.54	19.0966	5.1511	42.7216	92.9803	48.2637	3.70728	0.45946
90	44.3	5.98	17.6219	5.5911	39.7784	92.4968	46.1674	3.15177	0.43005
120	40.5	5.52	16.2242	5.1311	40.0596	92.9549	46.4043	3.16193	0.43095

Table A15: Metallization at T=1100°C, 20 % CH_4 in H_2 reducing gas.

Time (min.)	Mn_{tot}	Fe_{tot}	Mn^0	Fe^0	Metallization (%)			Mn^0/Fe^0	Mn_{met}/ Fe_{met}
					Mn_{met}	Fe_{met}	Total Met.		
0	0	0	0	0	0	0	0	0	0
10	44.2	5.46	7.9560	2.1840	18.0000	40.0000	20.4188	3.64285	0.45000
20	44.2	5.46	18.0908	5.0711	40.9294	92.8775	46.6410	3.56743	0.44068
30	43.5	5.58	19.8563	5.1911	45.6467	93.0306	51.0339	3.82506	0.49066
60	43.5	5.60	18.8448	5.2111	43.3214	93.0556	48.9938	3.61628	0.46554
90	45.1	6.13	17.2840	5.7411	38.3235	93.6560	44.9444	3.01057	0.40919
120	45.4	6.11	18.0265	5.7211	39.7058	93.6352	46.1028	3.15088	0.42404

Table A16: Metallization at T=1100°C, 30 % CH_4 in H_2 reducing gas.

Time (min.)	Mn_{tot}	Fe_{tot}	Mn^0	Fe^0	Metallization (%)			Mn^0/Fe^0	Mn_{met}/ Fe_{met}
					Mn_{met}	Fe_{met}	Total Met.		
0	0	0	0	0	0	0	0	0	0
10	42.6	5.45	7.6680	2.1210	18.0000	38.9190	20.3725	4.39678	0.46250
20	42.6	5.45	17.8183	5.0611	41.8272	92.8644	47.6160	3.52063	0.45041
30	45.8	5.71	19.9437	5.3211	43.5451	93.1893	49.0483	3.74804	0.46727
60	41.0	5.53	16.4340	5.1411	40.0830	92.9677	46.3681	4.67942	0.43115
90	45.6	6.29	17.9103	5.9011	39.2770	93.8174	45.8883	3.03507	0.41865
120	45.7	6.56	17.1253	6.1711	37.4732	94.0718	44.5778	2.77508	0.39834

Table A17: Metallization at T=1200°C, 10 % CH_4 in H_2 reducing gas.

Time (min.)	Mn_{tot}	Fe_{tot}	Mn^0	Fe^0	Metallization (%)			Mn^0/Fe^0	Mn_{met}/ Fe_{met}
					Mn_{met}	Fe_{met}	Total Met.		
0	0	0	0	0	0	0	0	0	0
10	47.1	5.49	9.4200	2.1400	20.0000	39.0000	21.9800	4.27000	0.51280
20	47.1	5.49	23.3439	5.1011	49.5625	92.9164	54.0882	3.71837	0.53341
30	45.4	5.85	21.0582	5.4611	46.3839	93.3523	51.7450	4.63212	0.49687
60	42.5	5.69	19.6781	5.3011	46.3015	93.1654	51.8350	3.71207	0.49698
90	46.4	6.41	18.7103	6.0211	40.3240	93.9331	46.8310	3.10745	0.42928
120	45.5	6.48	17.3678	6.0911	38.7102	93.9986	45.1307	2.85134	0.41181

Table A18: Metallization at T=1200°C, 20 % CH_4 in H_2 reducing gas.

Time (min.)	Mn_{tot}	Fe_{tot}	Mn^0	Fe^0	Metallization (%)			Mn^0/Fe^0	Mn_{met}/ Fe_{met}
					Mn_{met}	Fe_{met}	Total Met.		
0	0	0	0	0	0	0	0	0	0
10	42.3	5.51	10.5750	2.4795	25.0000	45.0000	32.7287	4.26400	0.55555
20	42.3	5.51	17.8345	5.1211	42.1619	92.9421	48.0142	3.48255	0.45363
30	44.8	5.63	19.7655	5.2411	44.1195	93.0925	49.5868	3.77125	0.47393
60	43.3	5.74	18.5816	5.3511	42.9137	93.2249	48.8024	3.47248	0.46032
90	45.9	6.22	18.4632	5.8311	40.2248	93.7477	46.6123	3.16633	0.42907
120	45.4	6.51	17.5207	6.1211	38.5918	94.0263	45.5438	2.86234	0.41043

Table A19: Metallization at T=1200°C, 30 % CH_4 in H_2 reducing gas.

Time (min.)	Mn_{tot}	Fe_{tot}	Mn^0	Fe^0	Metallization (%)			Mn^0/Fe^0	Mn_{met}/ Fe_{met}
					Mn_{met}	Fe_{met}	Total Met.		
0	0	0	0	0	0	0	0	0	0
10	43.7	5.26	6.5550	1.7358	15.0000	33.0000	16.9338	3.77635	0.45454
20	43.7	5.26	20.0563	4.8711	45.8954	92.6067	50.9137	4.11740	0.49559
30	43.6	5.52	18.5655	5.1311	42.5815	92.9549	48.2423	3.61823	0.45808
60	43.5	5.54	19.0977	5.1511	43.9027	92.9803	49.4470	3.70749	0.47217
90	42.5	5.82	17.3398	5.4311	40.7978	93.3180	47.1237	3.19268	0.43719
120	43.7	5.95	16.1368	5.5611	38.9263	93.4640	43.7017	2.90172	0.41648

Table A20: Metallization at T=1250°C, 10 % CH_4 in H_2 reducing gas.

Time (min.)	Mn_{tot}	Fe_{tot}	Mn^0	Fe^0	Metallization (%)			Mn^0/Fe^0	Mn_{met}/ Fe_{met}
					Mn_{met}	Fe_{met}	Total Met.		
0	0	0	0	0	0	0	0	0	0
10	45.3	5.81	6.7950	2.3240	15.0000	40.0000	17.8400	2.92380	0.37500
20	45.3	5.81	18.6851	5.4211	41.2473	93.3065	47.1652	3.44670	0.44206
30	44.1	5.93	17.9276	5.5411	40.6521	93.4420	46.9093	3.23538	0.43505
60	49.5	6.91	19.0920	6.5211	38.5696	94.3721	45.4052	2.92772	0.40869
90	45.5	5.89	18.6321	5.5011	40.9498	93.3975	46.9610	3.38697	0.43844
120	46.5	6.12	17.4827	5.7311	37.5973	93.6456	44.1160	3.05049	0.40148

Table A21: Metallization at T=1250°C, 20 % CH_4 in H_2 reducing gas.

Time (min.)	Mn_{tot}	Fe_{tot}	Mn^0	Fe^0	Metallization (%)			Mn^0/Fe^0	Mn_{met}/ Fe_{met}
					Mn_{met}	Fe_{met}	Total Met.		
0	0	0	0	0	0	0	0	0	0
10	43.2	5.68	7.7760	1.8744	18.0000	33.0000	19.7430	4.14900	0.54545
20	43.2	5.68	17.9126	5.2911	41.4645	93.1534	47.4709	3.38542	0.44512
30	44.9	6.46	18.3483	6.0711	40.8648	93.9800	47.5455	3.02223	0.43482
60	39.6	5.66	16.3989	5.2711	41.4112	93.1291	47.8788	3.11109	0.44466
90	45.7	5.95	18.6425	5.5611	40.7933	93.4641	46.8609	3.35230	0.43645
120	45.9	6.13	18.5264	5.7411	40.3626	93.6560	46.6415	3.22697	0.43096

Table A22: Metallization at T=1250°C, 30 % CH_4 in H_2 reducing gas.

Time (min.)	Mn_{tot}	Fe_{tot}	Mn^0	Fe^0	Metallization (%)			Mn^0/Fe^0	Mn_{met}/ Fe_{met}
					Mn_{met}	Fe_{met}	Total Met.		
0	0	0	0	0	0	0	0	0	0
10	41.8	5.63	5.8520	1.8579	14.0000	33.0000	16.2553	3.14970	0.42424
20	41.8	5.63	16.6432	5.2400	39.8165	93.0925	46.1379	3.62179	0.42771
30	45.0	6.26	18.0058	5.8711	40.0127	93.7872	46.5799	3.06685	0.42663
60	43.9	6.14	17.6322	5.7511	38.7977	93.6663	45.5302	3.06588	0.41421
90	44.2	5.95	17.5851	5.5611	39.7852	93.4640	46.1539	3.16216	0.42567
120	46.2	6.04	18.3840	5.6511	39.7920	93.5614	46.0089	3.25317	0.42530

SUMMARY TABLES FOR THE METALLIZATION DATA

The tabulated data below summarises the metallization values presented above in the metallization data tables, for summary and direct graphical comparisions.

The effect of changing the concentration of methane keeping temperature and carrier gas constant.

Table A23: Total metallization values at 1050 °C in argon carrier gas.

	(%) Total Met.	
Time (min.)	10% CH_4 in Ar	30% CH_4 in Ar
0	0	0
10	9.1900	12.0200
20	27.8883	31.6761
30	27.8337	31.0121
60	27.3462	30.7576
90	27.9415	31.5779
120	28.2346	31.0528

Table A24: Total metallization values at 1100 ºC in argon carrier gas.

	(%) Total Met.		
Time (min.)	10% CH_4 in Ar	20% CH_4 in Ar	30% CH_4 in Ar
0	0	0	0
10	12.2300	21.7518	20.9210
20	35.2016	55.6929	69.1580
30	35.9003	58.1129	67.6572
60	36.2619	50.1111	66.8128
90	36.4904	68.5224	65.3711
120	35.6643	70.1651	67.1406

Table A25: Total metallization values at 1200 ºC in argon carrier gas.

	(%) Total Met.		
Time (min.)	10% CH_4 in Ar	20% CH_4 in Ar	30% CH_4 in Ar
0	0	0	0
10	19.3260	29.8710	21.5110
20	72.3319	60.8801	68.8256
30	73.0751	72.2917	68.7159
60	68.4760	64.7217	68.3294
90	69.2953	66.0234	68.8193
120	68.1699	62.5030	68.9270

Table A26: Total metallization values at 1250 ºC in argon carrier gas.

	(%) Total Met.	
Time (min.)	10% CH_4 in Ar	30% CH_4 in Ar
0	0	0
10	23.2400	18.6333
20	65.7647	64.2805
30	65.4402	63.4915
60	64.3654	63.1864
90	65.3516	63.0613
120	64.5580	60.8946

Table A27: Total metallization values at 1050 ºC in hydrogen carrier gas.

	(%) Total Met.		
Time (min.)	10% CH_4 in Ar	20% CH_4 in Ar	30% CH_4 in Ar
0	0	0	0
10	19.9038	11.7433	18.3391
20	46.1020	16.2622	46.3165
30	46.2795	47.4332	47.8392
60	48.6865	47.2745	46.3299
90	45.0761	46.3616	44.5352
120	45.0691	48.0011	43.6021

Table A28: Total metallization values at 1100 ºC in hydrogen carrier gas.

	(%) Total Met.		
Time (min.)	10% CH_4 in Ar	20% CH_4 in Ar	30% CH_4 in Ar
0	0	0	0
10	20.2400	20.1488	20.3725
20	44.9799	46.6410	47.6160
30	53.5312	51.0339	49.0483
60	48.2637	48.9938	46.3681
90	46.1674	44.9444	45.8883
120	46.4043	46.1028	44.5778

Table A29: Total metallization values at 1200 ºC in hydrogen carrier gas.

	(%) Total Met.		
Time (min.)	10% CH_4 in Ar	20% CH_4 in Ar	30% CH_4 in Ar
0	0	0	0
10	21.9800	32.7287	16.9338
20	54.0082	48.0142	50.9137
30	51.7450	49.5868	48.2423
60	51.8350	48.8024	49.4470
90	46.8310	46.6123	47.1237
120	45.1307	45.5438	43.7017

Table A30: Total metallization values at 1250 ºC in hydrogen carrier gas.

	(%) Total Met.		
Time (min.)	10% CH_4 in Ar	20% CH_4 in Ar	30% CH_4 in Ar
0	0	0	0
10	17.8400	19.7430	16.2553
20	47.1652	47.4709	46.1379
30	46.9093	47.5455	46.5799
60	45.4052	47.8788	45.5302
90	46.9610	46.8609	46.1539
120	44.1160	46.6415	46.0089

The effect of changing temperature on the total metallization for a constant gas composition.

Table A31: Total metallization values at 10 % CH_4 in argon carrier gas for different temperatures

	(%) Total Met. For 10 % CH_4 in Ar			
Time (min.)	T=1050ºC	T= 1100ºC	T=1200ºC	T= 1250ºC
0	0	0	0	0
10	9.1900	12.2300	19.3260	23.2400
20	27.8883	35.2016	72.3319	65.7647
30	27.8337	35.9003	73.0751	65.4402
60	27.3462	36.2619	68.4760	64.3654
90	27.9415	36.4904	69.2953	65.3516
120	28.2346	35.6643	68.1699	64.5580

Table A32: Total metallization values at 20 % CH_4 in argon carrier gas for different temperatures.

	(%) Total Met. For 20 % CH_4 in Ar			
Time (min.)	T=1050ºC	T= 1100ºC	T=1200ºC	T= 1250ºC
0	0	0	0	0
10	n/a	21.7518	29.8710	n/a
20	n/a	55.6929	60.8801	n/a
30	n/a	58.1129	72.2917	n/a
60	n/a	50.1111	64.7217	n/a
90	n/a	68.5224	66.0234	n/a
120	n/a	70.1651	62.5030	n/a

Table A33: Total metallization values at 30 % CH_4 in argon carrier gas for different temperatures.

	(%) Total Met. For 30 % CH_4 in Ar			
Time (min.)	T=1050°C	T= 1100°C	T=1200°C	T= 1250°C
0	0	0	0	
10	12.0200	20.9210	21.5110	18.6333
20	31.6761	69.1580	68.8256	64.2805
30	31.0121	67.6572	68.7159	63.4915
60	30.7576	66.8128	68.3294	63.1864
90	31.5779	65.3711	68.8193	63.0613
120	31.0528	67.1406	68.9270	60.8946

Table A34: Total metallization values at 10 % CH_4 in Hydrogen carrier gas for different temperatures.

	(%) Total Met. For 10 % CH_4 in H_2			
Time (min.)	T=1050°C	T= 1100°C	T=1200°C	T= 1250°C
0	0	0	0	0
10	19.9038	20.2400	21.9800	17.8400
20	46.1020	44.9799	54.0082	47.1652
30	46.2795	53.5312	51.7450	46.9093
60	48.6865	48.2637	51.8350	45.4052
90	45.0761	46.1674	46.8310	46.9610
120	45.0691	46.4043	45.1307	44.1160

Table A35: Total metallization values at 20 % CH_4 in Hydrogen carrier gas for different temperatures.

	(%) Total Met. For 20 % CH_4 in H_2			
Time (min.)	T=1050°C	T= 1100°C	T=1200°C	T= 1250°C
0	0	0	0	0
10	11.7433	20.1488	32.7287	19.7430
20	16.2622	46.6410	48.0142	47.4709
30	47.4332	51.0339	49.5868	47.5455
60	47.2745	48.9938	48.8024	47.8788
90	46.3616	44.9444	46.6123	46.8609
120	48.0011	46.1028	45.5438	46.6415

Table A36: Total metallization values at 30 % CH_4 in Hydrogen carrier gas for different temperatures.

	(%) Total Met. For 30 % CH_4 in H_2			
Time (min.)	T=1050°C	T= 1100°C	T=1200°C	T= 1250°C
0	0	0	0	0
10	18.3391	20.3725	16.9338	16.2553
20	46.3165	47.6160	50.9137	46.1379
30	47.8392	49.0483	48.2423	46.5799
60	46.3299	46.3681	49.4470	45.5302
90	44.5352	45.8883	47.1237	46.1539
120	43.6021	44.5778	43.7017	46.0089

The comparision of the total metallization values for the different carrier gasses

Table A37: Total metallization values at 10% CH_4 in Ar and H_2 carrier gases for different temperature.

	(%) Total Met. For 10 % CH_4 in Ar				(%) Total Met. For 10 % CH_4 in H_2			
Time (min.)	T=1050°C	T= 1100°C	T=1200°C	T= 1250°C	T=1050°C	T= 1100°C	T=1200°C	T= 1250°C
0	0	0	0	0	0	0	0	0
10	9.1900	12.2300	19.3260	23.2400	19.9038	20.2400	21.9800	17.8400
20	27.8883	35.2016	72.3319	65.7647	46.1020	44.9799	54.0082	47.1652
30	27.8337	35.9003	73.0751	65.4402	46.2795	53.5312	51.7450	46.9093
60	27.3462	36.2619	68.4760	64.3654	48.6865	48.2637	51.8350	45.4052
90	27.9415	36.4904	69.2953	65.3516	45.0761	46.1674	46.8310	46.9610
120	28.2346	35.6643	68.1699	64.5580	45.0691	46.4043	45.1307	44.1160

Table A38: Total metallization values at 20% CH_4 in Ar and H_2 carrier gases for different temperature.

	(%) Total Met. For 20 % CH_4 in Ar				(%) Total Met. For 20 % CH_4 in H_2			
Time (min.)	T=1050°C	T= 1100°C	T=1200°C	T= 1250°C	T=1050°C	T= 1100°C	T=1200°C	T= 1250°C
0	0	0	0	0	0	0	0	0
10	n/a	21.7518	29.8710	n/a	11.7433	20.1488	32.7287	19.7430
20	n/a	55.6929	60.8801	n/a	16.2622	46.6410	48.0142	47.4709
30	n/a	58.1129	72.2917	n/a	47.4332	51.0339	49.5868	47.5455
60	n/a	50.1111	64.7217	n/a	47.2745	48.9938	48.8024	47.8788
90	n/a	68.5224	66.0234	n/a	46.3616	44.9444	46.6123	46.8609
120	n/a	70.1651	62.5030	n/a	48.0011	46.1028	45.5438	46.6415

Table A39: Total metallization values at 30% CH_4 in Ar and H_2 carrier gases for different temperature.

	(%) Total Met. For 30 % CH_4 in Ar				(%) Total Met. For 30 % CH_4 in H_2			
Time (min.)	T=1050°C	T= 1100°C	T=1200°C	T= 1250°C	T=1050°C	T= 1100°C	T=1200°C	T= 1250°C
0	0	0	0	0	0	0	0	0
10	12.0200	20.9210	21.5110	18.6333	18.3391	20.3725	16.9338	16.2553
20	31.6761	69.1580	68.8256	64.2805	46.3165	47.6160	50.9137	46.1379
30	31.0121	67.6572	68.7159	63.4915	47.8392	49.0483	48.2423	46.5799
60	30.7576	66.8128	68.3294	63.1864	46.3299	46.3681	49.4470	45.5302
90	31.5779	65.3711	68.8193	63.0613	44.5352	45.8883	47.1237	46.1539
120	31.0528	67.1406	68.9270	60.8946	43.6021	44.5778	43.7017	46.0089

Table A40: The final total metallization values as a function of temperature and reducing gas.

	Final Total Metallization Values (%)					
Temp(°C)	10% CH_4 in Ar	20% CH_4 in Ar	30% CH_4 in Ar	10% CH_4 in H_2	20% CH_4 in H_2	30% CH_4 in H_2
1050°C	28.2346	n/a	31.0528	45.0691	48.0011	43.6021
1100°C	35.6643	70.1651	67.1406	46.4043	46.1028	44.5778
1200°C	68.1699	62.5030	68.9270	45.1307	45.5438	43.7017
1250°C	64.5580	n/a	60.8946	44.1160	46.6415	46.0089

The comparision of the Mn_{met}: Fe_{met} ratios.

Table A41: The resulting manganese to iron (Mn_{met}: Fe_{met}) ratios for the reduction tests using 10% and 30% methane in the argon carrier gas.

	10 % CH_4 in Ar				30 % CH_4 in Ar			
Time (min.)	T=1050°C	T= 1100°C	T=1200°C	T= 1250°C	T=1050°C	T= 1100°C	T=1200°C	T= 1250°C
0	0	0	0	0	0	0	0	0
10	0.24137	0.30303	0.56250	0.64700	0.33333	0.62500	0.58823	0.56250
20	0.27806	0.36323	0.74106	0.63541	0.32857	0.79701	0.65166	0.62901
30	0.27982	0.32443	0.74686	0.63058	0.32741	0.79215	0.64939	0.63355
60	0.28369	0.34360	0.81000	0.63446	0.32358	0.79561	0.64468	0.64086
90	0.28818	0.33976	0.72035	0.64328	0.33262	0.82537	0.67278	0.64293
120	0.29204	0.34810	0.70073	0.63321	0.32356	0.85311	0.70450	0.63824

Table A42: The resulting manganese to iron (Mn_{met}: Fe_{met}) ratios for the reduction tests using 10% and 30% methane in the hydrogen carrier gas.

	10 % CH_4 in H_2				30 % CH_4 in H_2			
Time (min.)	T=1050°C	T= 1100°C	T=1200°C	T= 1250°C	T=1050°C	T= 1100°C	T=1200°C	T= 1250°C
0	0	0	0	0	0	0	0	0
10	0.50000	0.46150	0.51280	0.37500	0.43333	0.46250	0.45454	0.42424
20	0.51991	0.42354	0.53341	0.44206	0.43605	0.45041	0.49559	0.42771
30	0.50295	0.51919	0.49687	0.43505	0.46000	0.46727	0.45808	0.42663
60	0.46654	0.45946	0.49698	0.40869	0.44022	0.43115	0.47217	0.41421
90	0.41798	0.43005	0.42928	0.43844	0.41080	0.41865	0.43719	0.42567
120	0.41026	0.43095	0.41181	0.40148	0.39636	0.39834	0.41648	0.42530

Table A43: Comparision of the manganese to iron (Mn_{met}: Fe_{met}) ratios for tests using 10% methane in concentration for the two different carrier gasses.

	10 % CH_4 in Ar				10 % CH_4 in H_2			
Time (min.)	T=1050°C	T= 1100°C	T=1200°C	T= 1250°C	T=1050°C	T= 1100°C	T=1200°C	T= 1250°C
0	0	0	0	0	0	0	0	0
10	0.24137	0.30303	0.56250	0.64700	0.50000	0.46150	0.51280	0.37500
20	0.27806	0.36323	0.74106	0.63541	0.51991	0.42354	0.53341	0.44206
30	0.27982	0.32443	0.74686	0.63058	0.50295	0.51919	0.49687	0.43505
60	0.28369	0.34360	0.81000	0.63446	0.46654	0.45946	0.49698	0.40869
90	0.28818	0.33976	0.72035	0.64328	0.41798	0.43005	0.42928	0.43844
120	0.29204	0.34810	0.70073	0.63321	0.41026	0.43095	0.41181	0.40148

Table A44: Comparision of the manganese to iron (Mn_{met}: Fe_{met}) ratios for tests using 30% methane in concentration for the two different carrier gasses.

	30 % CH_4 in Ar				30 % CH_4 in H_2			
Time (min.)	T=1050°C	T= 1100°C	T=1200°C	T= 1250°C	T=1050°C	T= 1100°C	T=1200°C	T= 1250°C
0	0	0	0	0	0	0	0	0
10	0.33333	0.62500	0.58823	0.56250	0.43333	0.46250	0.45454	0.42424
20	0.32857	0.79701	0.65166	0.62901	0.43605	0.45041	0.49559	0.42771
30	0.32741	0.79215	0.64939	0.63355	0.46000	0.46727	0.45808	0.42663
60	0.32358	0.79561	0.64468	0.64086	0.44022	0.43115	0.47217	0.41421
90	0.33262	0.82537	0.67278	0.64293	0.41080	0.41865	0.43719	0.42567
120	0.32356	0.85311	0.70450	0.63824	0.39636	0.39834	0.41648	0.42530

Table A45: Summarry of the effect of reduction temperature on the final manganese to iron (Mn_{met}: Fe_{met}) ratios after a complete two hours reduction test run.

Temp(°C)	10% CH_4 in Ar	30% CH_4 in Ar	10% CH_4 in H_2	30% CH_4 in H_2
1050°C	0.29204	0.32356	0.41026	0.39636
1100°C	0.34810	0.85311	0.43095	0.39834
1200°C	0.70073	0.70450	0.41181	0.41648
1250°C	0.63321	0.63824	0.40148	0.42530

APPENDIX B

METALLIZATION CURVES AND X-RAY DIFFRACTION RESULTS

Methane + Argon

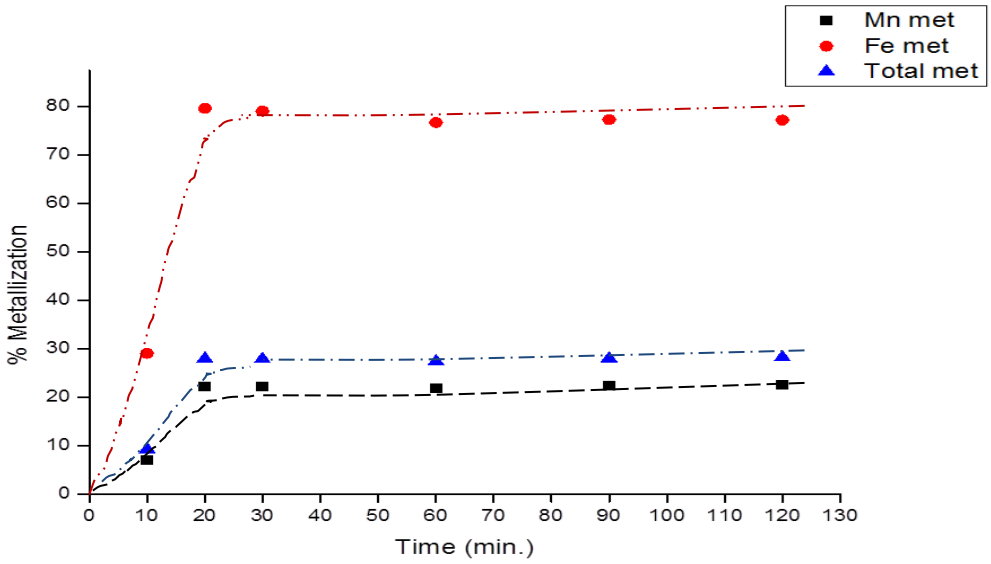

Figure B.1 Progress of metallization versus time for tests using 10 % CH_4 in Ar at T= 1050 °C

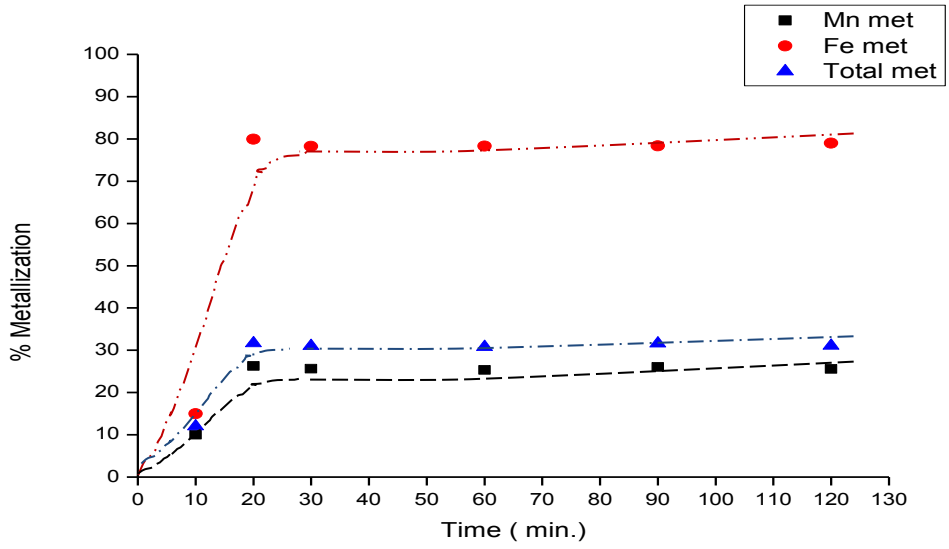

Figure B.2 Progress of metallization versus time for tests using 30 % CH_4 in Ar at T= 1050 °C

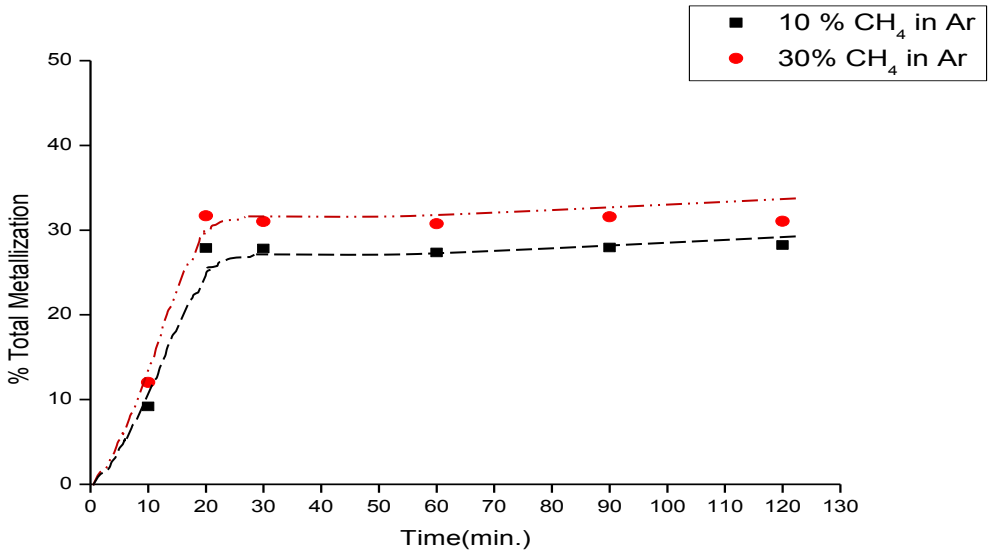

Figure B.3 Summary of total metallization versus time at 1050 ºC in Ar

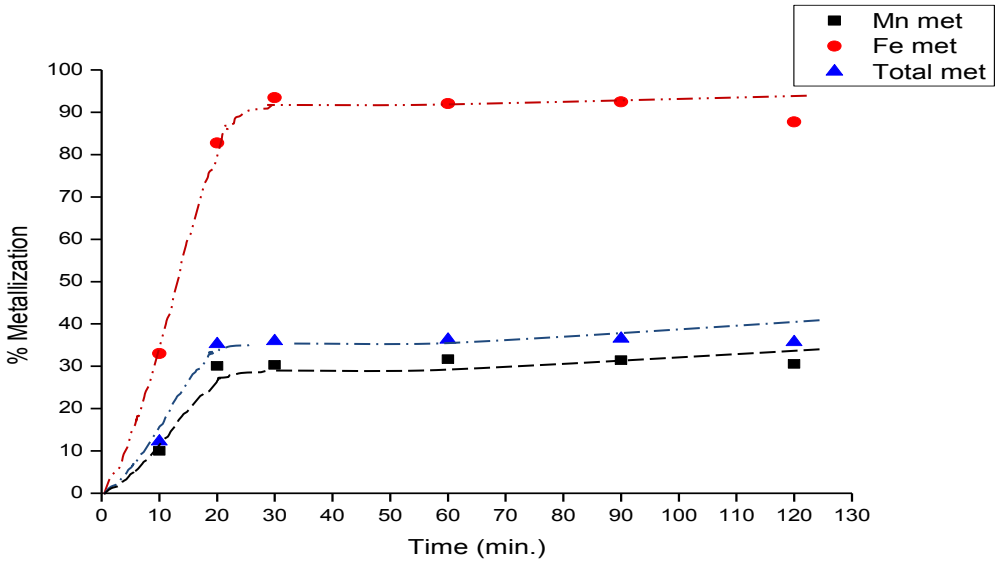

Figure B.4 Progress of metallization versus time for tests using 10 % CH_4 in Ar at T= 1100 ºC

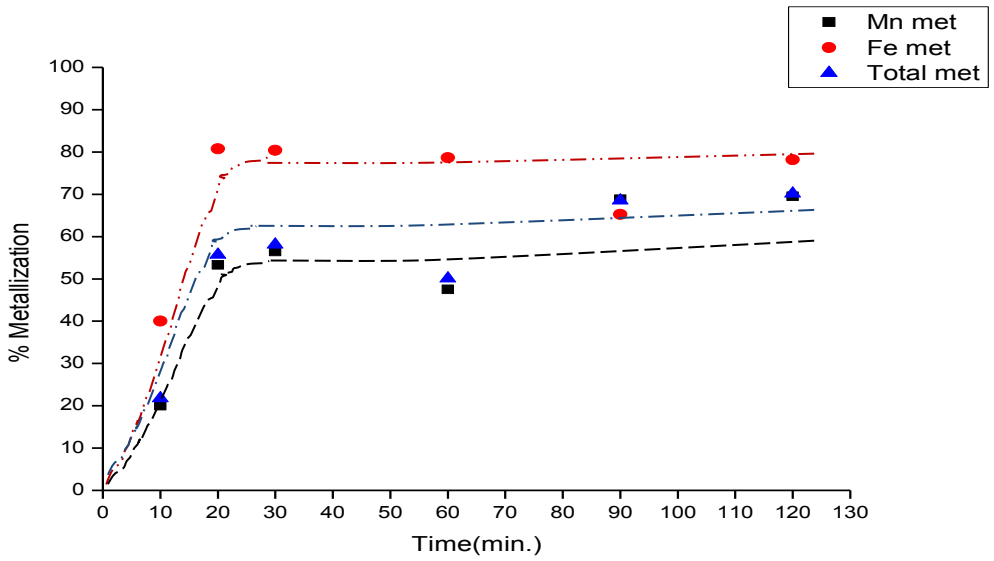

Figure B.5 Progress of metallization versus time for tests using 20 % CH_4 in Ar at T= 1100 °C

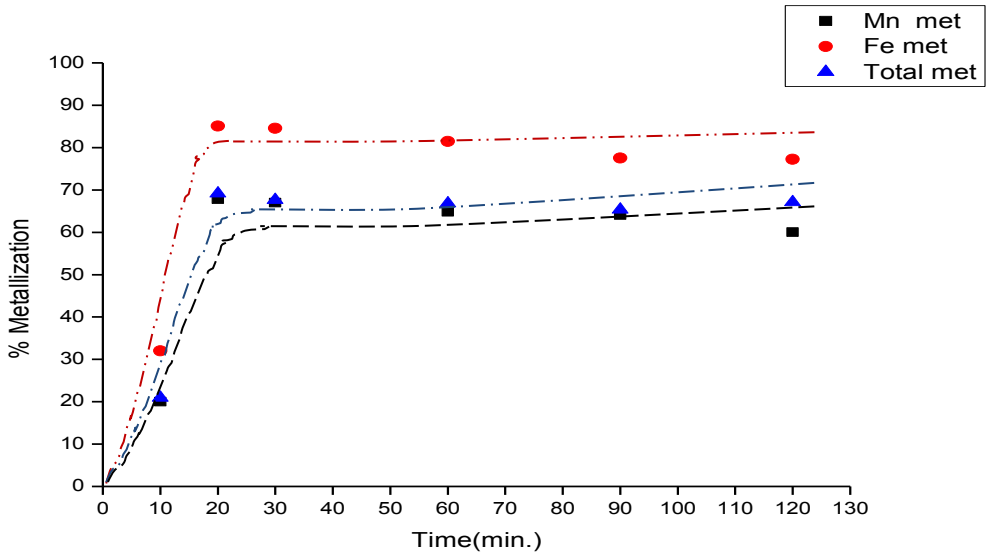

Figure B.6 Progress of metallization versus time for tests using 30 % CH_4 in Ar at T= 1100 °C

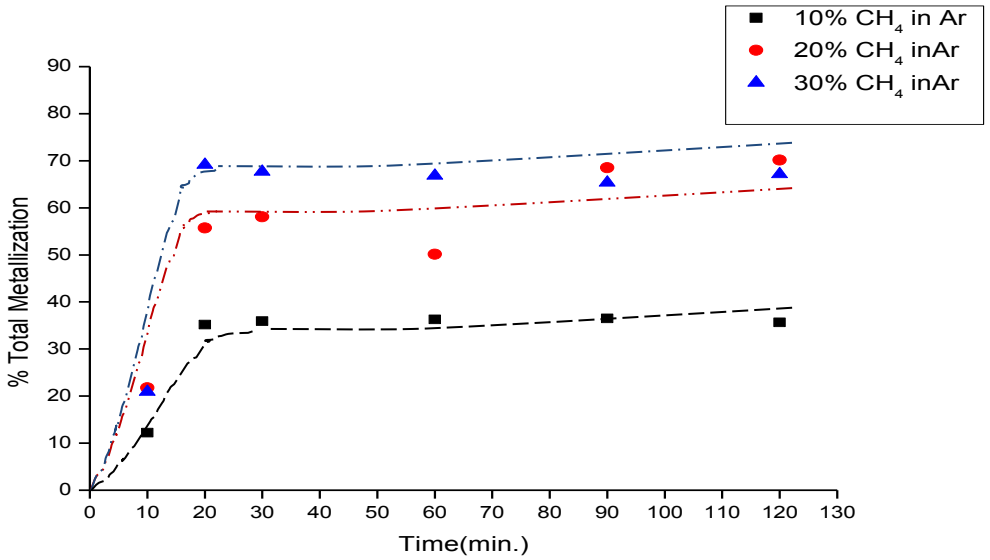

Figure B.7 Summary of total metallization at 1100 ºC in Ar.

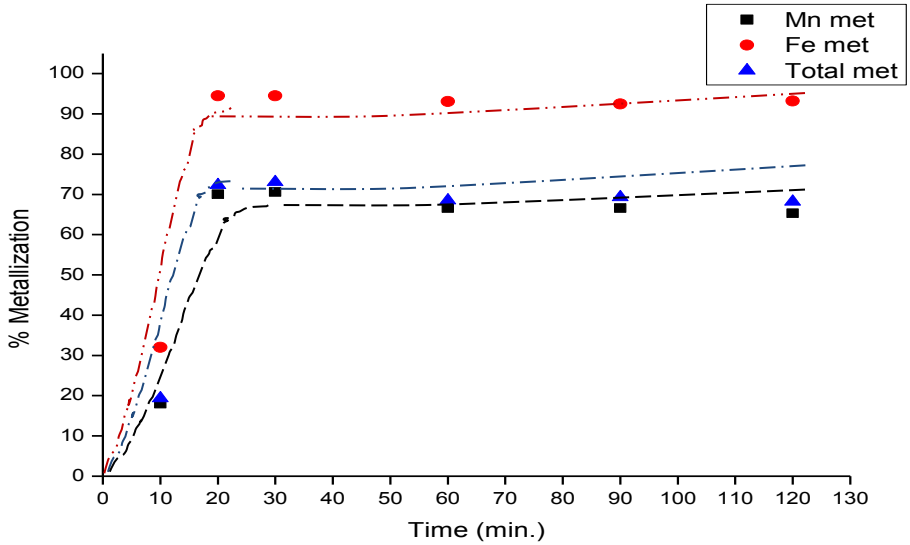

Figure B.8 Progress of metallization versus time for tests using 10 % CH_4 in Ar at T= 1200 ºC

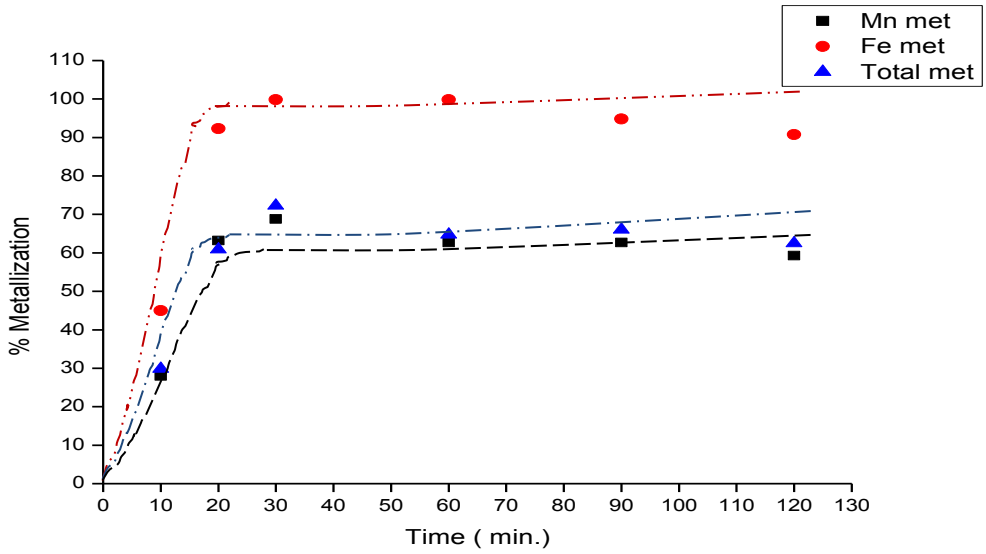

Figure B.9 Progress of metallization versus time for tests using 20 % CH_4 in Ar at T= 1200 °C

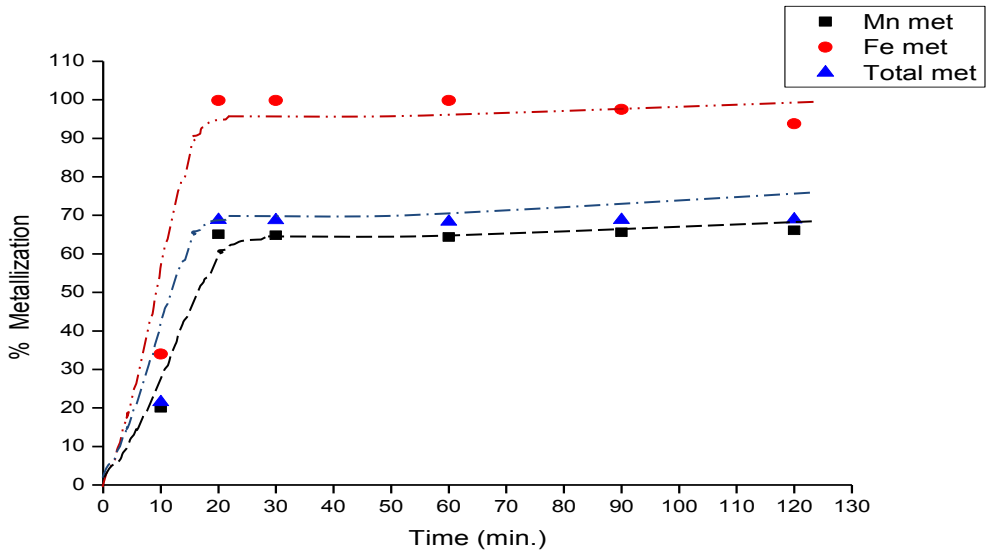

Figure B.10 Progress of metallization versus time for tests using 30 % CH_4 in Ar at T= 1200 °C

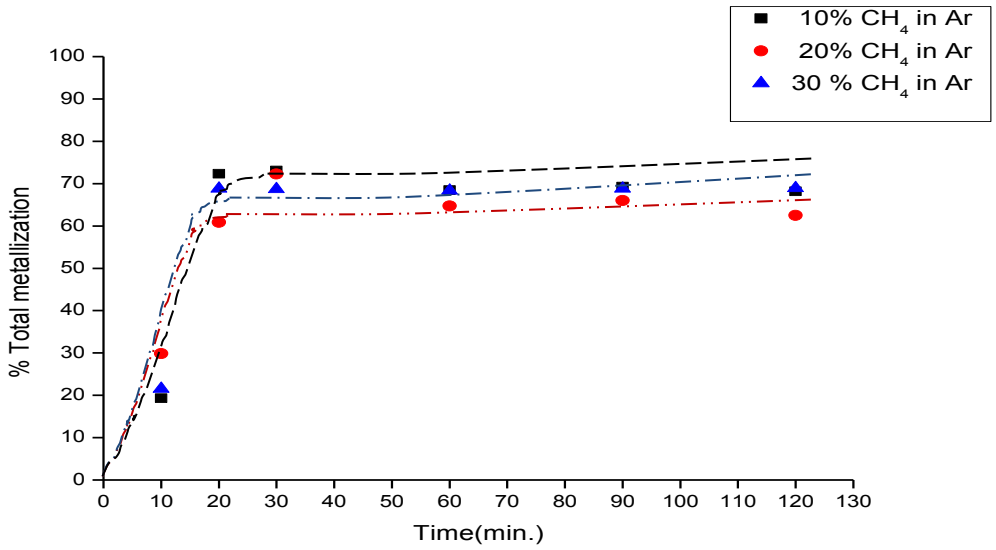

Figure B.11 Summary of a Total metallization at 1200 ºC in Ar

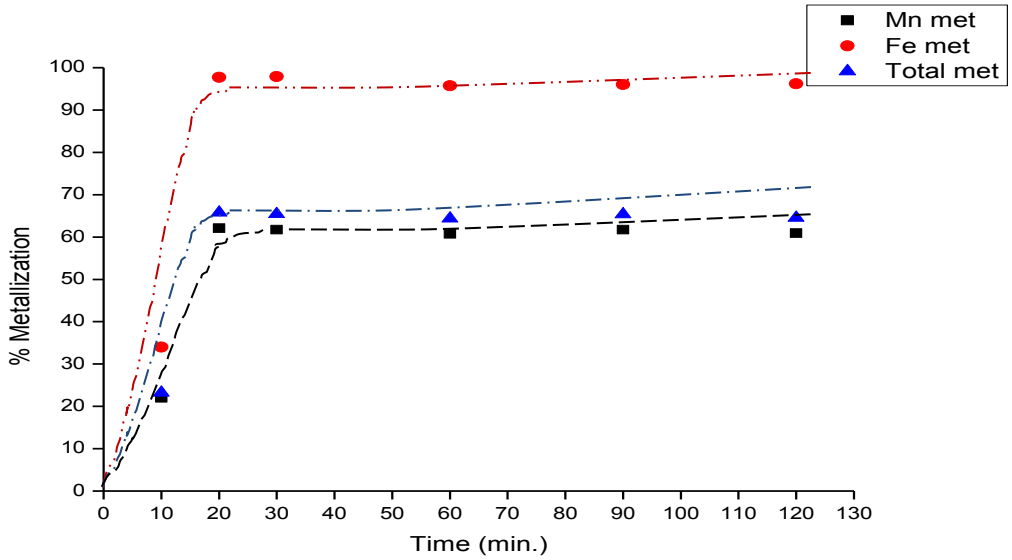

Figure B.12 Progress of metallization versus time for tests using 10 % CH_4 in Ar at T= 1250 ºC

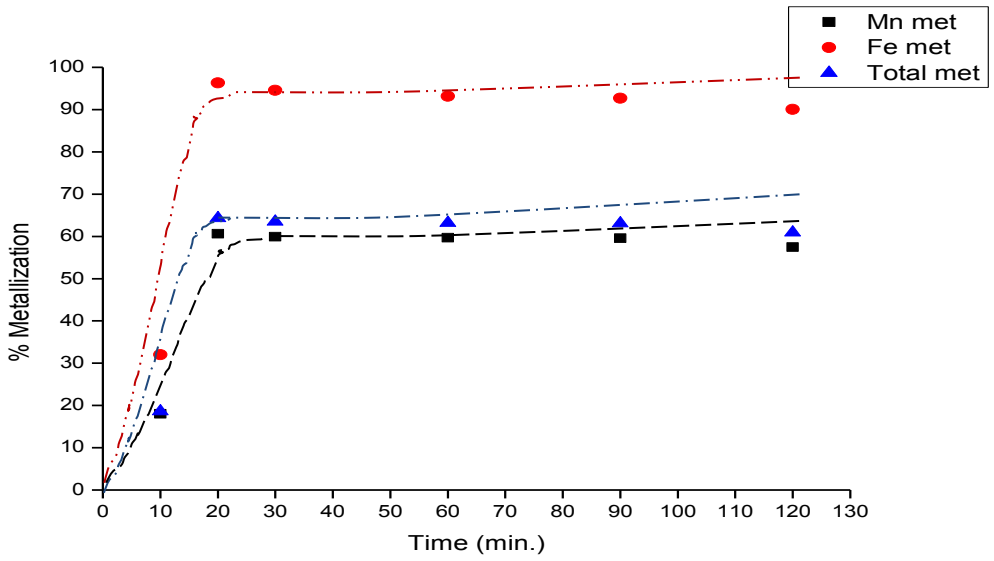

Figure B.13 Progress of metallization versus time for tests using 30 % CH_4 in Ar at T= 1250 ^oC

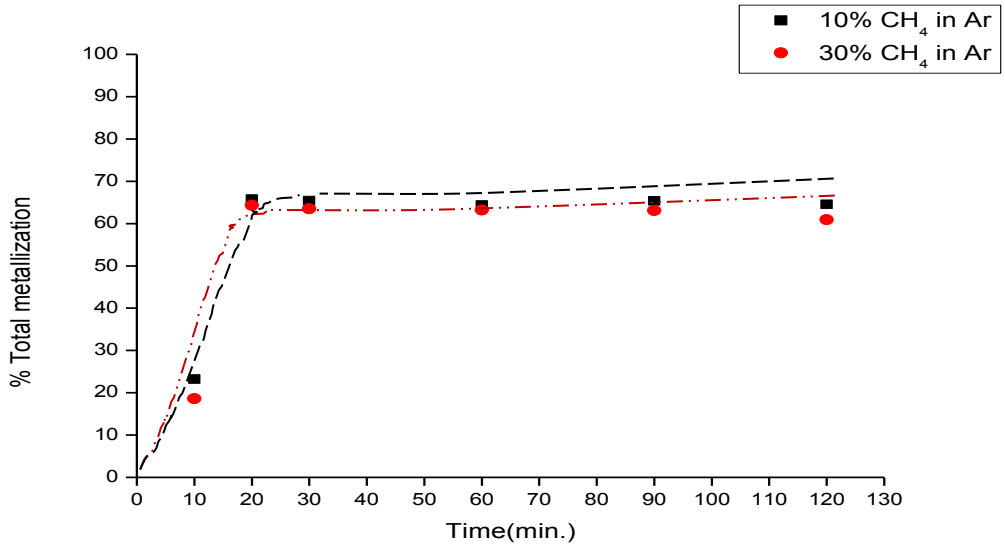

Figure B.14 Summary of total metallization at 1250 ^oC in Ar

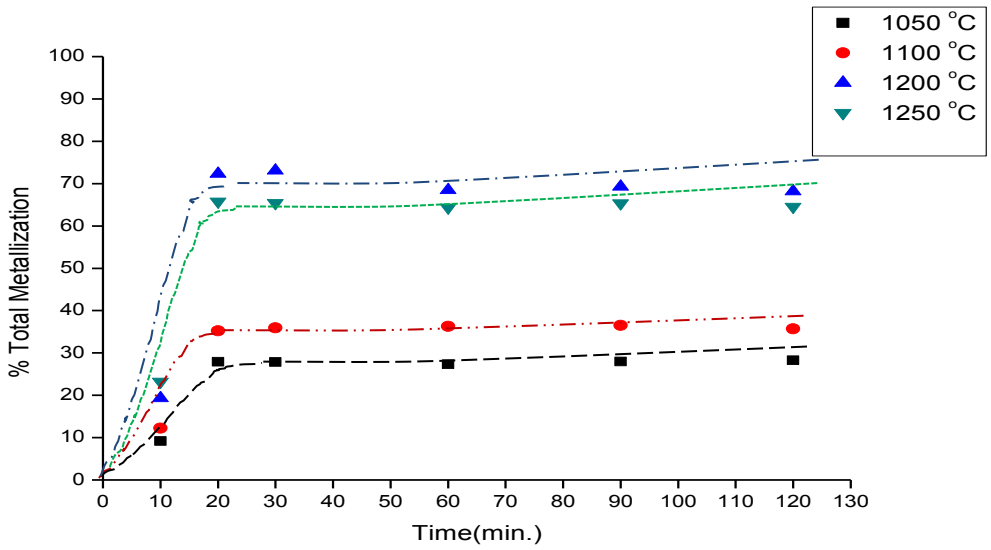

Figure B.15 Total metallization for 10 % CH_4 in Ar at different temperature

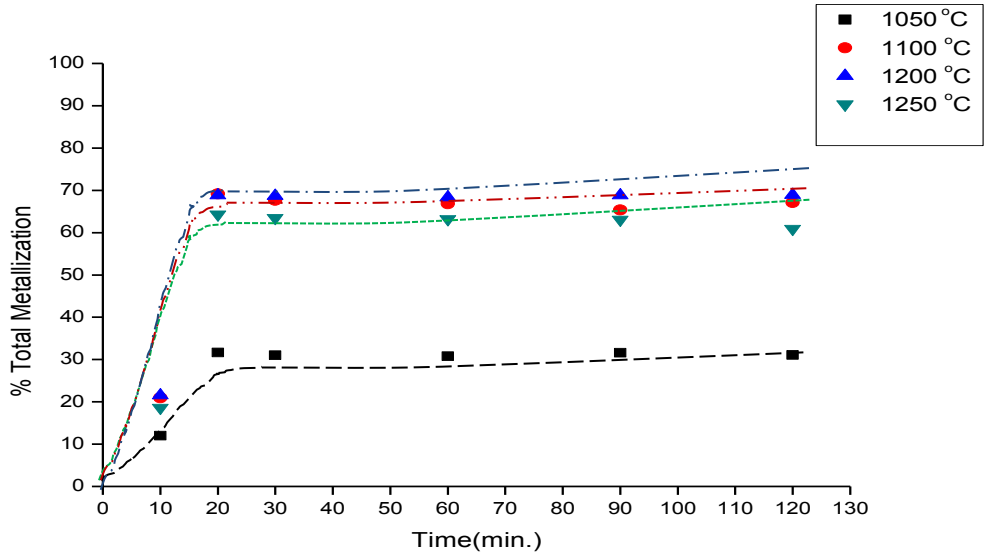

Figure B.16 Total Metallization for 30 % CH_4 in Ar at different temperature

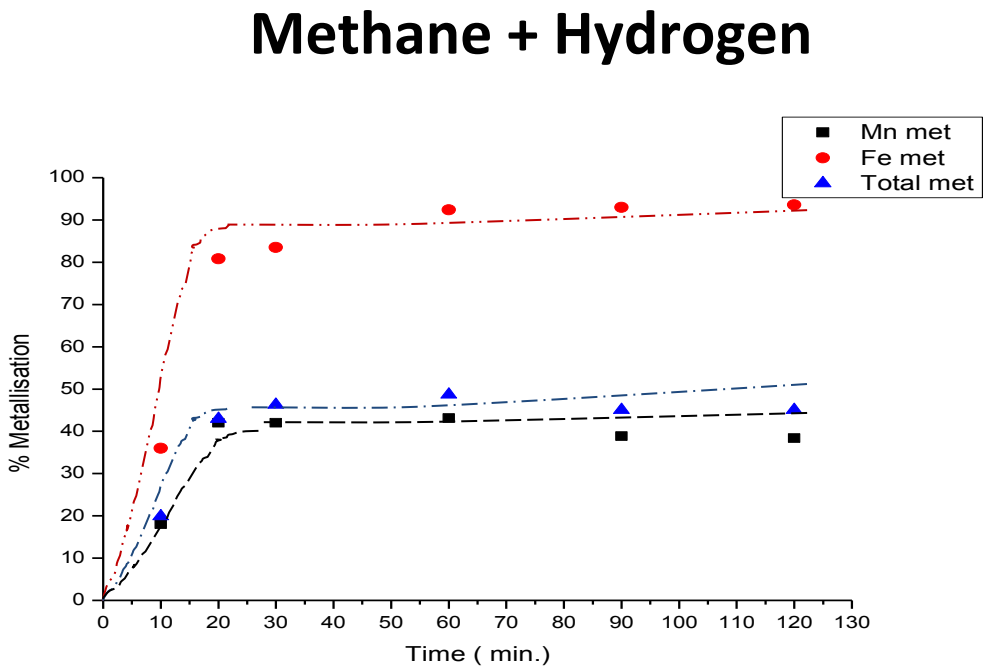

Figure B.17 Progress of metallization versus time for tests using 10 % CH_4 in H_2 at T= 1050 ºC

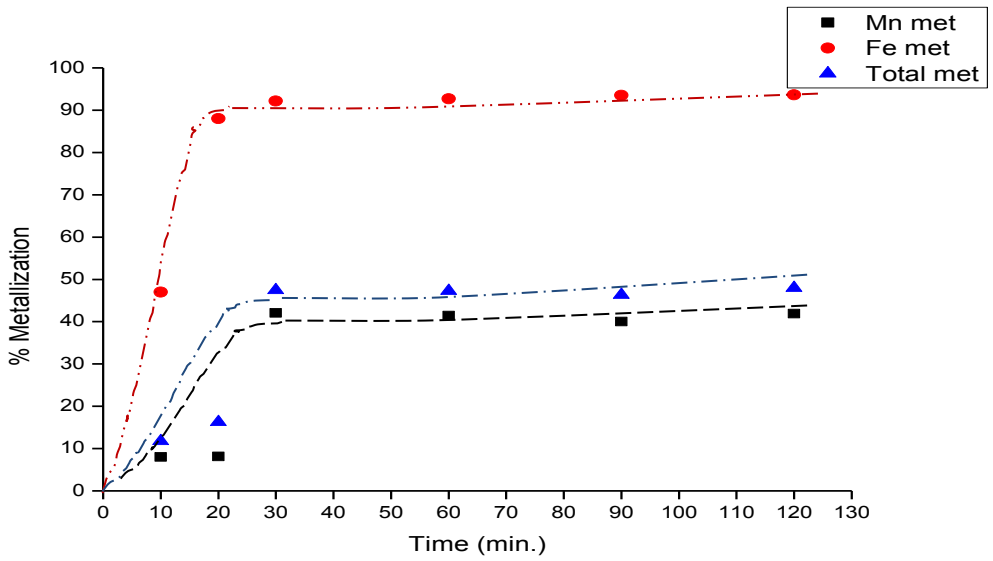

Figure B.18 Progress of metallization versus time for tests using 20 % CH_4 in H_2 at T= 1050 ºC

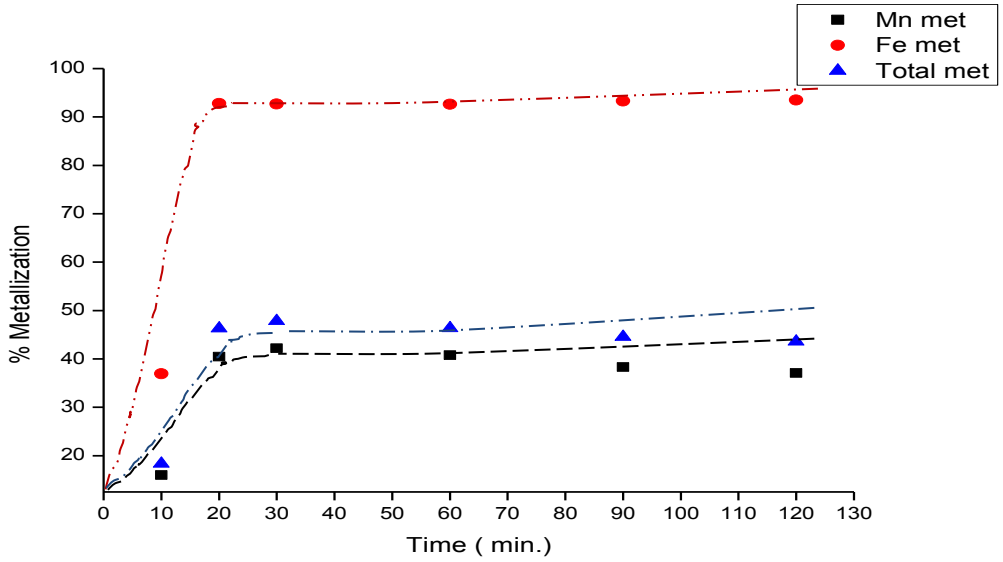

Figure B.19 Progress of metallization versus time for tests using 30 % CH_4 in H_2 at T= 1050 ºC

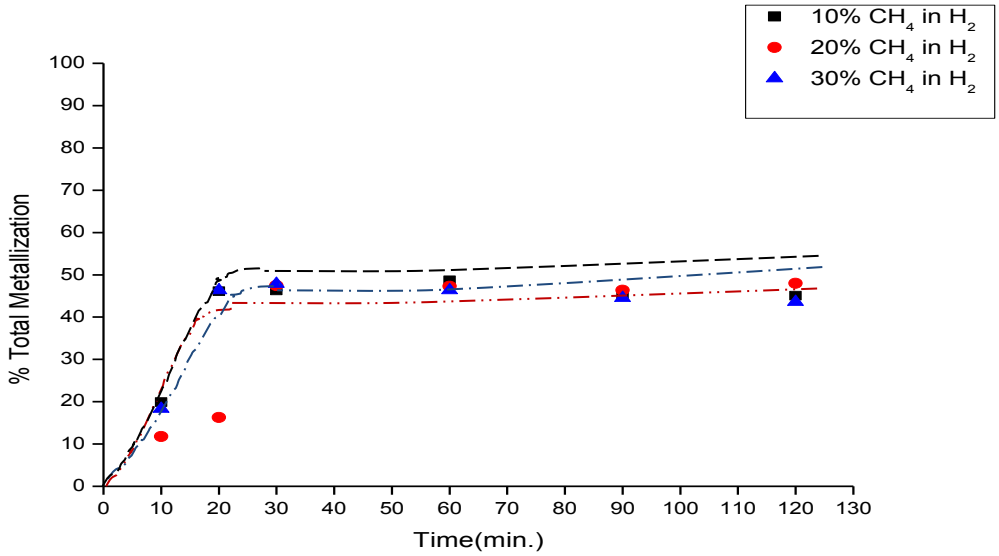

Figure B.20 Summary of Total metallization at 1050 ºC in H_2

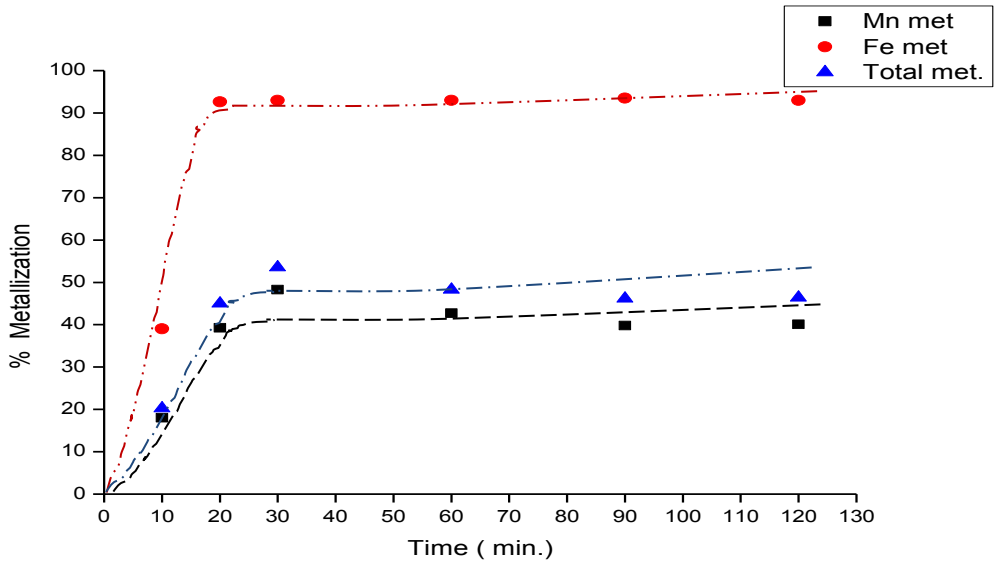

Figure B.21 Progress of metallization versus time for tests using 10 % CH_4 in H_2 at T= 1100 ^oC

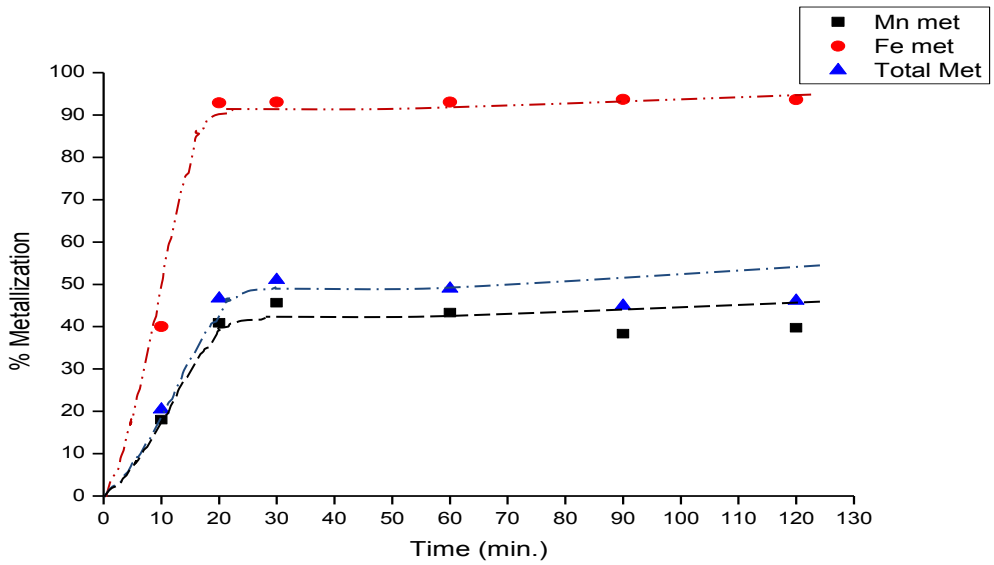

Figure B.22 Progress of metallization versus time for tests using 20 % CH_4 in H_2 at T= 1100 ^oC

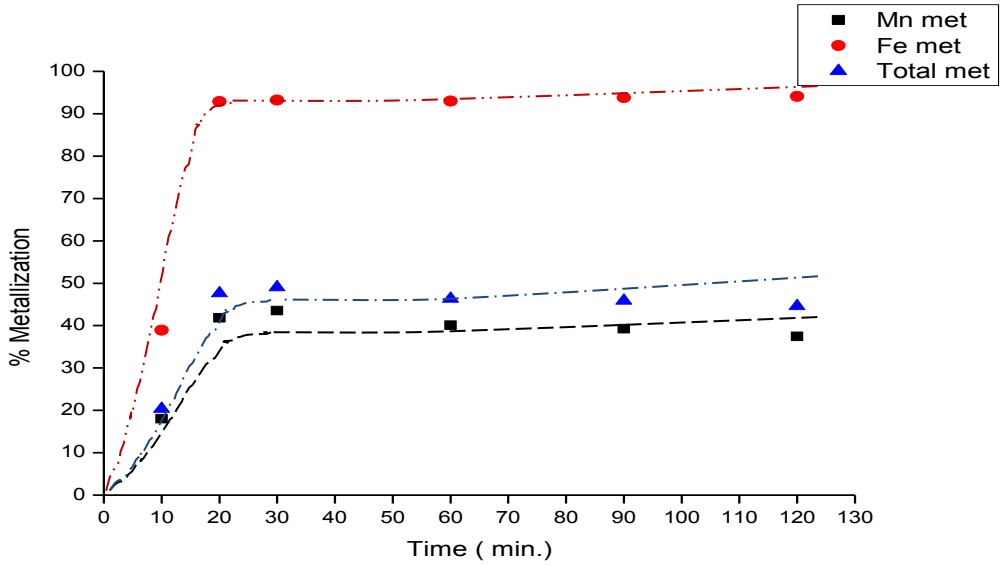

Figure B.23 Progress of metallization versus time for tests using 30 % CH_4 in H_2 at T= 1100 ^oC

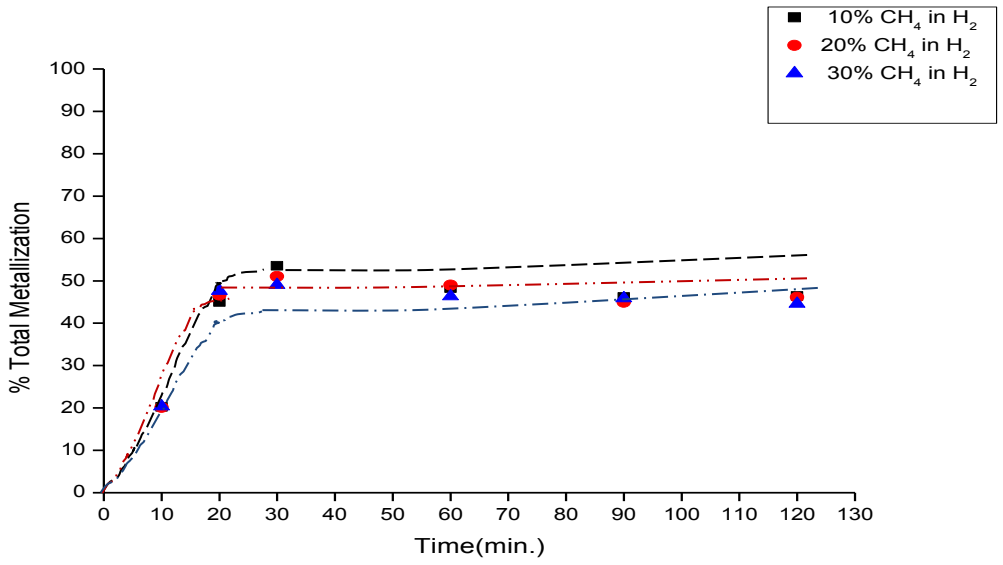

Figure B.24 Summary of total metallization at 1100 ^oC in H_2

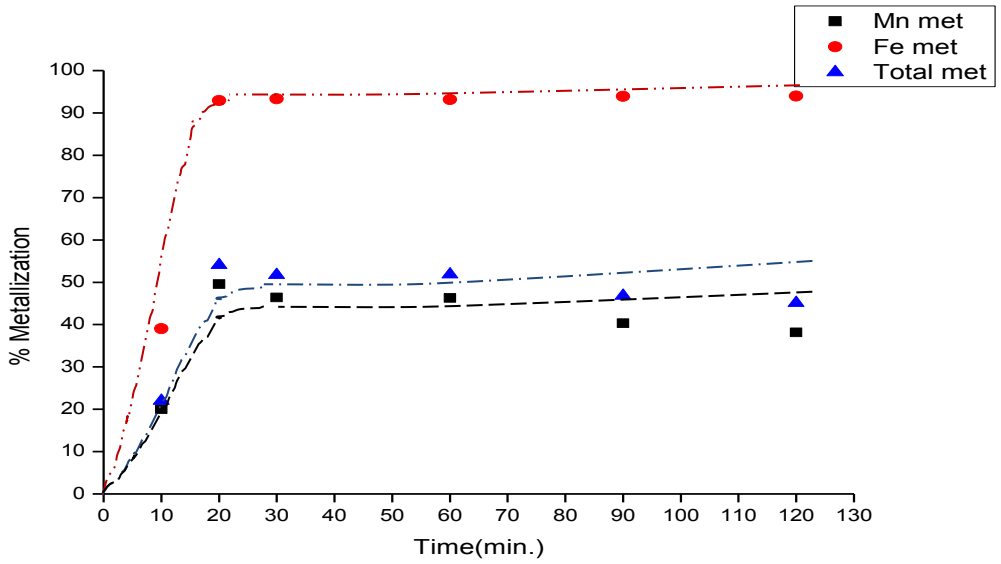

Figure B.25 Progress of metallization versus time for tests using 10 % CH_4 in H_2 at T= 1200 ^oC

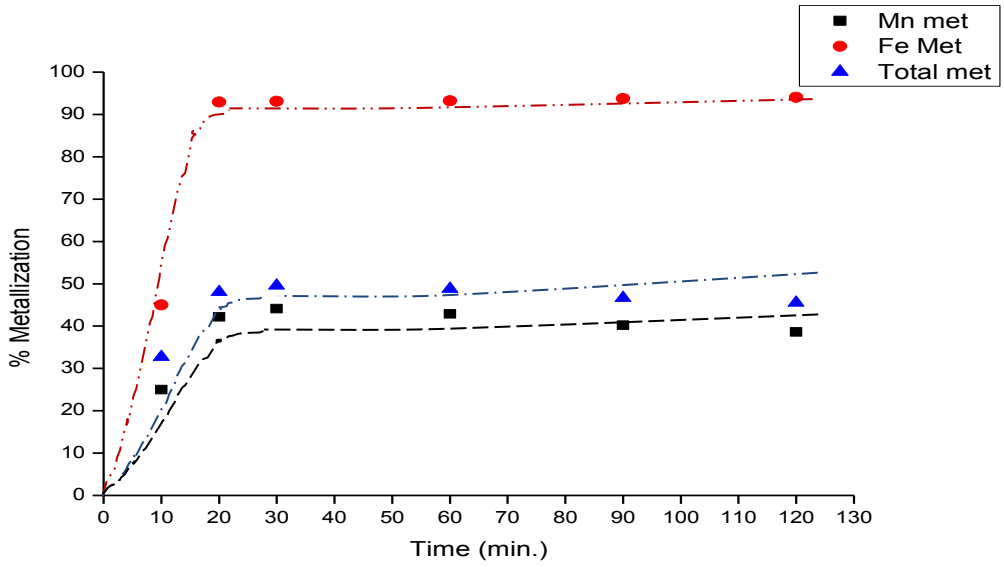

Figure B.26 Progress of metallization versus time for tests using 20 % CH_4 in H_2 at T= 1200 ^oC

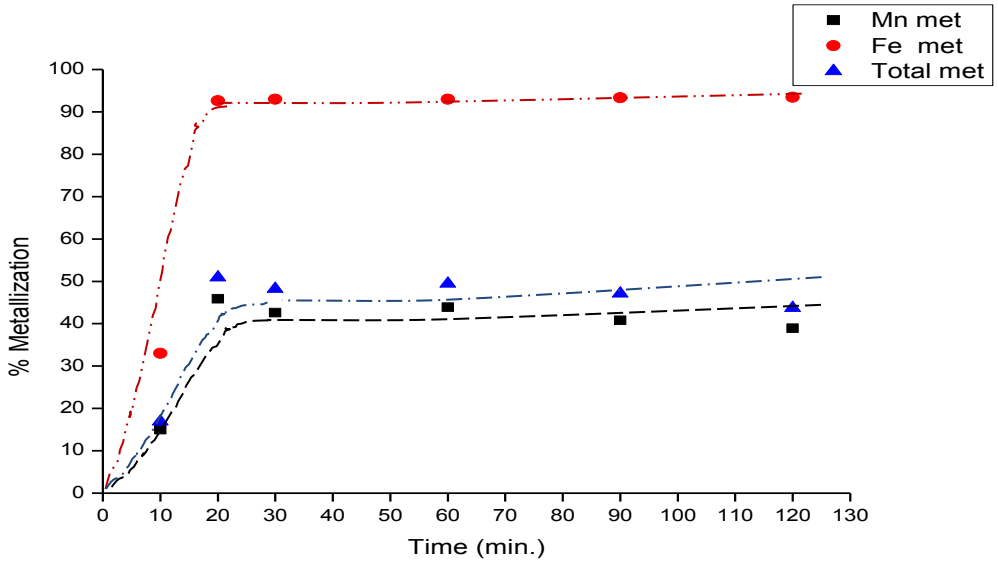

Figure B.27 Progress of metallization versus time for tests using 30 % CH_4 in H_2 at T= 1200 ^oC

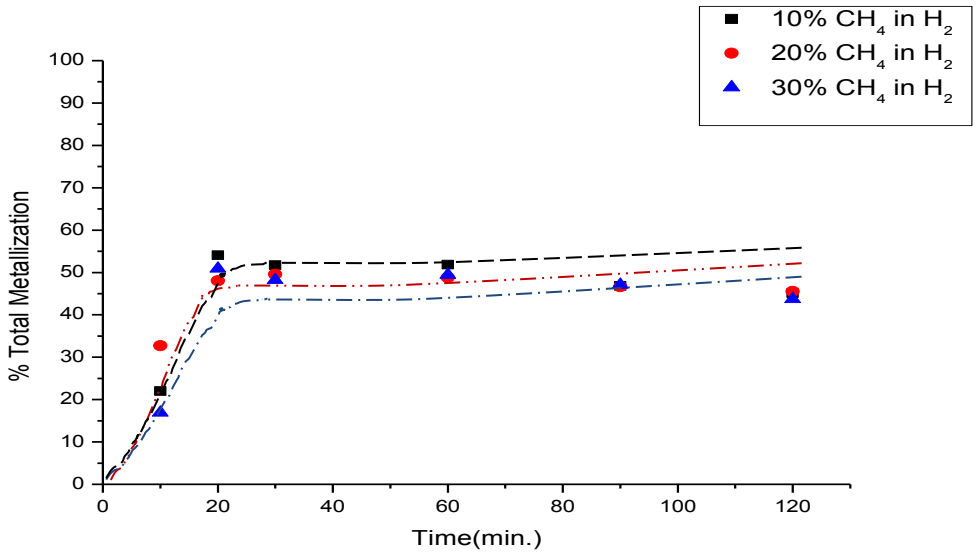

Figure B.28 Summary of total metallization at 1200 ^oC in H_2

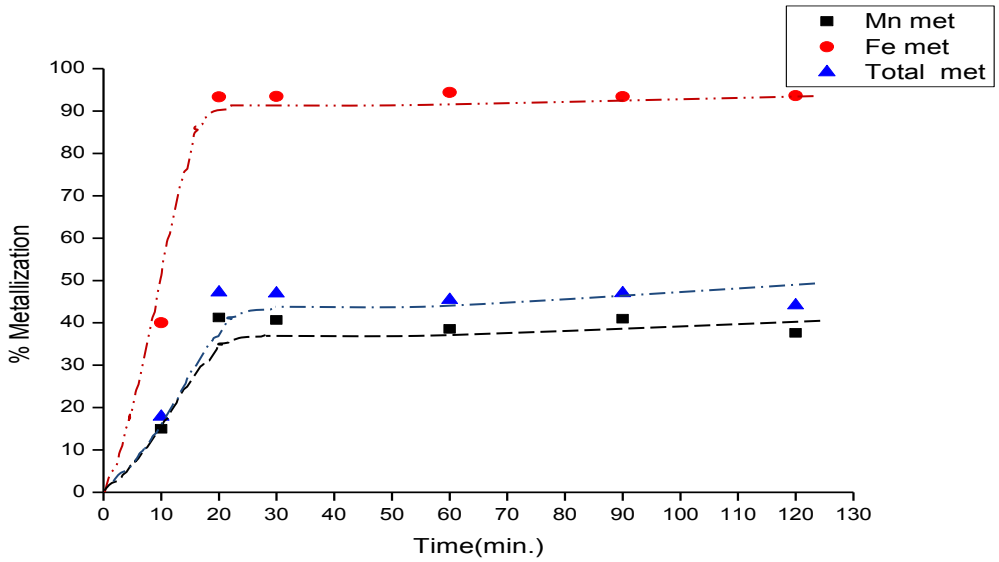

Figure B.29 Progress of metallization versus time for tests using 10 % CH_4 in H_2 at T= 1250 °C

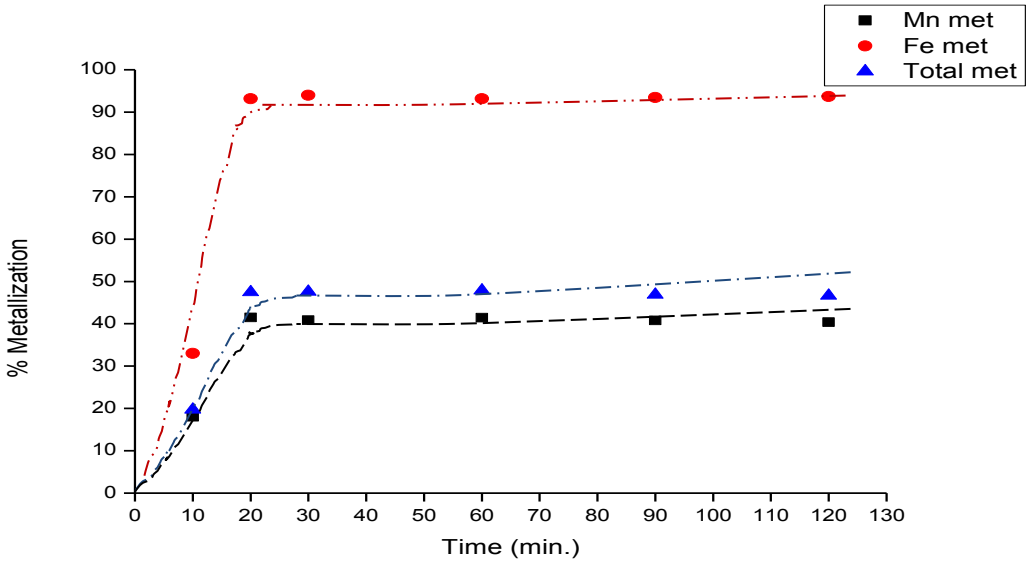

Figure B.30 Progress of metallization versus time for tests using 20 % CH_4 in H_2 at T= 1250 °C

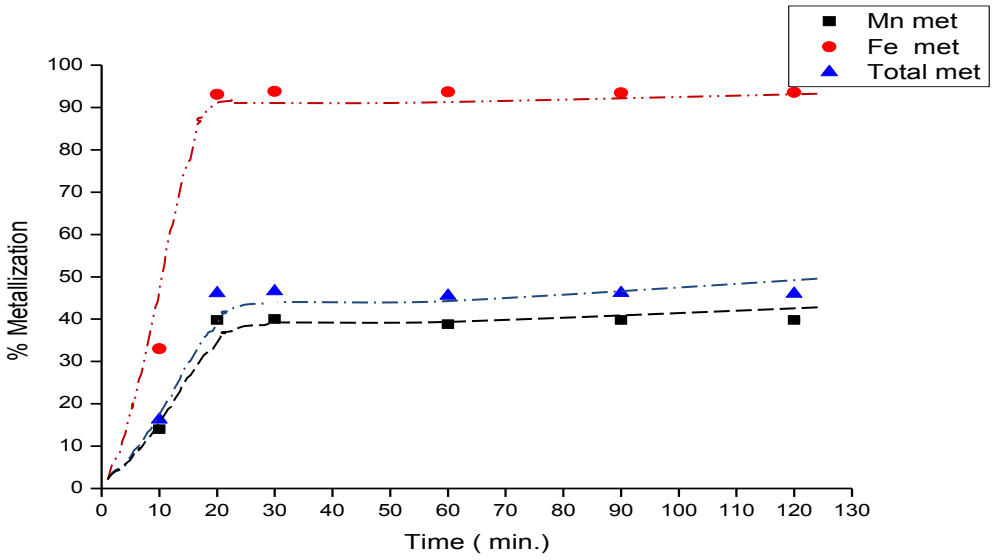

Figure B.31 Progress of metallization versus time for tests using 30 % CH_4 in H_2 at T= 1250 ^oC

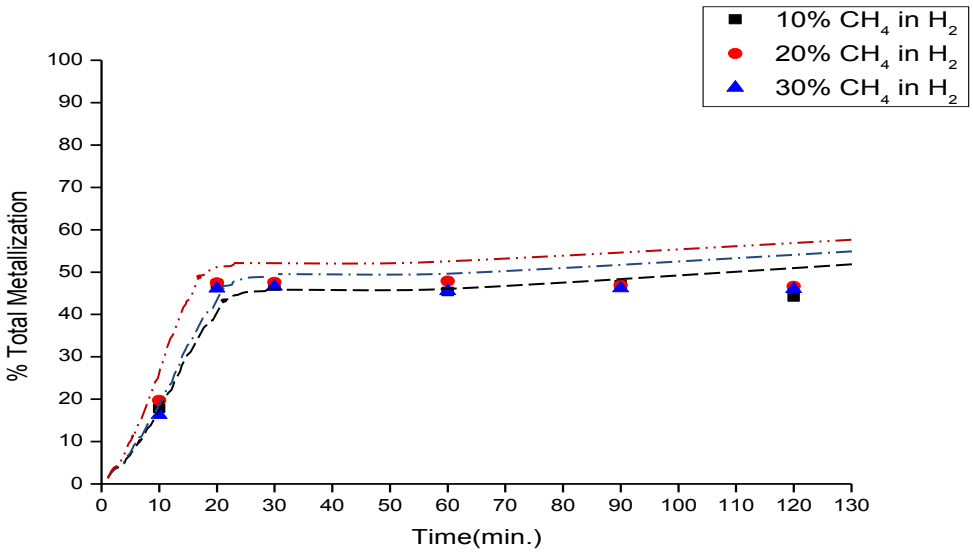

Figure B. 32 Summary of Total metallization at 1250 ^oC in H_2

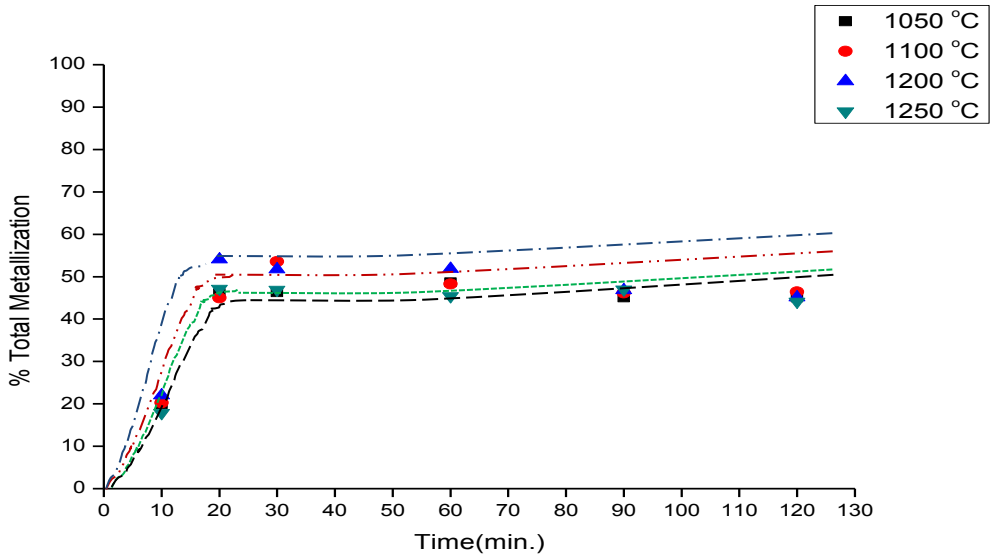

Figure B.33 Summary of Total metallization for 10% CH_4 in H_2 at different temperatures

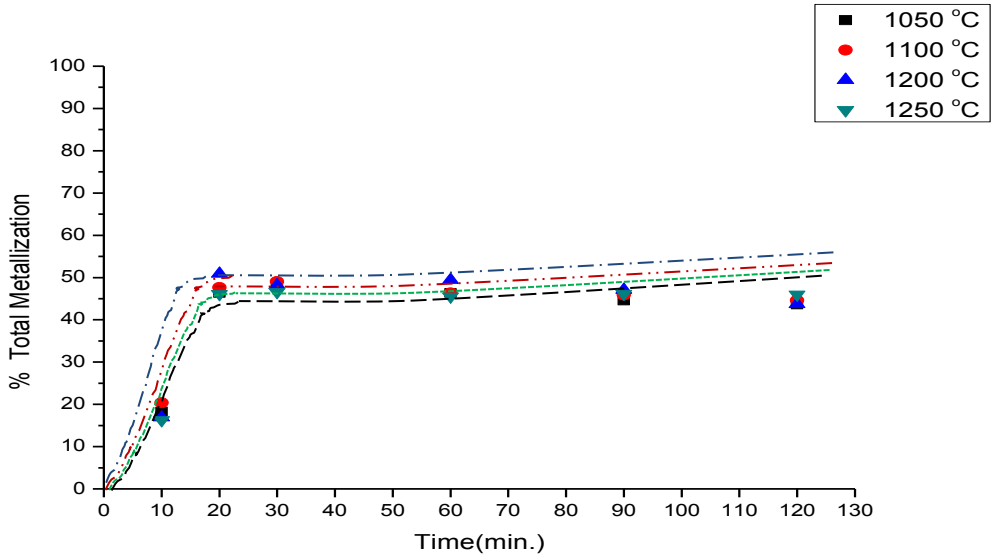

Figure B.34 Summary of Total metallization for 30% CH_4 in H_2 at different temperatures

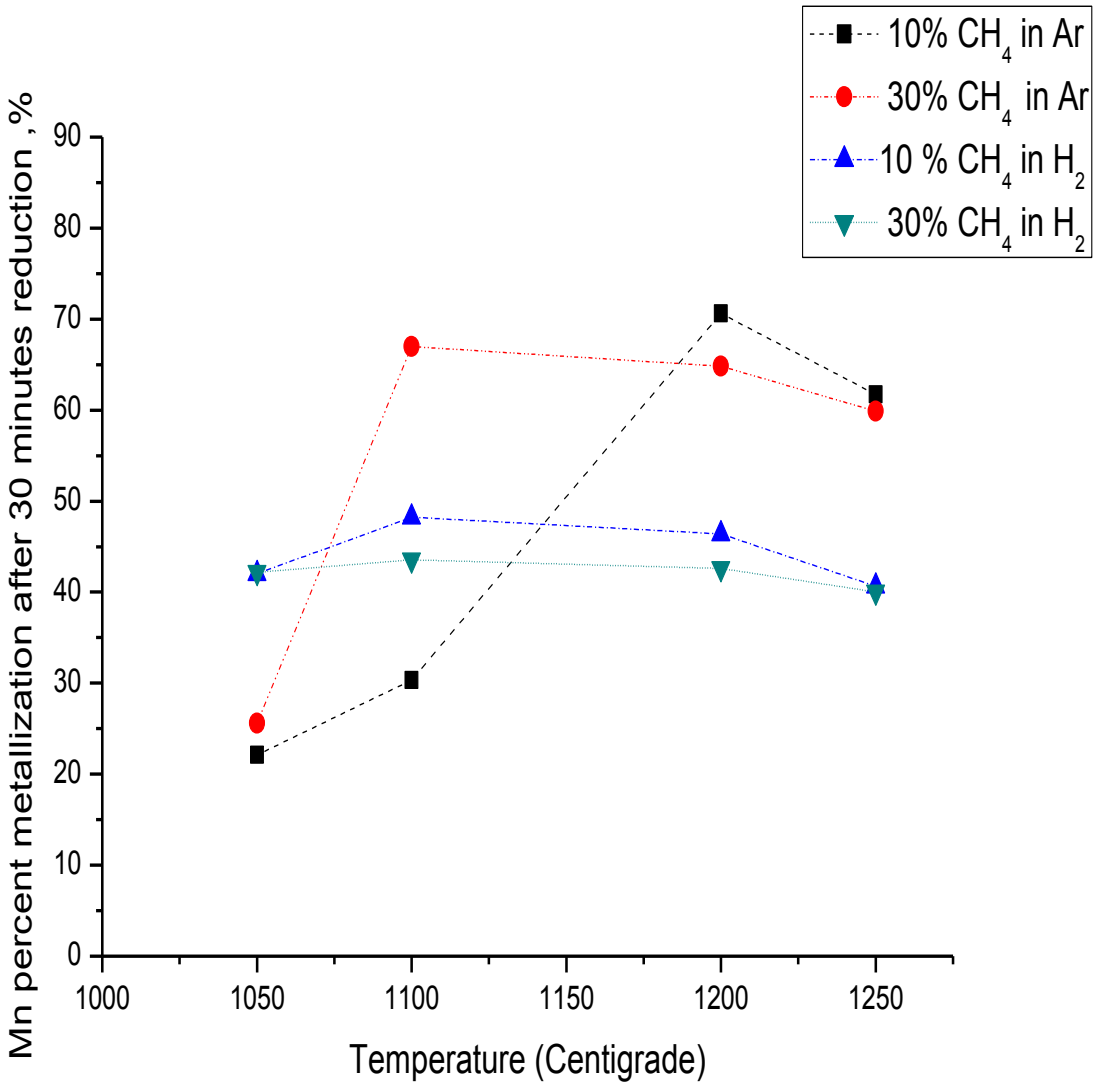

Figure B.35 % Mn metallization for 30 minutes at different concentration and temperatures

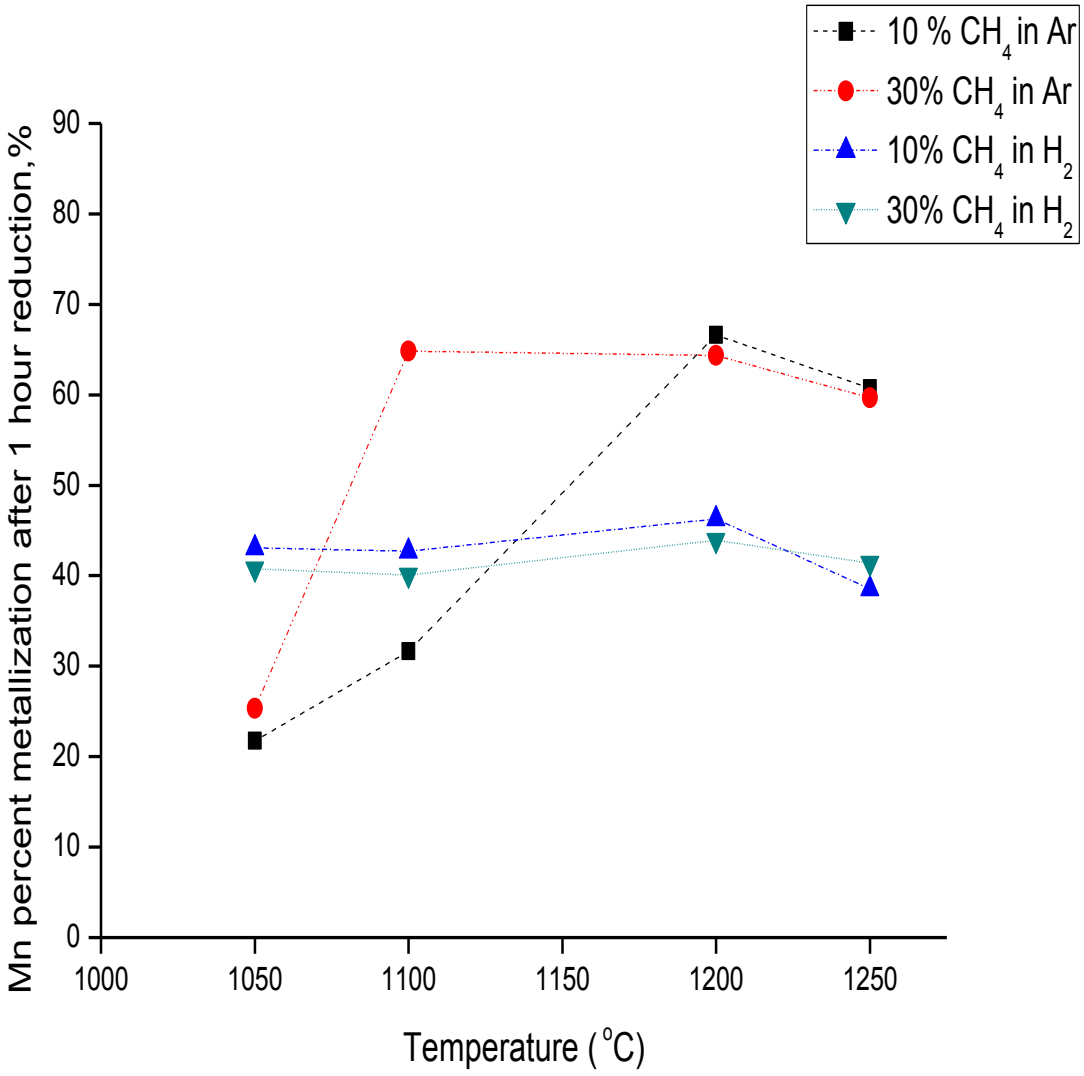

Figure B.36 % Mn metallization for 1 hour at different concentration and temperatures

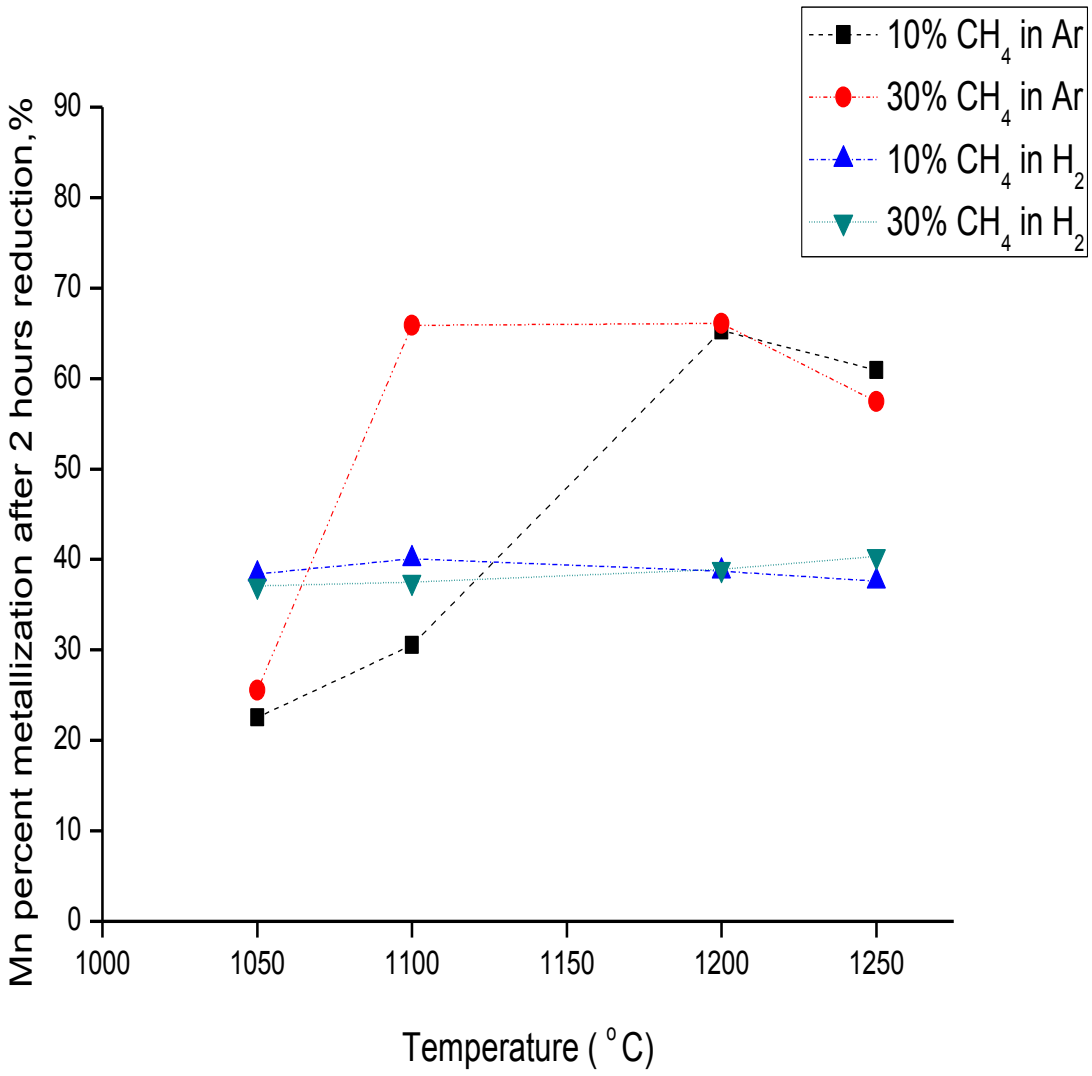

Figure B.37 % Mn metallization for 2 hour at different concentration and temperatures

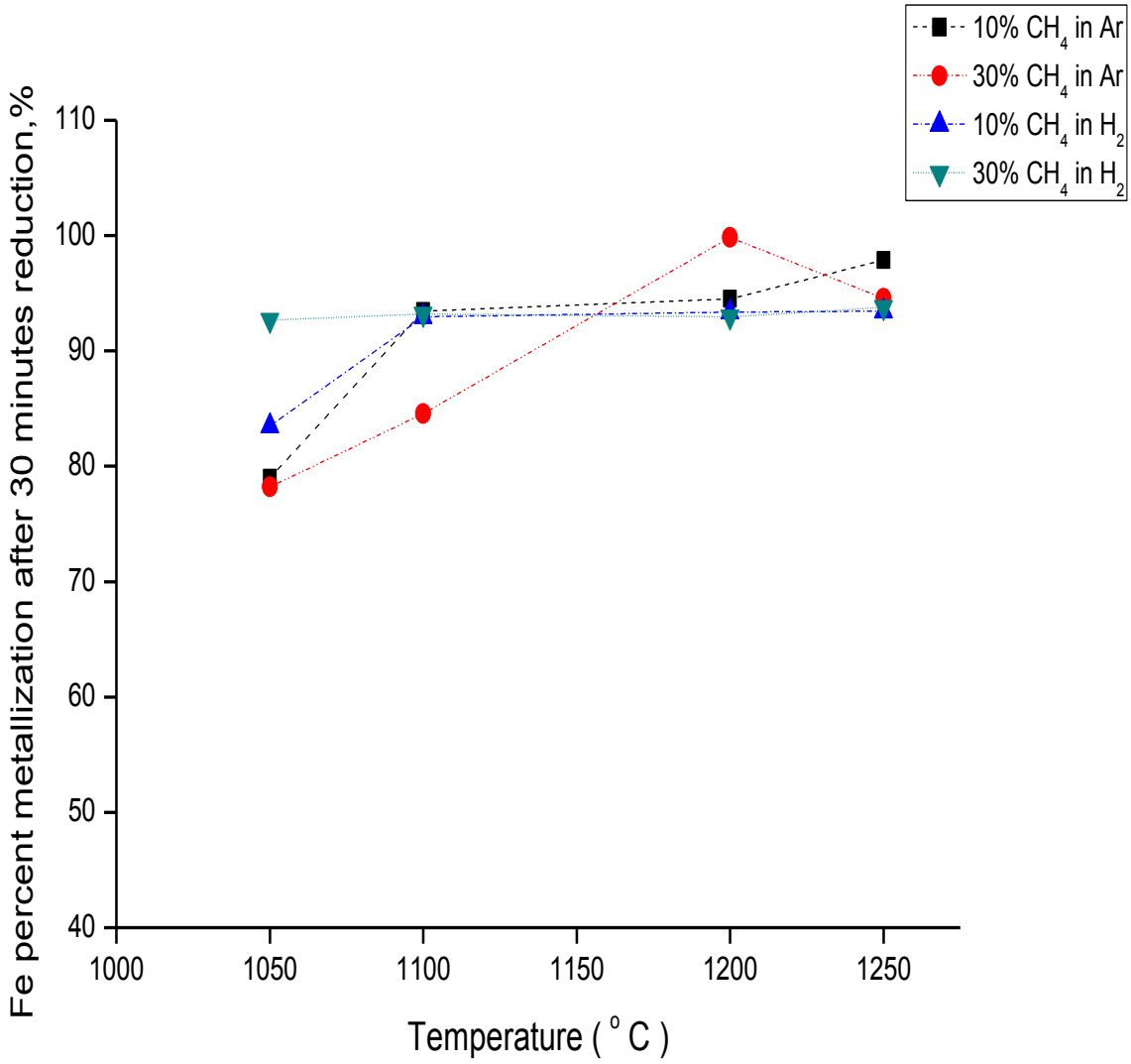

Figure B. 38 % Fe metallization for 30 minutes at different concentration and temperatures

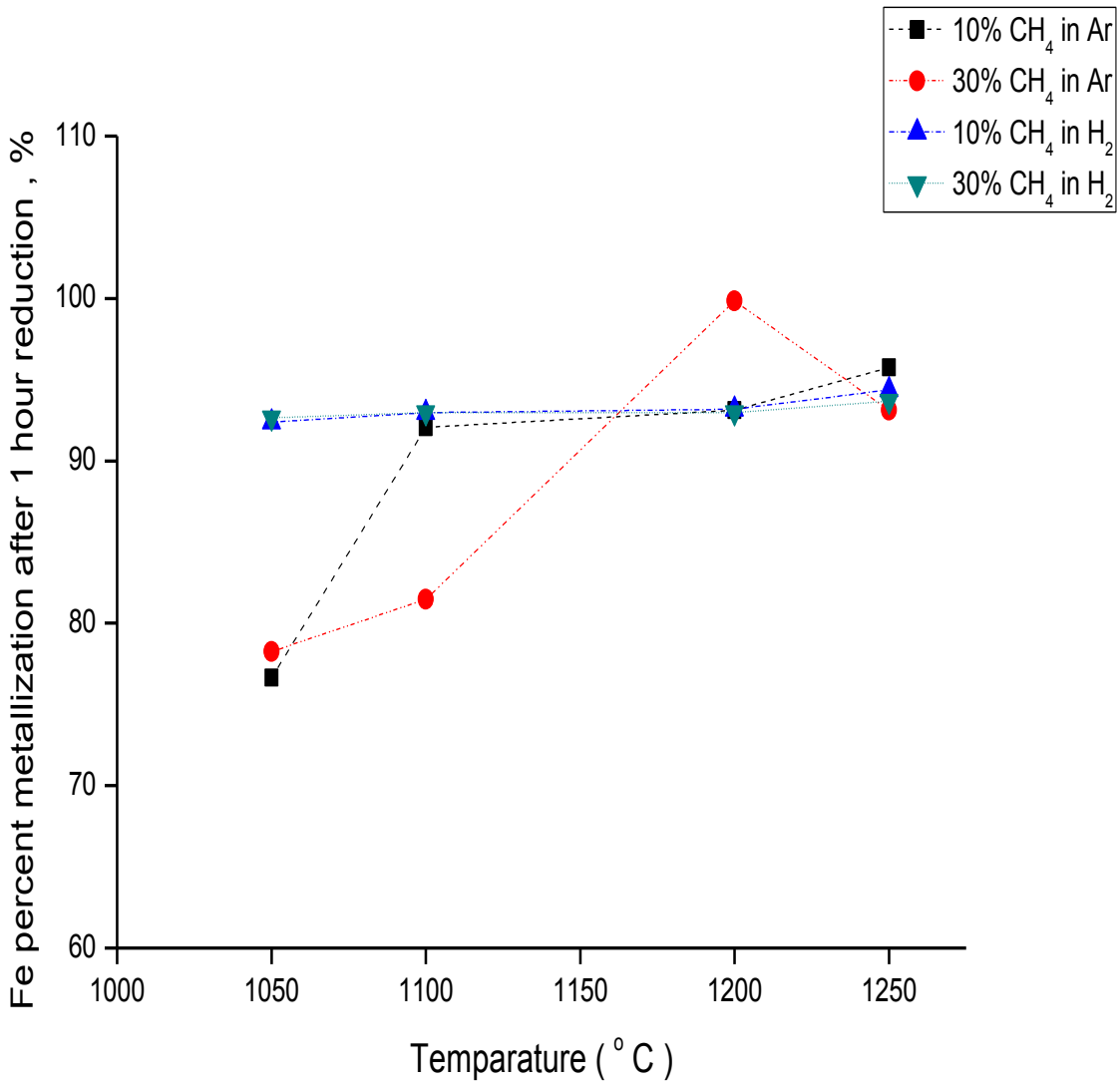

Figure B. 39 % Fe metallization for 1 hour at different concentration and temperatures

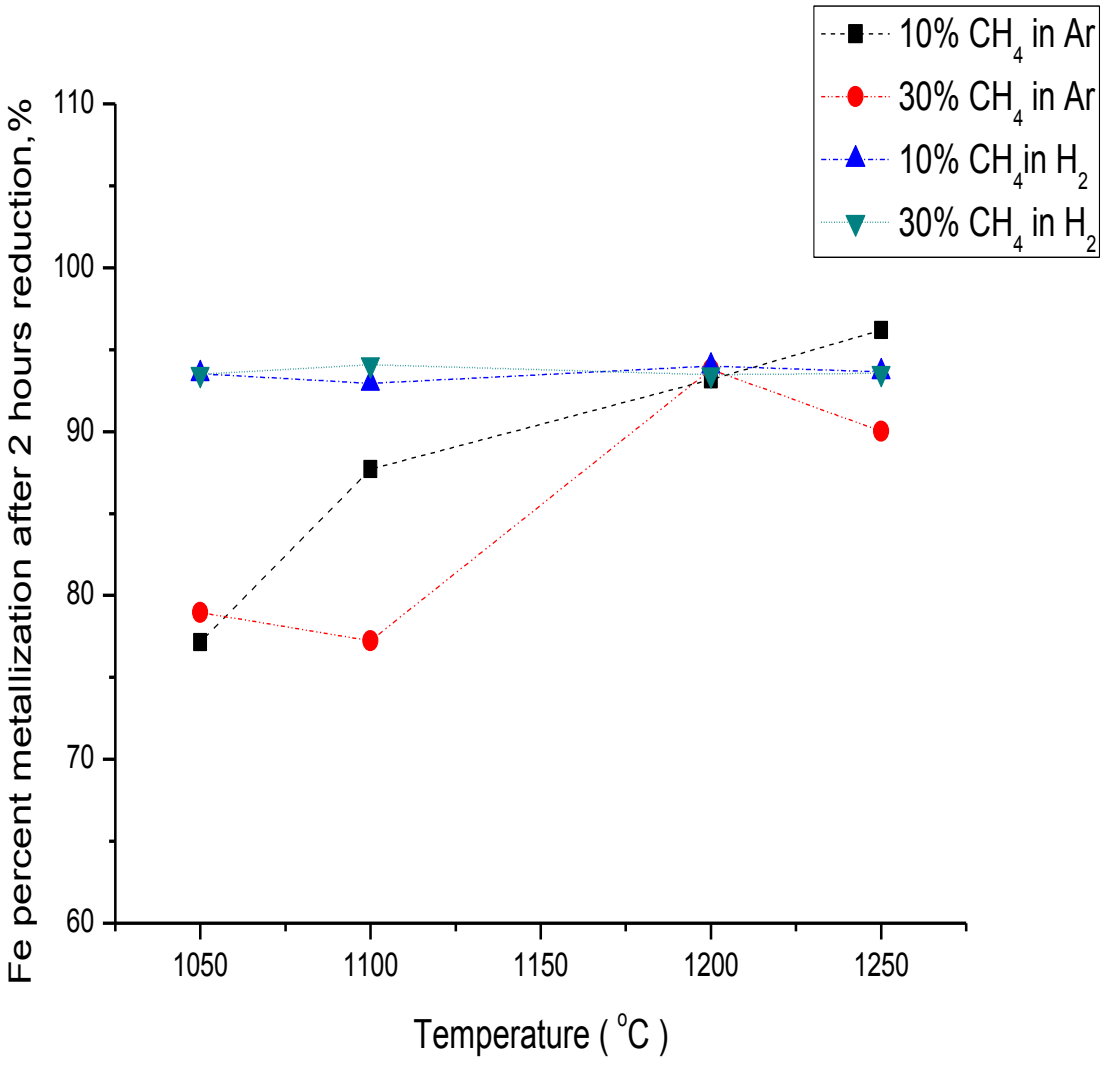

Figure B. 40 % Fe metallization for 2 hours at different concentration and temperatures

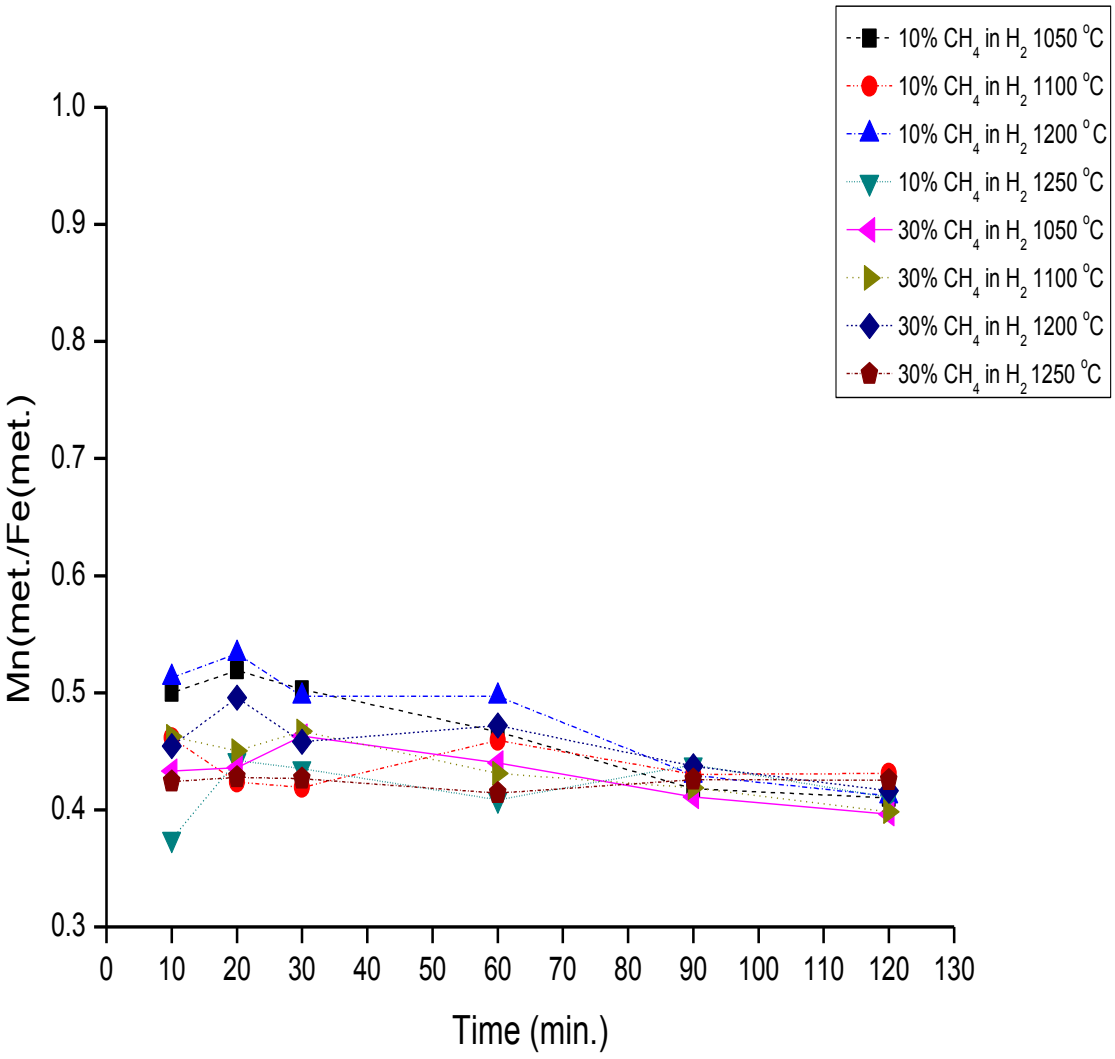

Figure B. 41 Mn /Fe metallization ratios at different concentrations in H_2

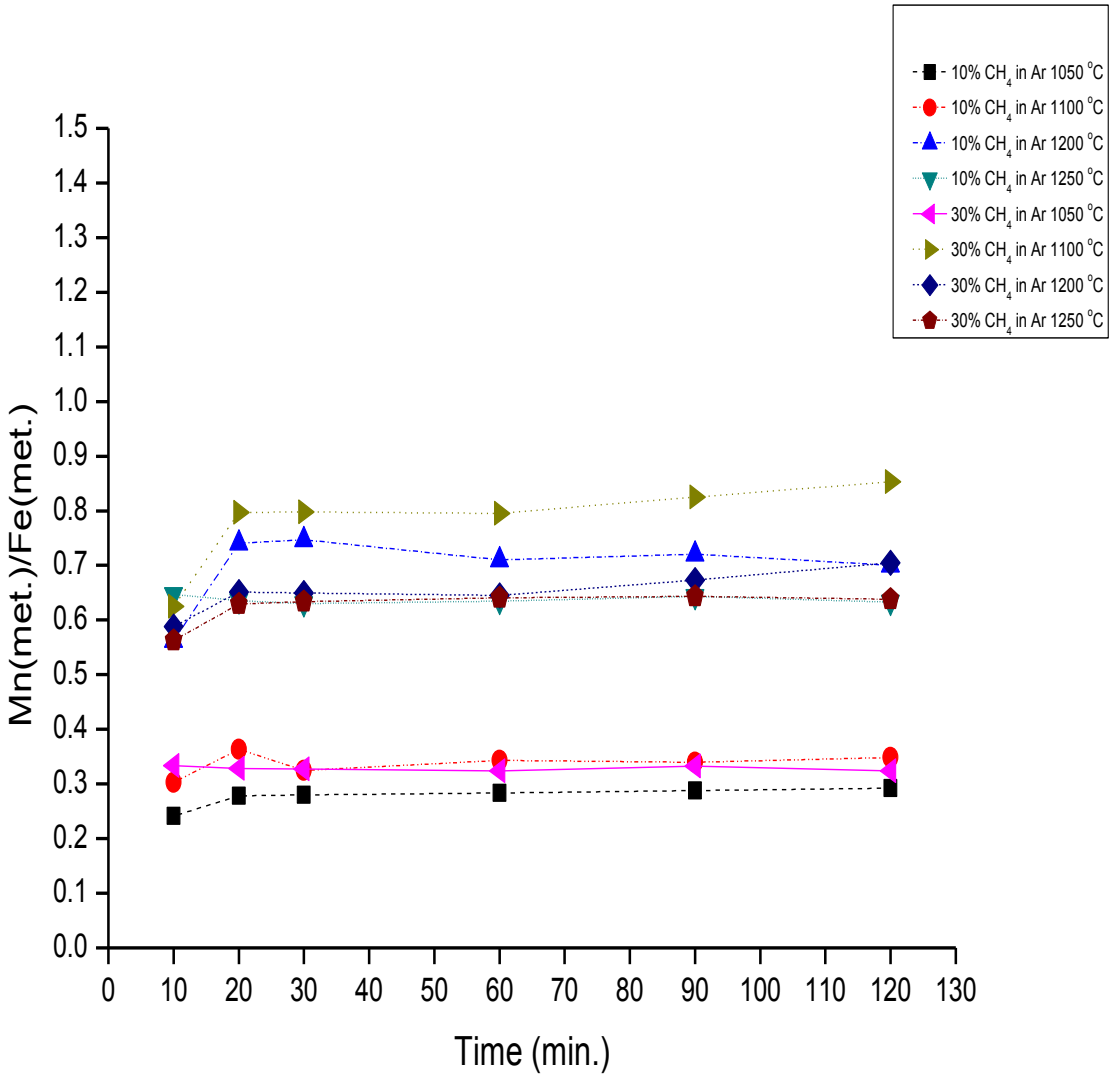

Figure B.42 Mn /Fe metallization ratios at different concentrations in Ar

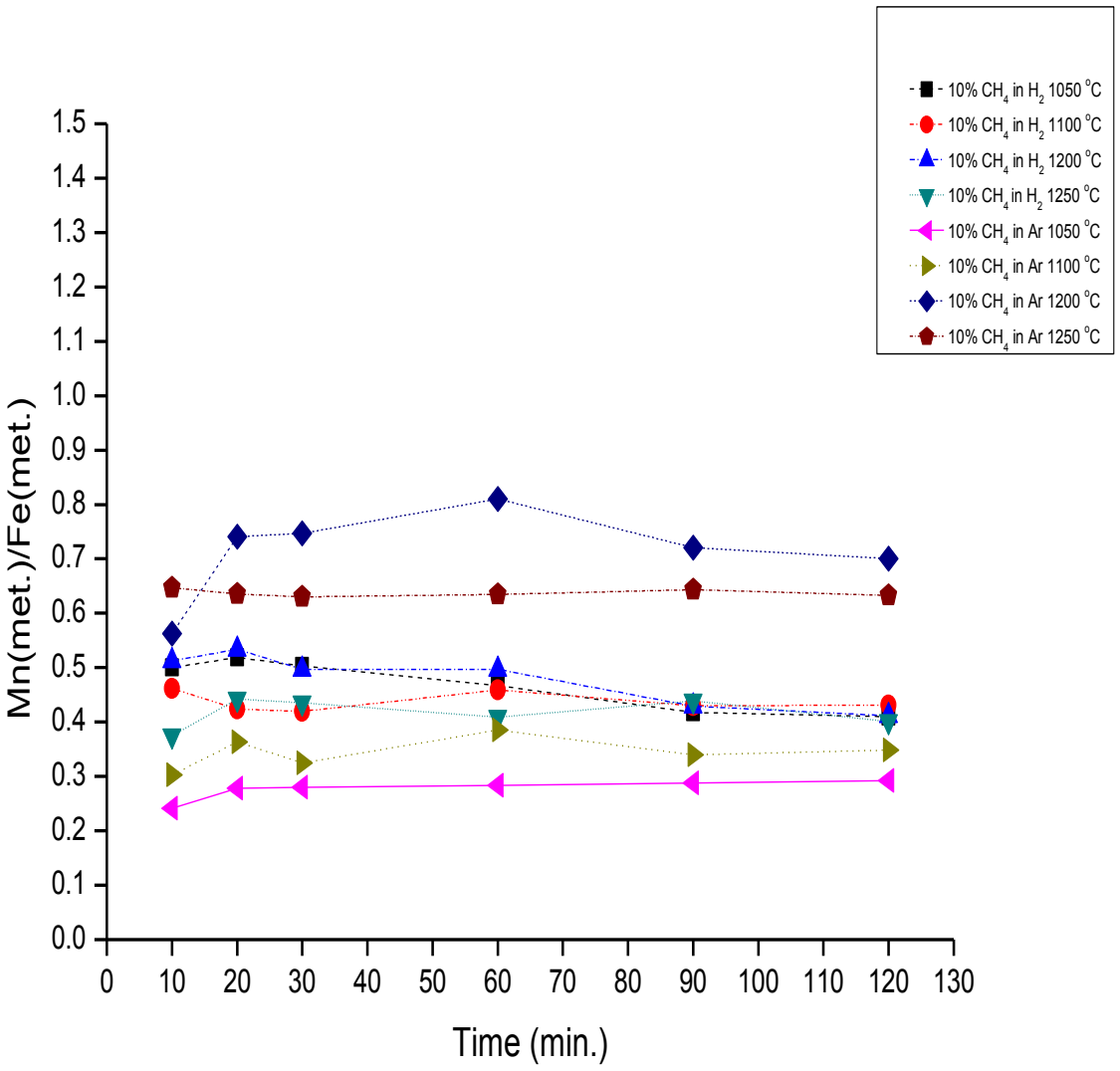

Figure B.43 Mn/Fe metallization ratios at 10% CH_4 concentrations in H_2 and Ar

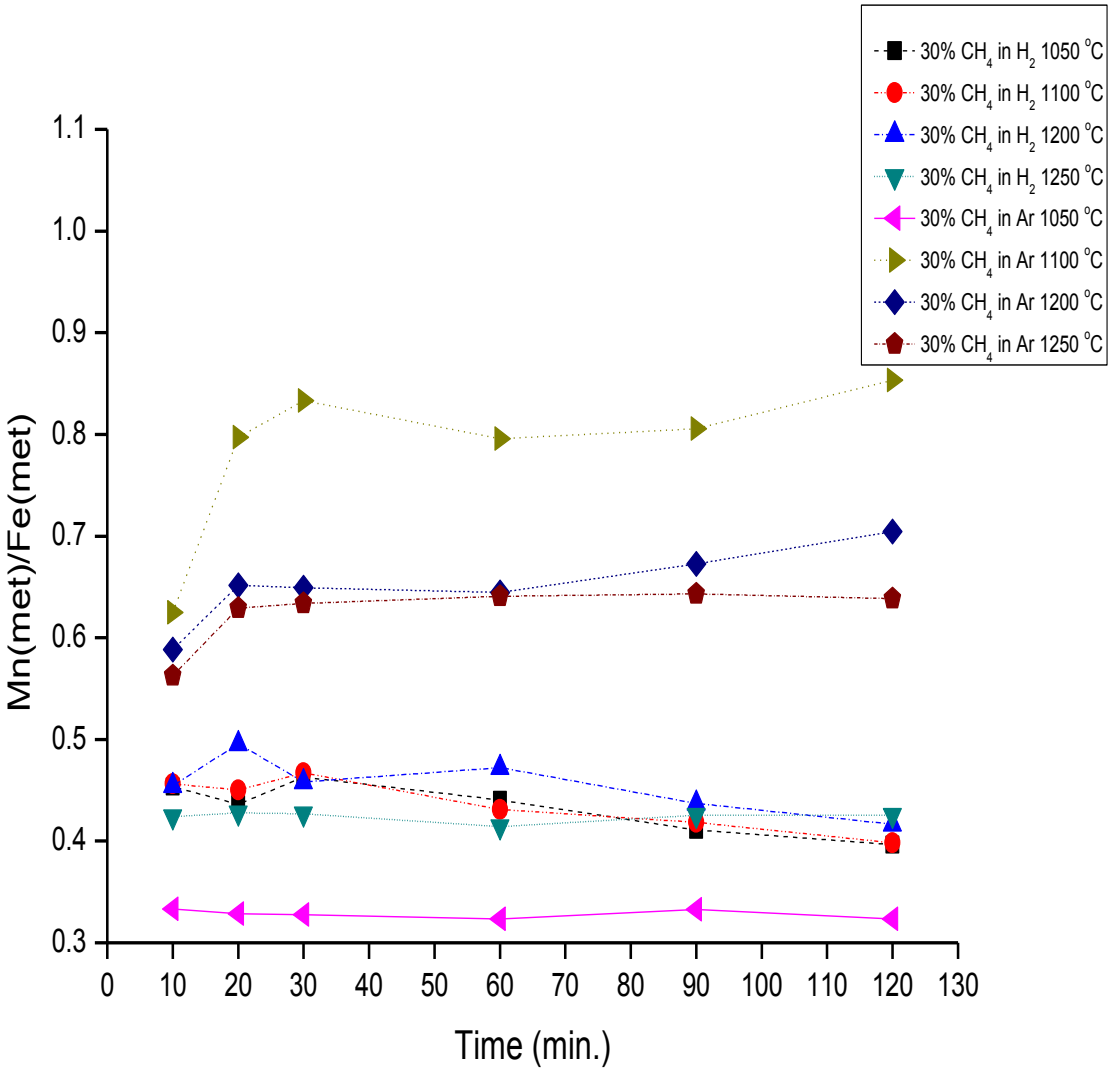

Figure B.44 Mn/Fe metallization ratios at 30 % concentrations in H_2 and Ar

X-RAY DIFFRACTION RESULTS

X-RD Phases present in the partially reduced manganese under different reducing conditions.

Table B1: X-RD Phases present in the partially reduced manganese under the different reducing conditions of 10 % methane, argon and 10% methane, hydrogen gas mixtures at all temperatures.

T(°C)	Reducing Medium	Reduction Time (min.)	Phases Detected
1050°C	10% CH_4 in Ar	20	Mn_5C_2; Mn_7C_3; $Mn_{15}C_4$; $Mn_{23}C_6$; Fe_7C_3; Fe_3C; $Mn_2Fe(CO)_{14}$; Ca_2FeMnO_5; $Fe_{2.7}Mn_{0.3}C$; $Fe_{1.8}Mn_{1.2}C_2$; $Fe_{1.1}Mn_{3.9}C_2$
		30	Mn_5C_2; Mn_7C_3; $Mn_{15}C_4$; $Mn_{23}C_6$; Fe_7C_3; Fe_3C; $Mn_2Fe(CO)_{14}$; Ca_2FeMnO_5; $Fe_{2.7}Mn_{0.3}C$; $Fe_{1.8}Mn_{1.2}C_2$; $Fe_{1.1}Mn_{3.9}C_2$
		60	Mn_5C_2; Mn_7C_3; $Mn_{15}C_4$; $Mn_{23}C_6$; Fe_7C_3; Fe_3C; $Mn_2Fe(CO)_{14}$; Ca_2FeMnO_5; $Fe_{2.7}Mn_{0.3}C$; $Fe_{1.8}Mn_{1.2}C_2$; $Fe_{1.1}Mn_{3.9}C_2$
		90	Mn_5C_2; Mn_7C_3; $Mn_{15}C_4$; $Mn_{23}C_6$; Fe_7C_3; Fe_3C; $Mn_2Fe(CO)_{14}$; Ca_2FeMnO_5; $Fe_{2.7}Mn_{0.3}C$; $Fe_{1.8}Mn_{1.2}C_2$; $Fe_{1.1}Mn_{3.9}C_2$
		120	Mn_5C_2; Mn_7C_3; $Mn_{15}C_4$; $Mn_{23}C_6$; Fe_7C_3; Fe_3C; $Mn_2Fe(CO)_{14}$; Ca_2FeMnO_5; $Fe_{2.7}Mn_{0.3}C$; $Fe_{1.8}Mn_{1.2}C_2$; $Fe_{1.1}Mn_{3.9}C_2$
1050°C	10% CH_4 in H_2	20	Mn_7C_3; Mn_5C_2; $Mn_{23}C_6$; Fe_7C_3; Fe_3C; Ca_2FeMn0_5; $Mn_2Fe(CO)_{14}$
		30	Mn_7C_3; Mn_5C_2; $Mn_{23}C_6$; Fe_7C_3; Fe_3C; Ca_2FeMn0_5; $MnFe_2O_4$; $FeMn_2O_4$
		60	Mn_7C_3; Mn_5C_2; $Mn_{23}C_6$; Fe_7C_3; Fe_3C; Ca_2FeMn0_5;$MnFe_2O_4$; $FeMn_2O_4$; $Fe_3Mn_3O_8$
		90	$Mn_{15}C_4$; Mn_5C_2; Fe_3C; $Mn_2Fe(CO)_{14}$

		120	$Mn_{15}C_4$; Mn_5C_2; Fe_3C
1100°C	10% CH_4 in Ar	20	Most dominant ones (highest abundance to lowest) : $CaMn_20_4$; Mn_7C_3; $FeO_{(0.099)}MnO_{(0.901)}$; Fe $_7C_3$ Others: Mn_5C_2; $Mn_{23}C_6$; C; MnO; Ca_2FeMnO_5
		30	Most dominant ones: $CaMn_20_4$; Mn_7C_3; $FeO_{(0.099)}MnO_{(0.901)}$; Fe $_7C_3$; MnO Others: Mn_5C_2; $Mn_{23}C_6$; C; Ca_2FeMnO_5; $Mn_2Fe(C0)_{14}$
		60	Most dominant ones: FeO $_{(0.099)}$ MnO $_{(0.901)}$; $CaMn_20_4$; Mn_7C_3; Fe $_7C_3$ Others:Mn_5C_2; $Mn_{23}C_6$; C; MnO; Ca_2FeMnO_5; $Mn_2Fe(C0)_{14}$
		90	Most dominant ones: $FeO_{(0.099)}MnO_{(0.901)}$; $CaMn_20_4$; Mn_7C_3; Fe $_7C_3$ Others:Mn_5C_2; $Mn_{23}C_6$; C; MnO; Ca_2FeMnO_5; $Mn_2Fe(C0)_{14}$
		120	Most dominant ones: $CaMn_20_4$; MnO; Mn_7C_3; Mn_5C_2; Fe $_7C_3$ Others: $Mn_{23}C_6$; C; Ca_2FeMnO_5; $Mn_2Fe(C0)_{14}$
1100°C	10% CH_4 in H_2	20	$Mn_{15}C_4$; Mn_5C_2; $Mn_2Fe(CO)_{14}$; Fe $_{1.8}$ Mn $_{1.2}$C; Fe $_{2.7}$ Mn $_{0.3}$ C
		30	$Mn_{15}C_4$; Mn_5C_2; $Mn_2Fe(CO)_{14}$; Fe $_{1.8}$ Mn $_{1.2}$C; Fe $_{2.7}$ Mn $_{0.3}$ C
		60	Mn_5C_2; Fe_3C; $CaMn_2O_4$; $Mn_2Fe(CO)_{14}$
		90	$Mn_{15}C_4$; Mn_5C_2; Fe_3C; Mn_2O_3
		120	$Mn_{15}C_4$; Mn_5C_2; $Mn_2Fe(CO)_{14}$
1200°C	10% CH_4 in Ar	20	Mn_7C_3; Mn_5C_2; $Mn_{15}C_4$; $Mn_{23}C_6$; Fe_7C_3; Fe_3C; $Mn_2Fe(CO)_{14}$; Ca_2FeMnO_5; Fe $_{2.7}$Mn $_{0.3}$ C; Fe $_{1.8}$ Mn $_{1.2}$ C_2; Fe $_{1.1}$ Mn $_{3.9}$ C_2
		30	Mn_7C_3; Mn_5C_2; $Mn_{15}C_4$; $Mn_{23}C_6$; Fe_7C_3; Fe_3C; $Mn_2Fe(CO)_{14}$; Ca_2FeMnO_5; Fe $_{2.7}$Mn $_{0.3}$ C; Fe $_{1.8}$ Mn $_{1.2}$ C_2; Fe $_{1.1}$ Mn $_{3.9}$ C_2
		60	Most dominant ones: $CaMn_20_4$; Mn_5C_2; $Mn_2Fe(C0)_{14}$ Others: Fe_3C

		90	Mn_7C_3; Mn_5C_2; $Mn_{15}C_4$; $Mn_{23}C_6$; Fe_7C_3; Fe_3C; $Mn_2Fe(CO)_{14}$; Ca_2FeMnO_5; $Fe_{2.7}Mn_{0.3}C$; $Fe_{1.8}Mn_{1.2}C_2$; $Fe_{1.1}Mn_{3.9}C_2$
		120	Mn_5C_2; Mn_7C_3; $Mn_{15}C_4$; $Mn_{23}C_6$; Fe_7C_3; Fe_3C; $Mn_2Fe(CO)_{14}$; Ca_2FeMnO_5; $CaMn_2O_4$; $Fe_{2.7}Mn_{0.3}C$; $Fe_{1.8}Mn_{1.2}C_2$; $Fe_{1.1}Mn_{3.9}C_2$
1200°C	10% CH_4 in H_2	20	$Mn_{15}C_4$; Mn_5C_2; $Mn_2Fe(CO)_{14}$; $Fe_{1.8}Mn_{1.2}C$;$Fe_{2.7}Mn_{0.3}C$
		30	$Mn_{15}C_4$; Mn_5C_2; $Mn_2Fe(CO)_{14}$; $Fe_{1.8}Mn_{1.2}C$; $Fe_{2.7}Mn_{0.3}C$
		60	Mn_5C_2; Fe_3C; $CaMn_2O_4$; $Mn_2Fe(CO)_{14}$
		90	$Mn_{15}C_4$; Mn_5C_2; Fe_3C; $Mn_2Fe(CO)_{14}$
		120	$Mn_{15}C_4$; Mn_5C_2; $Mn_2Fe(CO)_{14}$; $Fe_{1.8}Mn_{1.2}C$; $Fe_{2.7}Mn_{0.3}C$
1250°C	10% CH_4 in Ar	20	Mn_5C_2; Mn_7C_3; $Mn_{15}C_4$; $Mn_{23}C_6$; Fe_7C_3; Fe_3C; $Mn_2Fe(CO)_{14}$; Ca_2FeMnO_5; $Fe_{2.7}Mn_{0.3}C$; $Fe_{1.8}Mn_{1.2}C_2$; $Fe_{1.1}Mn_{3.9}C_2$
		30	Mn_5C_2; Mn_7C_3; $Mn_{15}C_4$; $Mn_{23}C_6$; Fe_7C_3; Fe_3C; $Mn_2Fe(CO)_{14}$; Ca_2FeMnO_5; $Fe_{2.7}Mn_{0.3}C$; $Fe_{1.8}Mn_{1.2}C_2$; $Fe_{1.1}Mn_{3.9}C_2$
		60	Mn_5C_2; Mn_7C_3; $Mn_{15}C_4$; $Mn_{23}C_6$; Fe_7C_3; Fe_3C; $Mn_2Fe(CO)_{14}$; Ca_2FeMnO_5; $Fe_{2.7}Mn_{0.3}C$; $Fe_{1.8}Mn_{1.2}C_2$; $Fe_{1.1}Mn_{3.9}C_2$
		90	Mn_5C_2; Mn_7C_3; $Mn_{15}C_4$; $Mn_{23}C_6$; Fe_7C_3; Fe_3C; $Mn_2Fe(CO)_{14}$; Ca_2FeMnO_5; $Fe_{2.7}Mn_{0.3}C$; $Fe_{1.8}Mn_{1.2}C_2$; $Fe_{1.1}Mn_{3.9}C_2$
		120	Mn_5C_2; Mn_7C_3; $Mn_{15}C_4$; $Mn_{23}C_6$; Fe_7C_3; Fe_3C; $Mn_2Fe(CO)_{14}$; Ca_2FeMnO_5; $Fe_{2.7}Mn_{0.3}C$; $Fe_{1.8}Mn_{1.2}C_2$; $Fe_{1.1}Mn_{3.9}C_2$

1250°C	10% CH_4 in H_2	20	$Mn_{15}C_4$; Mn_5C_2; $Mn_2Fe(CO)_{14}$; $Fe_{1.8}Mn_{1.2}C$; $Fe_{2.7}Mn_{0.3}C$
		30	$Mn_{15}C_4$; Mn_5C_2; $Mn_2Fe(CO)_{14}$; $Fe_{1.8}Mn_{1.2}C$; $Fe_{2.7}Mn_{0.3}C$
		60	Mn_5C_2; Fe_7C_3; $CaMn_2O_4$; $Mn_2Fe(CO)_{14}$
		90	$Mn_{15}C_4$; Mn_5C_2; Fe_3C; $Mn_2Fe(CO)_{14}$
		120	$Mn_{15}C_4$; Mn_5C_2; $Mn_2Fe(CO)_{14}$; $Fe_{1.8}Mn_{1.2}C$; $Fe_{2.7}Mn_{0.3}C$

Table B2: X-RD Phases present in the partially reduced manganese under the different reducing conditions of 20 % methane, argon and 20% methane, hydrogen gas mixtures at all temperatures.

T(°C)	Reducing Medium	Reduction Time (min.)	Phases Detected
1050°C	20% CH_4 in H_2	20	Mn_5C_2; Mn_7C_3; $Mn_{23}C_6$; MnO; Mn_3O_4; $CaMn_2O_4$; $Mn_2Fe(CO)_{14}$; $FeO_{(0.099)}MnO_{(0.901)}$; Fe_7C_3
		30	Mn_5C_2; Mn_7C_3; $Mn_{23}C_6$; MnO; Mn_3O_4; $CaMn_2O_4$; $FeO_{(0.099)}MnO_{(0.901)}$; Fe_7C_3
		60	Mn_5C_2; Mn_7C_3; $Mn_{23}C_6$; MnO; Mn_3O_4; $CaMn_2O_4$; $FeO_{(0.099)}MnO_{(0.901)}$; Fe_7C_3
		90	$Mn_{15}C_4$; Mn_5C_2; Fe_3C; $Mn_2Fe(CO)_{14}$
		120	$Mn_{15}C_4$; Mn_5C_2; Fe_3C; $Mn_2Fe(CO)_{14}$

1100°C	20% CH_4 in Ar	20	Most dominant ones: $CaMn_2O_4$; Mn_3O_4; MnO; Mn_7C_3; Mn_5C_2; Fe_7C_3 Others: $Mn_{23}C_6$; $FeO_{(0.099)}MnO_{(0.901)}$; $Mn_2Fe(C0)_{14}$
		30	Most dominant ones: $CaMn_2O_4$; MnO; Mn_7C_3; Mn_5C_2; Fe_7C_3 Others: $Mn_{23}C_6$; Mn; Mn_3O_4; $FeO_{(0.099)}MnO_{(0.901)}$
		60	Most dominant ones: $FeO_{(0.099)}MnO_{(0.901)}$; Mn_7C_3; MnO $CaMn_2O_4$ Others:Mn_5C_2; $Mn_{23}C_6$; Mn; Mn_3O_4; $FeO_{(0.099)}MnO_{(0.901)}$
		90	Most dominant ones: $CaMn_2O_4$; Mn_7C_3; Mn_5C_2 Others: $Mn_{23}C_6$; Fe_3C; Mn_3O_4; $Mn_2Fe(C0)_{14}$
		120	Most dominant ones: $CaMn_2O_4$; Mn_7C_3; Mn_5C_2; Fe_3C Others:Mn_3O_4
1100°C	20% CH_4 in H_2	20	Mn_5C_2; Fe_3C; $Mn_2Fe(CO)_{14}$; $CaMn_2O_4$; Ca_2FeMnO_5
		30	$Mn_{15}C_4$; $Mn_2Fe(CO)_{14}$; $Fe_{1.8}Mn_{1.2}C$; $Fe_{2.7}Mn_{0.3}C$
		60	Mn_5C_2; Fe_3C; $CaMn_2O_4$; Ca_2FeMnO_5
		90)	$Mn_{15}C_4$; Mn_5C_2; $Mn_2Fe(CO)_{14}$; $Fe_{1.8}Mn_{1.2}C$; $Fe_{2.7}Mn_{0.3}C$
		120	$Mn_{15}C_4$; Mn_5C_2; $Mn_2Fe(CO)_{14}$; $Fe_{1.8}Mn_{1.2}C$; $Fe_{2.7}Mn_{0.3}C$
1200°C	20% CH_4 in Ar	20	Most dominant ones: $CaMn_2O_4$; Mn_5C_2 Others: Fe_3C; $Mn_2Fe(C0)_{14}$; Ca_2FeMnO_5; $Fe_{1.1}Mn_{3.9}C_2$
		30	Mn_7C_3; Mn_5C_2; $Mn_{15}C_4$; $Mn_{23}C_6$; Fe_7C_3; Fe_3C; $Mn_2Fe(CO)_{14}$; Ca_2FeMnO_5; $Fe_{2.7}Mn_{0.3}C$; $Fe_{1.8}Mn_{1.2}C_2$;$Fe_{1.1}Mn_{3.9}C_2$; $CaMn_2O_4$
		60	Most dominant ones: $CaMn_2O_4$; Mn_5C_2 Others: Fe_3C; Ca_2FeMnO_5; $Fe_{1.1}Mn_{3.9}C_2$
		90	Mn_5C_2; Mn_7C_3; $Mn_{15}C_4$; $Mn_{23}C_6$; Fe_7C_3; Fe_3C; $Mn_2Fe(CO)_{14}$; Ca_2FeMnO_5; $Fe_{2.7}Mn_{0.3}C$; $Fe_{1.8}Mn_{1.2}C_2$; $Fe_{1.1}Mn_{3.9}C_2$
		120	Mn_5C_2; Mn_7C_3; $Mn_{15}C_4$; $Mn_{23}C_6$; Fe_7C_3; Fe_3C; $Mn_2Fe(CO)_{14}$; Ca_2FeMnO_5; $Fe_{2.7}Mn_{0.3}C$; $Fe_{1.8}Mn_{1.2}C_2$; $Fe_{1.1}Mn_{3.9}C_2$

1200°C	20% CH_4 in H_2	20	Mn_5C_2; Fe_3C; $Mn_2Fe(CO)_{14}$; $CaMn_2O_4$; Ca_2FeMnO_5
		30	$Mn_{15}C_4$; Mn_5C_2; $Mn_2Fe(CO)_{14}$; $Fe_{1.8}Mn_{1.2}C$; $Fe_{2.7}Mn_{0.3}C$
		60	Mn_5C_2; Fe_3C; $Mn_2Fe(CO)_{14}$; $CaMn_2O_4$
		90	$Mn_{15}C_4$; Mn_5C_2; $Mn_2Fe(CO)_{14}$; $Fe_{1.8}Mn_{1.2}C$; $Fe_{2.7}Mn_{0.3}C$
		120	Mn_5C_2; Fe_3C; $Mn_2Fe(CO)_{14}$; $Fe_{1.8}Mn_{1.2}C$; $Fe_{2.7}Mn_{0.3}C$
1250°C	20% CH_4 in H_2	20	Mn_5C_2; Fe_3C; $Mn_2Fe(CO)_{14}$; $CaMn_2O_4$; Ca_2FeMnO_5
		30	$Mn_{15}C_4$; Mn_5C_2; $Mn_2Fe(CO)_{14}$; $Fe_{1.8}Mn_{1.2}C$; $Fe_{2.7}Mn_{0.3}C$
		60	Mn_5C_2; Fe_3C;;$CaMn_2O_4$; Ca_2FeMnO_5
		90	$Mn_{15}C_4$; Mn_5C_2; $Mn_2Fe(CO)_{14}$; $Fe_{1.8}Mn_{1.2}C$; $Fe_{2.7}Mn_{0.3}C$
		120	$Mn_{15}C_4$; Mn_5C_2; $Mn_2Fe(CO)_{14}$; $Fe_{1.8}Mn_{1.2}C$; $Fe_{2.7}Mn_{0.3}C$

Table B3: X-RD Phases present in the partially reduced manganese under the different reducing conditions of 30 % methane, argon and 30% methane, hydrogen gas mixtures at all temperatures.

T(°C)	Reducing Medium	Reduction Time (min.)	Phases Detected
1050°C	30% CH_4 in Ar	20	Mn_5C_2; Mn_7C_3; $Mn_{15}C_4$; $Mn_{23}C_6$; Fe_7C_3; Fe_3C; $Mn_2Fe(CO)_{14}$; Ca_2FeMnO_5; $Fe_{2.7}Mn_{0.3}C$; $Fe_{1.8}Mn_{1.2}C_2$; $Fe_{1.1}Mn_{3.9}C_2$
		30	Mn_5C_2; Mn_7C_3; $Mn_{15}C_4$; $Mn_{23}C_6$; Fe_7C_3; Fe_3C; $Mn_2Fe(CO)_{14}$; Ca_2FeMnO_5; $Fe_{2.7}Mn_{0.3}C$; $Fe_{1.8}Mn_{1.2}C_2$; $Fe_{1.1}Mn_{3.9}C_2$
		60	Mn_5C_2; Mn_7C_3; $Mn_{15}C_4$; $Mn_{23}C_6$; Fe_7C_3; Fe_3C; $Mn_2Fe(CO)_{14}$; Ca_2FeMnO_5; $Fe_{2.7}Mn_{0.3}C$; $Fe_{1.8}Mn_{1.2}C_2$; $Fe_{1.1}Mn_{3.9}C_2$
		90	Mn_5C_2; Mn_7C_3; $Mn_{15}C_4$; $Mn_{23}C_6$; Fe_7C_3; Fe_3C; $Mn_2Fe(CO)_{14}$; Ca_2FeMnO_5; $Fe_{2.7}Mn_{0.3}C$; $Fe_{1.8}Mn_{1.2}C_2$; $Fe_{1.1}Mn_{3.9}C_2$
		120	Mn_5C_2; Mn_7C_3; $Mn_{15}C_4$; $Mn_{23}C_6$; Fe_7C_3; Fe_3C; $Mn_2Fe(CO)_{14}$; Ca_2FeMnO_5; $Fe_{2.7}Mn_{0.3}C$; $Fe_{1.8}Mn_{1.2}C_2$; $Fe_{1.1}Mn_{3.9}C_2$
1050°C	30% CH_4 in H_2	20	Mn_5C_2; Mn_7C_3; Fe_3C; Mn_3O_4; $CaMn_2O_4$; $Mn_2Fe(CO)_{14}$
		30	Mn_5C_2; Mn_7C_3; Fe_3C; Mn_3O_4; $CaMn_2O_4$; $Mn_2Fe(CO)_{14}$
		60	Mn_5C_2; Mn_7C_3; Fe_3C; Mn_3O_4; $CaMn_2O_4$; $Mn_2Fe(CO)_{14}$
		90	Mn_5C_2; Mn_7C_3; Fe_3C
		120	$Mn_{15}C_4$; Mn_5C_2; $Mn_2Fe(CO)_{14}$; $Fe_{1.8}Mn_{1.2}C$; $Fe_{2.7}Mn_{0.3}C$
1100°C	30% CH_4 in Ar	20	Most dominant ones: $CaMn_20_4$; Mn_30_4; Mn_7C_3; Mn_5C_2 Others: Fe_3C; $Mn_2Fe(C0)_{14}$

		30	Most dominant ones: $CaMn_2O_4$; Mn_3O_4; Mn_5C_2 Others: Mn_7C_3; Fe_3C; $Mn_2Fe(C0)_{14}$
		60	Most dominant ones: $CaMn_2O_4$; Mn_3O_4; Mn_5C_2. Others: Mn_7C_3; Fe_3C; $Mn_2Fe(C0)_{14}$
		90	Mn_5C_2; Mn_7C_3; Fe_3C; Mn_3O_4; $CaMn_2O_4$; $Mn_2Fe(C0)_{14}$
		120	Most dominant ones:$CaMn_2O_4$; $FeO_{(0.099)}MnO_{(0.901)}$; Mn_5C_2; Mn_3O_4. Others: Fe_3C; $Mn_2Fe(C0)_{14}$
1100°C	30% CH_4 in H_2	20	$Mn_{15}C_4$; Mn_5C_2; $Mn_2Fe(CO)_{14}$; $Fe_{1.8}Mn_{1.2}C$; $Fe_{2.7}Mn_{0.3}C$
		30	Mn_5C_2; Fe_7C_3; $CaMn_2O_4$; Ca_2FeMnO_5
		60	Mn_5C_2; $CaMn_2O_4$
		90	$Mn_{15}C_4$; Mn_5C_2; $Mn_2Fe(CO)_{14}$; $Fe_{1.8}Mn_{1.2}C$; $Fe_{2.7}Mn_{0.3}C$
		120	$Mn_{15}C_4$; Mn_5C_2; $Mn_2Fe(CO)_{14}$; $Fe_{1.8}Mn_{1.2}C$; $Fe_{2.7}Mn_{0.3}C$
1200°C	30% CH_4 in Ar	20	Mn_5C_2; Mn_7C_3; $Mn_{15}C_4$; $Mn_{23}C_6$; Fe_7C_3; Fe_3C; $Mn_2Fe(CO)_{14}$; Ca_2FeMnO_5; $Fe_{2.7}Mn_{0.3}C$; $Fe_{1.8}Mn_{1.2}C_2$; $Fe_{1.1}Mn_{3.9}C_2$
		30	Most dominant ones: Fe_7C_3; Mn_5C_2; $CaMn_2O_4$ Others: Ca_2FeMnO_5
		60	Most dominant ones: Mn_5C_2; $CaMn_2O_4$
		90	Mn_5C_2; Mn_7C_3; $Mn_{15}C_4$; $Mn_{23}C_6$; Fe_7C_3; Fe_3C; $Mn_2Fe(CO)_{14}$; Ca_2FeMnO_5; $Fe_{2.7}Mn_{0.3}C$; $Fe_{1.8}Mn_{1.2}C_2$; $Fe_{1.1}Mn_{3.9}C_2$
		120	Mn_5C_2; Mn_7C_3; $Mn_{15}C_4$; $Mn_{23}C_6$; Fe_7C_3; Fe_3C; $Mn_2Fe(CO)_{14}$; Ca_2FeMnO_5; $Fe_{2.7}Mn_{0.3}C$; $Fe_{1.8}Mn_{1.2}C_2$; $Fe_{1.1}Mn_{3.9}C_2$

1200°C	30% CH_4 in H_2	20	$Mn_{15}C_4$; Mn_5C_2; $Mn_2Fe(CO)_{14}$; $Fe_{1.8}Mn_{1.2}C$; $Fe_{2.7}Mn_{0.3}C$
		30	Mn_5C_2; Fe_7C_3; $CaMn_2O_4$; Ca_2FeMnO_5
		60	Mn_5C_2; $CaMn_2O_4$
		90	$Mn_{15}C_4$; Mn_5C_2; $Mn_2Fe(CO)_{14}$; $Fe_{1.8}Mn_{1.2}C$; $Fe_{2.7}Mn_{0.3}C$
		120	$Mn_{15}C_4$; Mn_5C_2; $Mn_2Fe(CO)_{14}$; $Fe_{1.8}Mn_{1.2}C$; $Fe_{2.7}Mn_{0.3}C$
1250°C	30% CH_4 in Ar	20	Mn_5C_2; Mn_7C_3; $Mn_{15}C_4$; $Mn_{23}C_6$; Fe_7C_3; Fe_3C; $Mn_2Fe(CO)_{14}$; Ca_2FeMnO_5; $Fe_{2.7}Mn_{0.3}C$; $Fe_{1.8}Mn_{1.2}C_2$; $Fe_{1.1}Mn_{3.9}C_2$
		30	Mn_5C_2; Mn_7C_3; $Mn_{15}C_4$; $Mn_{23}C_6$; Fe_7C_3; Fe_3C; $Mn_2Fe(CO)_{14}$; Ca_2FeMnO_5; $Fe_{2.7}Mn_{0.3}C$; $Fe_{1.8}Mn_{1.2}C_2$; $Fe_{1.1}Mn_{3.9}C_2$
		60	Mn_5C_2; Mn_7C_3; $Mn_{15}C_4$; $Mn_{23}C_6$; Fe_7C_3; Fe_3C; $Mn_2Fe(CO)_{14}$; Ca_2FeMnO_5; $Fe_{2.7}Mn_{0.3}C$; $Fe_{1.8}Mn_{1.2}C_2$; $Fe_{1.1}Mn_{3.9}C_2$
		90	Mn_5C_2; Mn_7C_3; $Mn_{15}C_4$; $Mn_{23}C_6$; Fe_7C_3; Fe_3C; $Mn_2Fe(CO)_{14}$; Ca_2FeMnO_5; $Fe_{2.7}Mn_{0.3}C$; $Fe_{1.8}Mn_{1.2}C_2$; $Fe_{1.1}Mn_{3.9}C_2$
		120	Mn_5C_2; Mn_7C_3; $Mn_{15}C_4$; $Mn_{23}C_6$; Fe_7C_3; Fe_3C; $Mn_2Fe(CO)_{14}$; Ca_2FeMnO_5; $Fe_{2.7}Mn_{0.3}C$; $Fe_{1.8}Mn_{1.2}C_2$; $Fe_{1.1}Mn_{3.9}C_2$
1250°C	30% CH_4 in H_2	20	$Mn_{15}C_4$; Mn_5C_2; $Mn_2Fe(CO)_{14}$; $Fe_{1.8}Mn_{1.2}C$; $Fe_{2.7}Mn_{0.3}C$
		30	Mn_5C_2; Fe_7C_3; $CaMn_2O_4$; Ca_2FeMnO_5

		60	$Mn_{15}C_4$; Mn_5C_2; $Mn_2Fe(CO)_{14}$; $Fe_{1.8}Mn_{1.2}C$; $Fe_{2.7}Mn_{0.3}C$
		90	$Mn_{15}C_4$; Mn_5C_2; $Mn_2Fe(CO)_{14}$; $Fe_{1.8}Mn_{1.2}C$; $Fe_{2.7}Mn_{0.3}C$
		120	$Mn_{15}C_4$; Mn_5C_2; $Mn_2Fe(CO)_{14}$; $Fe_{1.8}Mn_{1.2}C$; $Fe_{2.7}Mn_{0.3}C$

APPENDIX C

SCANNING ELECTRON MICROSCOPE IMAGE OF REDUCED SAMPLES.

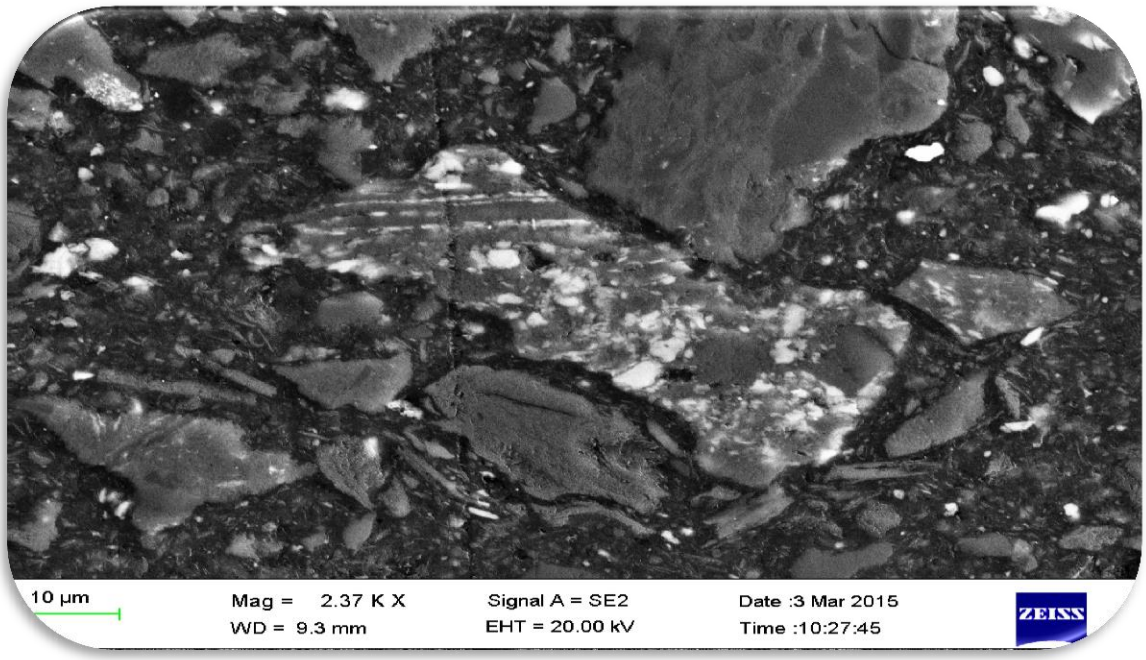

Figure C.1 10 % CH_4 in Ar for 20 minutes at 1050^{o}C

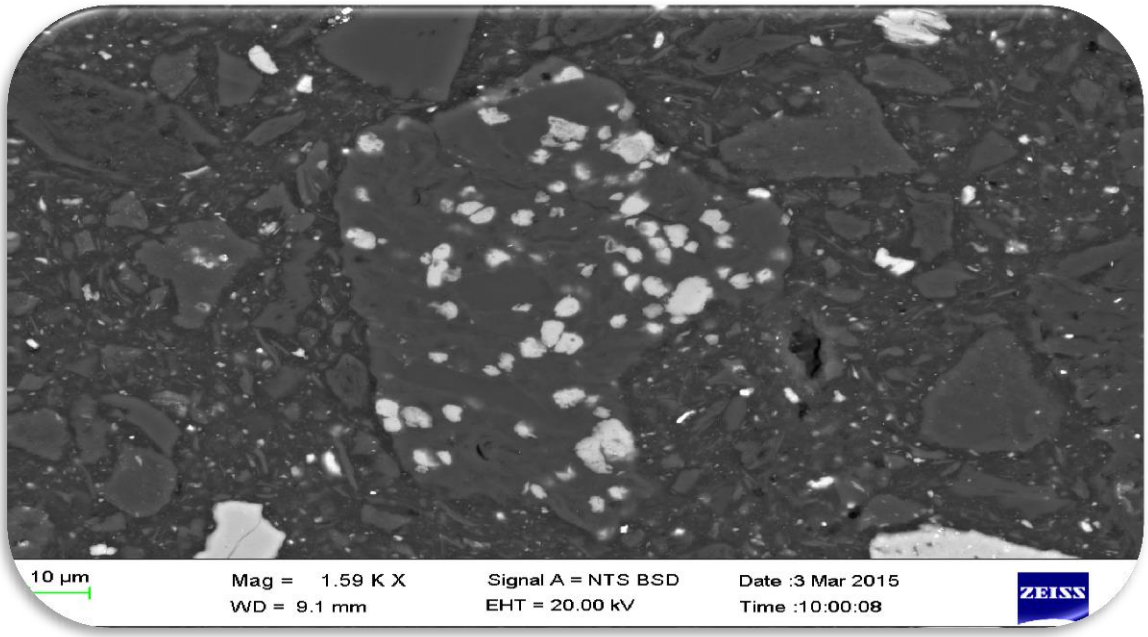

Figure C.2 10 % CH_4 in Ar for 30 minutes at 1050^{o}C

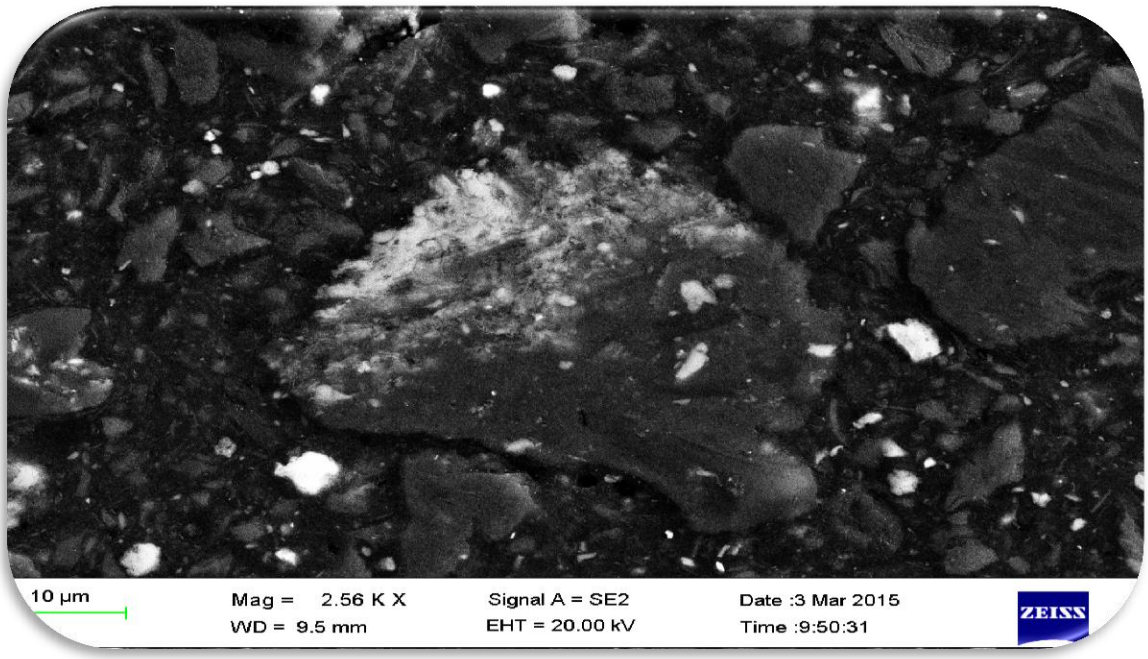

Figure C.3 10 % CH_4 in Ar for 60 minutes at 1050^{o}C

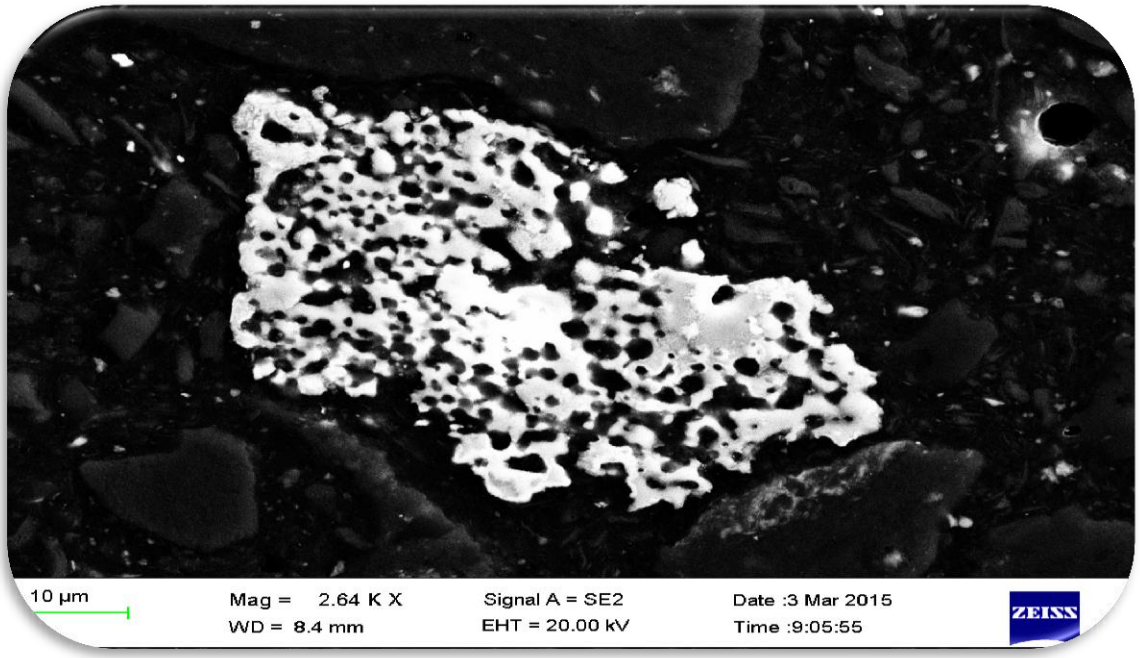

Figure C.4 10 % CH_4 in Ar for 90 minutes at 1050^{o}C

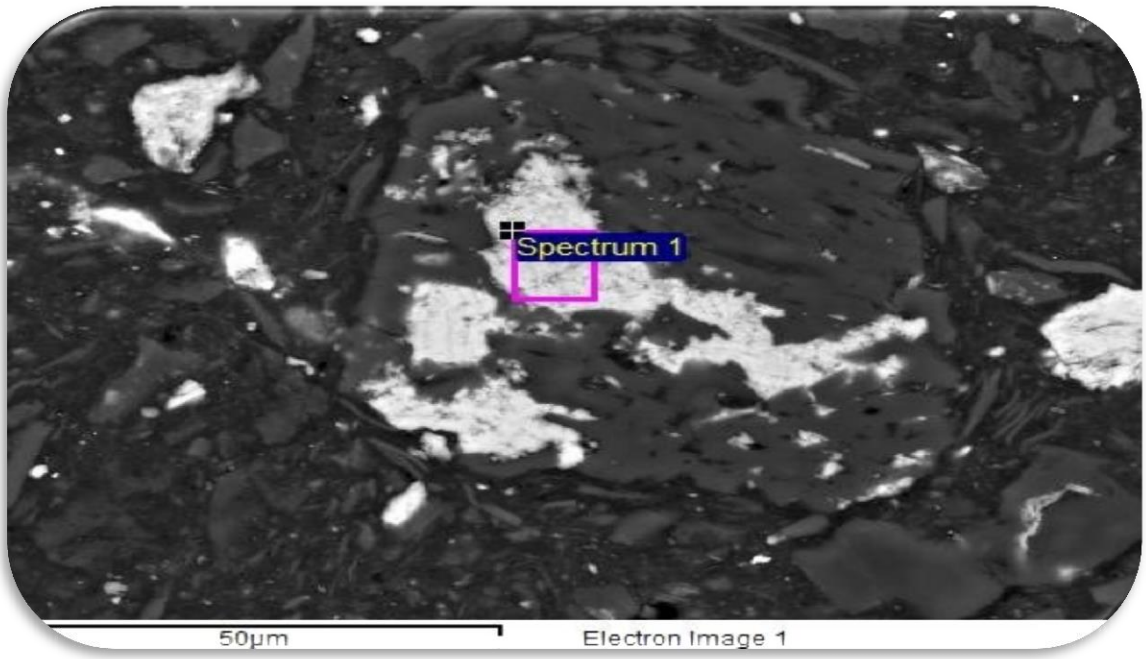

Figure C.5 10 % CH_4 in Ar for 120 minutes at 1050°C

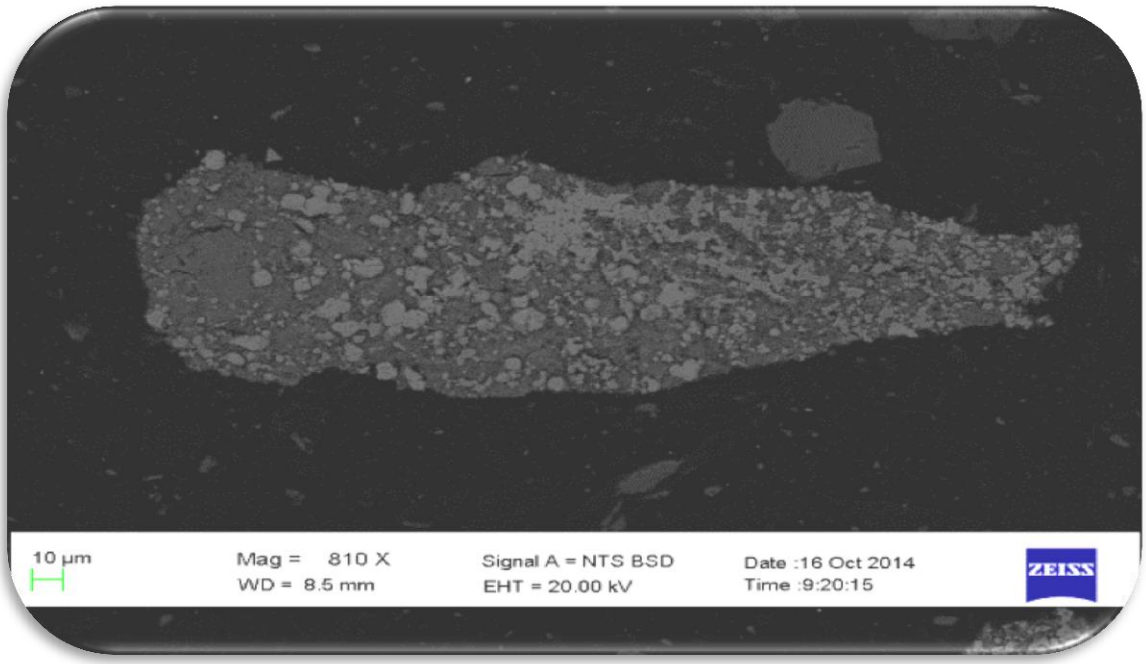

Figure C.6 10 % CH_4 in Ar for 20 minutes at 1100°C

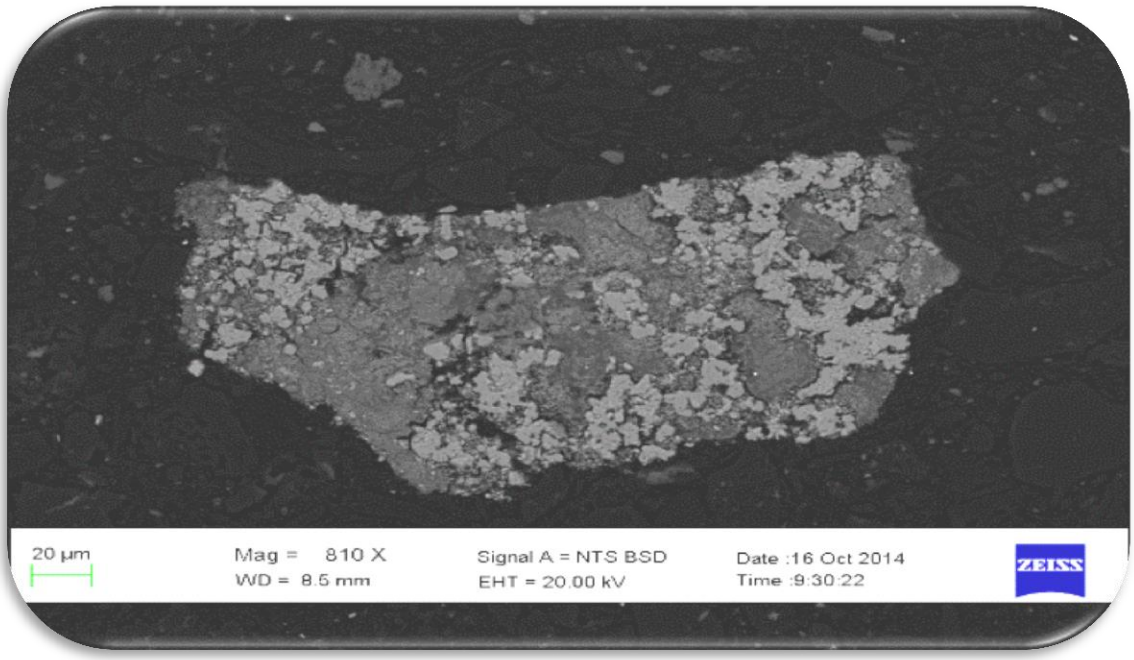

Figure C.7 10 % CH_4 in Ar for 30 minutes at 1100°C

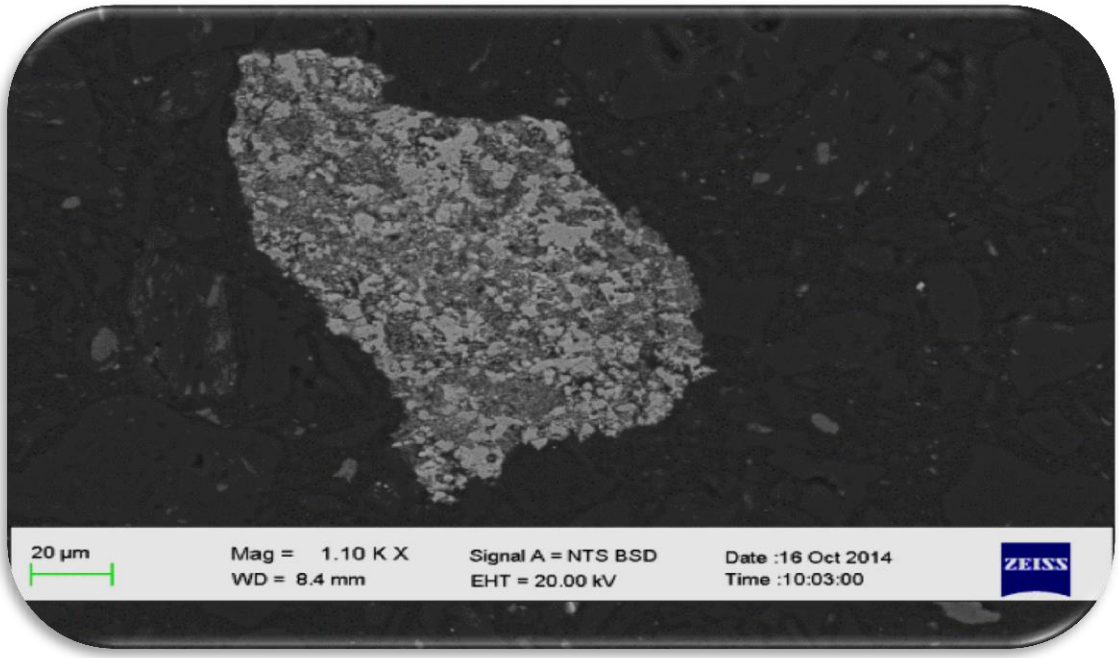

Figure C.8 10 % CH_4 in Ar for 60 minutes at 1100°C

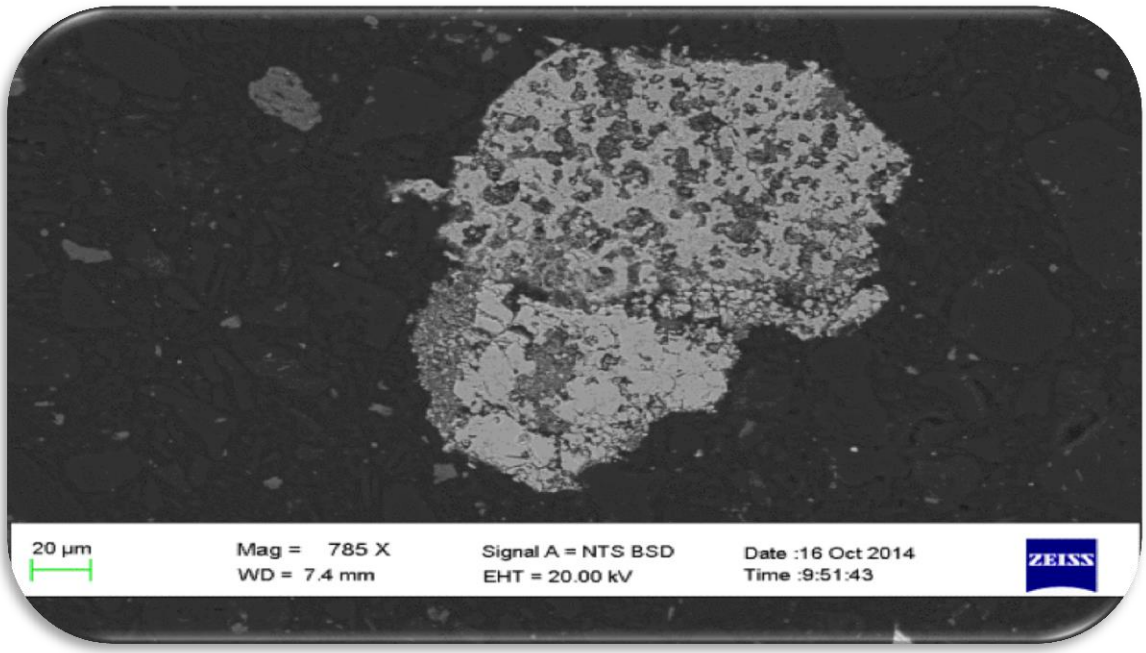

Figure C.9 10 % CH_4 in Ar for 90 minutes at 1100°C

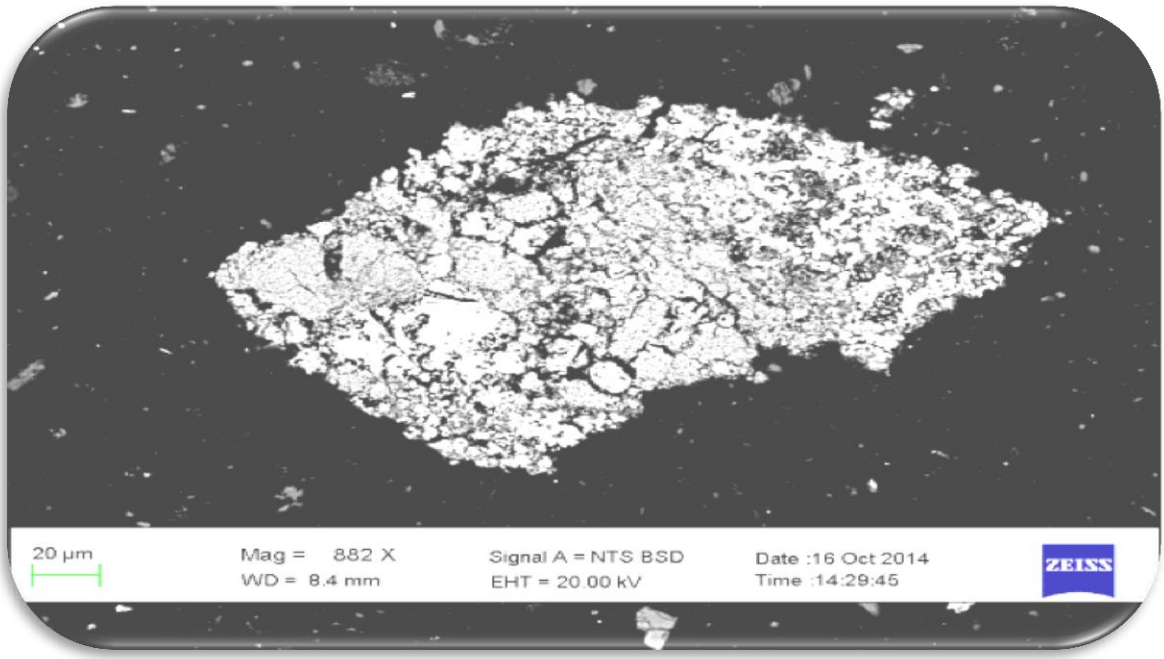

Figure C.10 10 % CH_4 in Ar for 120 minutes at 1100°C

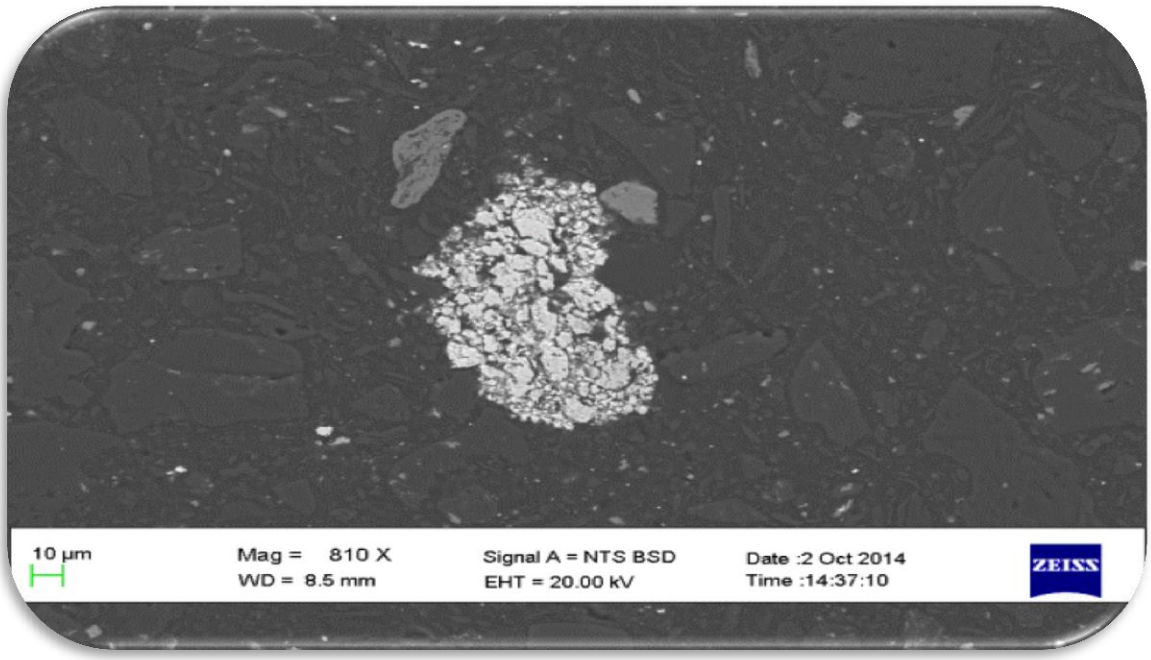

Figure C.11 10 % CH_4 in Ar for 20 minutes at 1200^{o}C

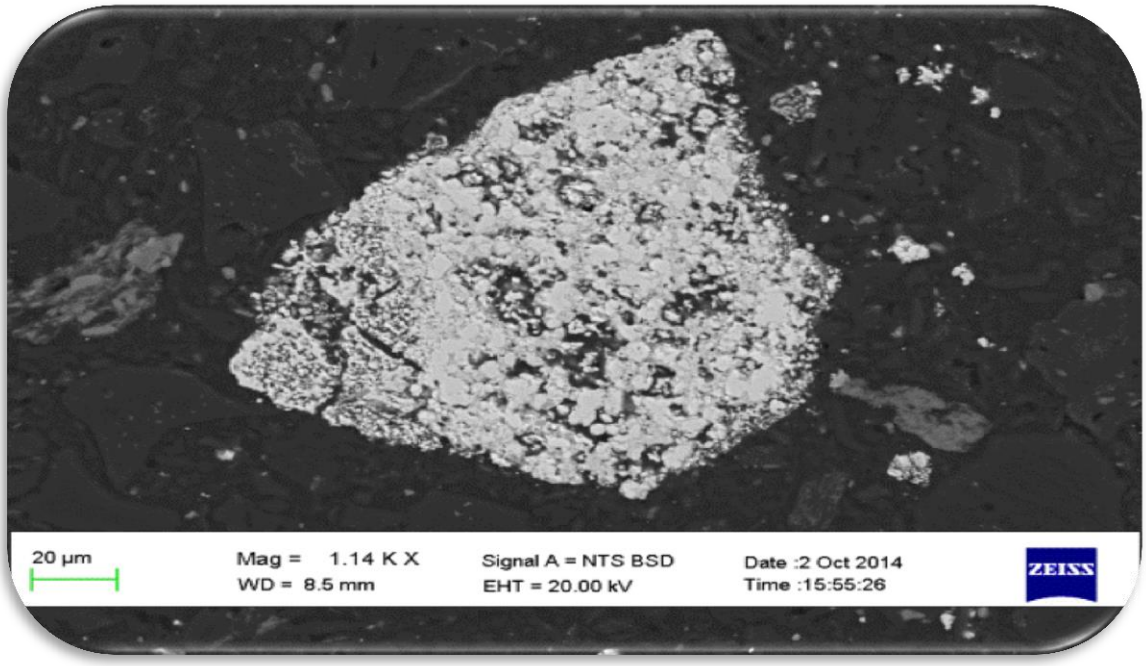

Figure C.12 10 % CH_4 in Ar for 30 minutes at 1200^{o}C

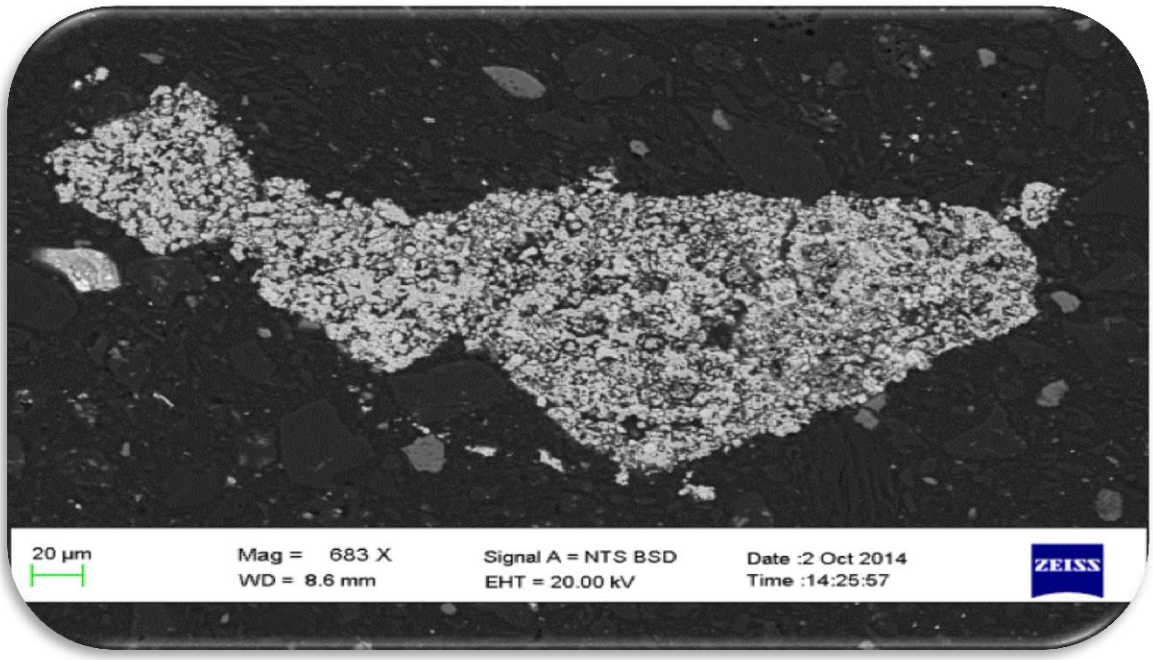

Figure C.13 10 % CH_4 in Ar for 60 minutes at 1200^{o}C

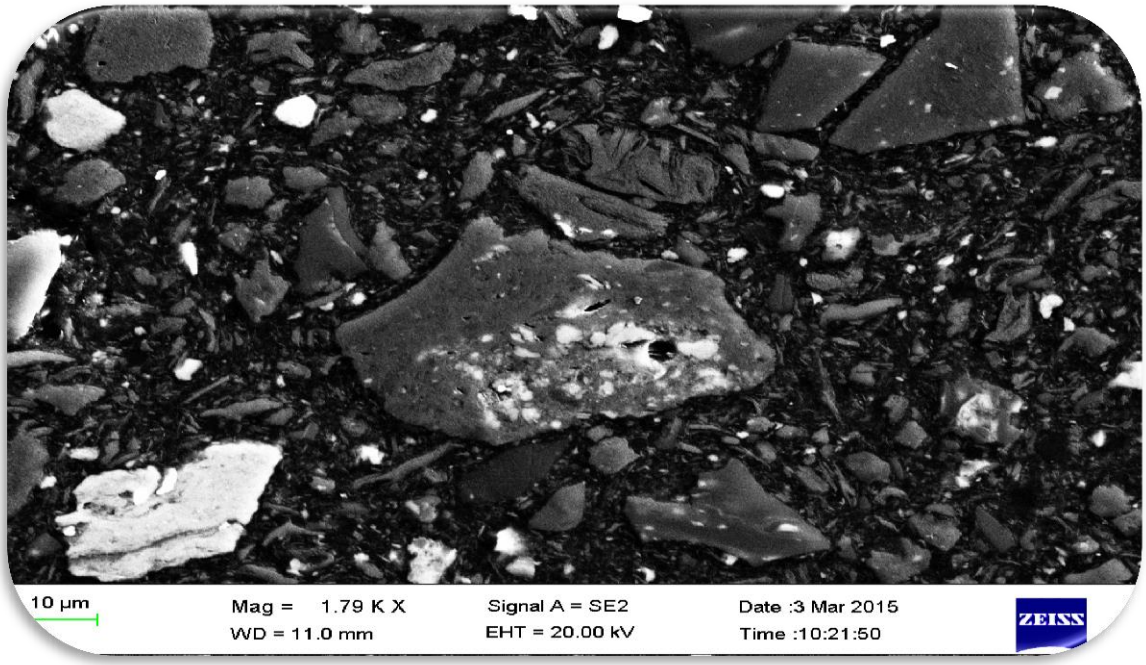

Figure C.14 10 % CH_4 in Ar for 90 minutes at 1200^{o}C

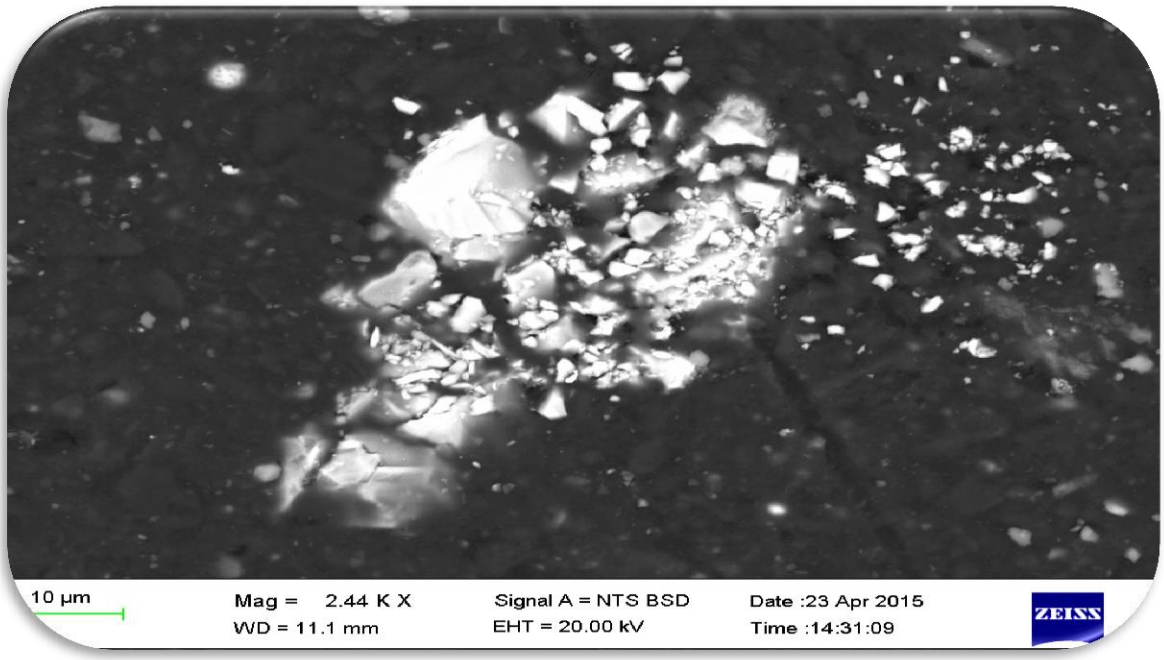

Figure C.15 10 % CH_4 in Ar for 120 minutes at 1200^{o}C

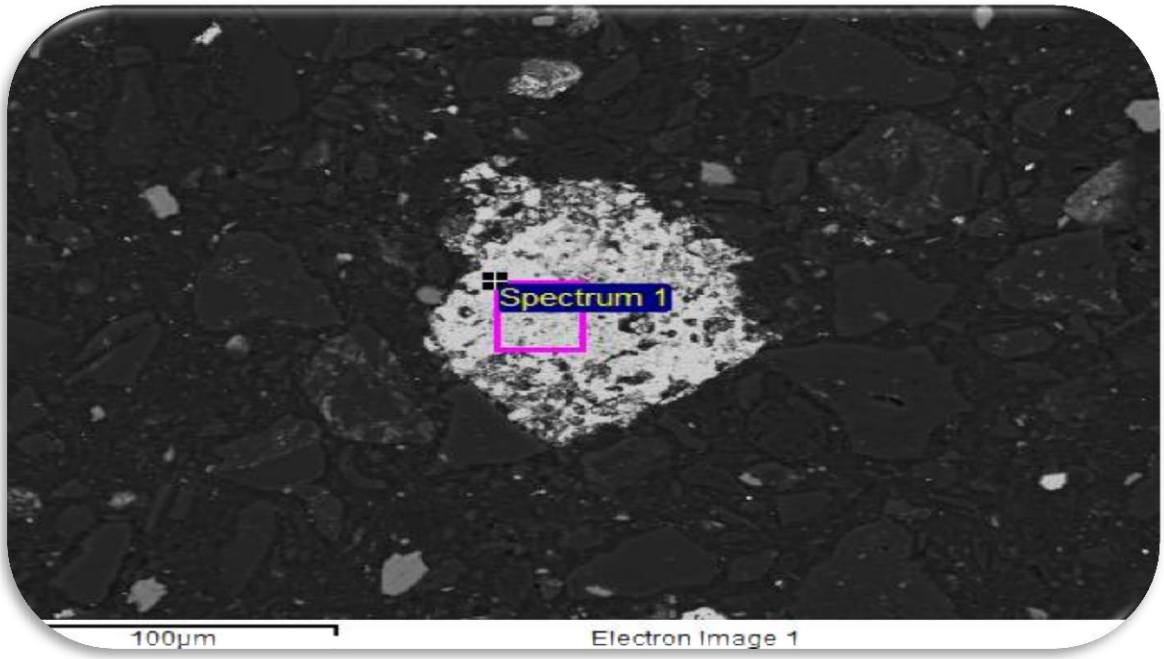

Figure C.16 10 % CH_4 in Ar for 20 minutes at 1250^{o}C

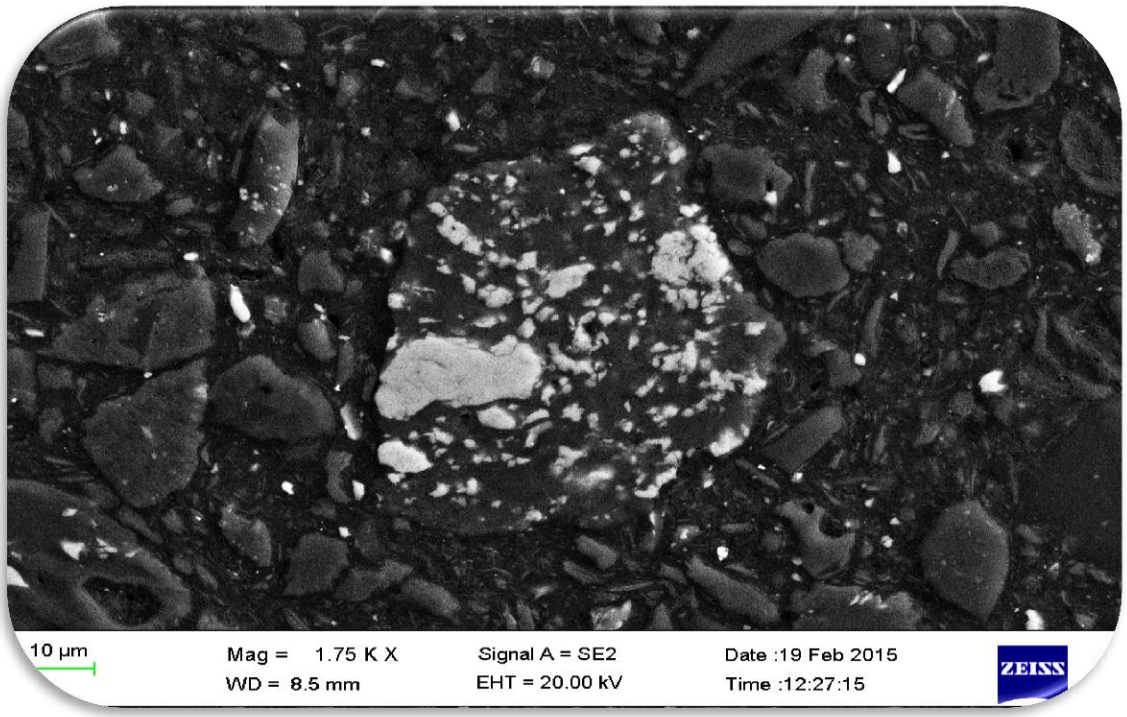

Figure C.17 10 % CH_4 in Ar for 30 minutes at 1250^{o}C

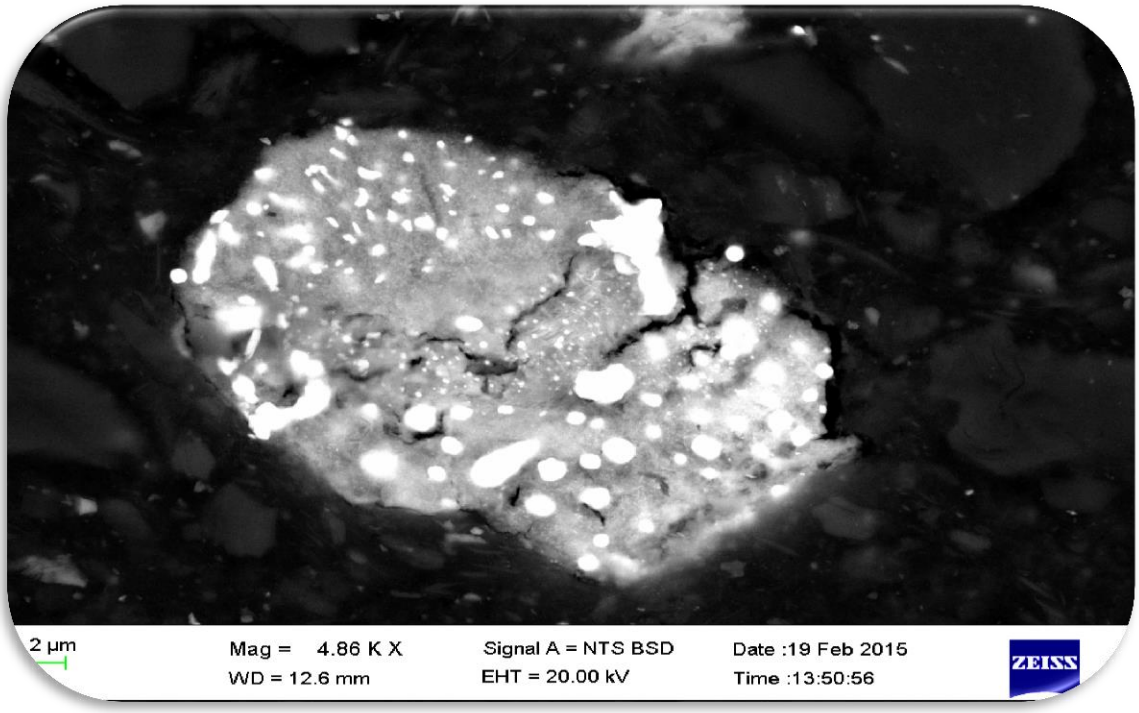

Figure C.18 10 % CH_4 in Ar for 60 minutes at 1250^{o}C

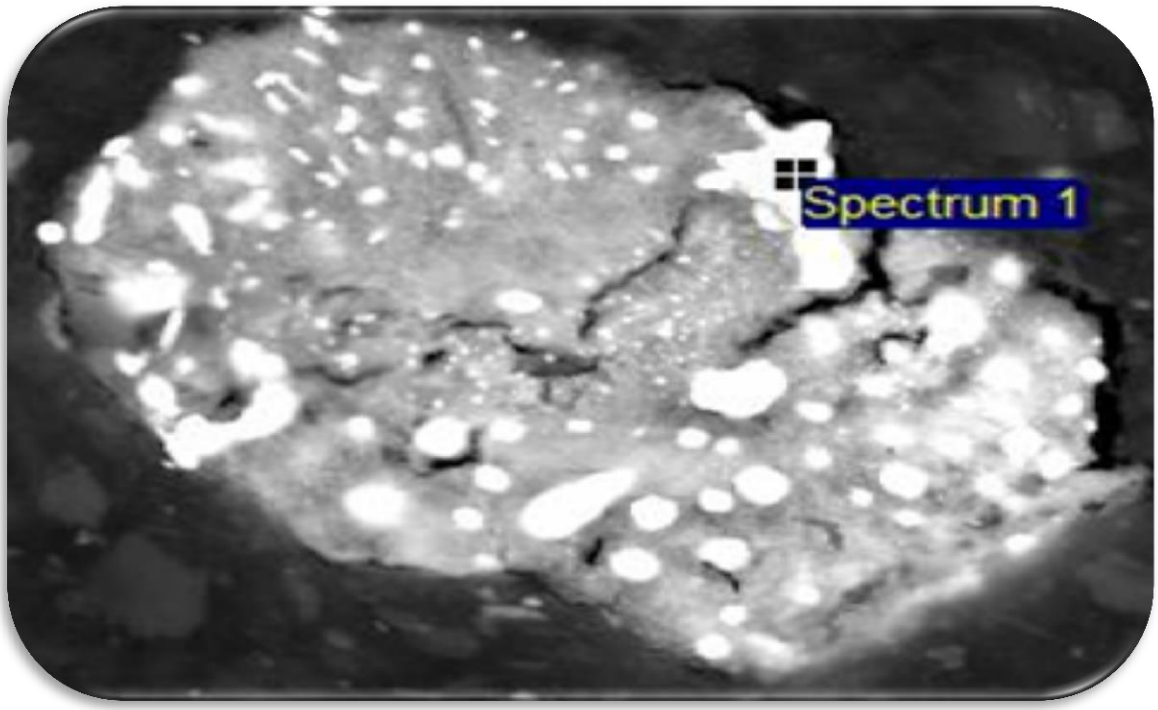

Figure C.19 10 % CH_4 in Ar for 90 minutes at 1250^oC

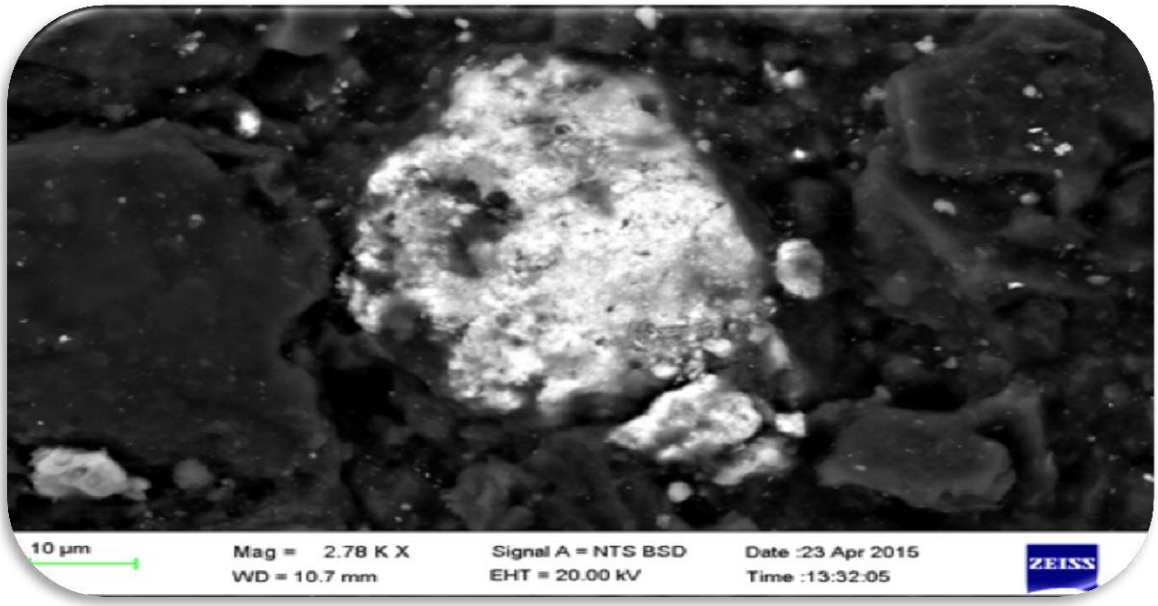

Figure C.20 10 % CH_4 in Ar for 120 minutes at 1250^oC

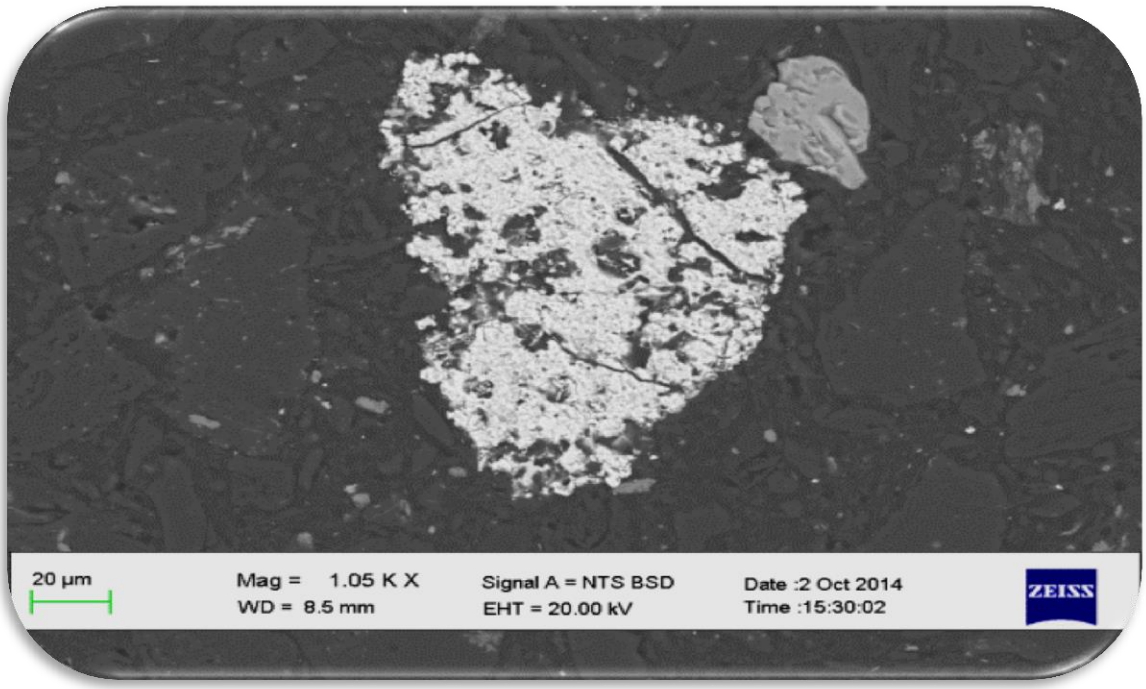

Figure C.21 20 % CH_4 in Ar for 20 minutes at 1100^{o}C

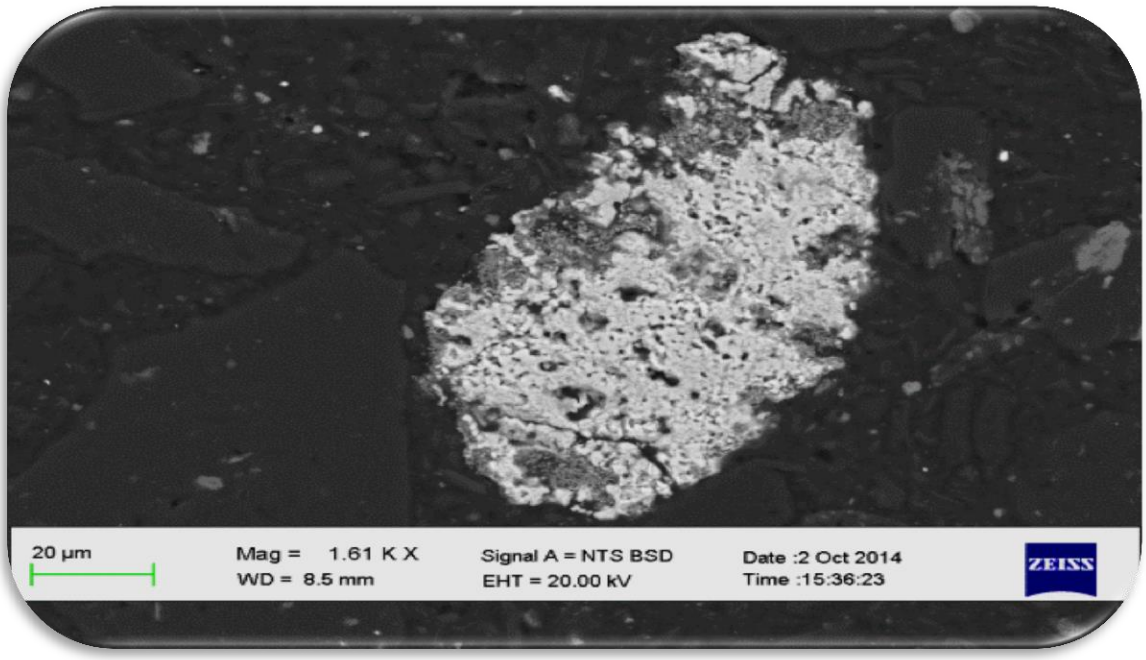

Figure C.22 20 % CH_4 in Ar for 30 minutes at 1100^{o}C

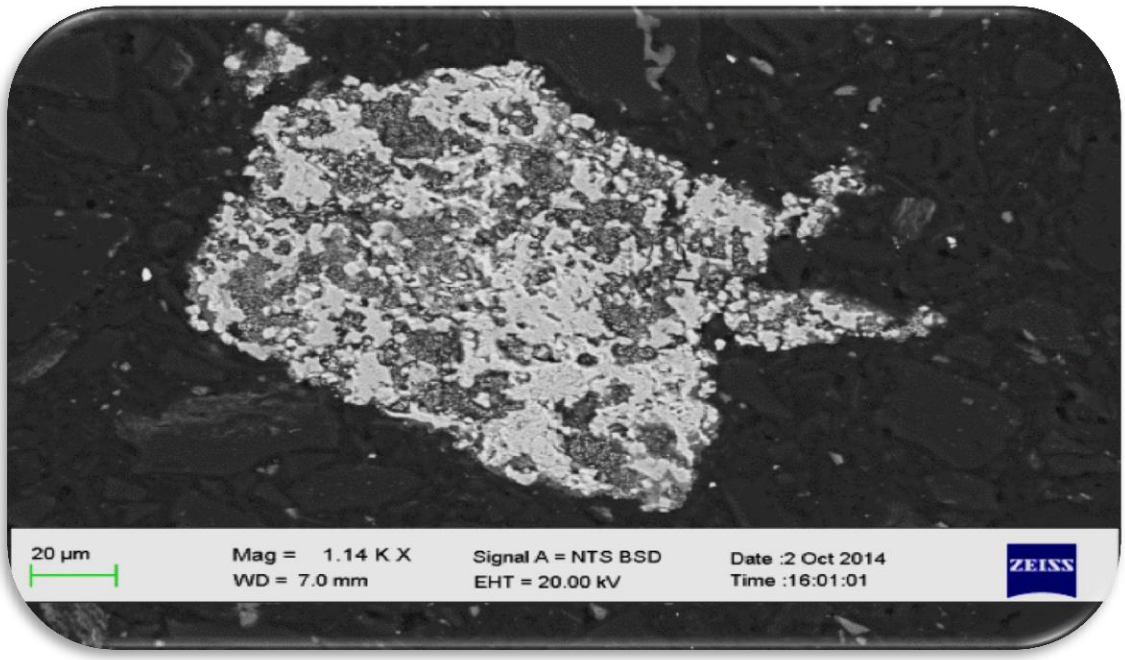

Figure C.23 20 % CH_4 in Ar for 60 minutes at 1100^{o}C

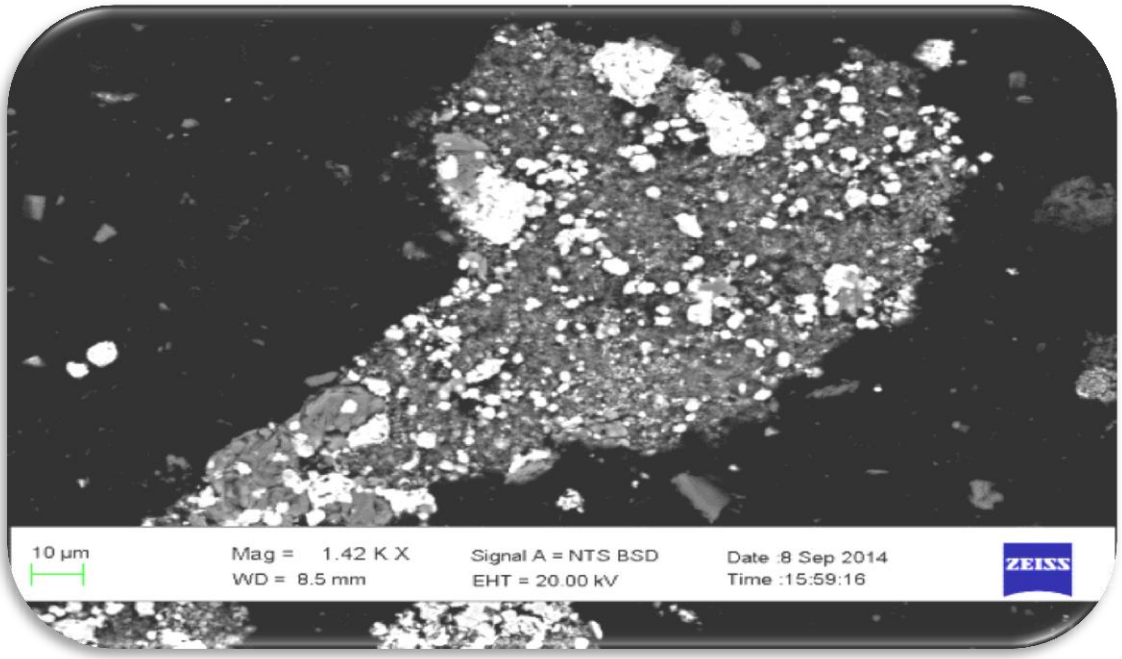

Figure C.24 20 % CH_4 in Ar for 90 minutes at 1100^{o}C

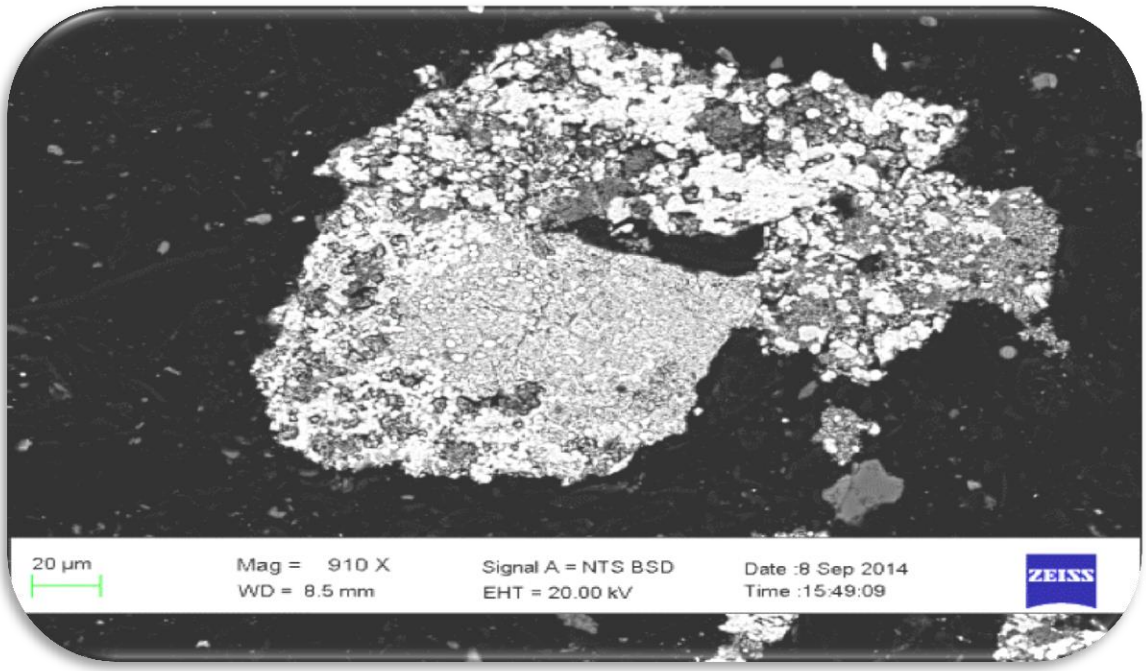

Figure C.25 20 % CH_4 in Ar for 120 minutes at 1100°C

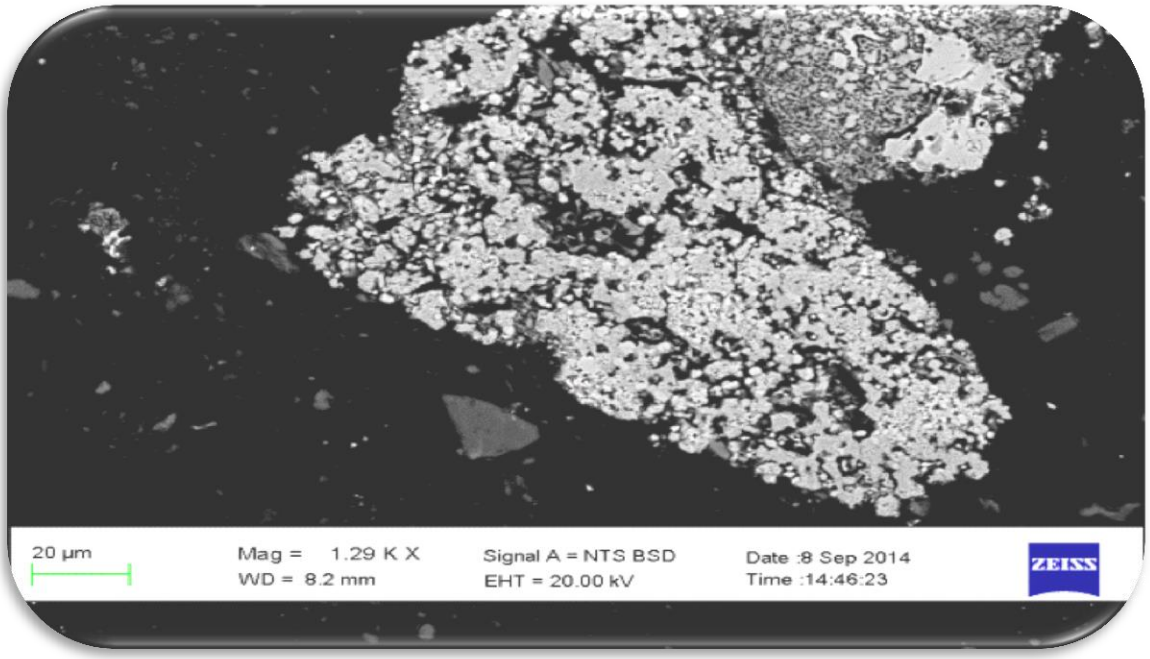

Figure C.26 20 % CH_4 in Ar for 20 minutes at 1200°C

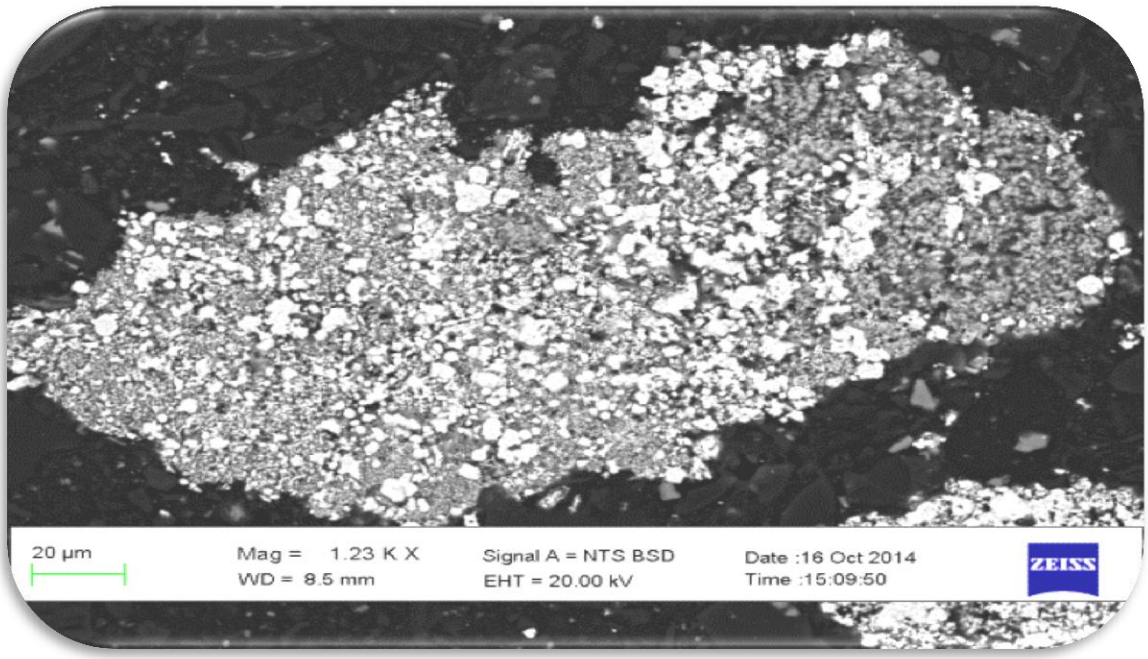

Figure C.27 20 % CH_4 in Ar for 30 minutes at 1200°C

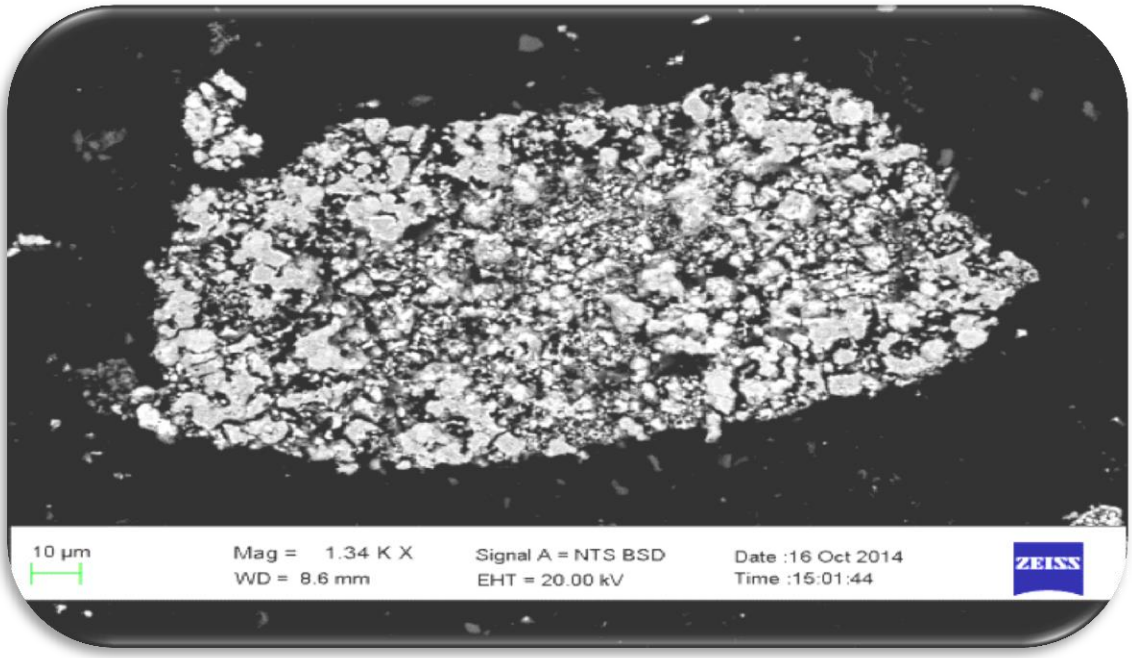

Figure C.28 20 % CH_4 in Ar for 60 minutes at 1200°C

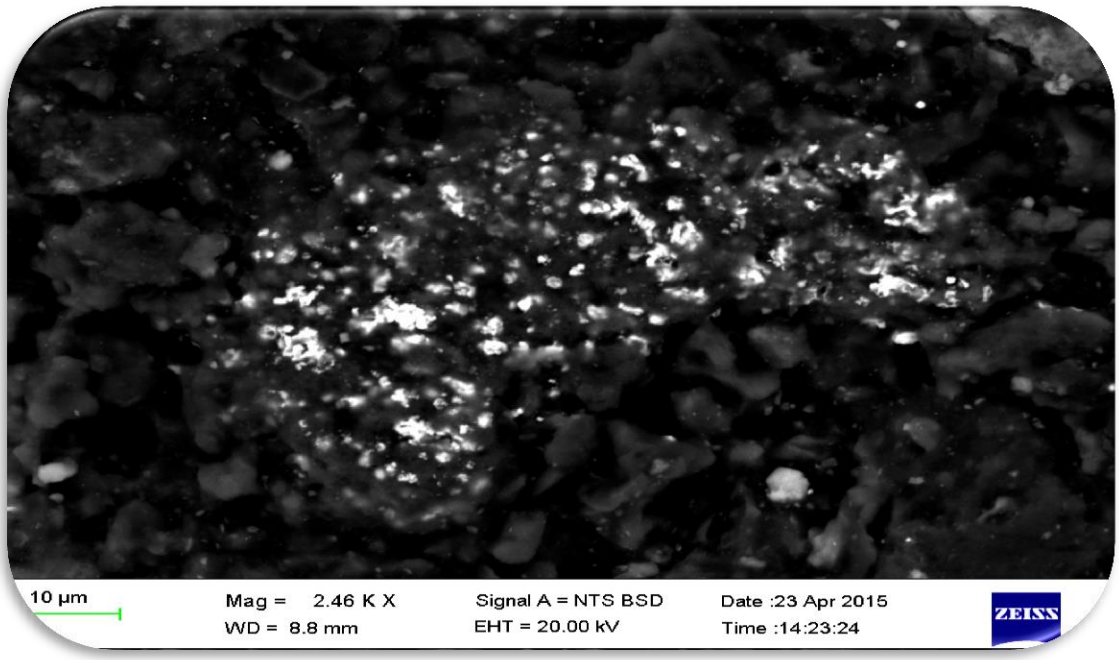

Figure C.29 20 % CH_4 in Ar for 90 minutes at 1200^{o}C

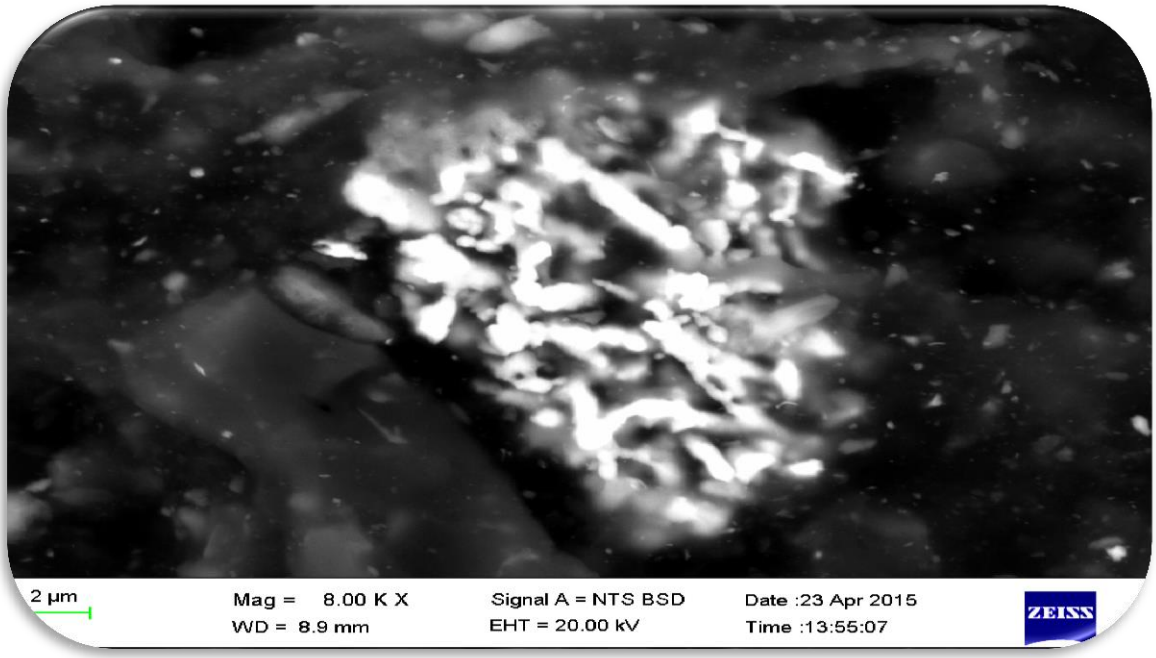

Figure C.30 20 % CH_4 in Ar for 120 minutes at 1200^{o}C

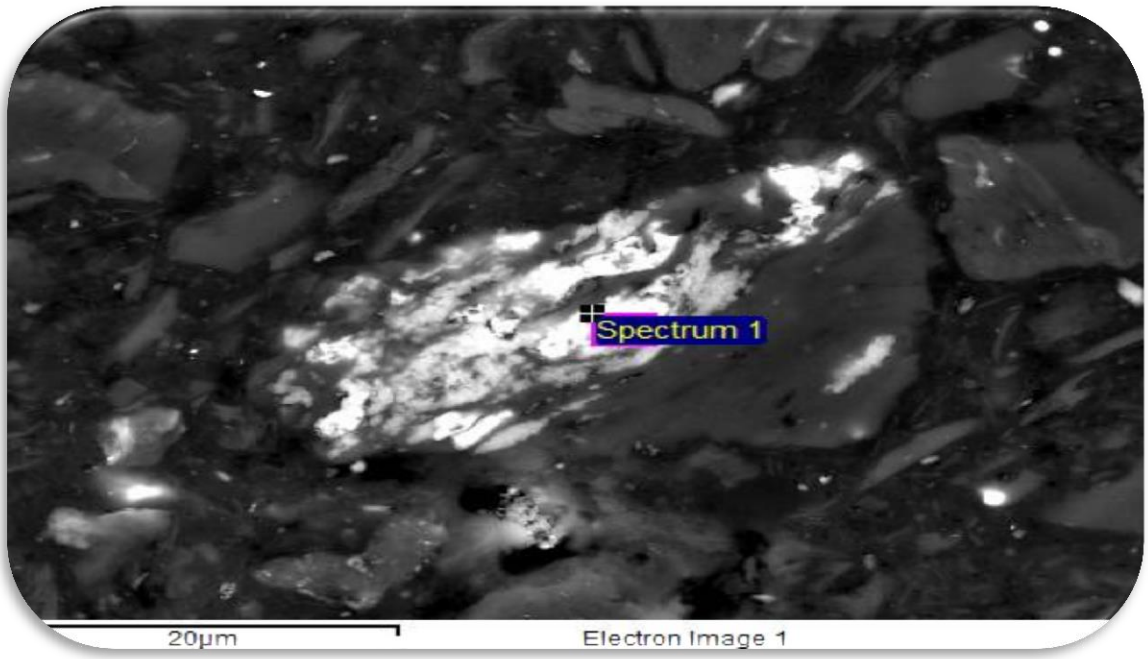

Figure C.31 30 % CH_4 in Ar for 20 minutes at 1050^{o}C

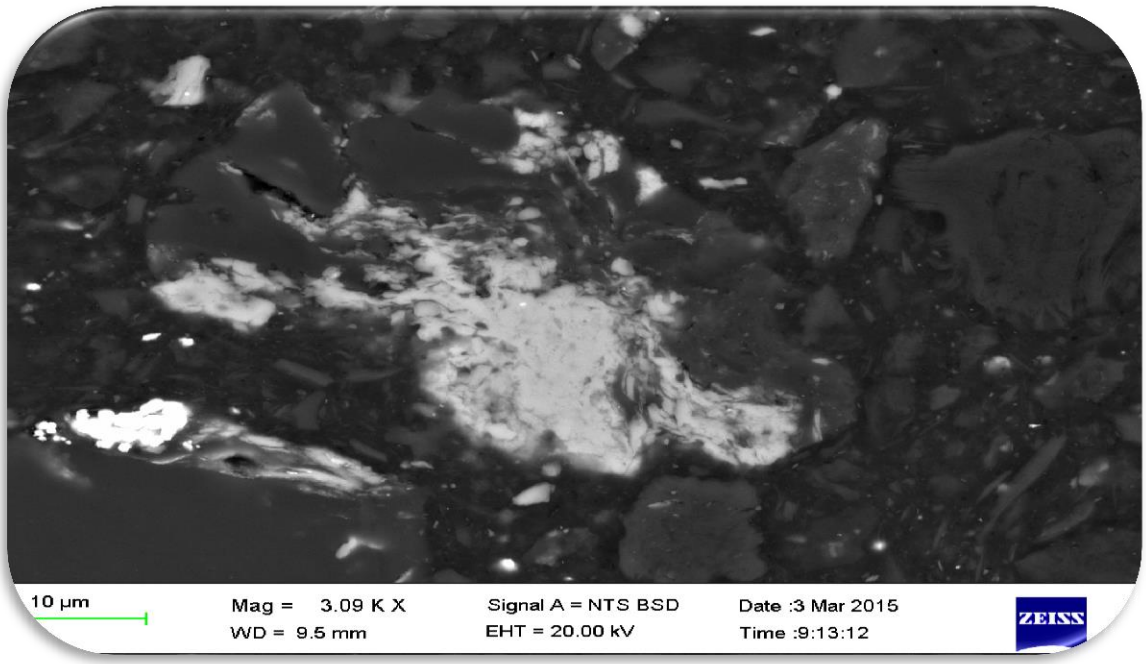

Figure C.32 30 % CH_4 in Ar for 30 minutes at 1050^{o}C

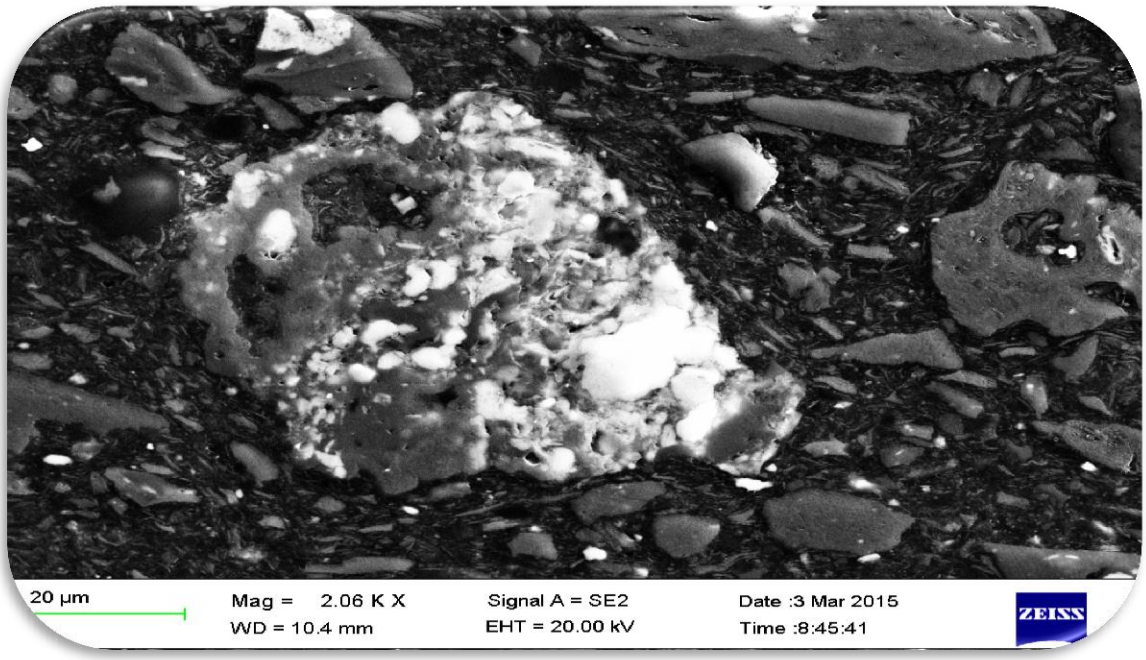

Figure C.33 30 % CH_4 in Ar for 60 minutes at 1050^{o}C

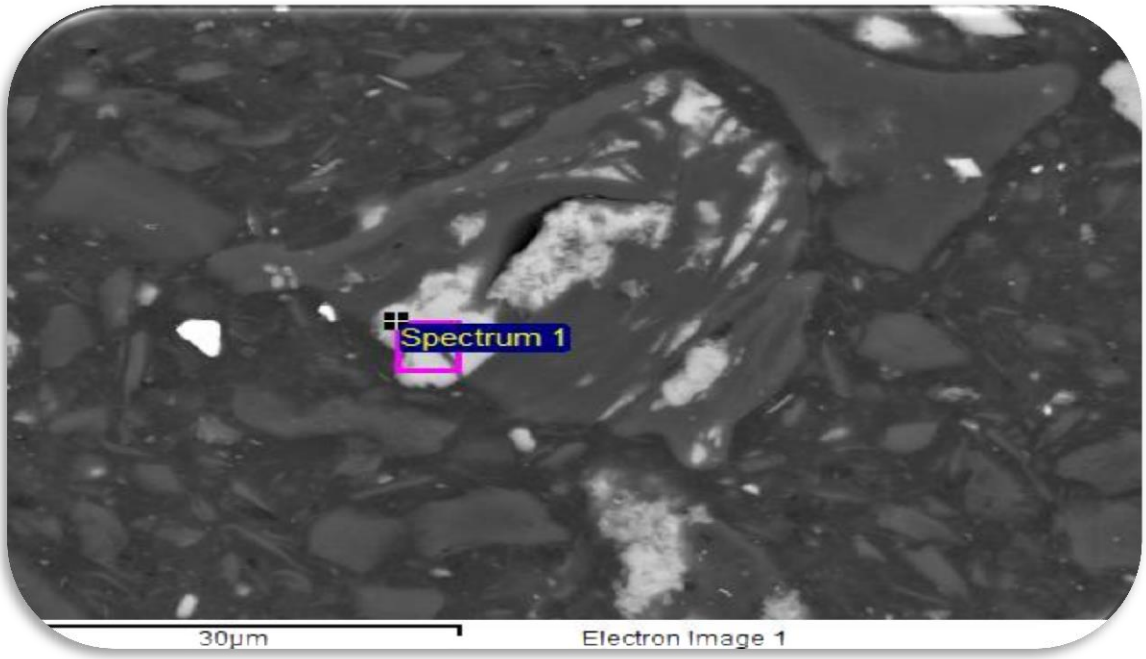

Figure C.34 30 % CH_4 in Ar for 90 minutes at 1050^{o}C

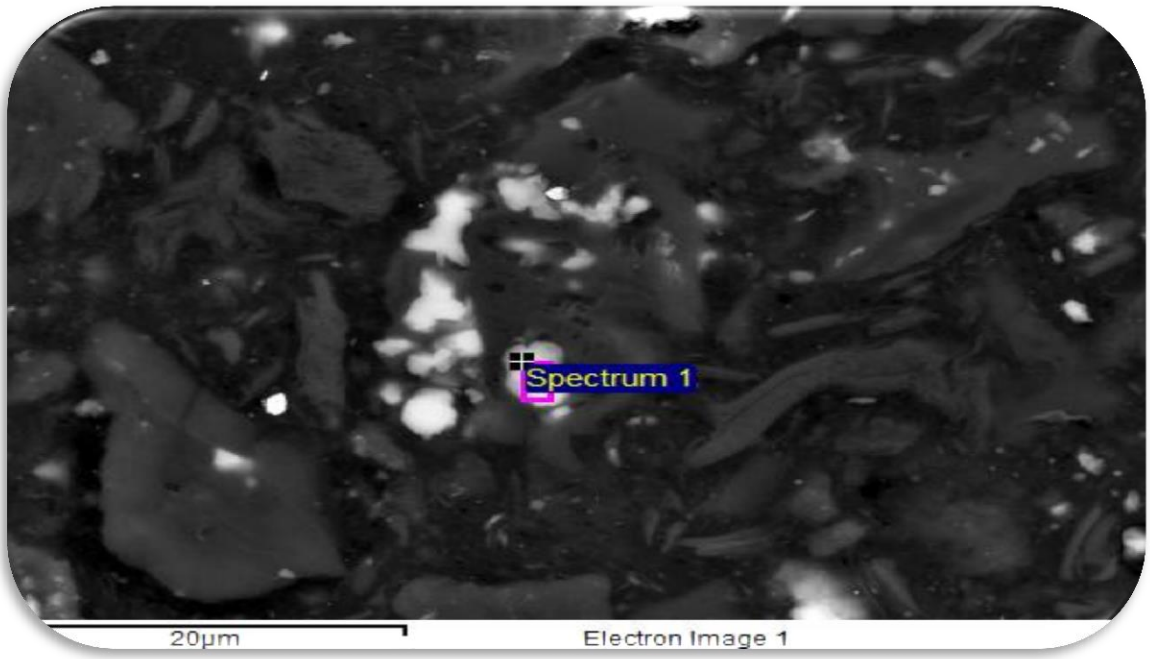

Figure C.35 30 % CH_4 in Ar for 120 minutes at 1050°C

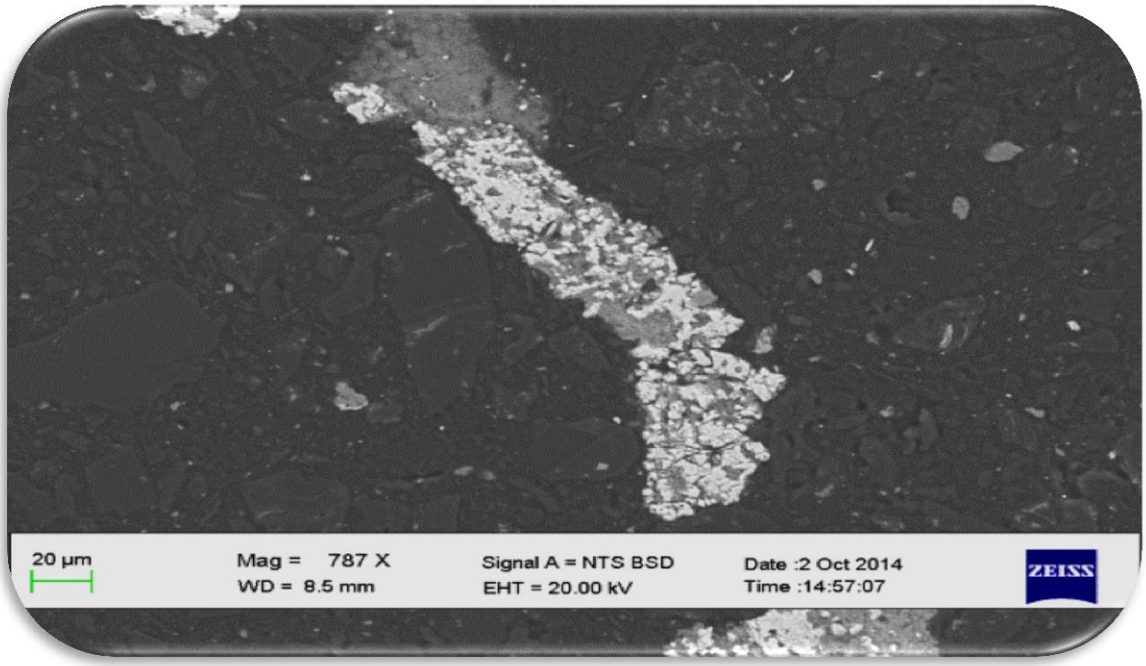

Figure C.36 30 % CH_4 in Ar for 20 minutes at 1100°C

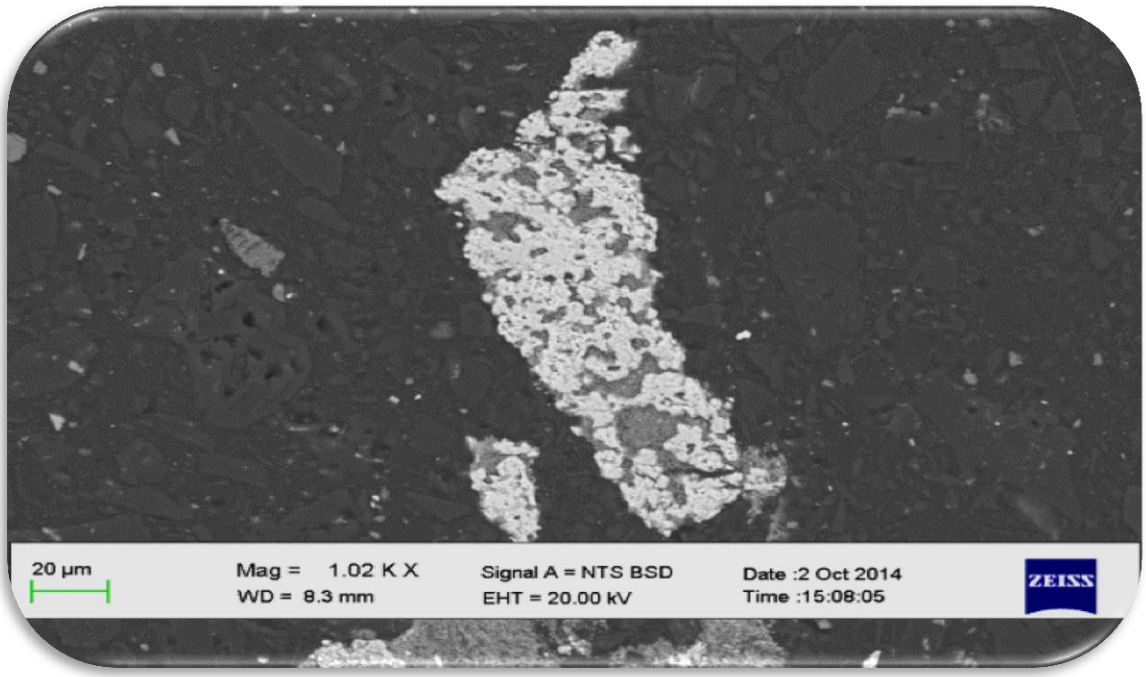

Figure C.37 30 % CH_4 in Ar for 30 minutes at 1100^{o}C

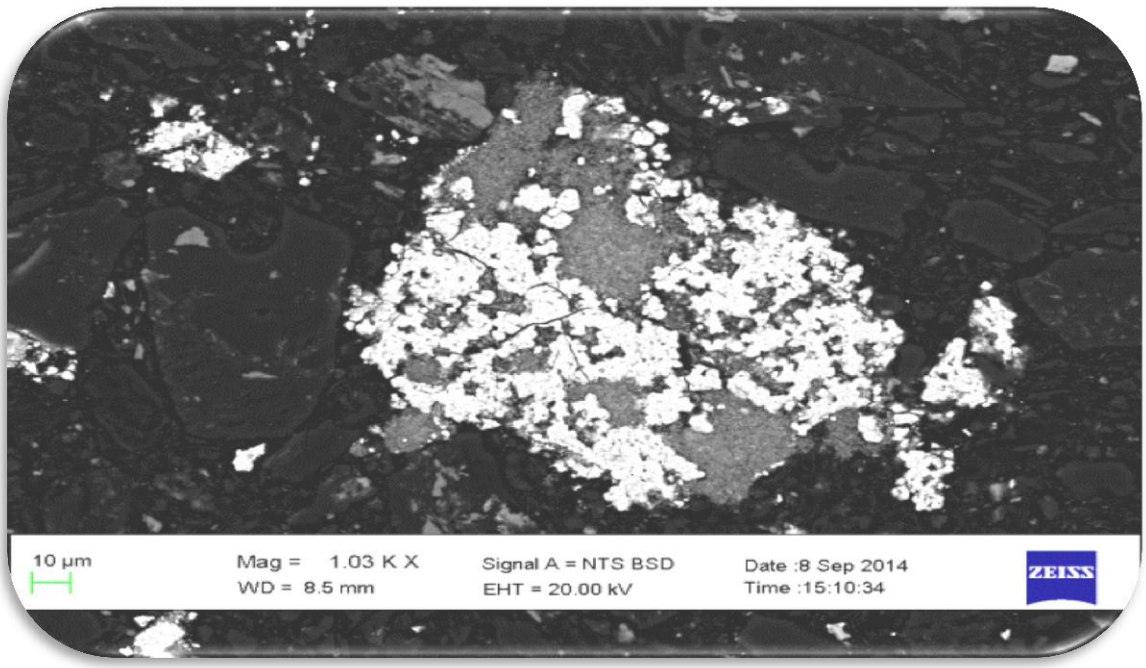

Figure C.38 30 % CH_4 in Ar for 60 minutes at 1100^{o}C

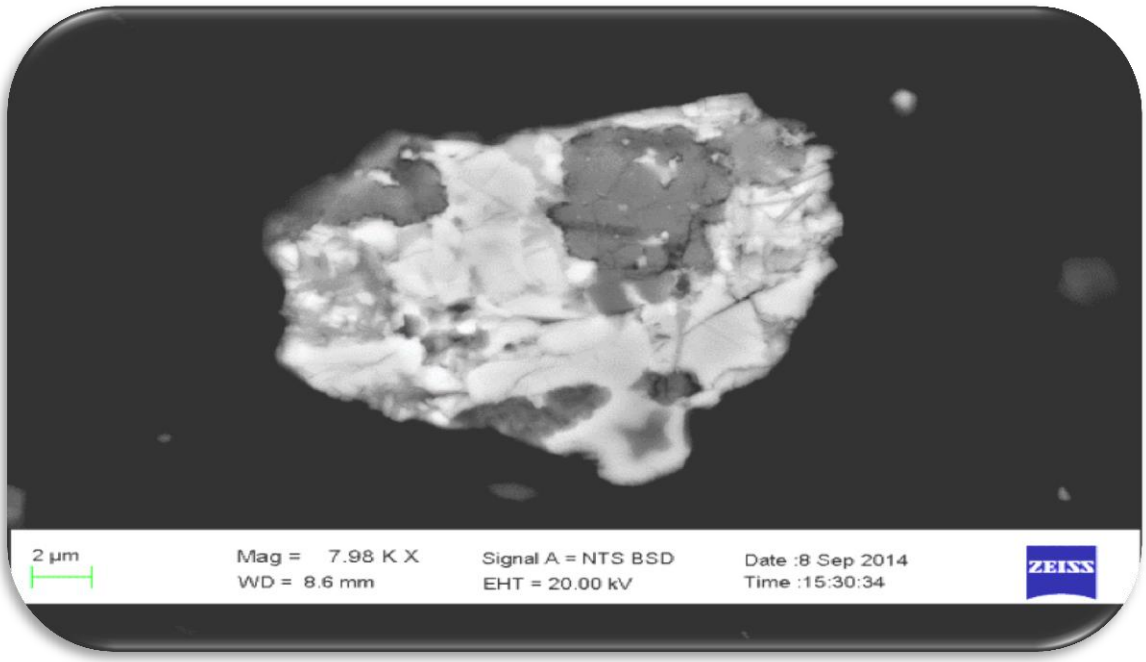

Figure C.39 30 % CH_4 in Ar for 90 minutes at 1100°C

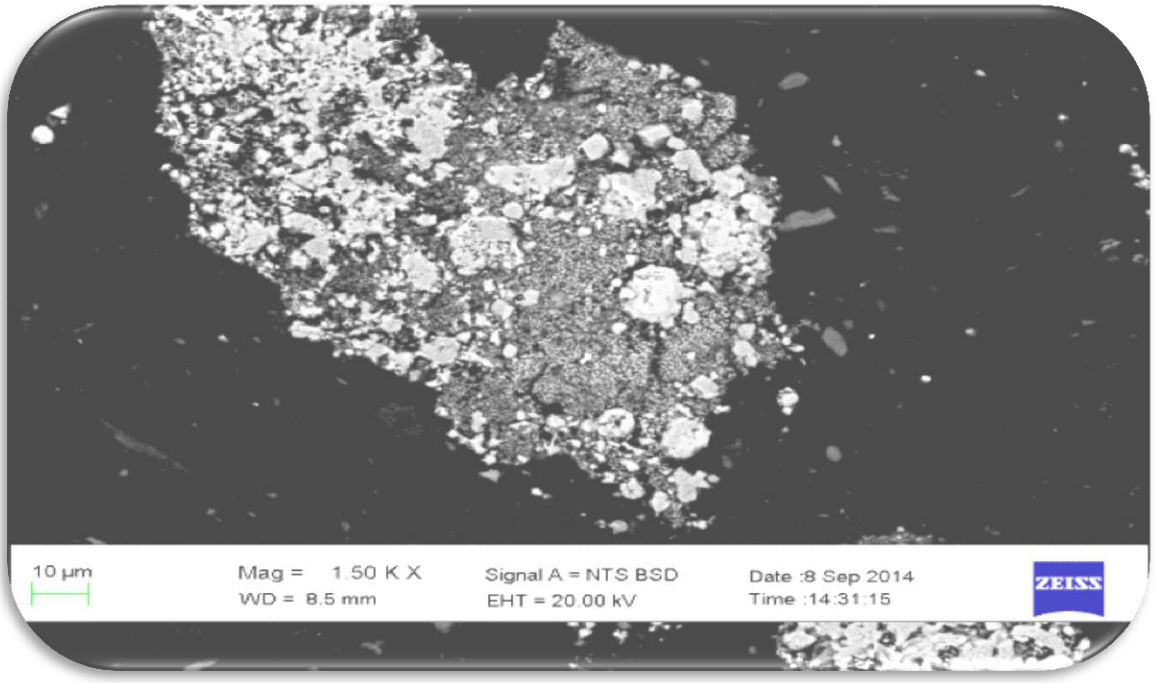

Figure C.40 30 % CH_4 in Ar for 120 minutes at 1100°C

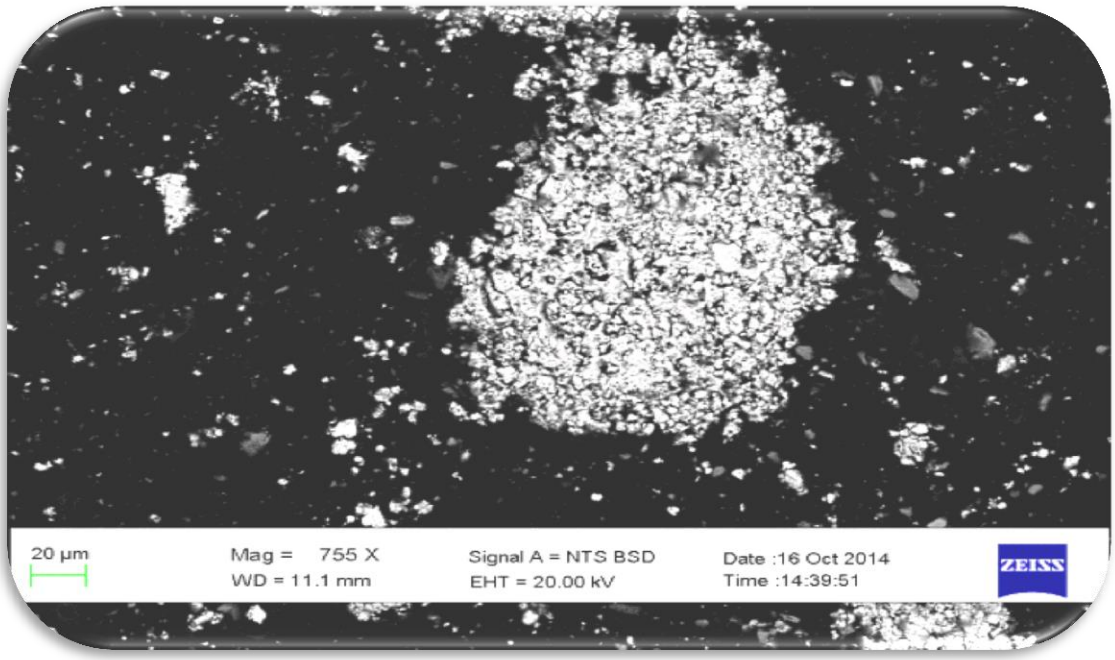

Figure C.41 30 % CH_4 in Ar for 20 minutes at 1200°C

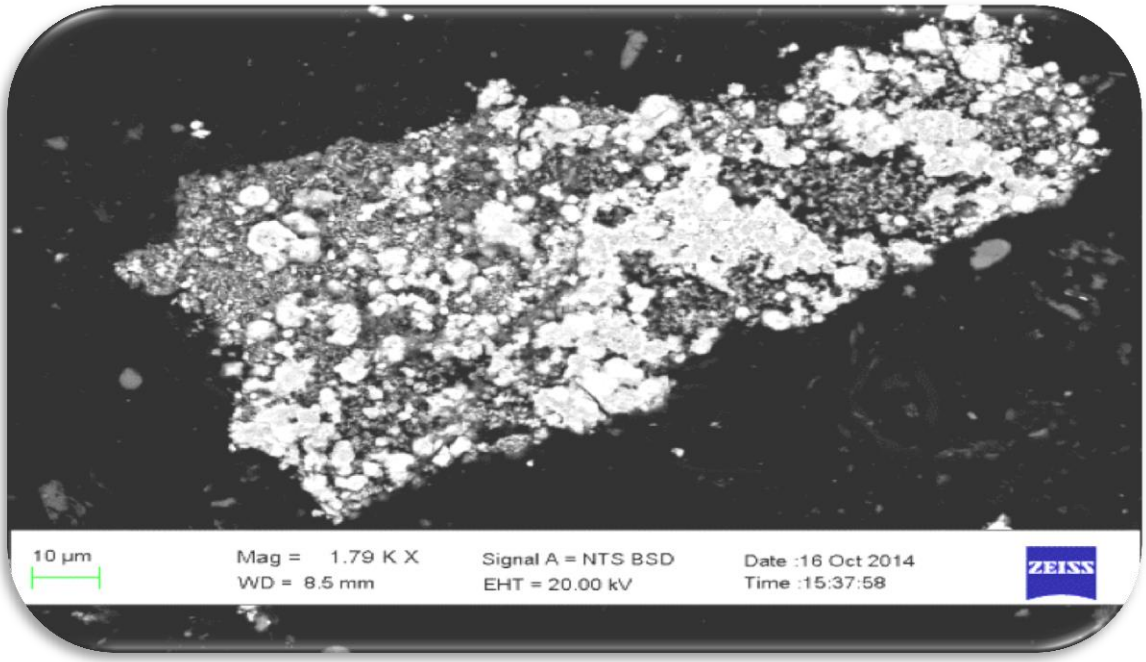

Figure C.42 30 % CH_4 in Ar for 30 minutes at 1200°C

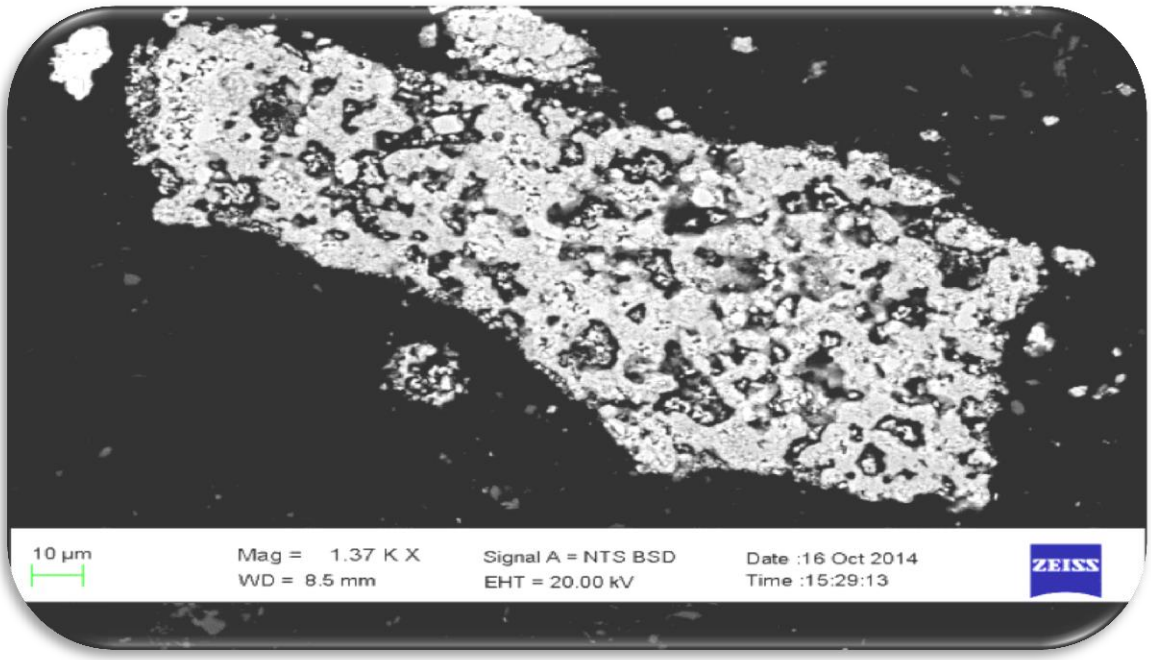

Figure C.43 30 % CH_4 in Ar for 60 minutes at 1200°C

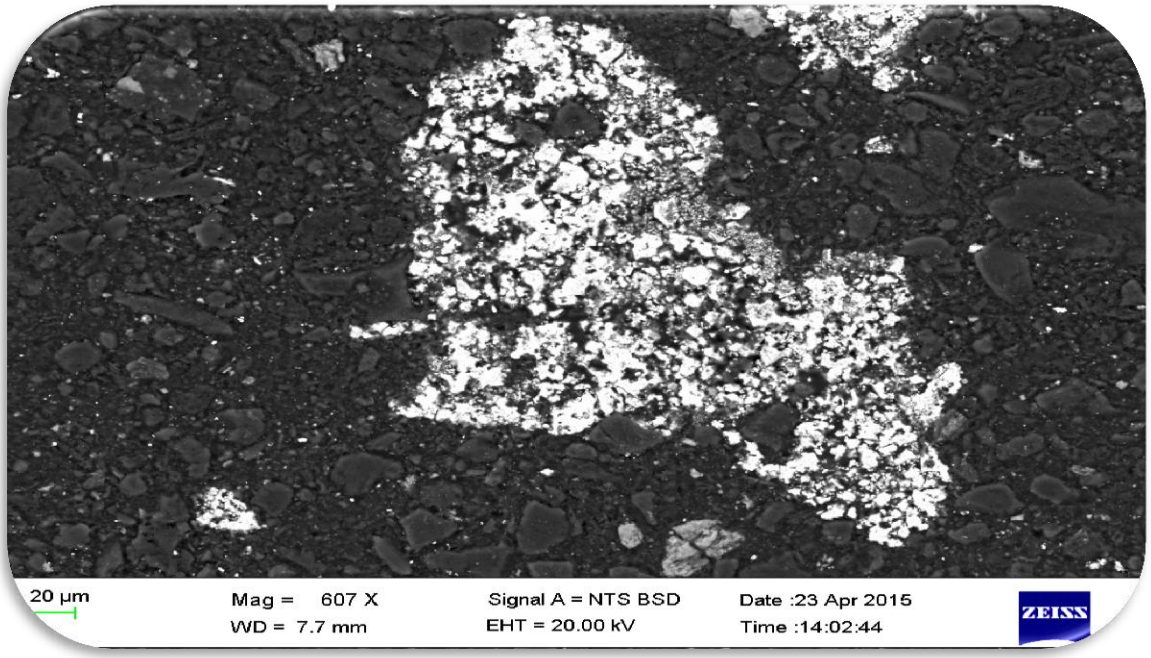

Figure C.44 30 % CH_4 in Ar for 90 minutes at 1200°C

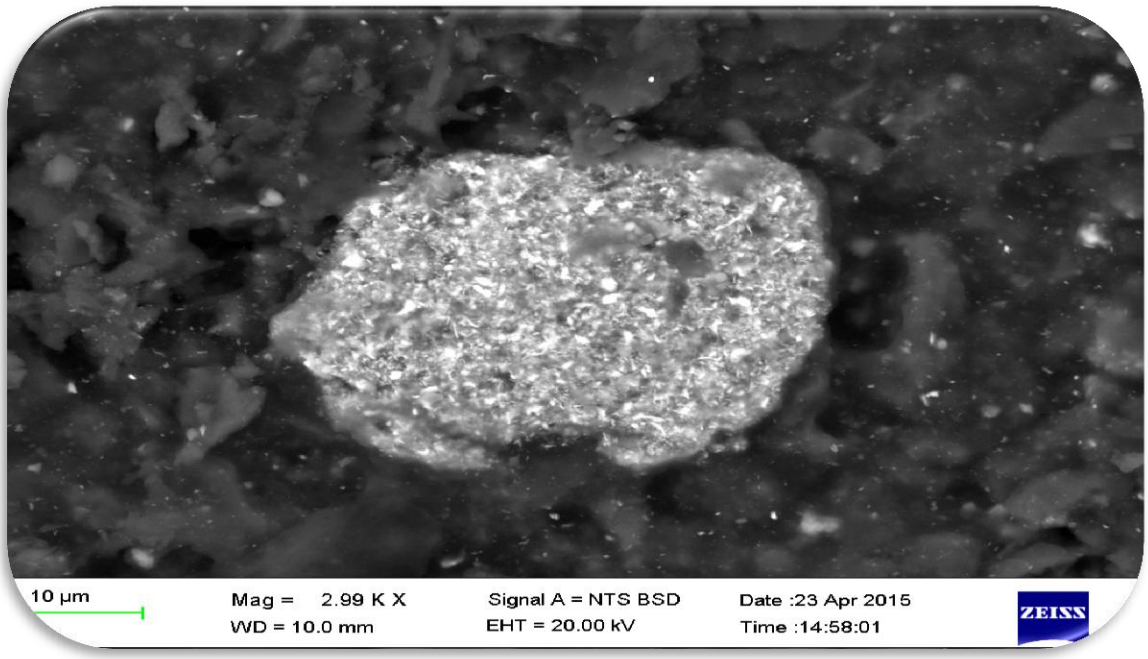

Figure C.45 30 % CH_4 in Ar for 120 minutes at 1200^{o}C

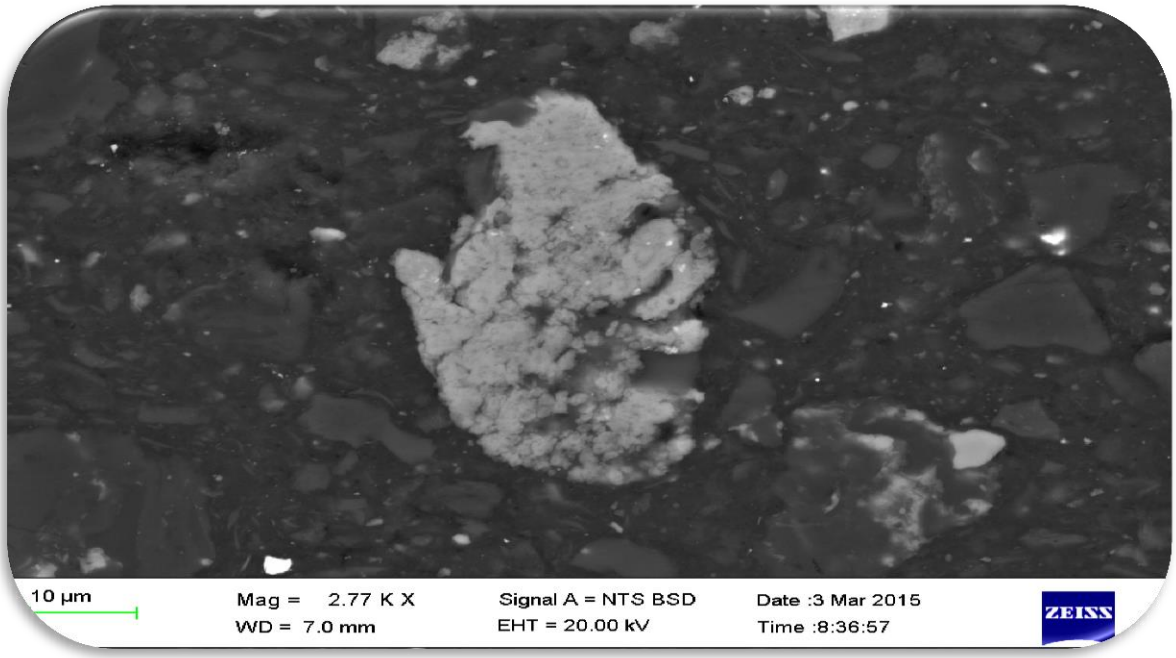

Figure C.46 30 % CH_4 in Ar for 20 minutes at 1250^{o}C

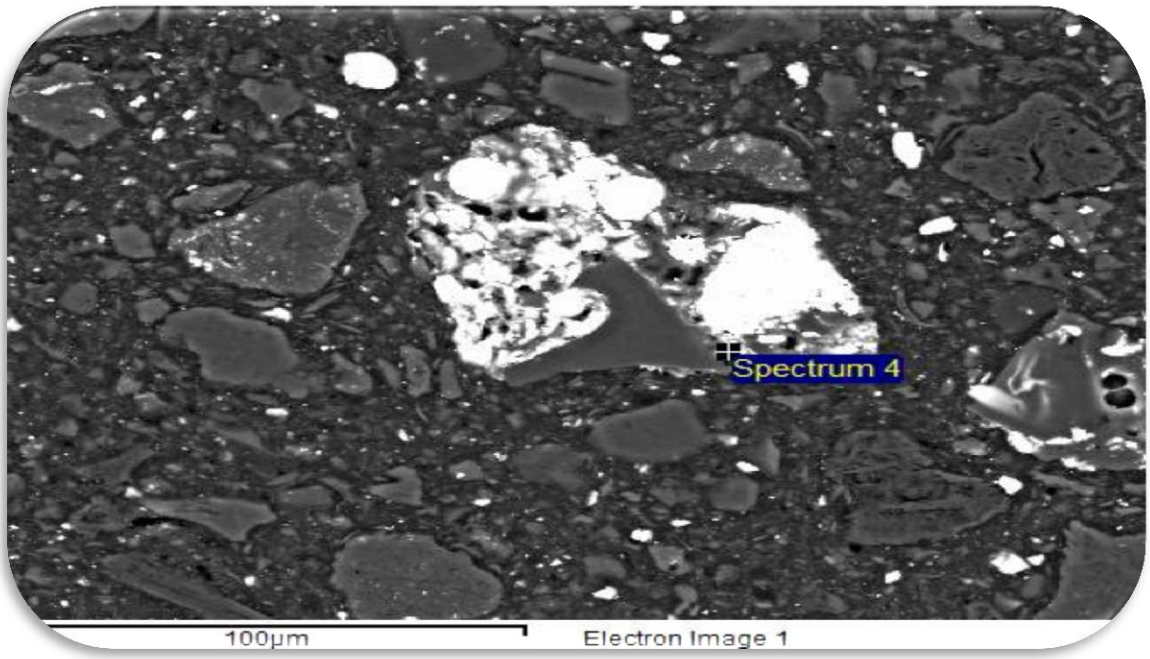

Figure C.47 30 % CH_4 in Ar for 30 minutes at 1250°C

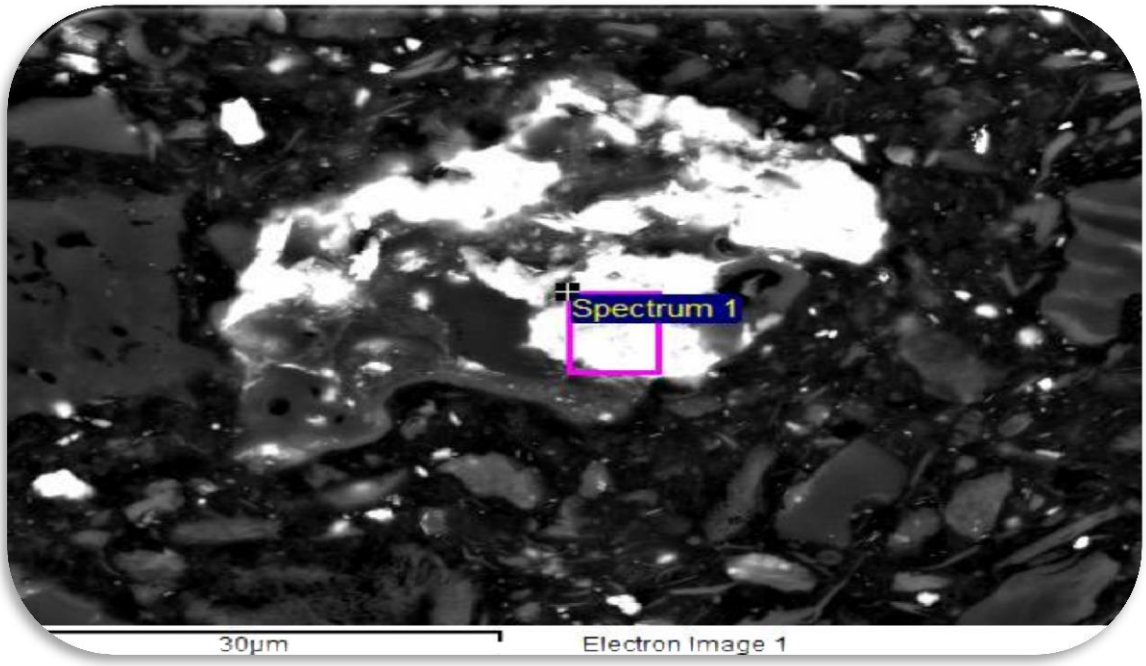

Figure C.48 30 % CH_4 in Ar for 60 minutes at 1250°C

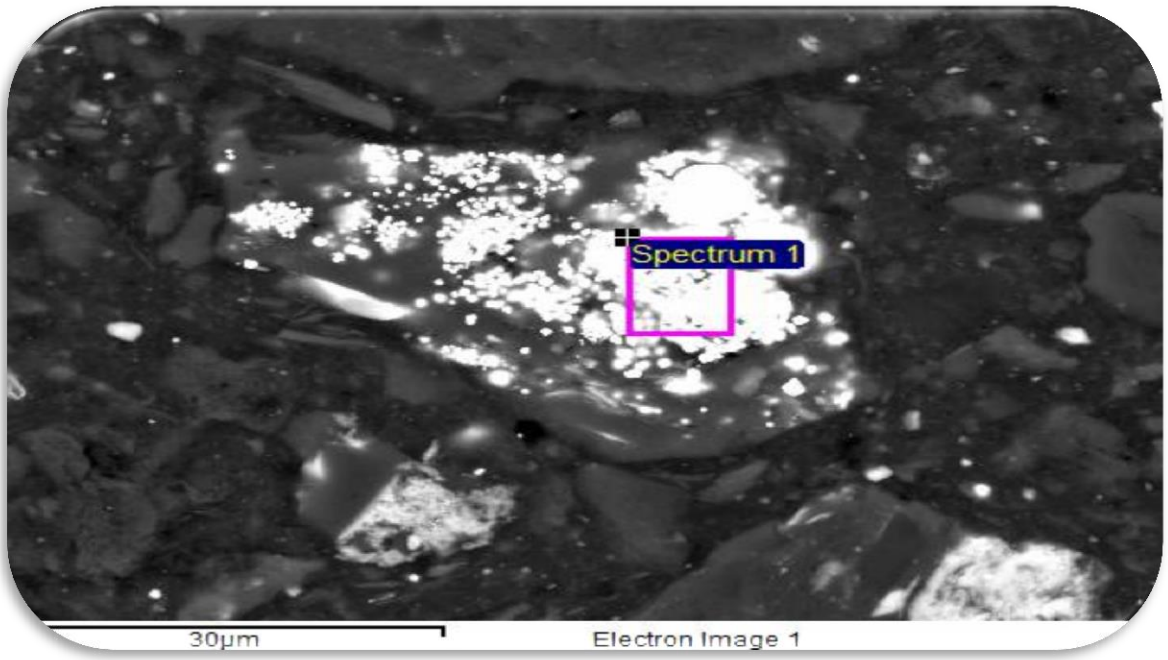

Figure C.49 30 % CH_4 in Ar for 90 minutes at 1250°C

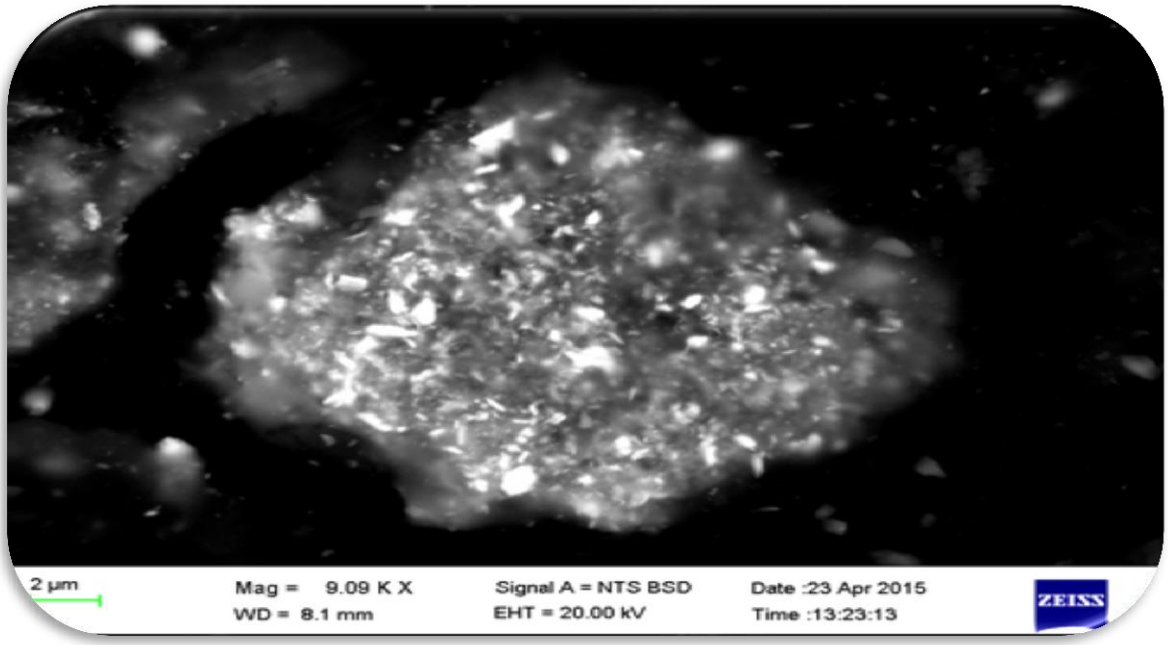

Figure C.50 30 % CH_4 in Ar for 120 minutes at 1250°C

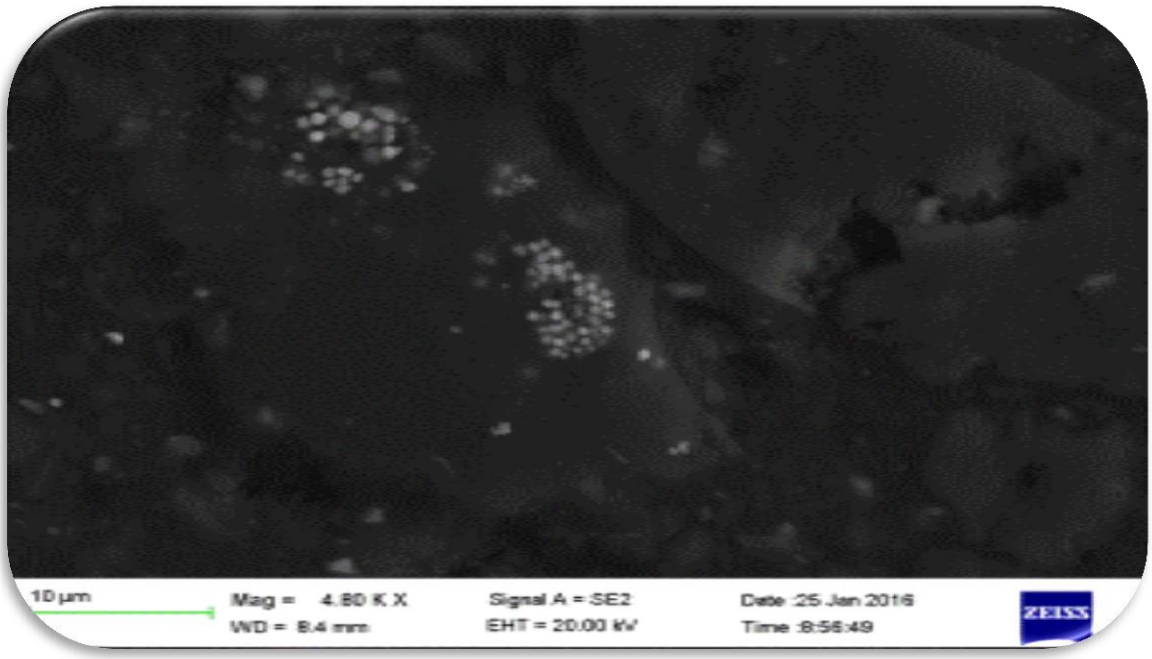

Figure C.51 10 % CH_4 in H_2 for 20 minutes at 1050°C

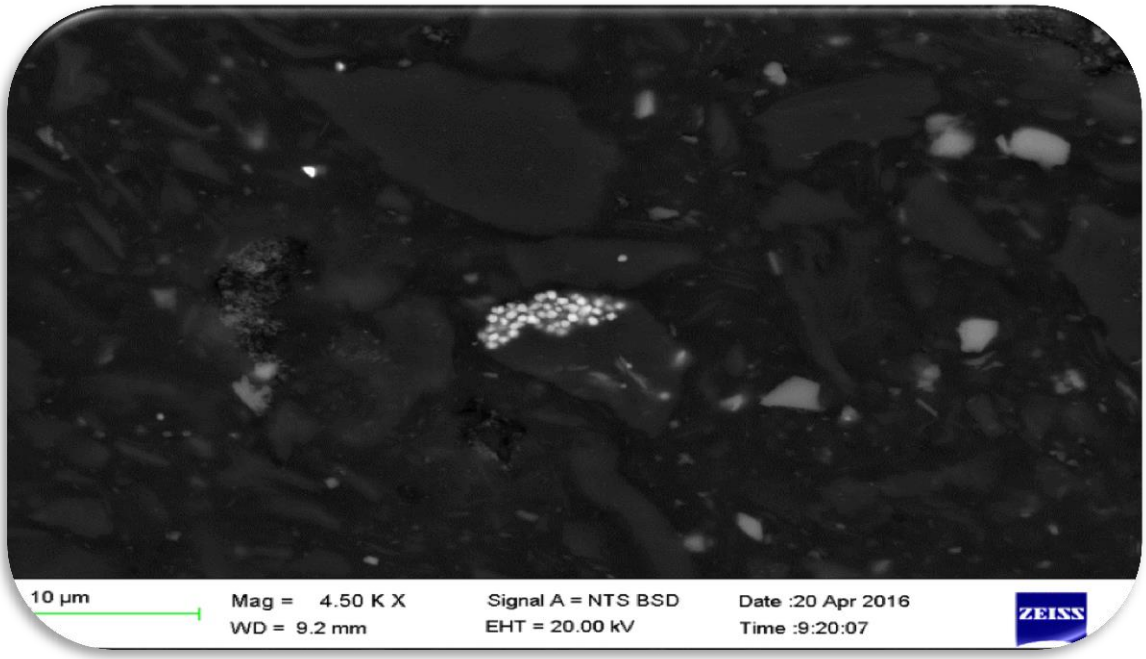

Figure C.52 10 % CH_4 in H_2 for 30 minutes at 1050°C

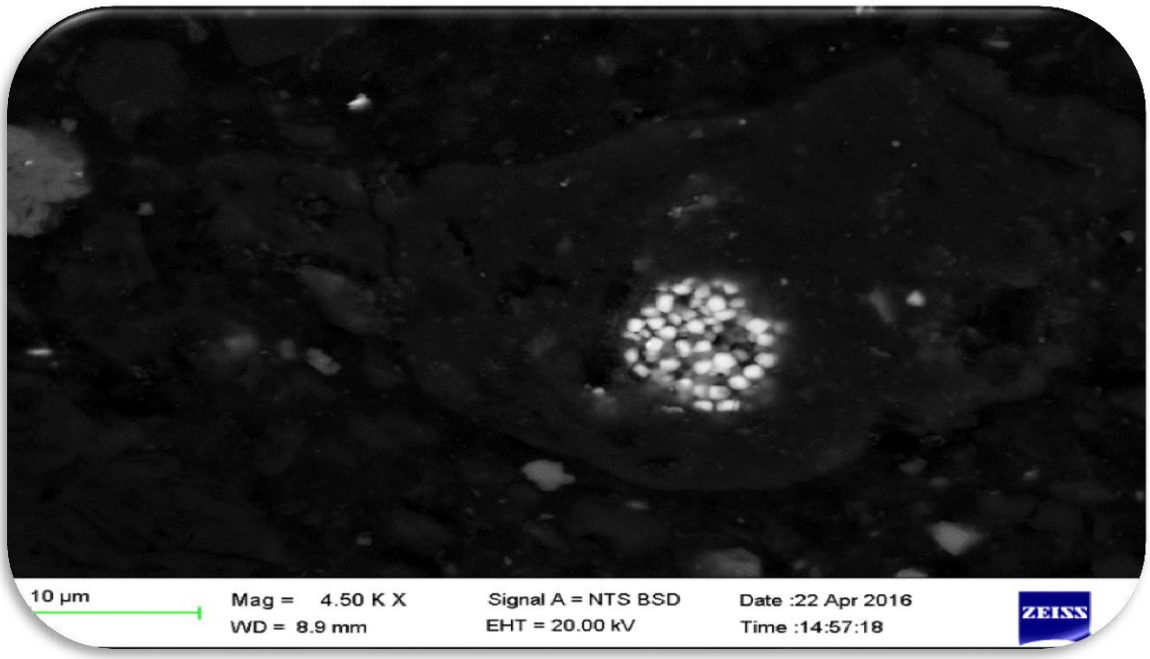

Figure C.53 10 % CH_4 in H_2 for 60 minutes at 1050^{o}C

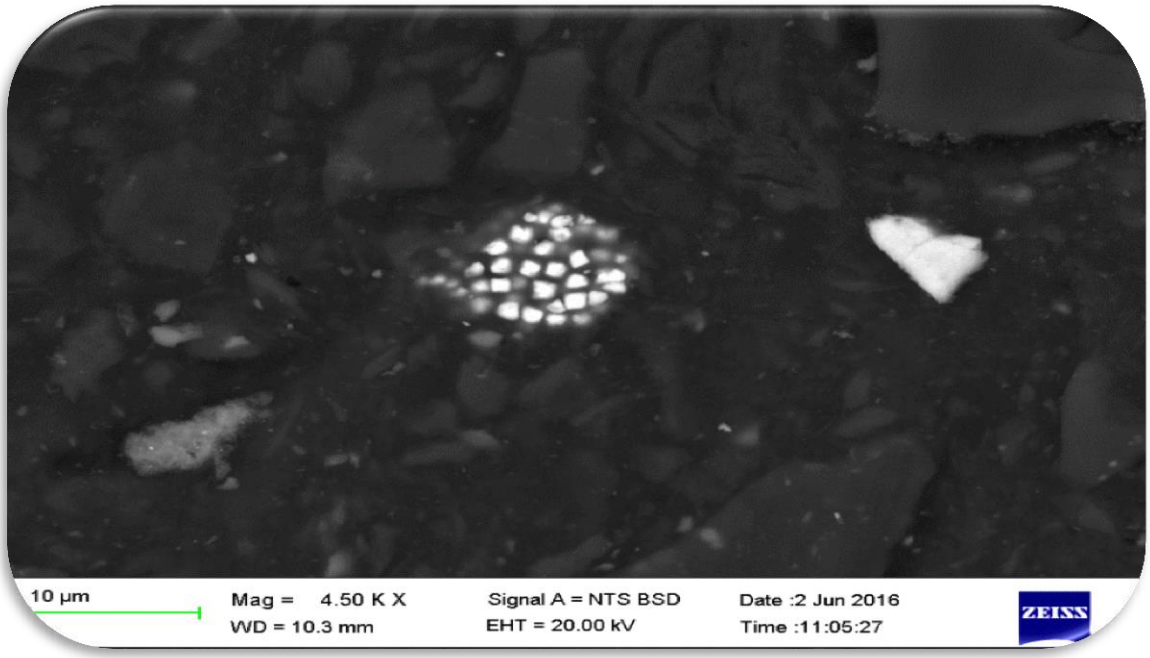

Figure C.54 10 % CH_4 in H_2 for 90 minutes at 1050^{o}C

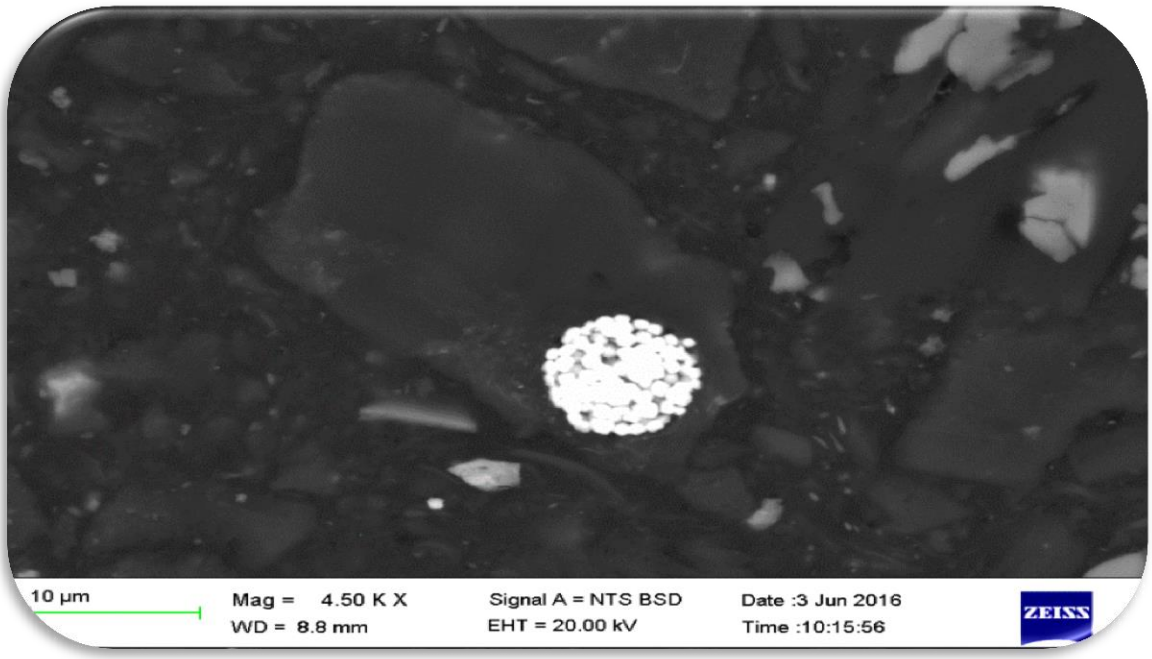

Figure C.55 10 % CH_4 in H_2 for 120 minutes at 1050^{o}C

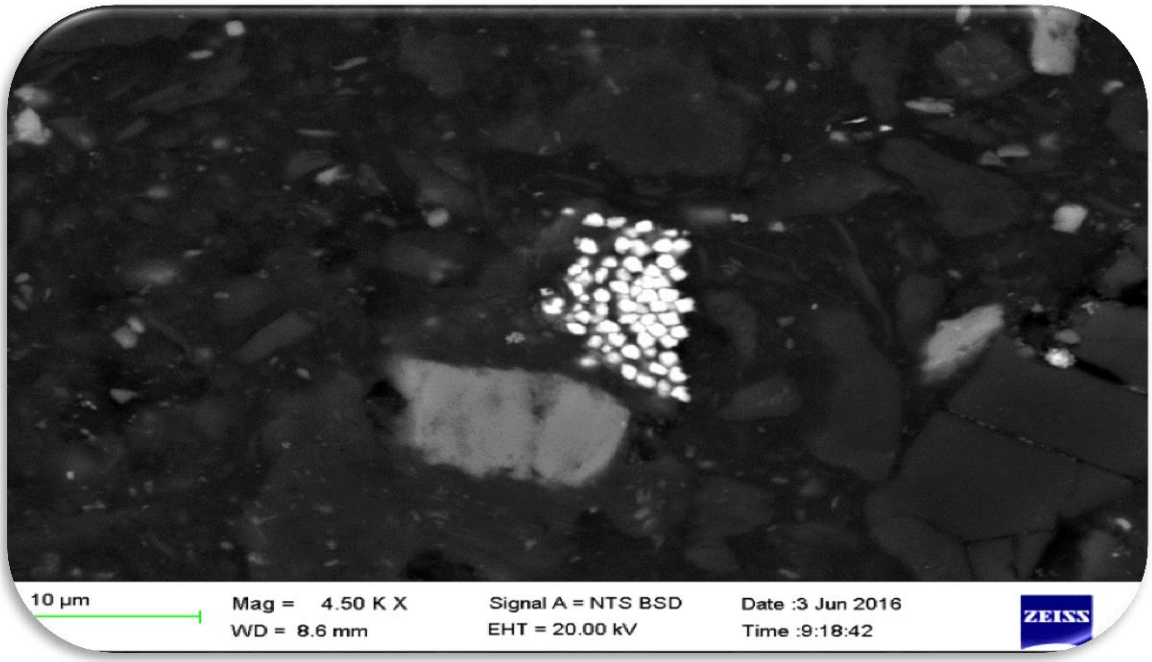

Figure C.56 10 % CH_4 in H_2 for 20 minutes at 1100^{o}C

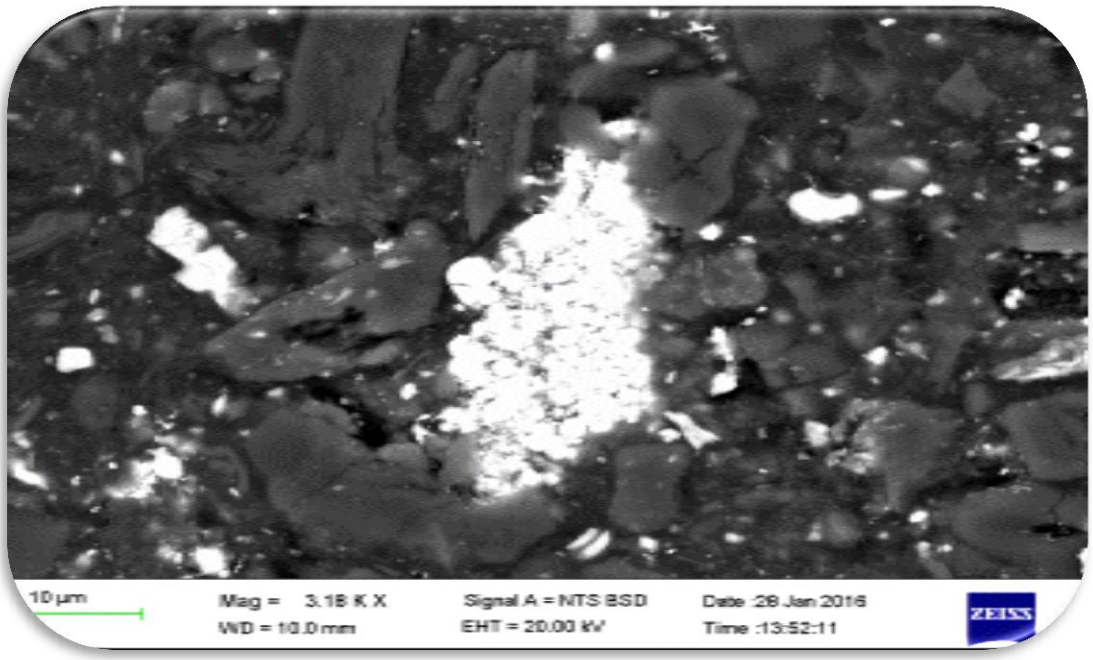

Figure C.57 10 % CH_4 in H_2 for 30 minutes at 1100°C

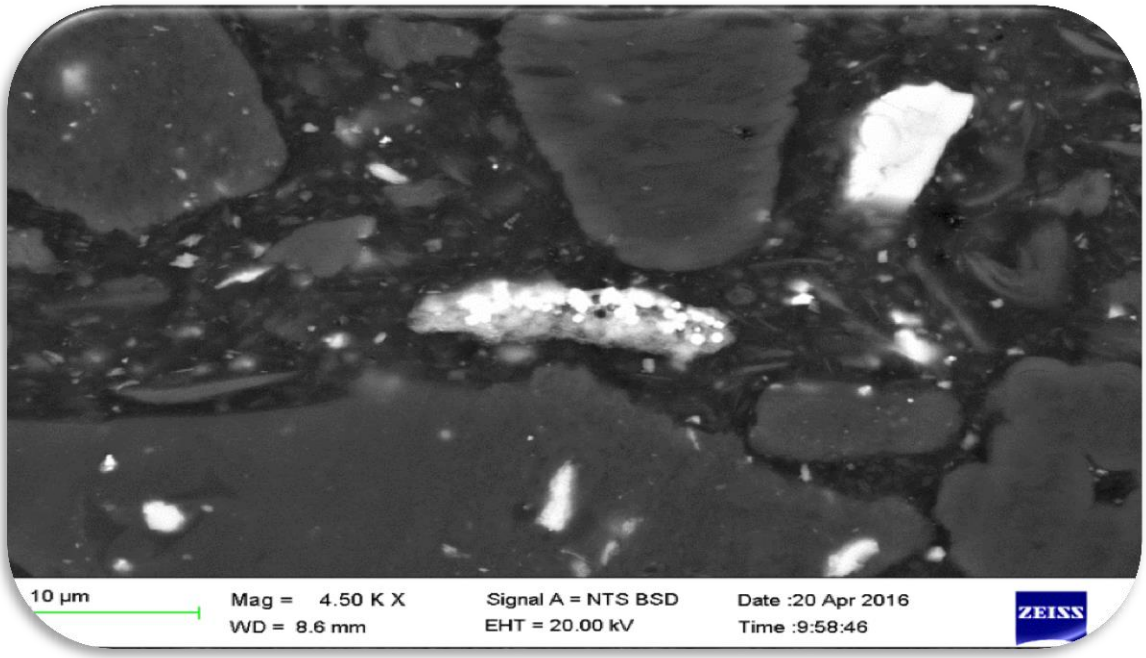

Figure C.58 10 % CH_4 in H_2 for 60 minutes at 1100°C

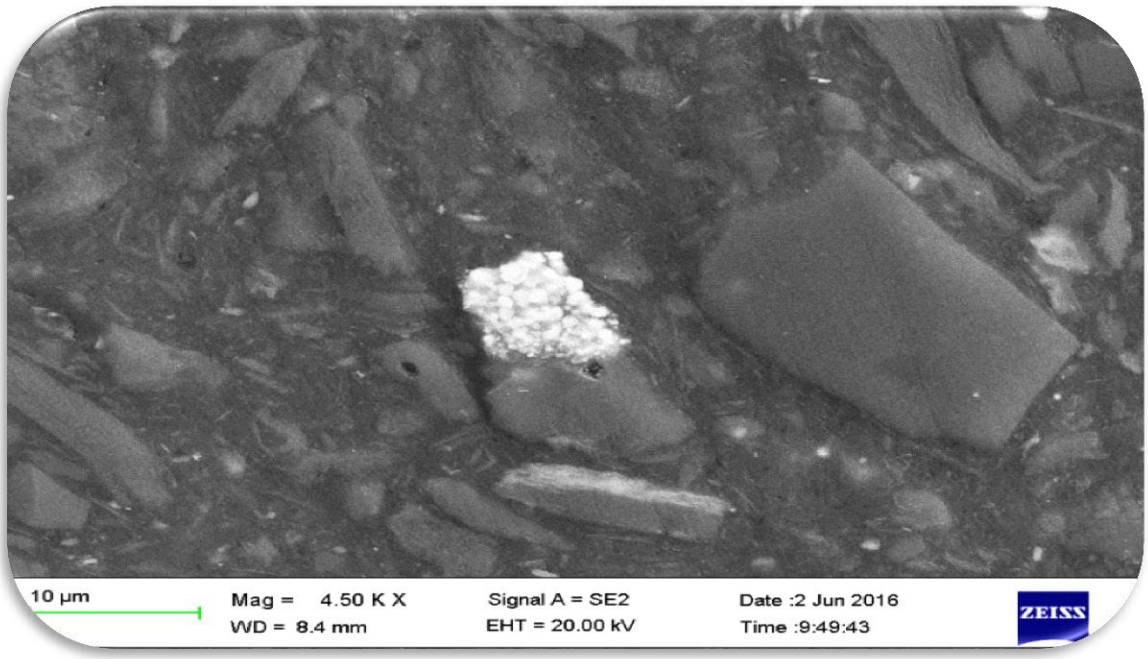

Figure C.59 10 % CH_4 in H_2 for 90 minutes at 1100°C

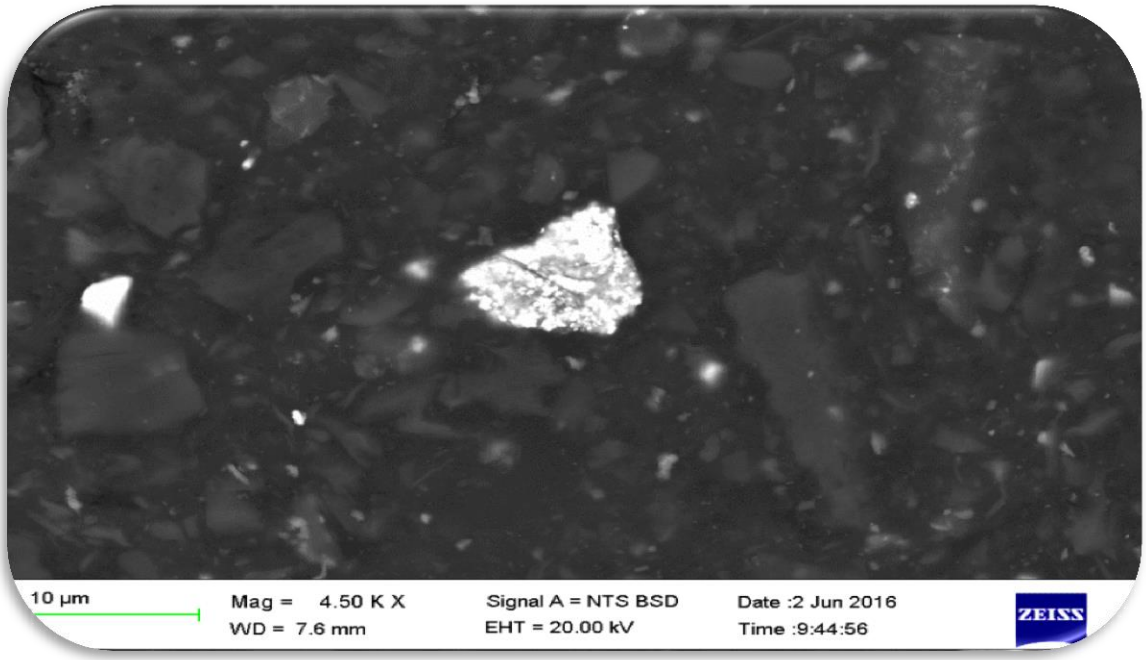

Figure C.60 10 % CH_4 in H_2 for 120 minutes at 1100°C

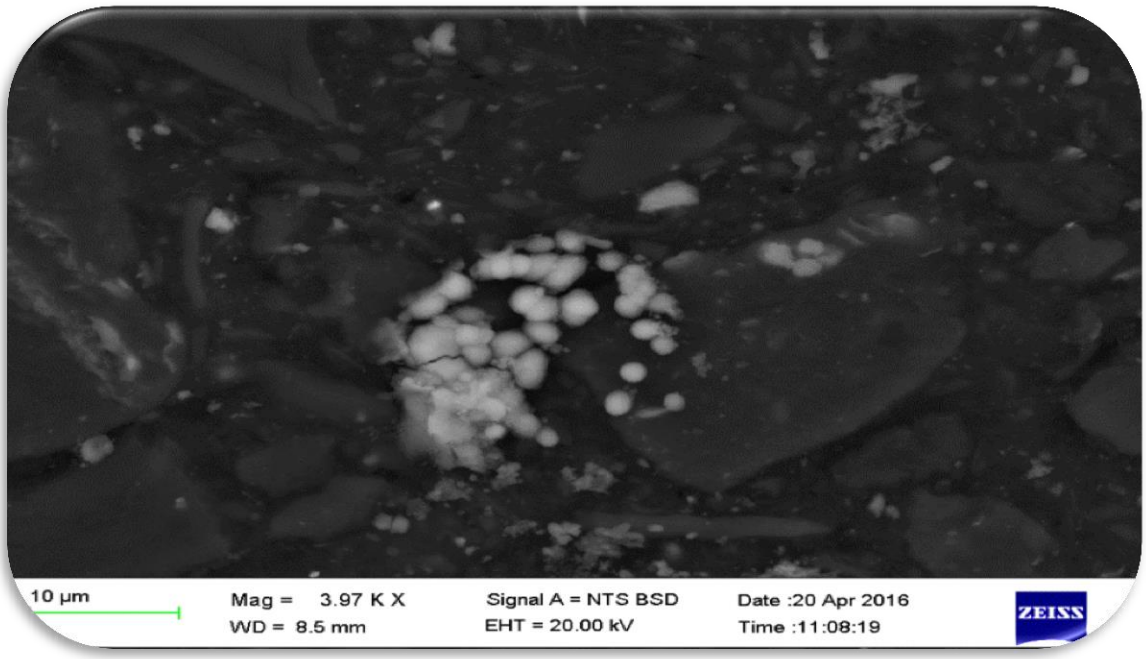

Figure C.61 10 % CH_4 in H_2 for 20 minutes at 1200^{o}C

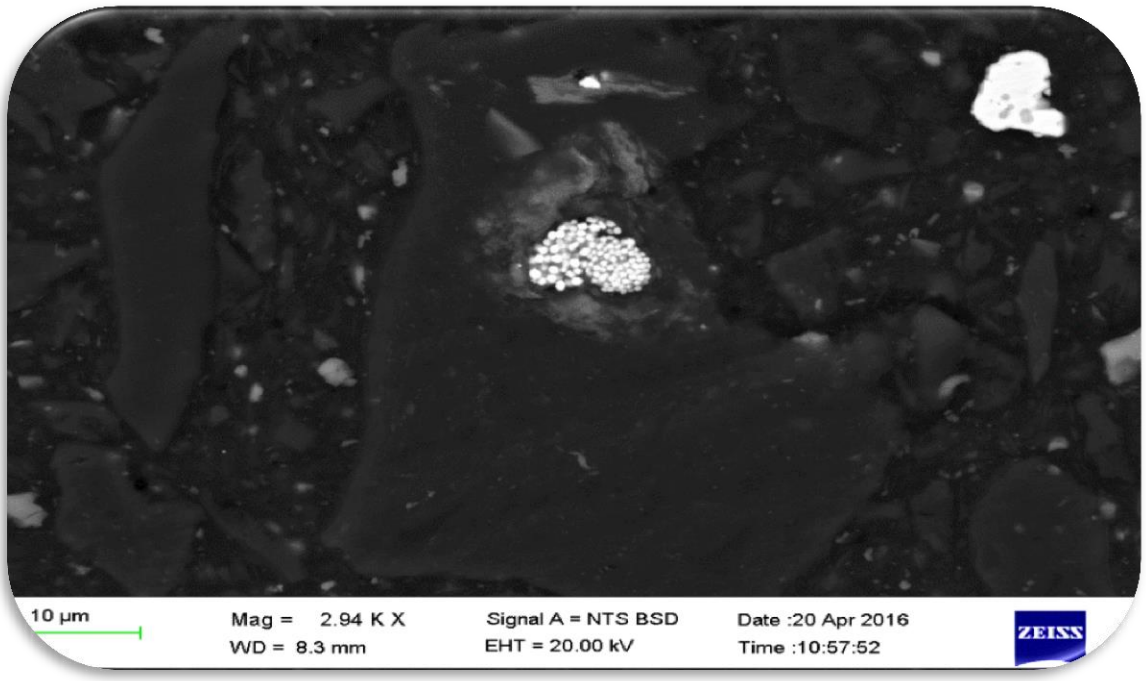

Figure C.62 10 % CH_4 in H_2 for 30 minutes at 1200^{o}C

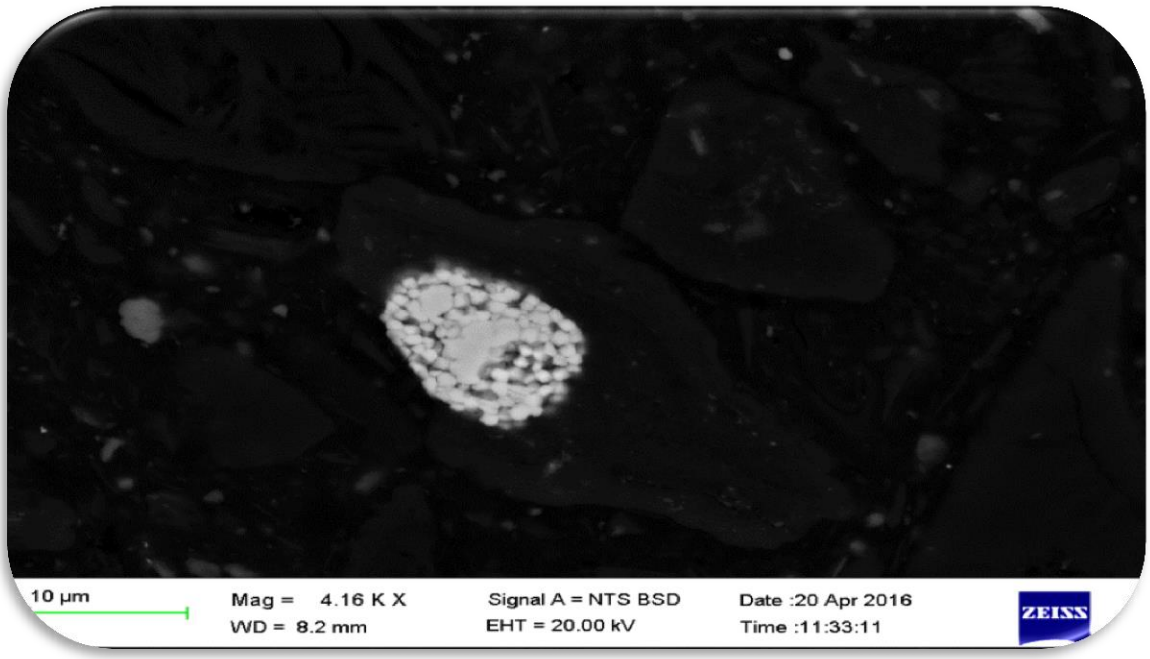

Figure C.63 10 % CH_4 in H_2 for 60 minutes at 1200^{o}C

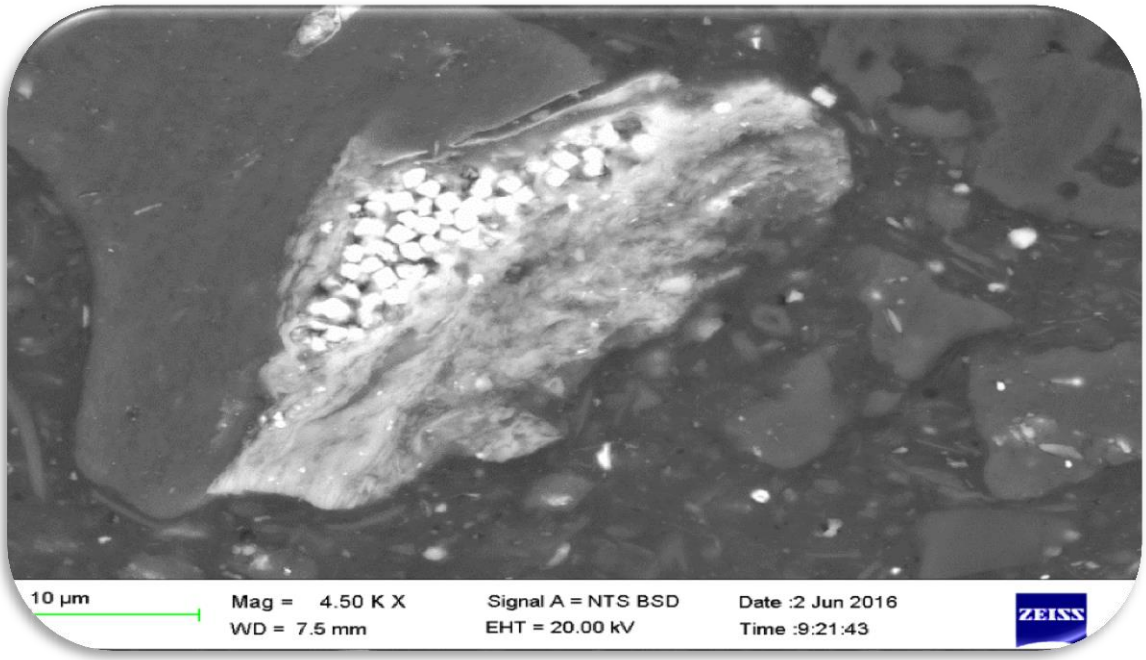

Figure C.64 10 % CH_4 in H_2 for 90 minutes at 1200^{o}C

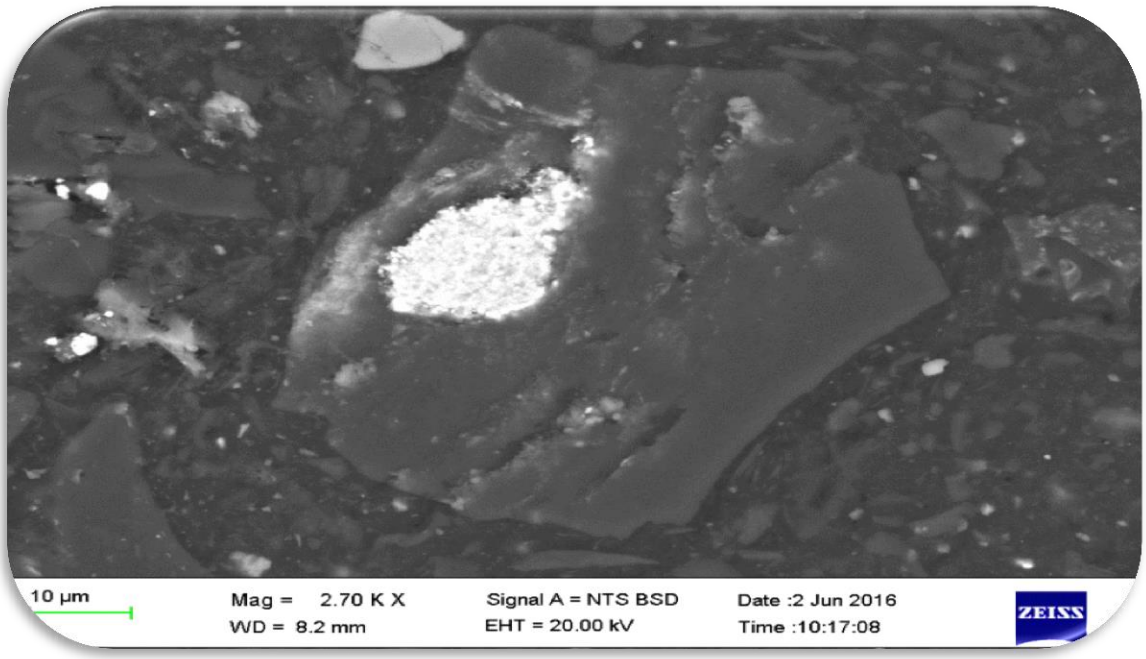

Figure C.65 10 % CH_4 in H_2 for 120 minutes at 1200^{o}C

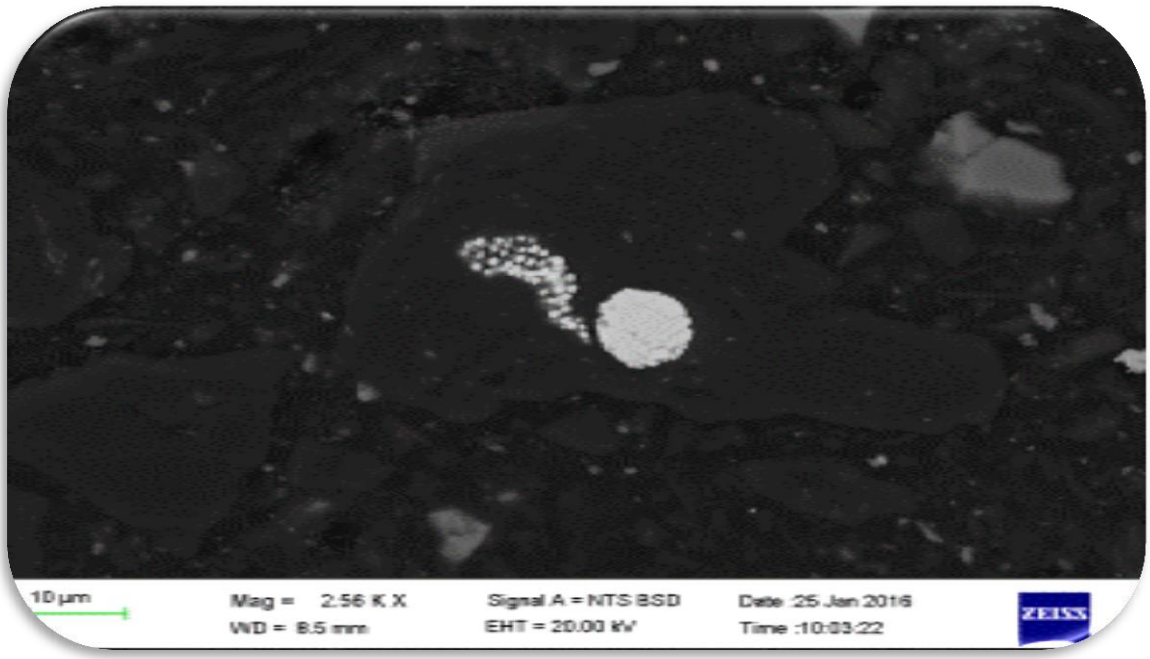

Figure C.66 10 % CH_4 in H_2 for 20 minutes at 1250^{o}C

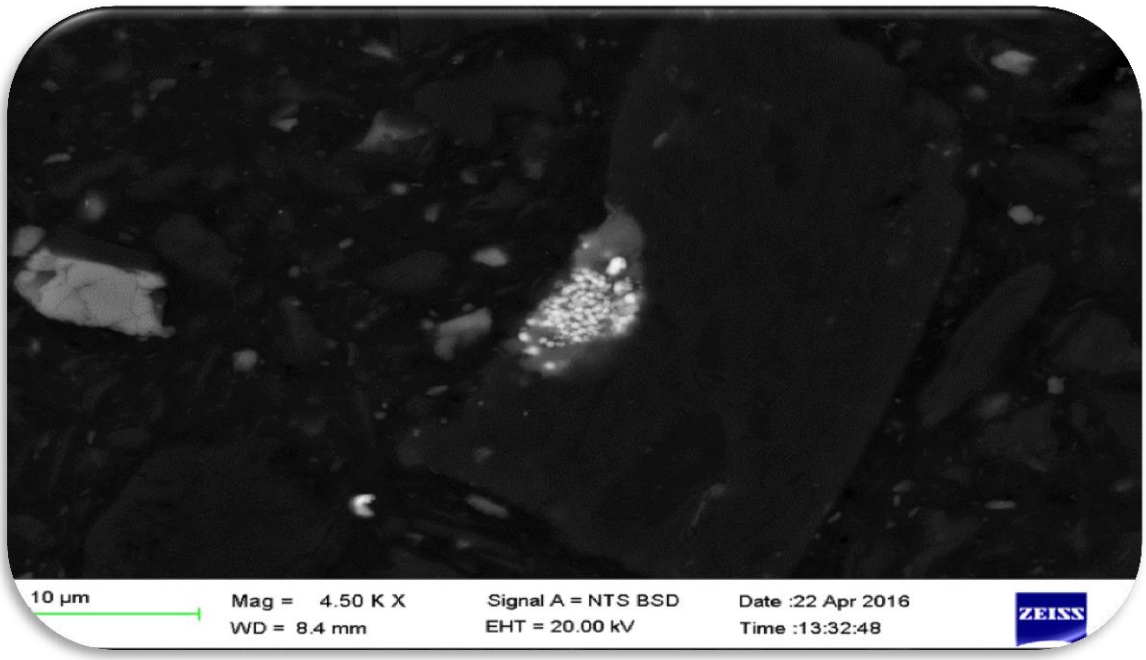

Figure C.67 10 % CH_4 in H_2 for 30 minutes at 1250^{o}C

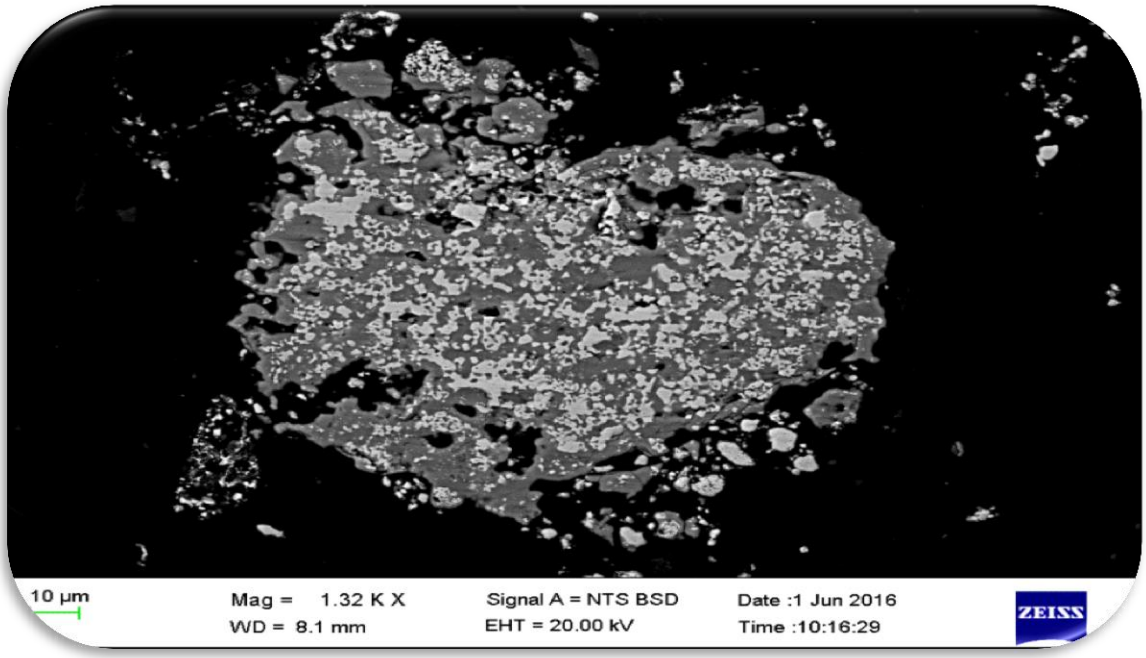

Figure C.68 10 % CH_4 in H_2 for 60 minutes at 1250^{o}C

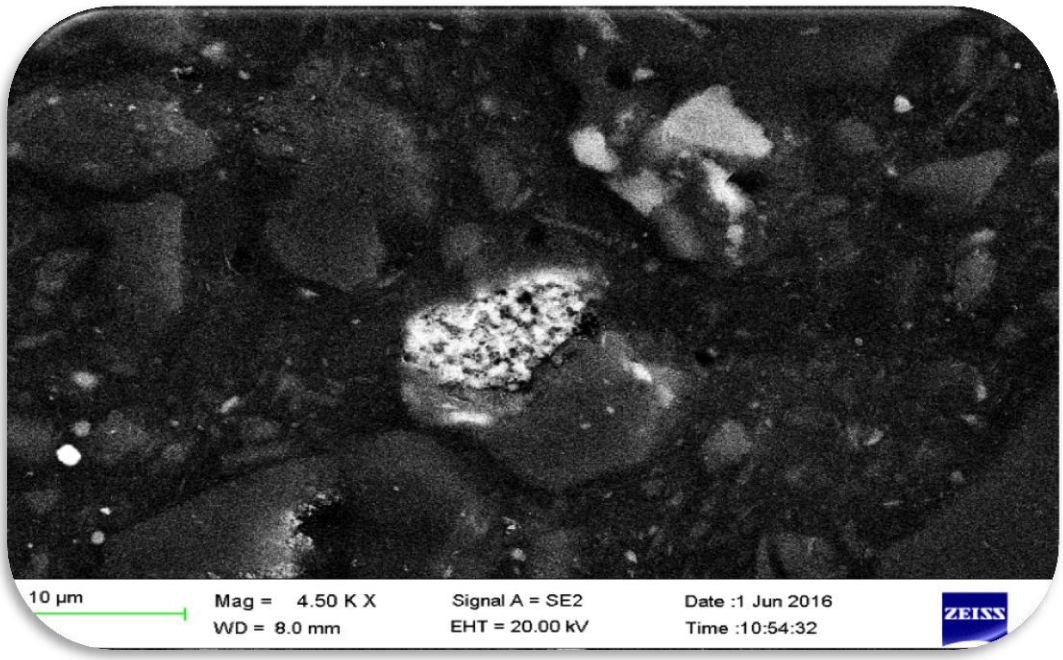

Figure C.69 10 % CH_4 in H_2 for 90 minutes at 1250^{o}C

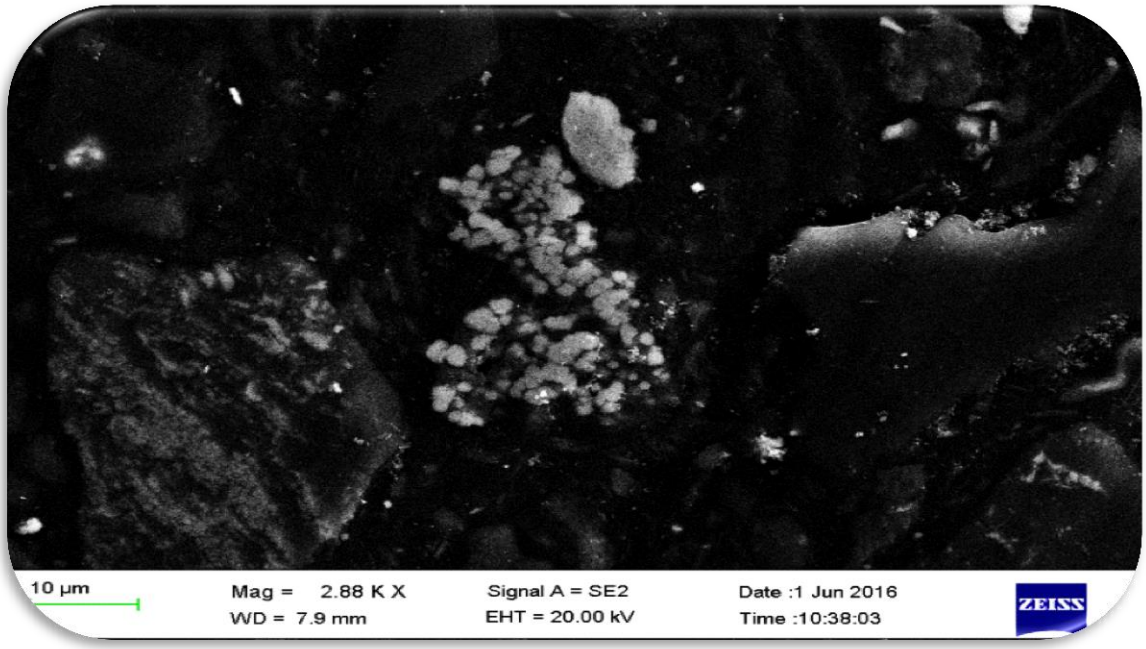

Figure C.70 10 % CH_4 in H_2 for 120 minutes at 1250^{o}C

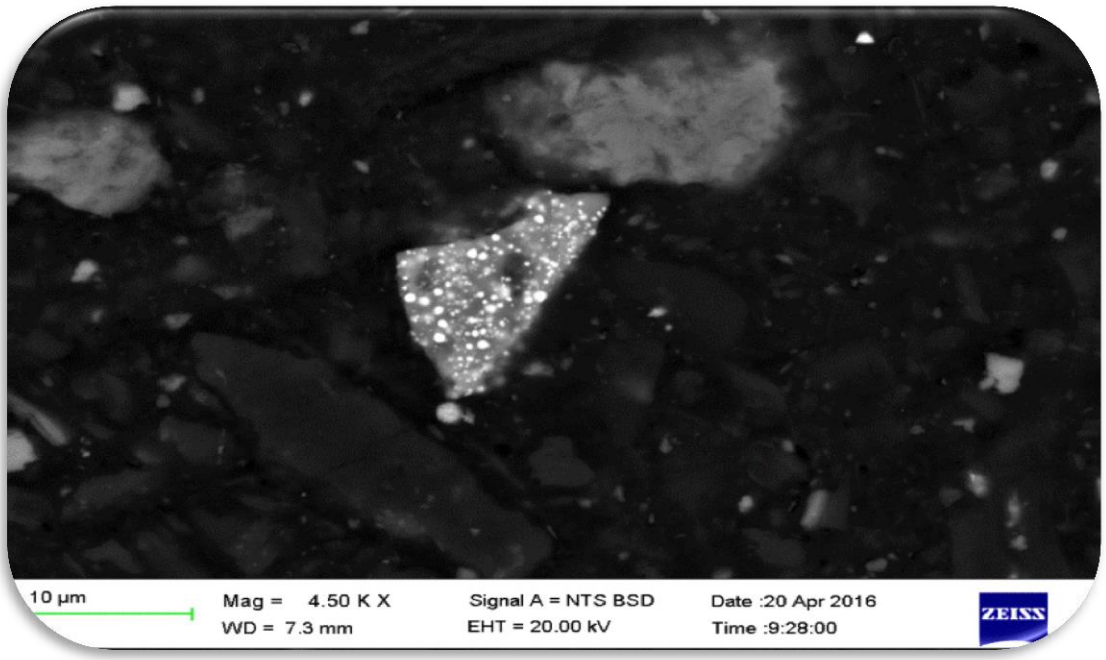

Figure C.71 20 % CH_4 in H_2 for 20 minutes at 1050^{o}C

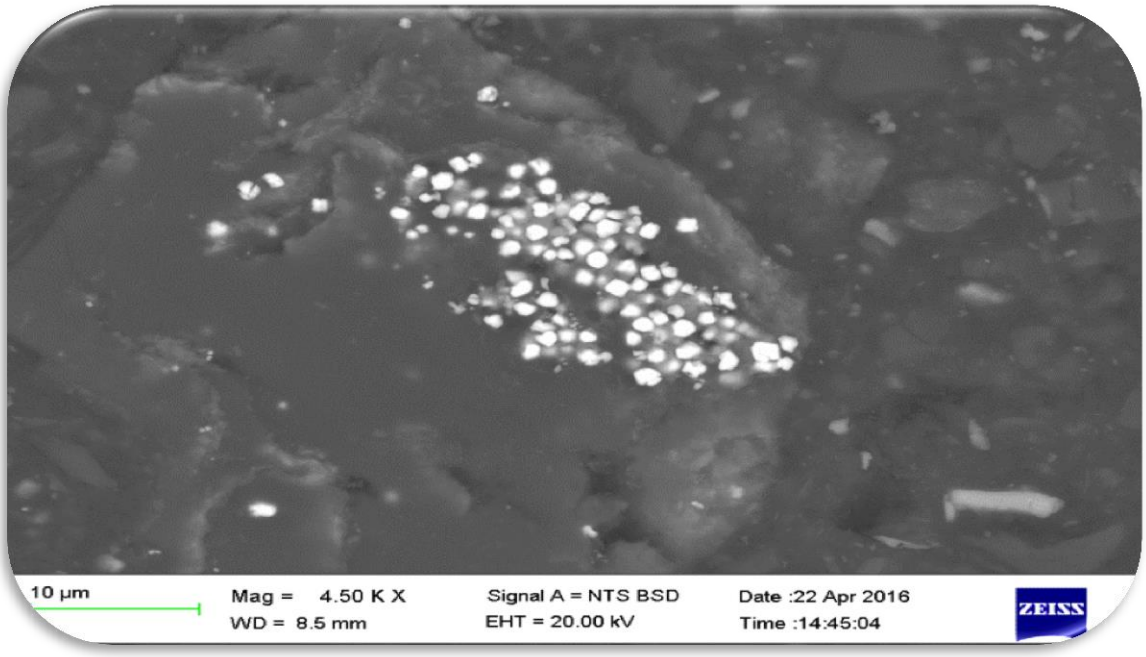

Figure C.72 20 % CH_4 in H_2 for 30 minutes at 1050^{o}C

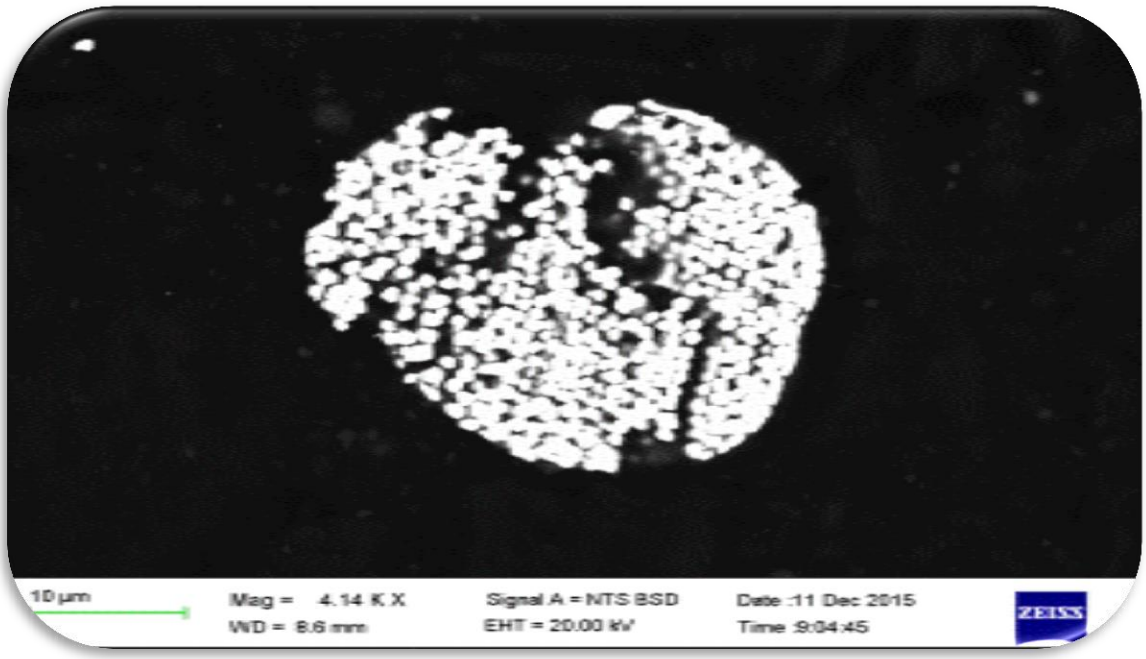

Figure C.73 20 % CH_4 in H_2 for 60 minutes at 1050^{o}C

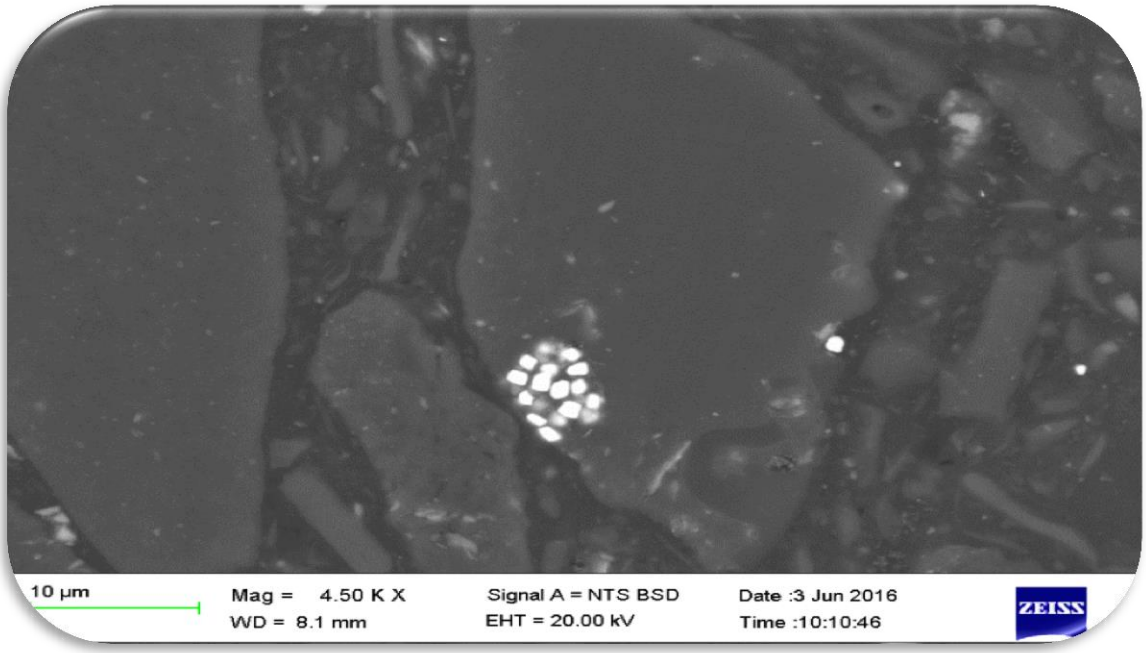

Figure C.74 20 % CH_4 in H_2 for 90 minutes at 1050^{o}C

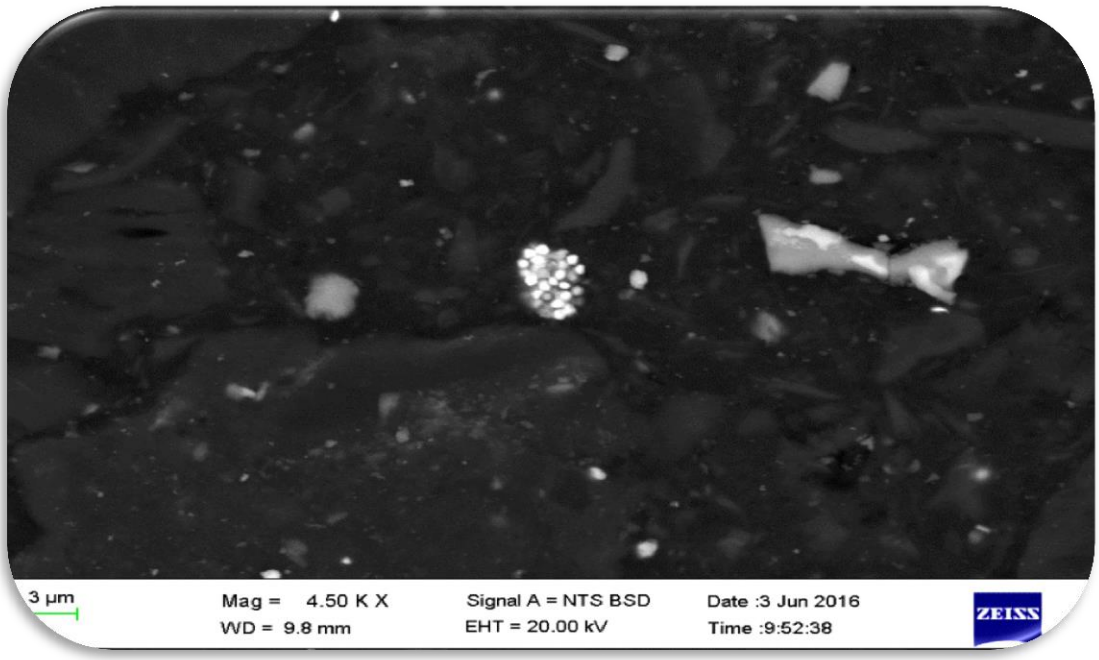

Figure C.75 20 % CH_4 in H_2 for 120 minutes at 1050^{o}C

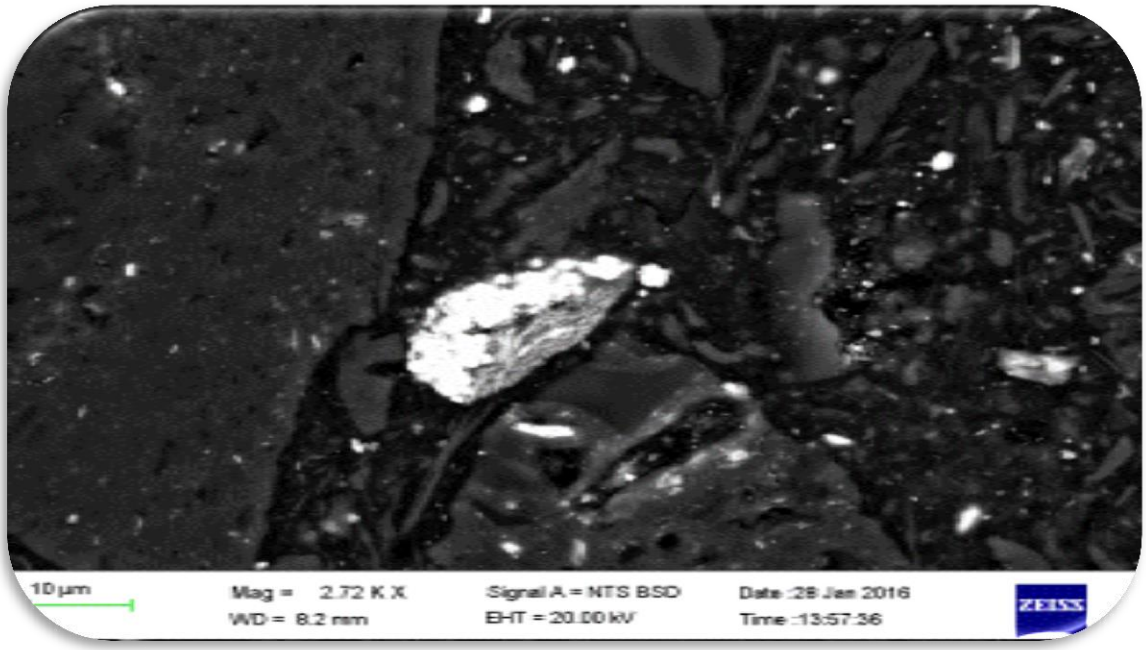

Figure C.76 20 % CH_4 in H_2 for 20 minutes at 1100^{o}C

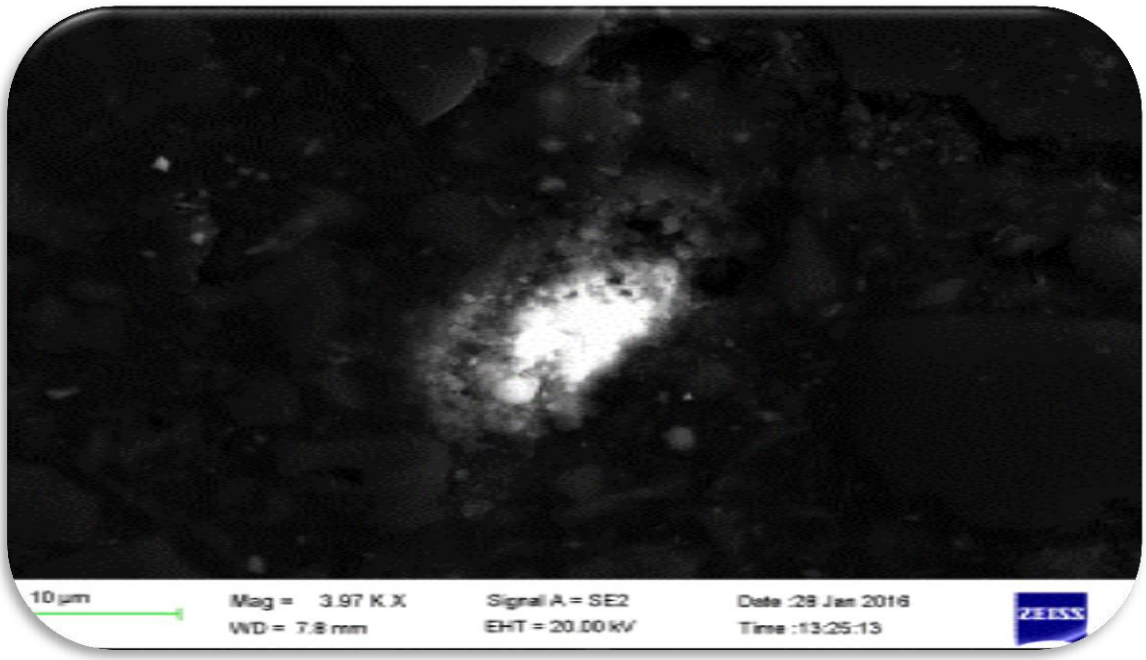

Figure C.77 20 % CH_4 in H_2 for 30 minutes at 1100^{o}C

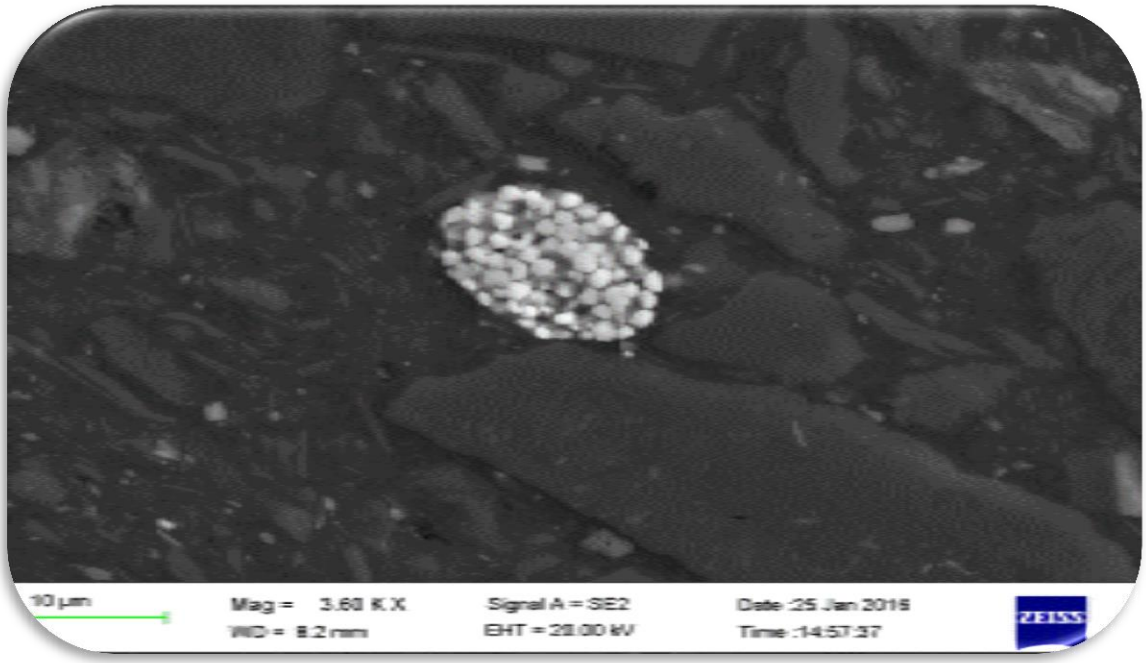

Figure C.78 20 % CH_4 in H_2 for 60 minutes at 1100^{o}C

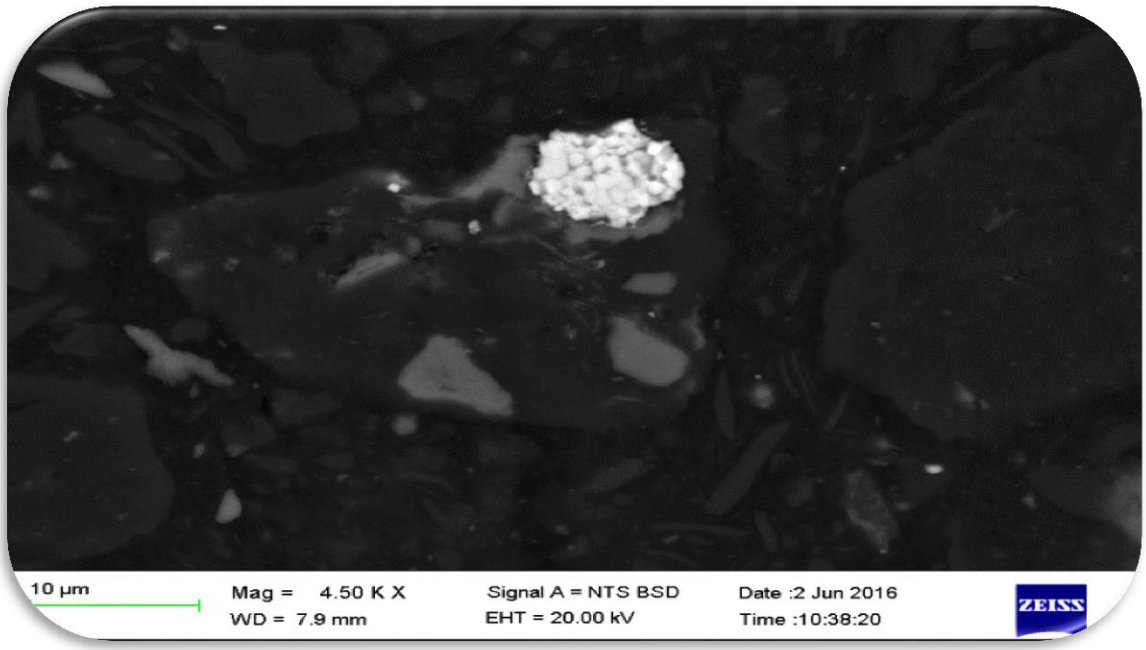

Figure C.79 20 % CH_4 in H_2 for 90 minutes at 1100^{o}C

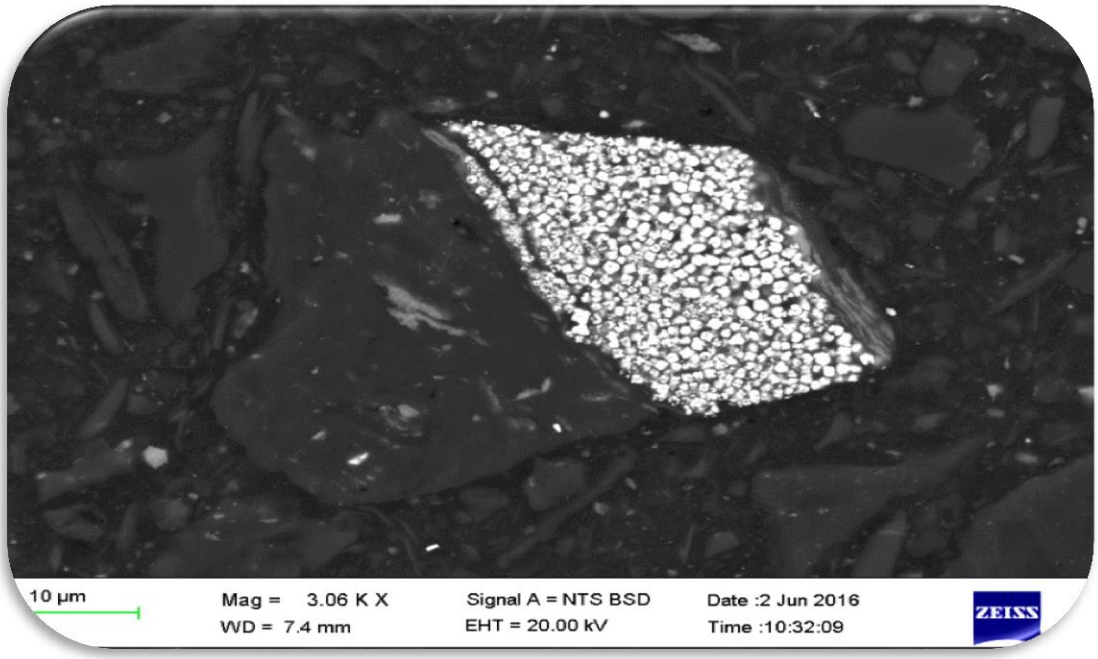

Figure C.80 20 % CH_4 in H_2 for 120 minutes at 1100^{o}C

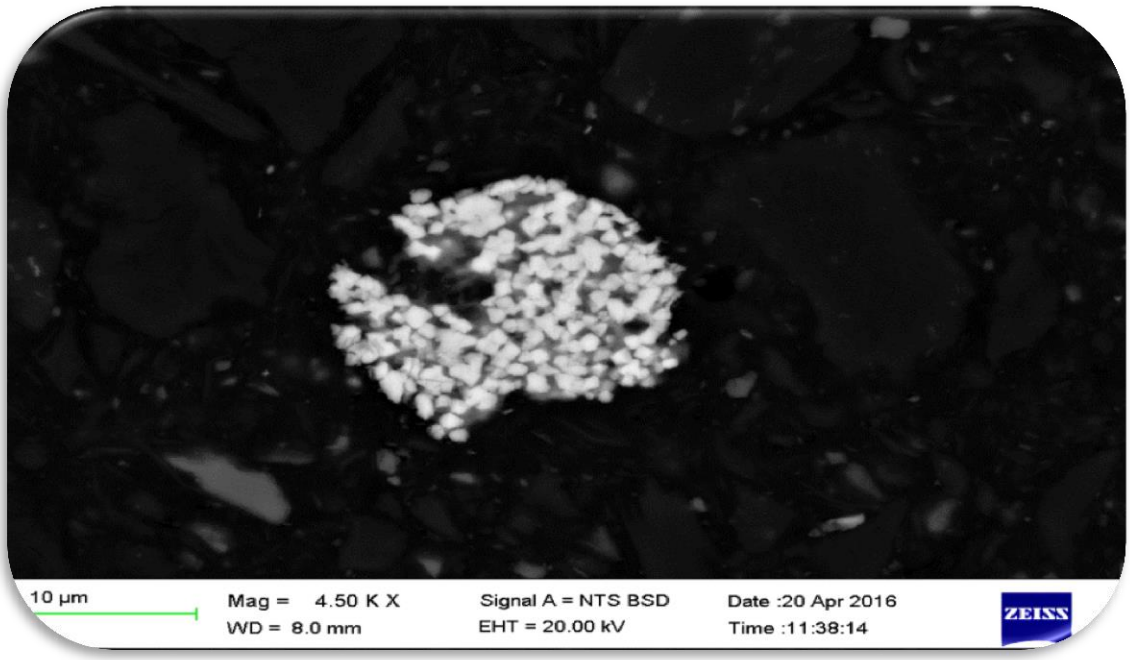

Figure C.81 20 % CH_4 in H_2 for 20 minutes at 1200^{o}C

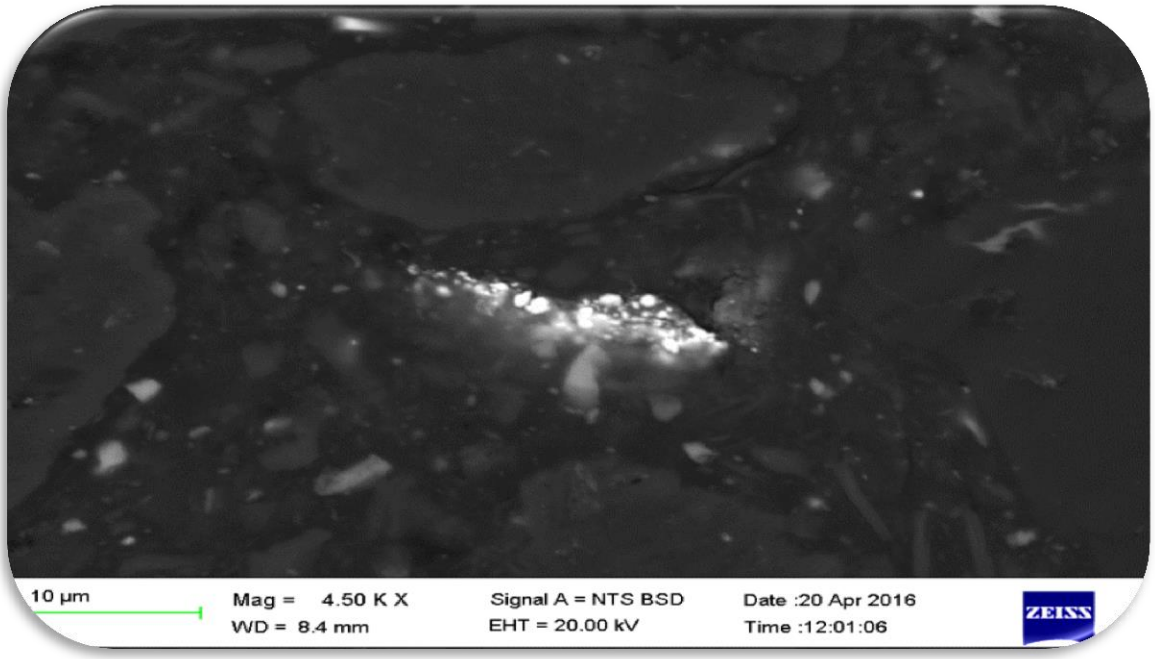

Figure C.82 20 % CH_4 in H_2 for 30 minutes at 1200^{o}C

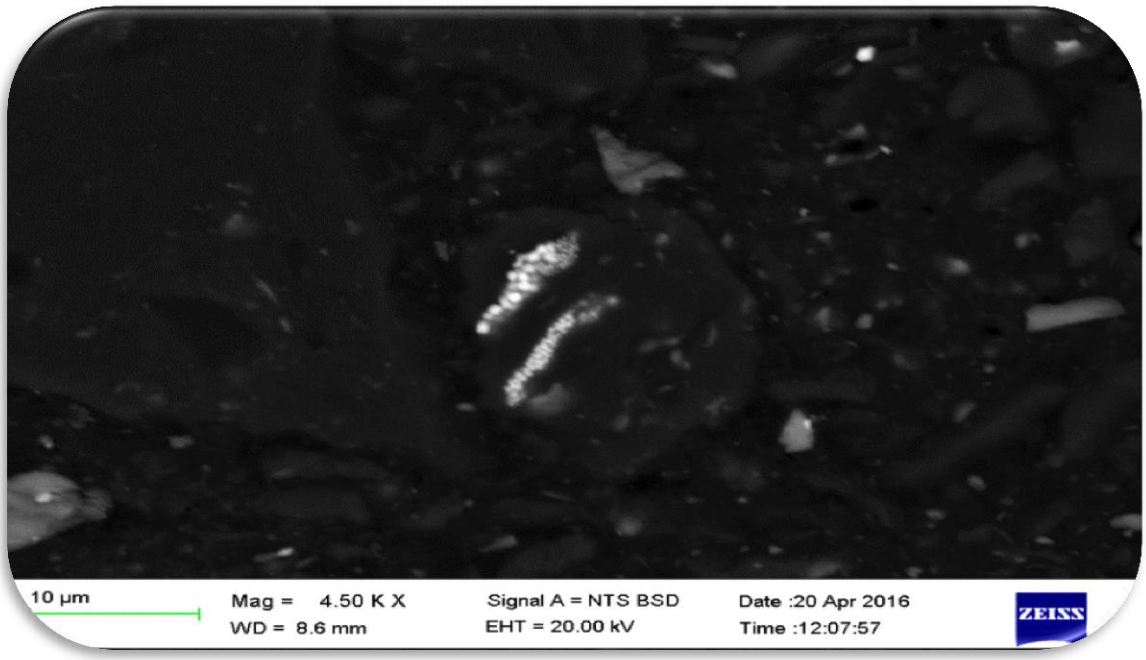

Figure C.83 20 % CH_4 in H_2 for 60 minutes at 1200^{o}C

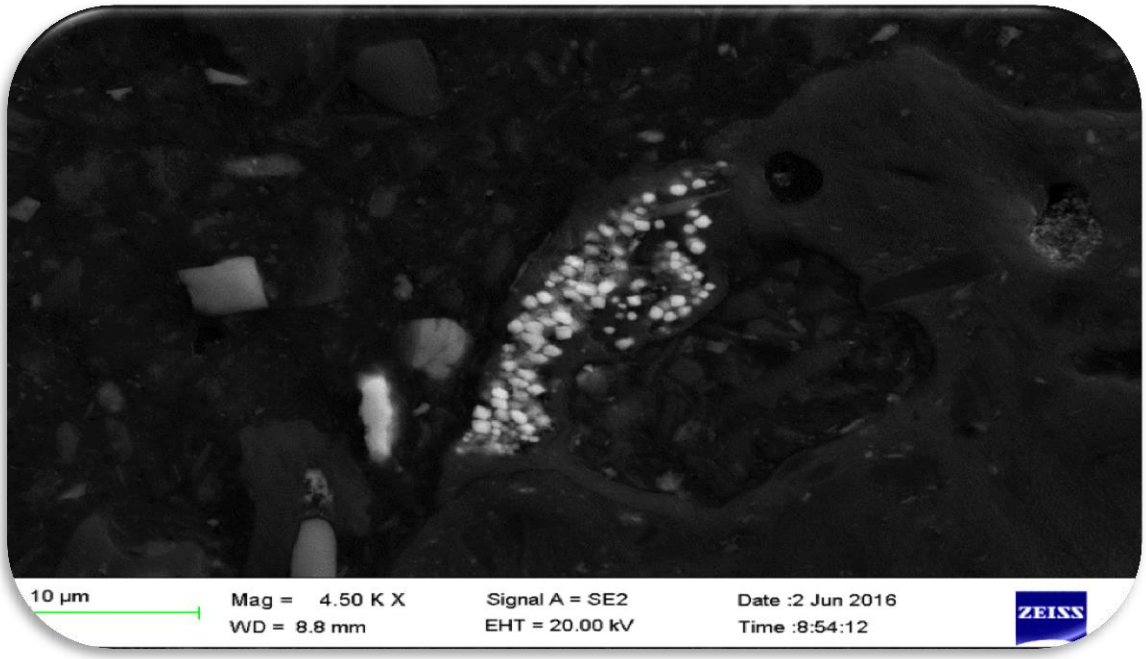

Figure C.84 20 % CH_4 in H_2 for 90 minutes at 1200^{o}C

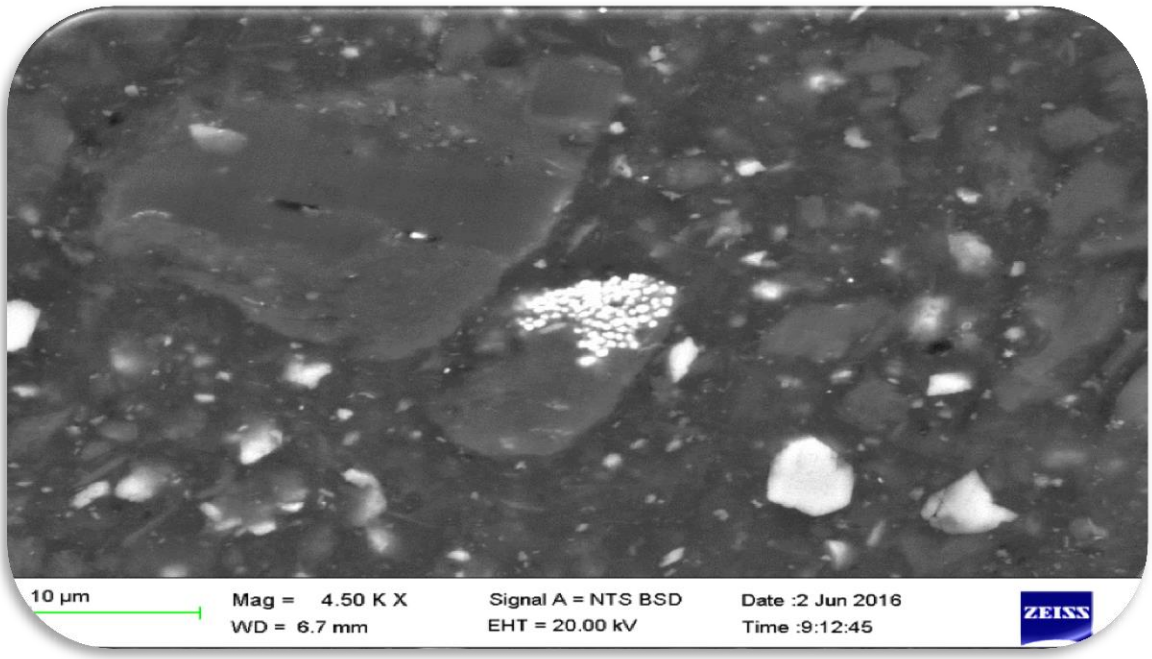

Figure C.85 20 % CH_4 in H_2 for 120 minutes at 1200°C

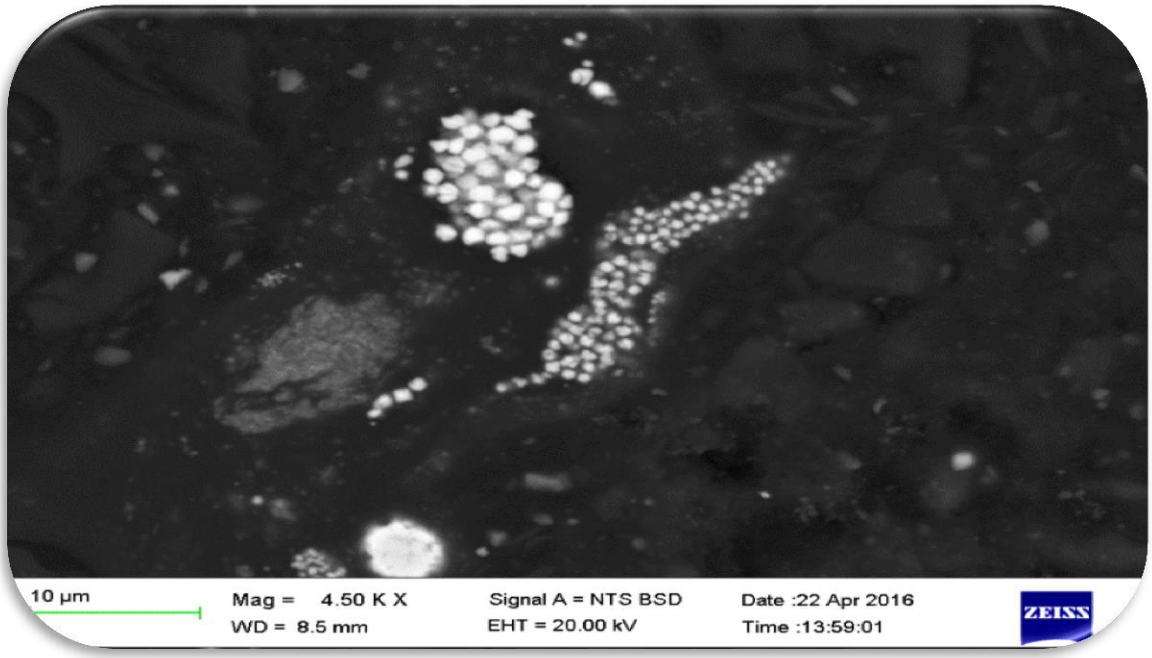

Figure C.86 20 % CH_4 in H_2 for 20 minutes at 1250°C

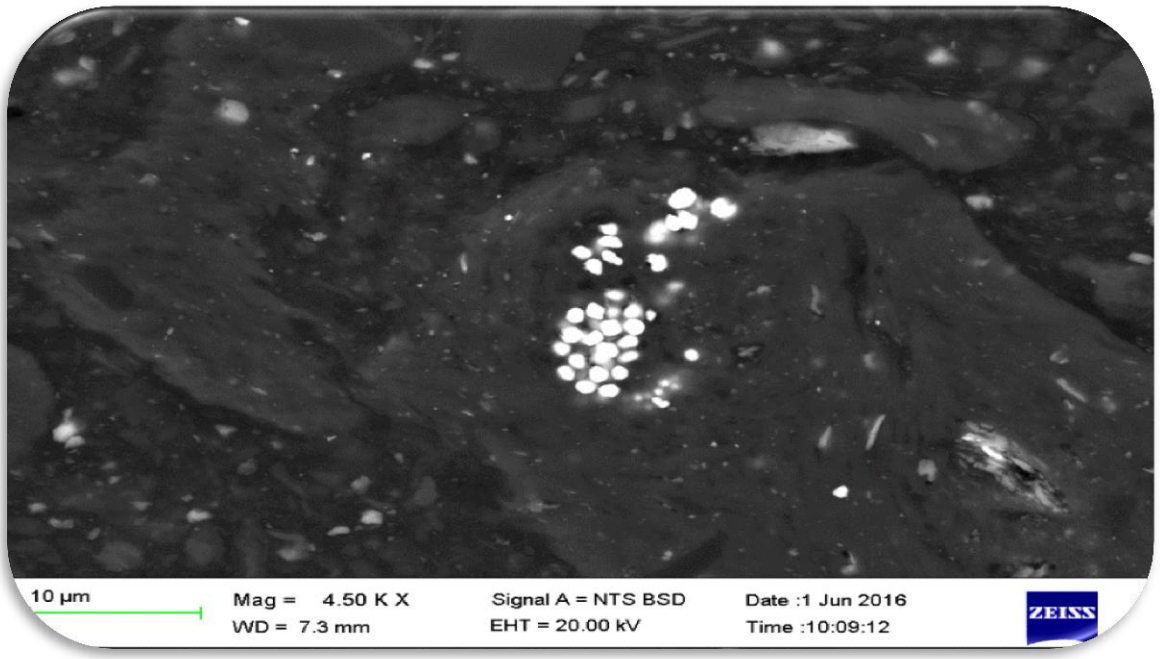

Figure C.87 20 % CH_4 in H_2 for 30 minutes at 1250^{o}C

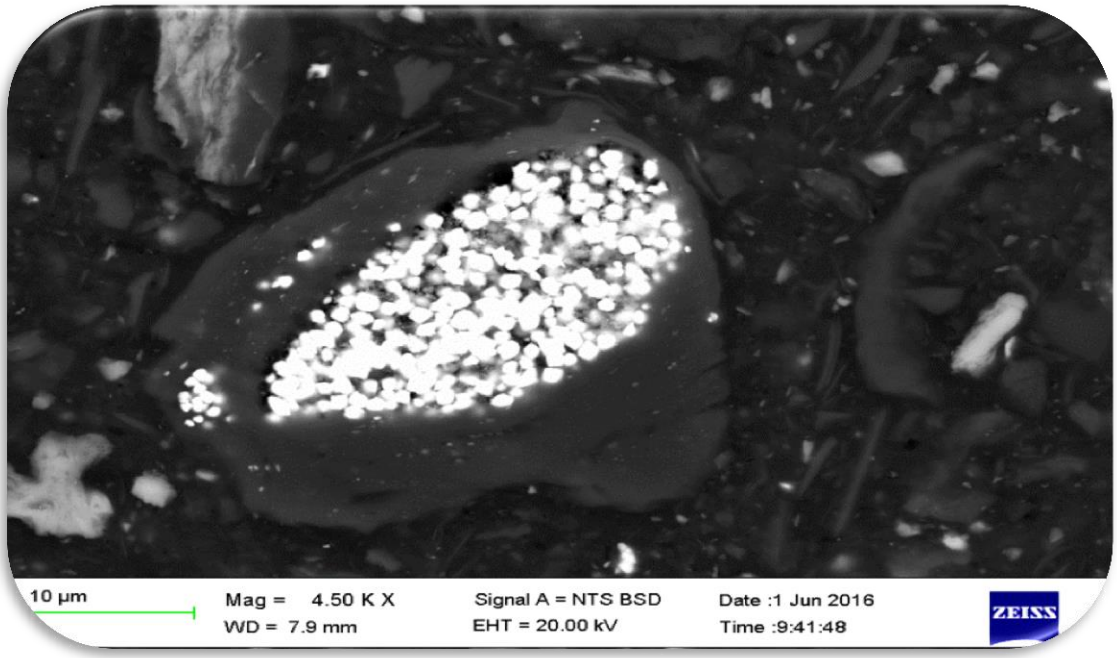

Figure C.88 20 % CH_4 in H_2 for 60 minutes at 1250^{o}C

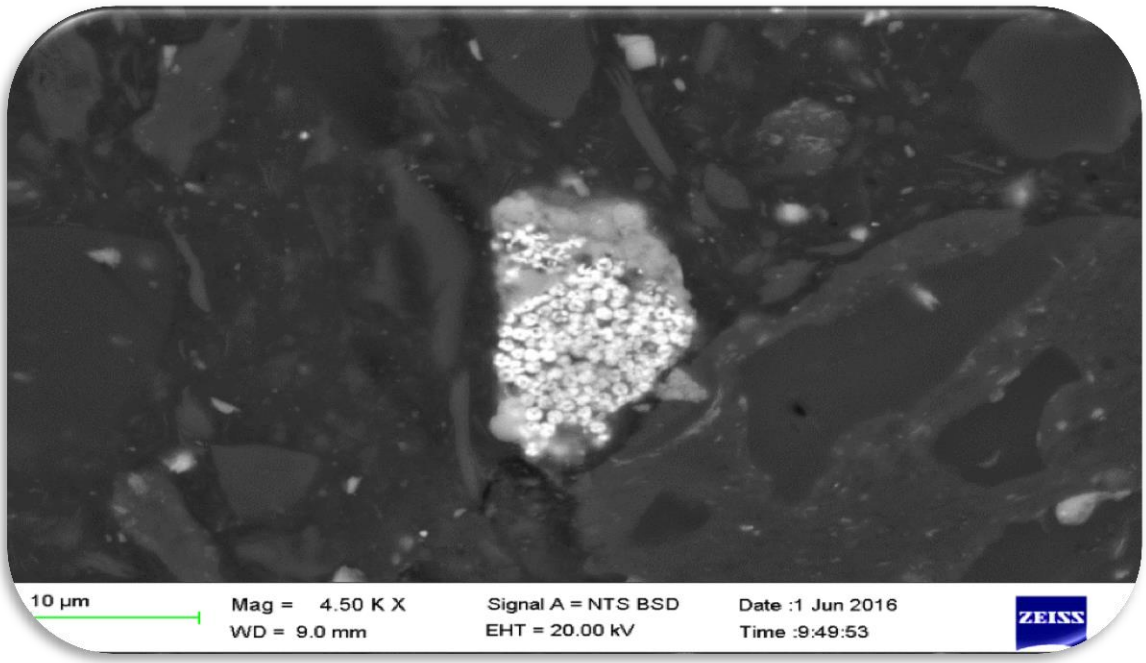

Figure C.89 20 % CH_4 in H_2 for 90 minutes at 1250^{o}C

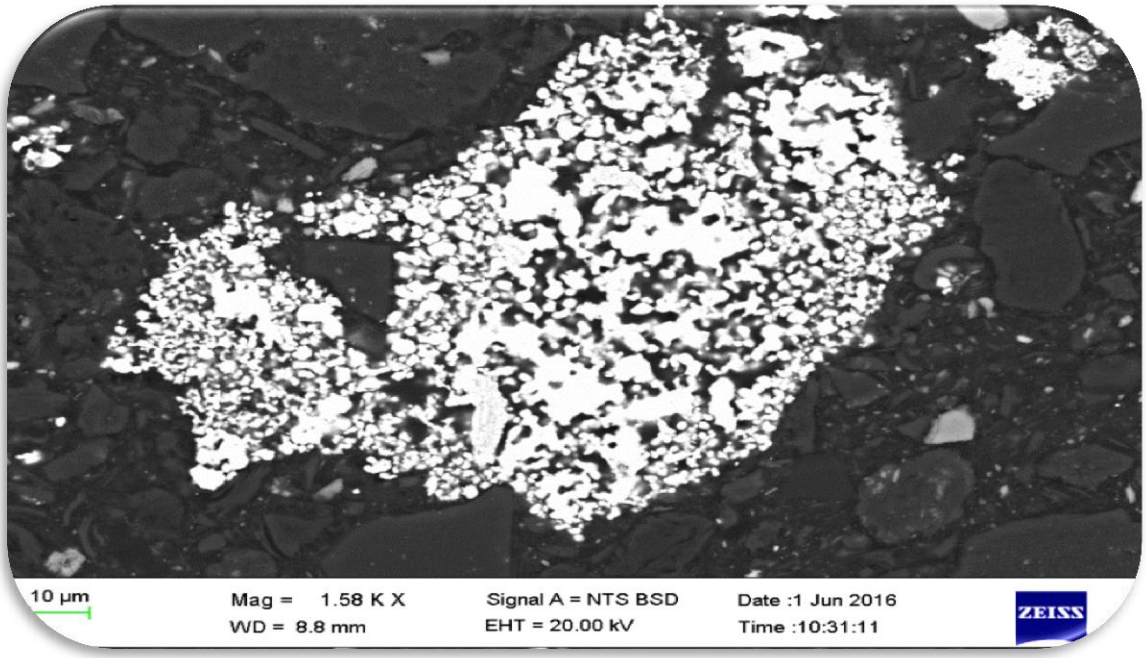

Figure C.90 20 % CH_4 in H_2 for 120 minutes at 1250^{o}C

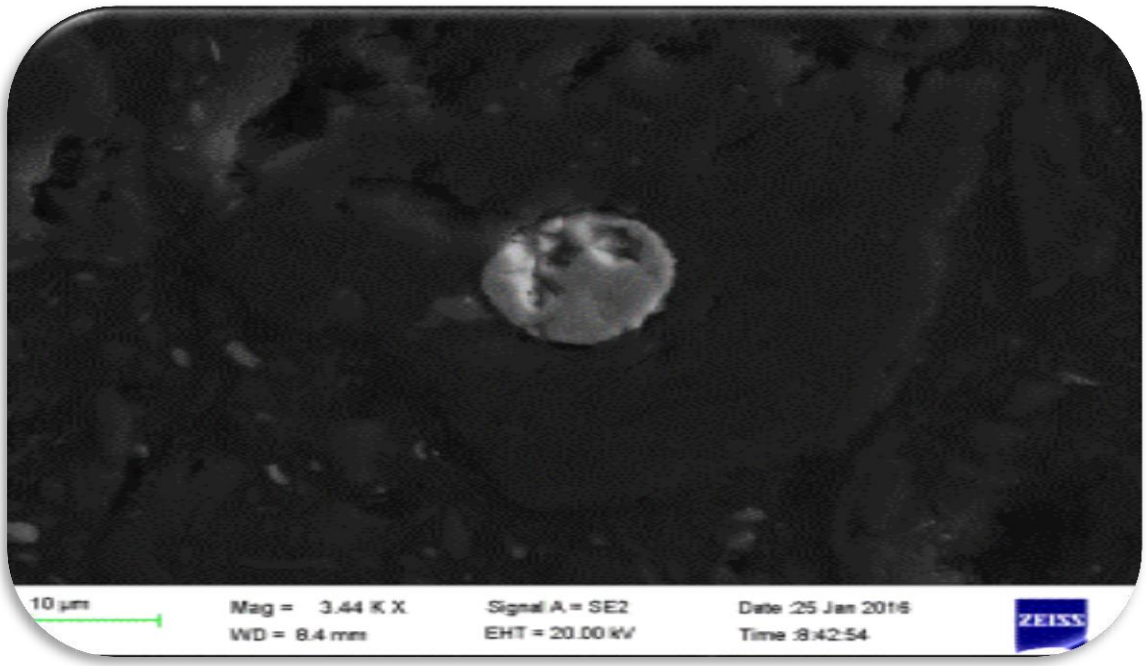

Figure C.91 30 % CH_4 in H_2 for 20 minutes at 1050°C

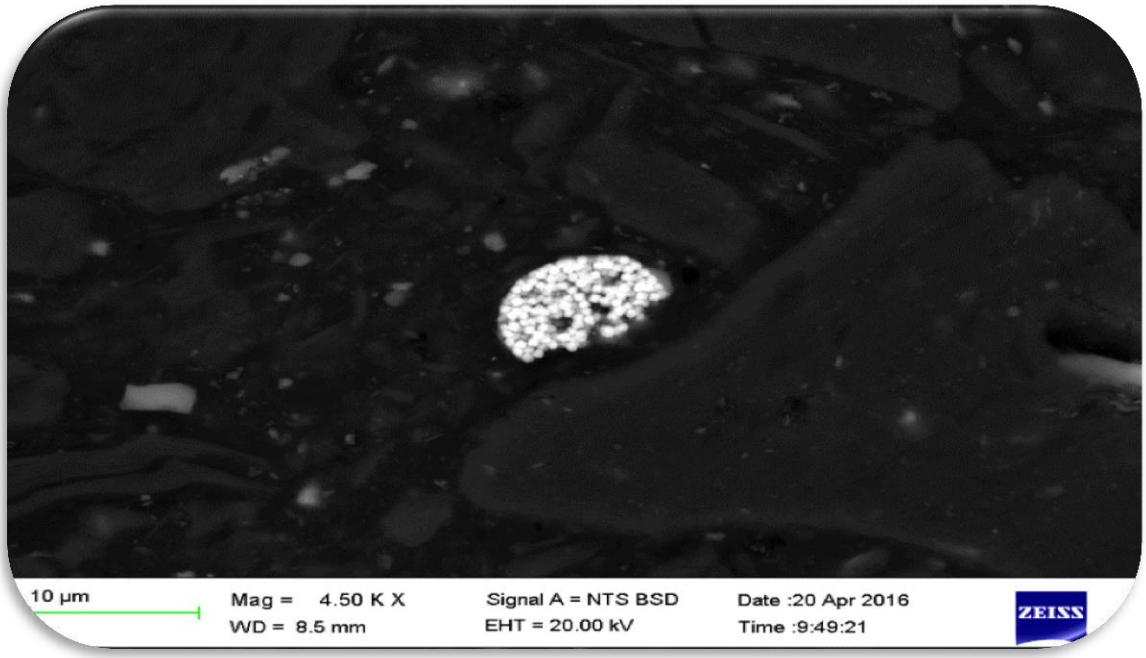

Figure C.92 30 % CH_4 in H_2 for 30 minutes at 1050°C

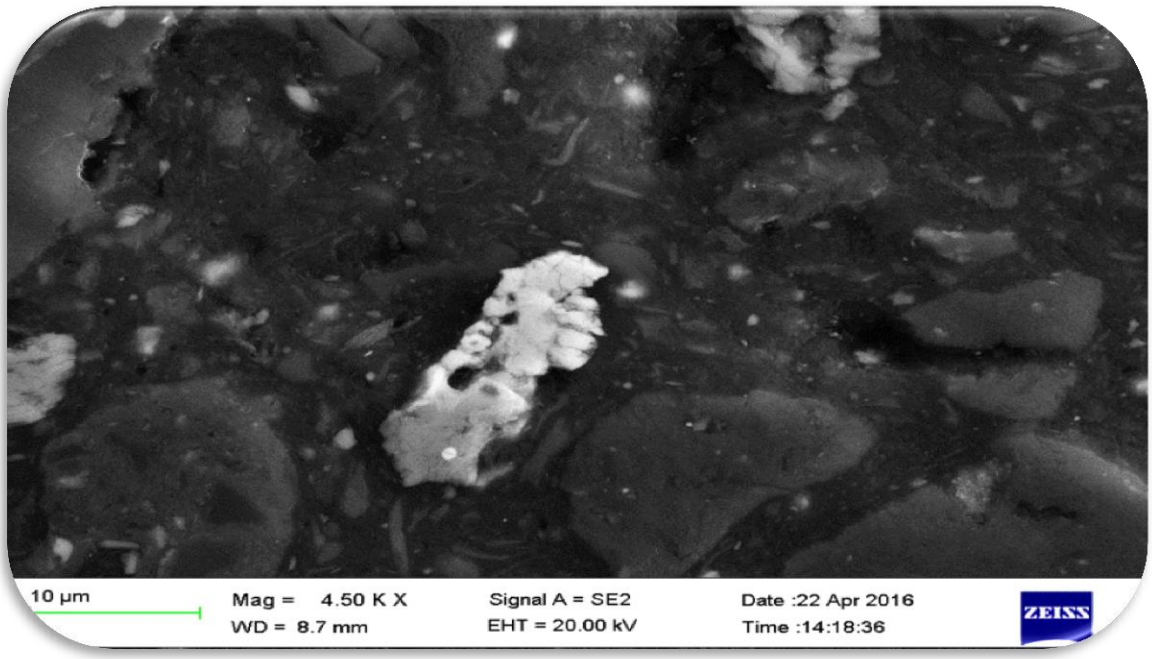

Figure C.93 30 % CH_4 in H_2 for 60 minutes at 1050°C

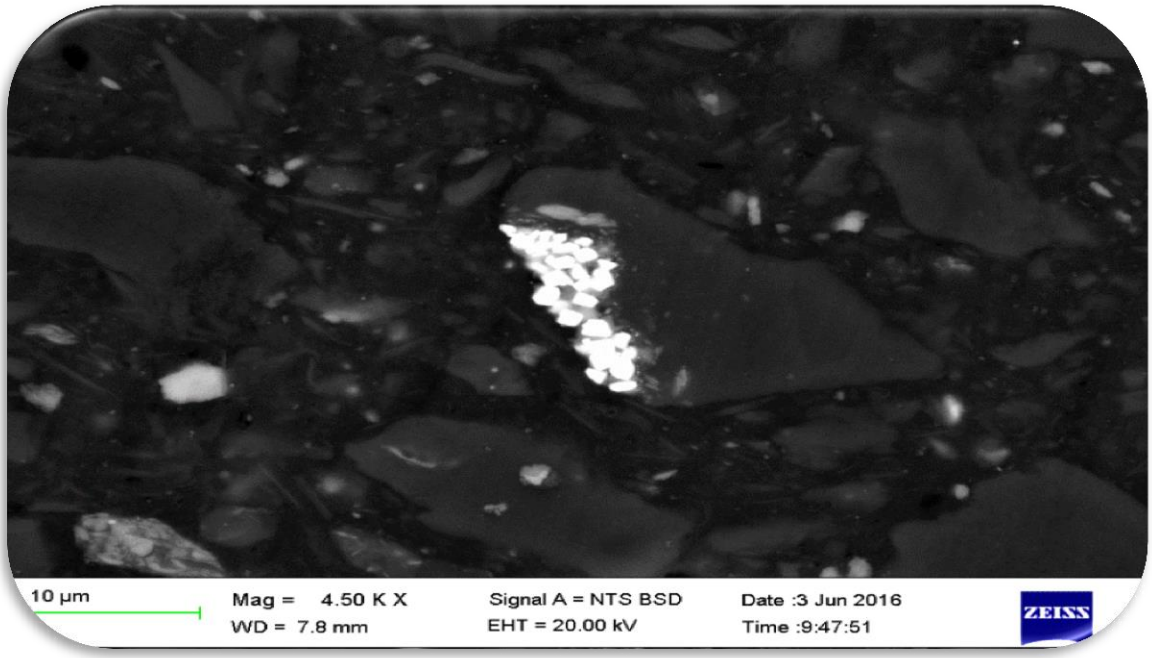

Figure C.94 30 % CH_4 in H_2 for 90 minutes at 1050°C

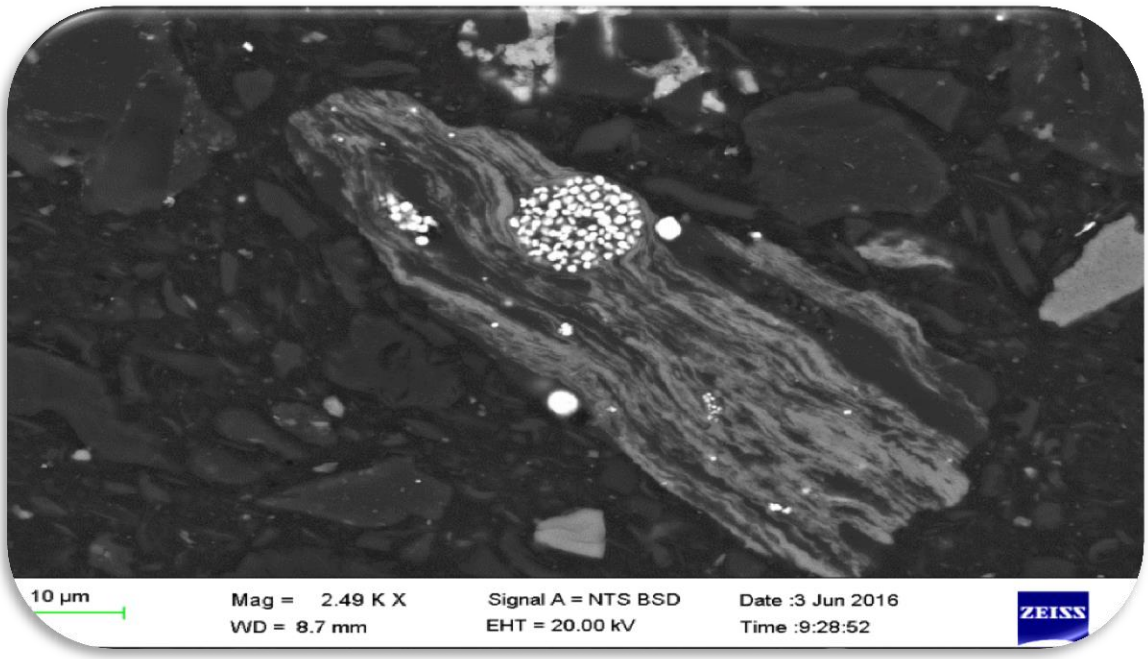

Figure C.95 30 % CH_4 in H_2 for 120 minutes at 1050^{o}C

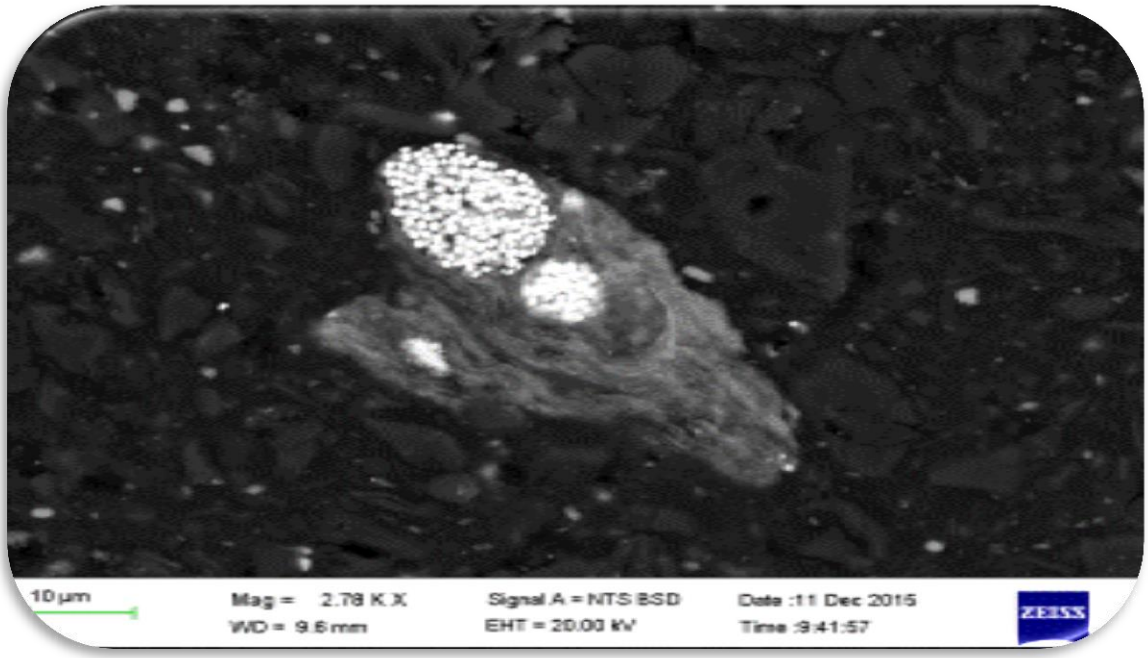

Figure C.96 30 % CH_4 in H_2 for 20 minutes at 1100^{o}C

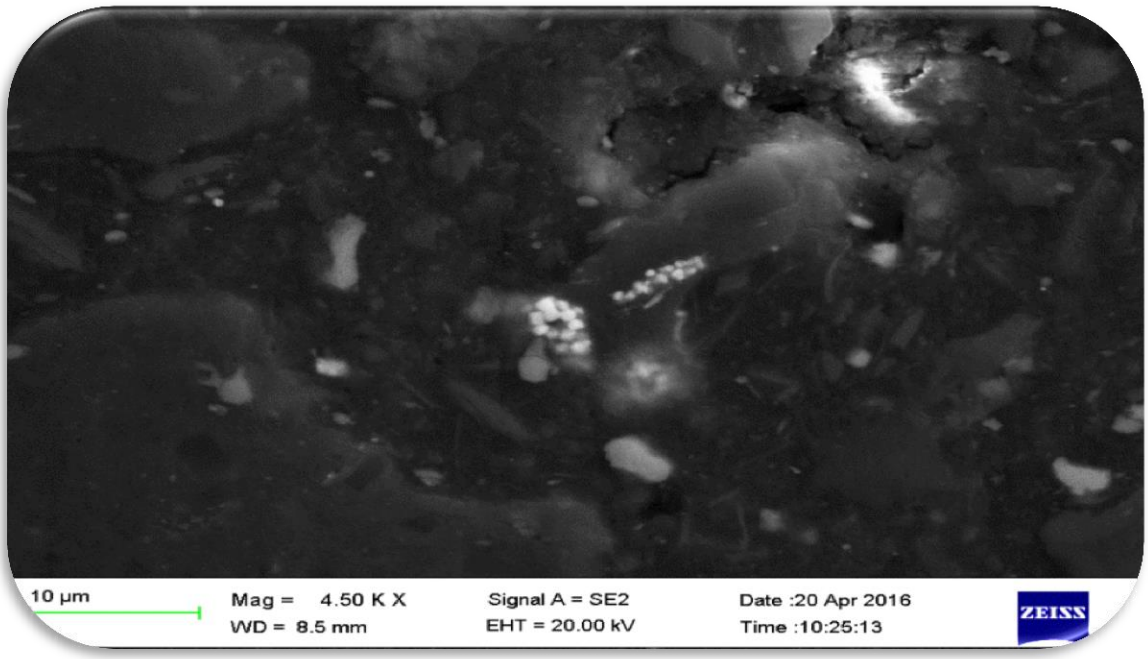

Figure C.97 30 % CH_4 in H_2 for 30 minutes at 1100^{o}C

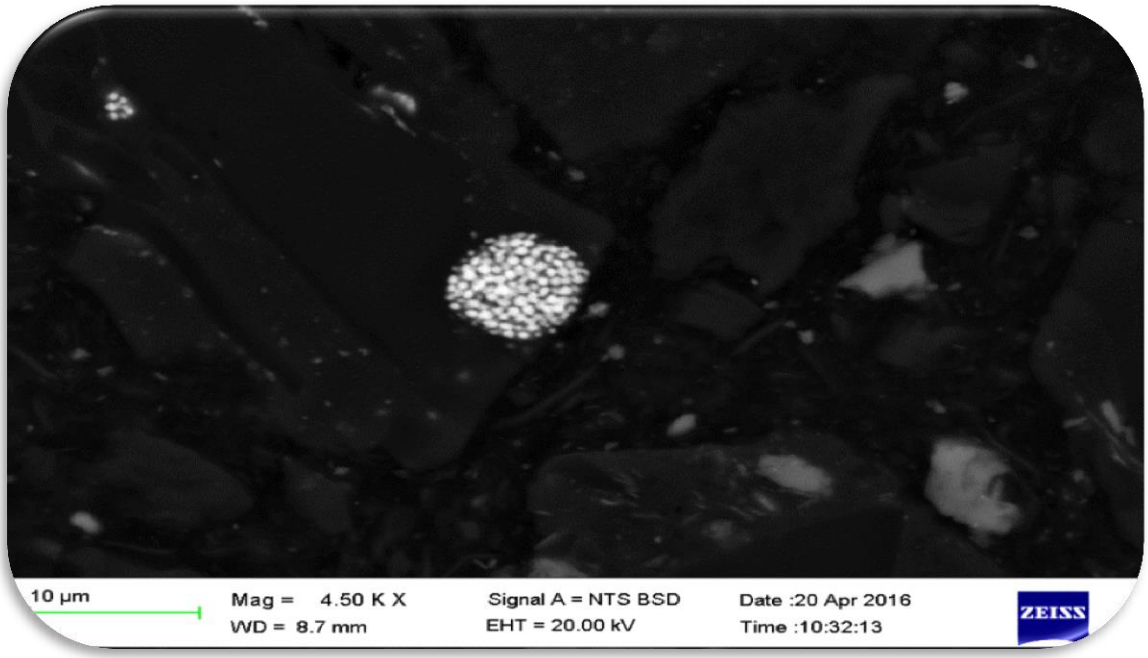

Figure C.98 30 % CH_4 in H_2 for 60 minutes at 1100^{o}C

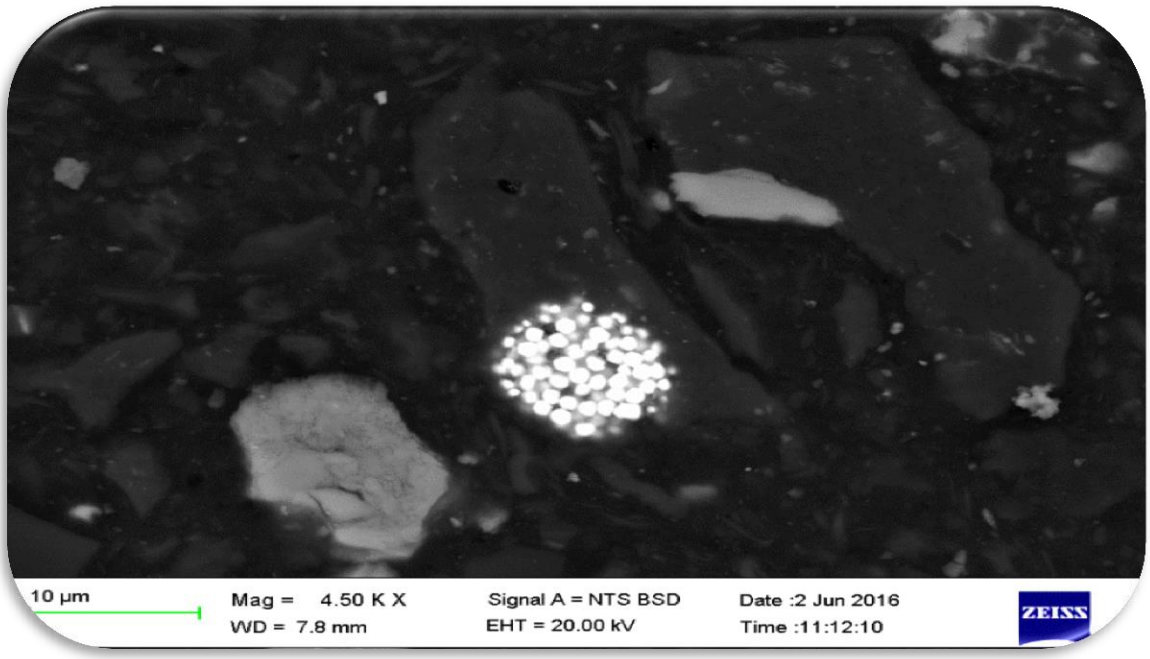

Figure C.99 30 % CH_4 in H_2 for 90 minutes at 1100°C

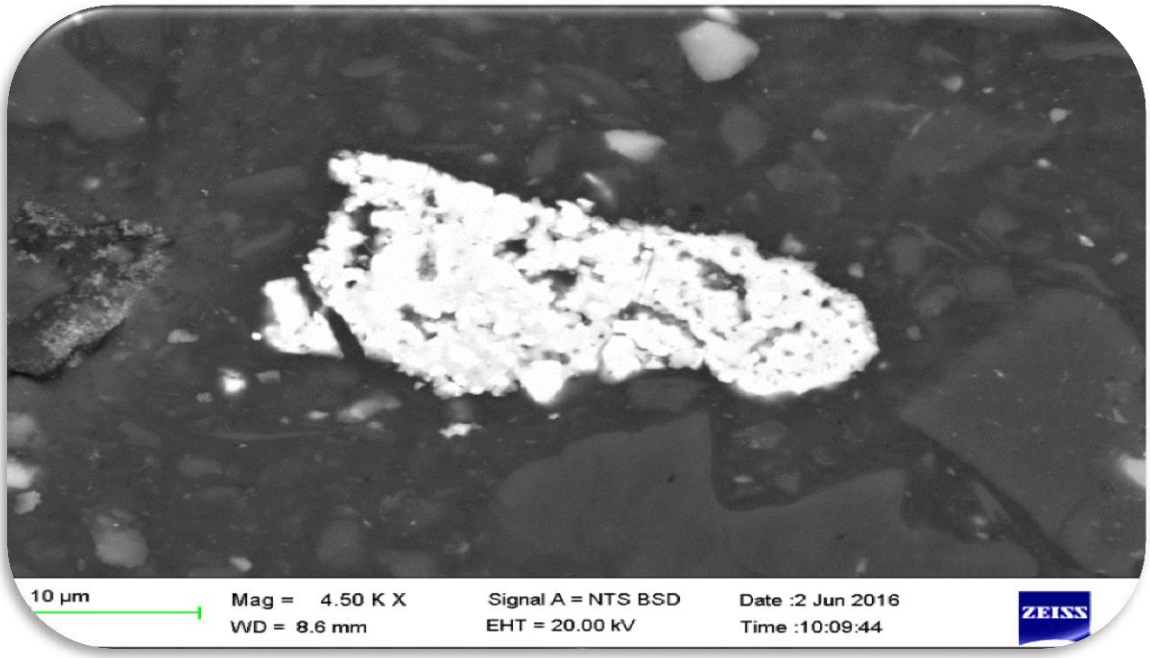

Figure C.100 30 % CH_4 in H_2 for 120 minutes at 1100°C

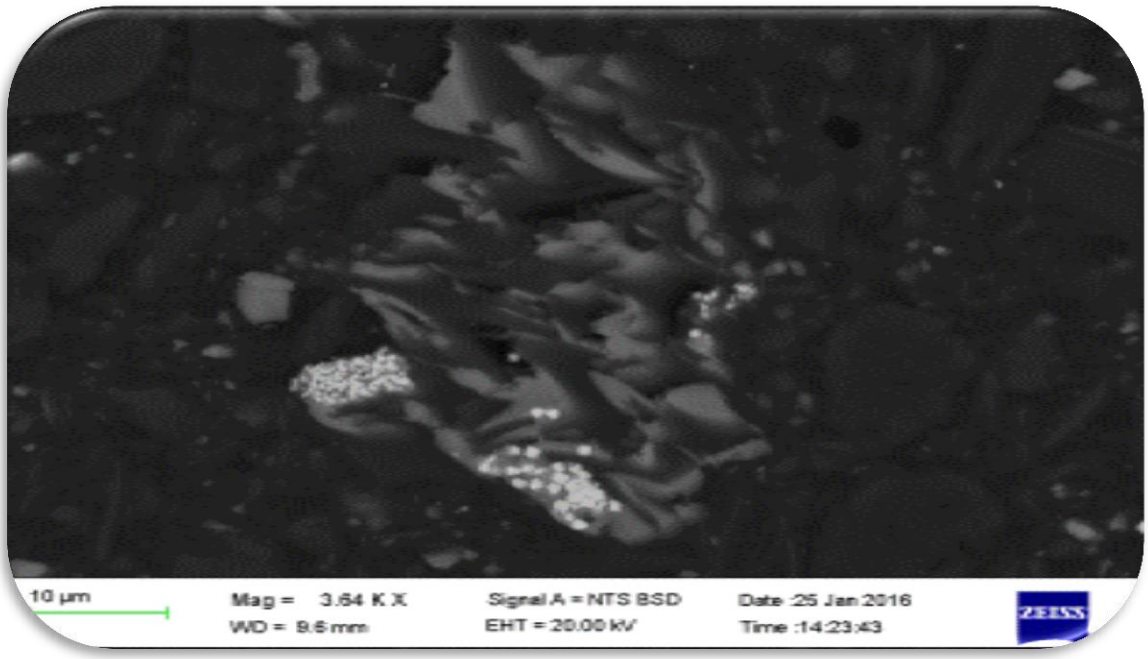

Figure C.101 30 % CH_4 in H_2 for 20 minutes at 1200°C

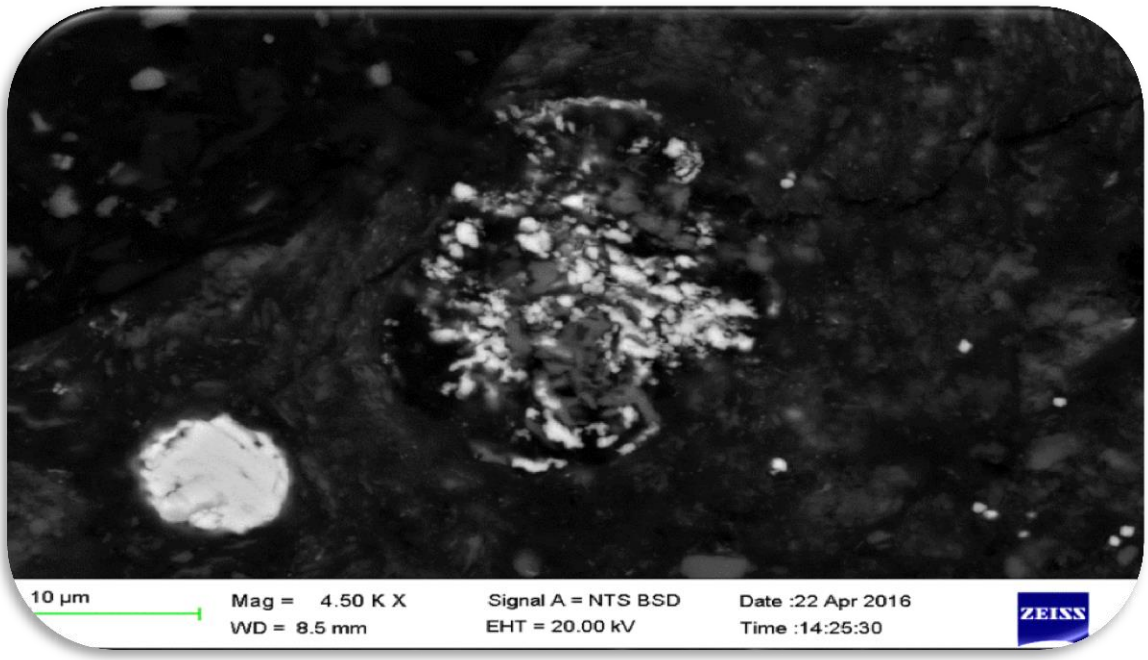

Figure C.102 30 % CH_4 in H_2 for 30 minutes at 1200°C

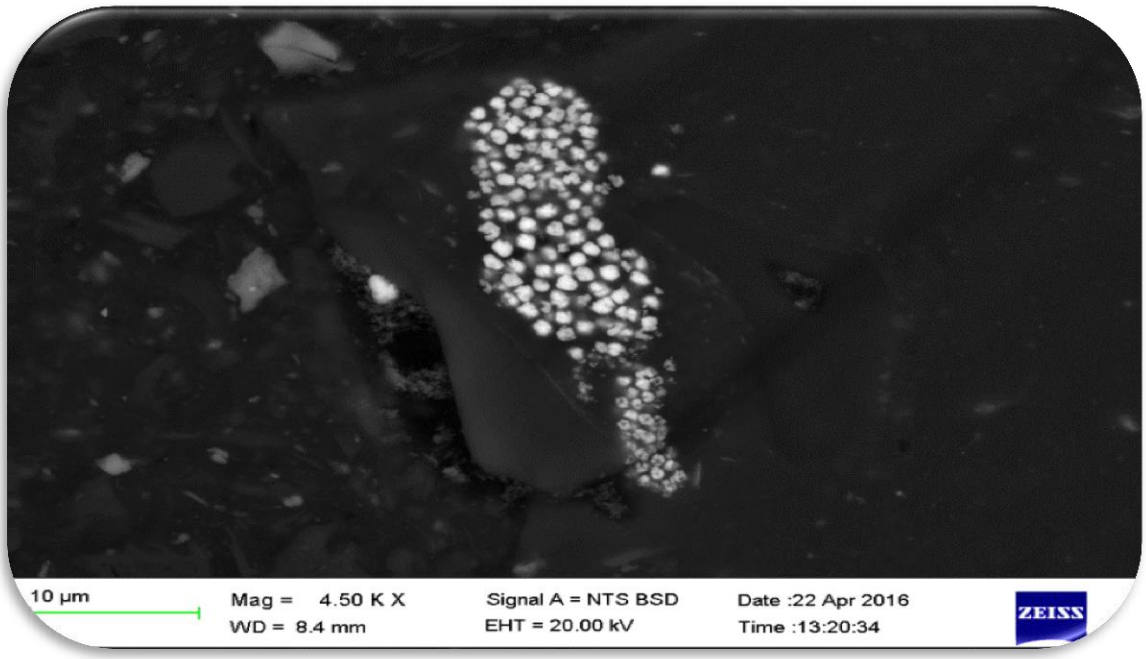

Figure C.103 30 % CH_4 in H_2 for 60 minutes at 1200°C

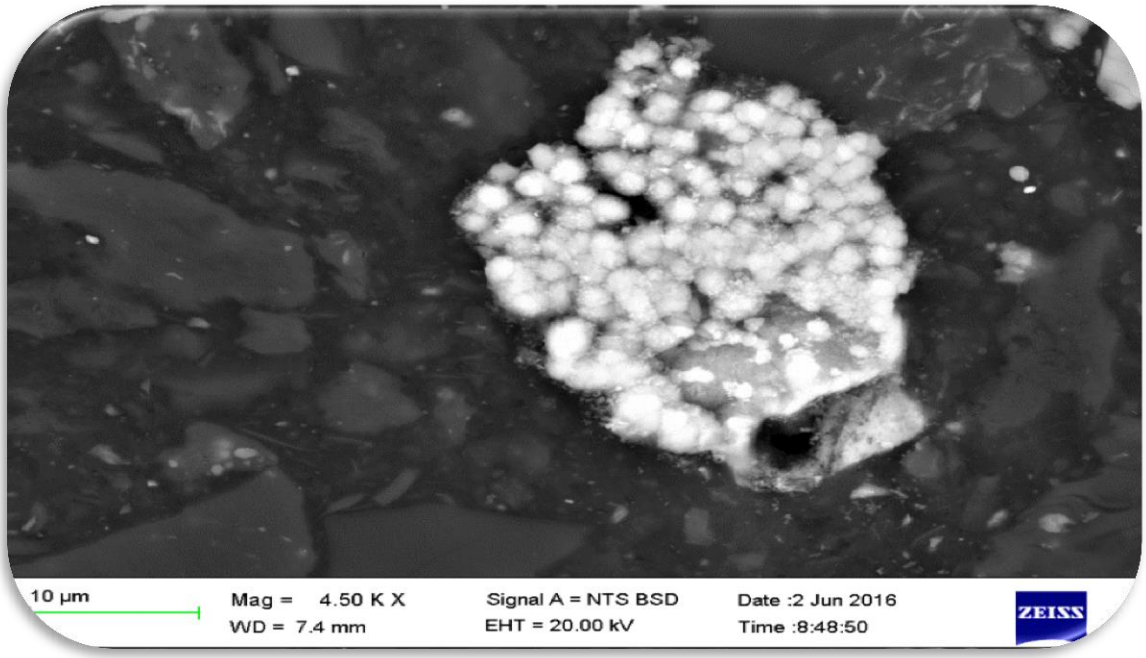

Figure C.104 30 % CH_4 in H_2 for 90 minutes at 1200°C

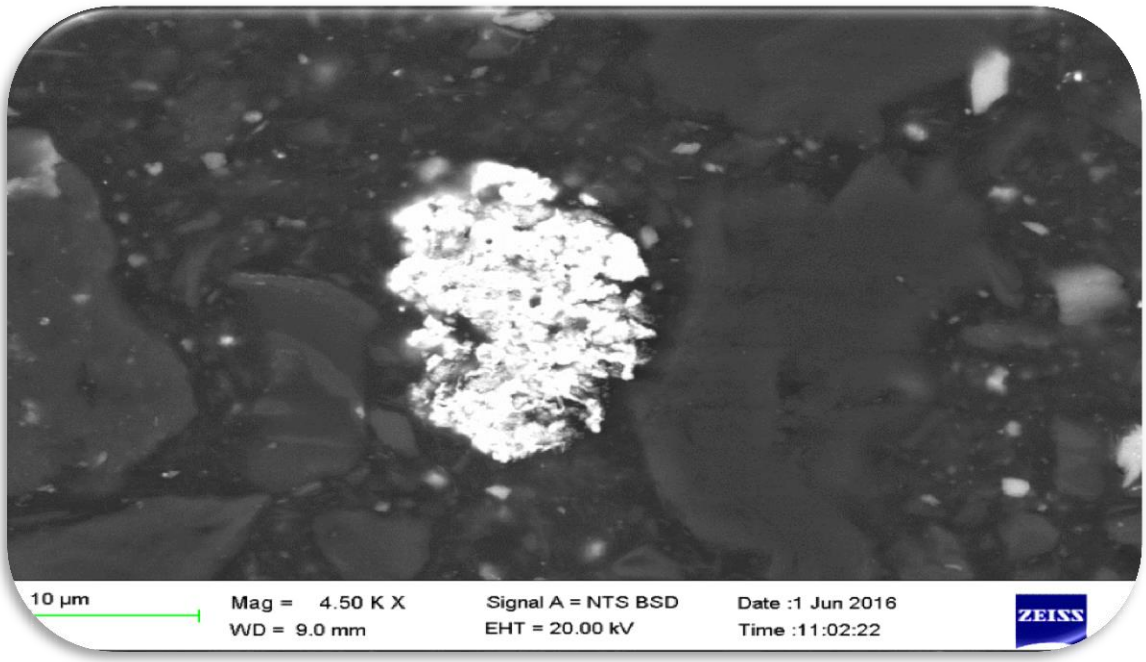

Figure C.105 30 % CH_4 in H_2 for 120 minutes at 1200^{o}C

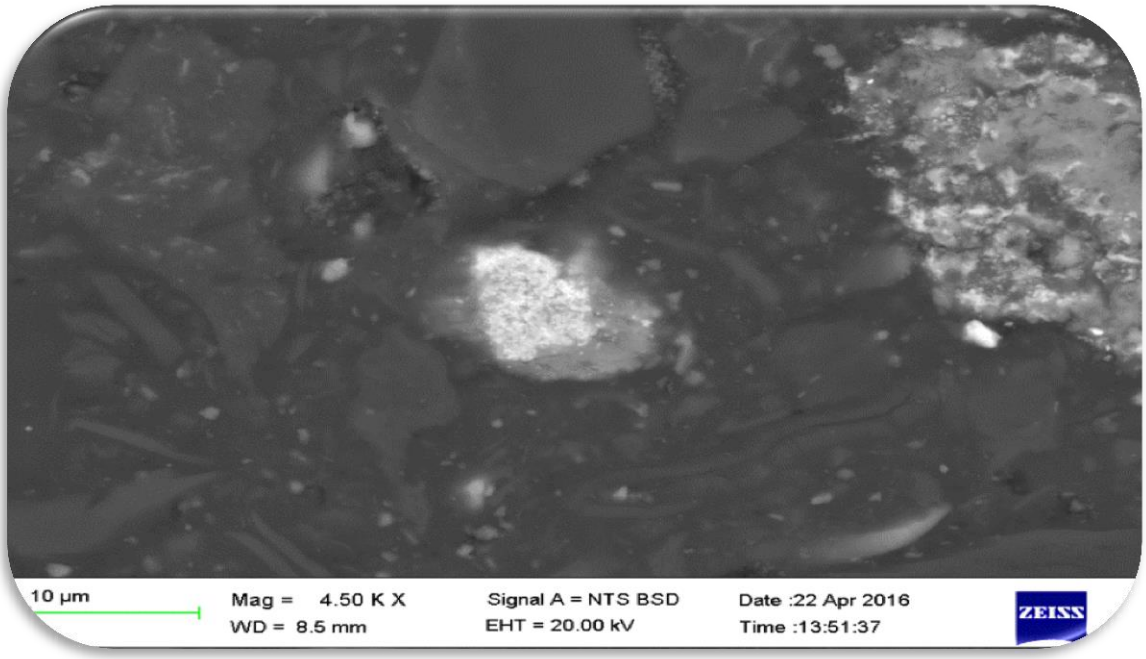

Figure C.106 30 % CH_4 in H_2 for 20 minutes at 1250^{o}C

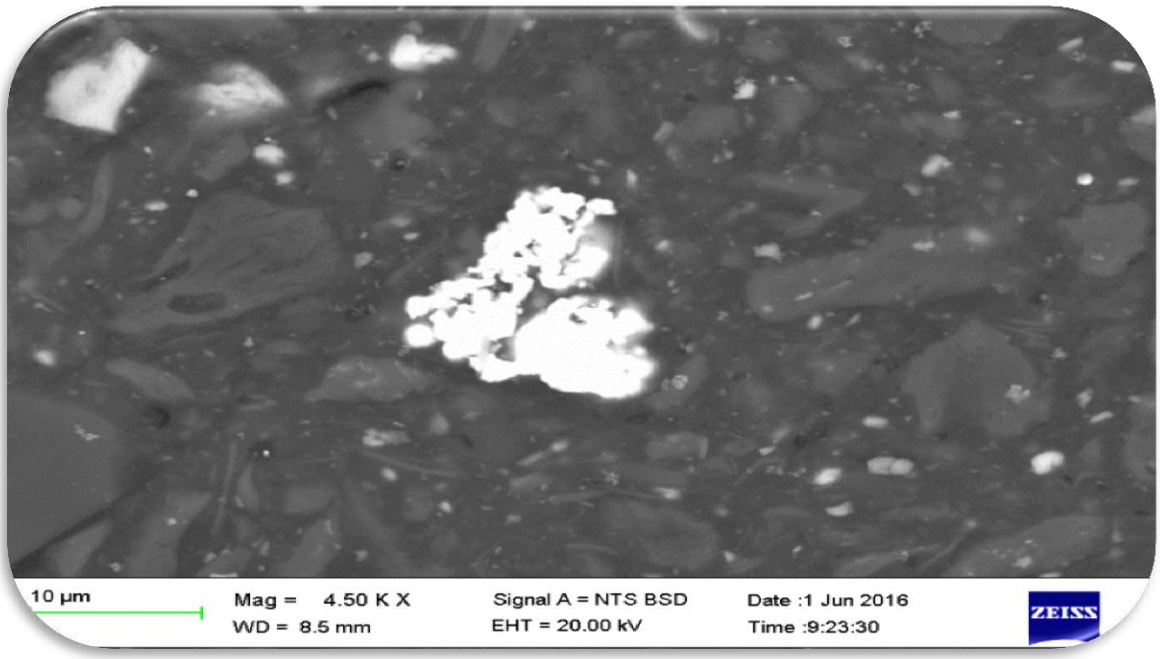

Figure C.107 30 % CH_4 in H_2 for 30 minutes at 1250^{o}C

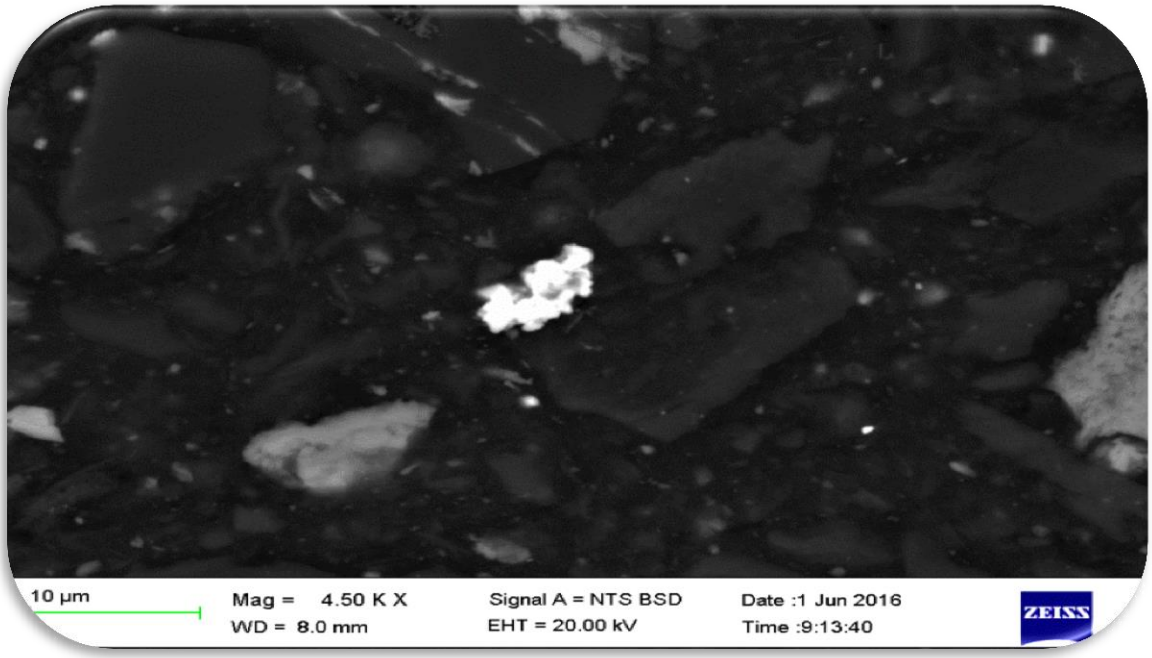

Figure C.108 30 % CH_4 in H_2 for 60 minutes at 1250^{o}C

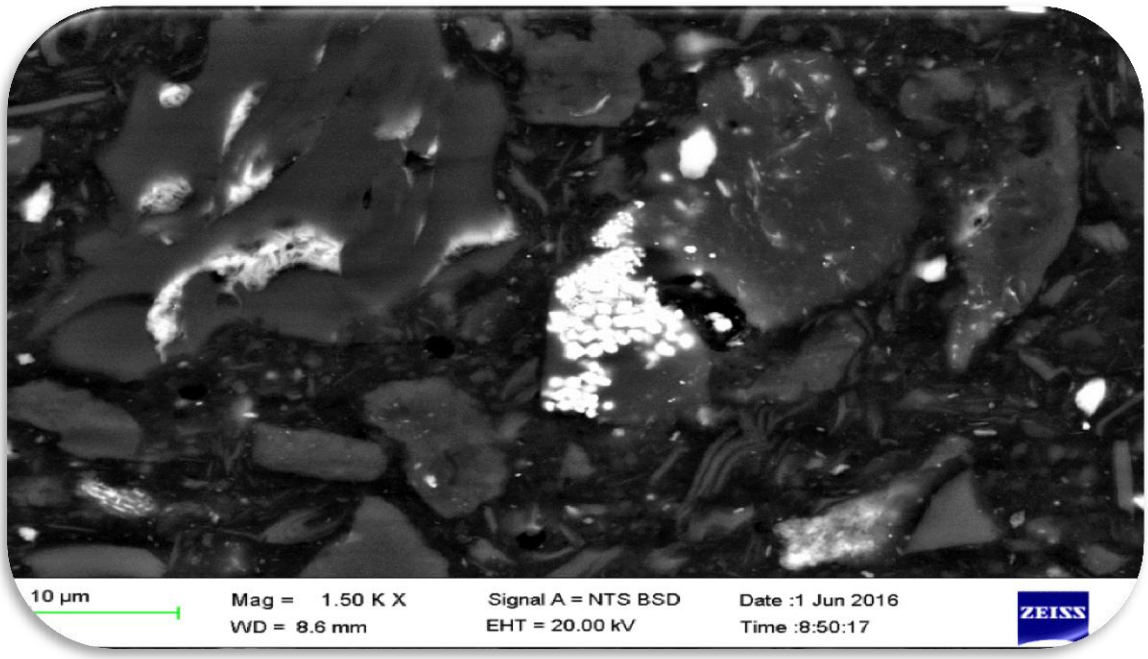

Figure C.109 30 % CH_4 in H_2 for 90 minutes at 1250^{o}C

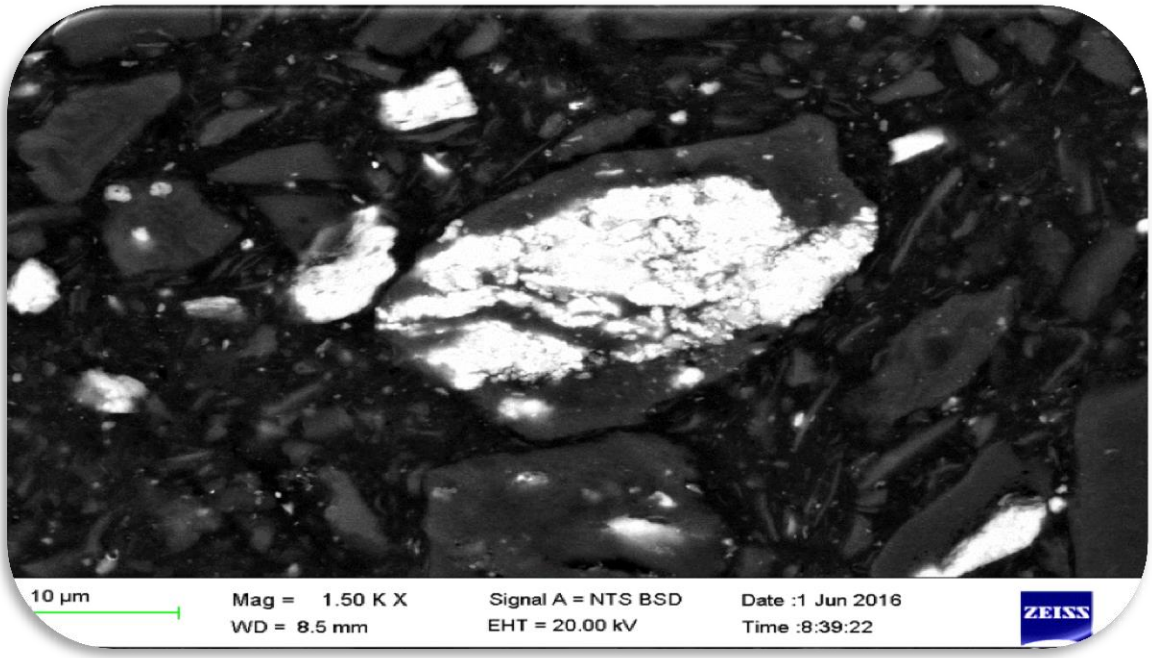

Figure C.110 30 % CH_4 in H_2 for 120 minutes at 1250^{o}C

APPENDIX D

CALCULATIONS FOR MATHEMATICAL MODELLING AND ANALYSIS

Total available oxygen from Chemical Analysis

Oxygen as Mn_2O_3 = (48/158)* (54.14) = 16.447 %

Oxygen as Fe_2O_3 = (48/160)* (6.728) = 2.01841%

Total oxygen = 18.4654%

The relative amount of Mn_2O_3 and Mn_3O_4 in manganese ores

Total manganese + iron content = 37.69 + 4.71 =42.4

In the following calculation, in order to simplify the mathematical model equations iron was treated as manganese and total manganese content was assumed to be that of manganese itself plus iron. This can also be justified since both metals have similar characteristics and similar atomic weights.

The molar ratio (Mn/O) can be calculated as:

(42.4/54.94) / (18.4654/16) = 0.77175/1.154087 = 1/ 1.495

In Mn_2O_3, the molar ratio is 1/1.5 and in Mn_3O_4 it is 1/1.33

So molar ratio of 1/1.5 corresponds to a high proportion of Mn_2O_3.

If (n) is the amount of Mn_2O_3, 1.5(n) + 1.33(1-n) =1.495

, n= 0.971 for Mamatwan ore.

From total amount of manganese in the ores Mn in Mn_2O_3 can be calculated as (total Mn*n)

= 42.4 *0.971.

= 41.1704%

And Mn in Mn_3O_4 = (42.4 -41.1704) = 1.2296 %.

Therefore, % Mn_2O_3 can be found as

(158/110) * 41.1704 = 59.1356 %

And % Mn_3O_4 as

(229/165) * 1.2296 =1.70563%

The concentration of Mn_2O_3 and Mn_3O_4 in the ores can be found as follows

$C_{Mn_2O_3} = density * (\% Mn_2O_3)/158.$

$C_{Mn_3O_4} = density * (\% Mn_3O_4)/229$

Density of Mawatwan ore from literature =4.5 gcm^{-3}

$C_{Mn_2O_3}$ = 4.5 *59.1356/158= 16842.417 moles m^{-3} ore

$C_{Mn_3O_4}$ = 4.5 *1.70653/229 = 335.3443 moles m^{-3} ore

Calculation of total concentration of oxygen available (C_{oxy})

Mn_2O_3 is assumed to be instantaneously reduced to Mn_3O_4 according to the reaction:

3 Mn_2O_3 + C = 2 Mn_3O_4 + CO

Thus the total concentration of Mn_3O_4 at the beginning of the first stage is:

$C_{Mn_3O_{4(f)}} = C_{Mn_3O_4} + \left(\frac{2}{3}\right) C_{Mn_2O_3}$

$C_{Mn_3O_{4(f)}}$ = 335.3443 + (2/3)* 16842.417

=11563.6223.

And the total amount of oxygen available can be calculated considering following reactions:

3 Mn_2O_3 + C = 2 Mn_3O_4 + CO

Mn_3O_4 + C = 3 MnO + CO.

$C_{oxy} = \frac{1}{6} * C_{Mn_2O_3} + 2 * C_{Mn_3O_{4(f)}}$

= 1/6 *(16842.417) + 2 *(11563.6223)

=2807.0695 + 23127.2446

= 25934.3141. moles m^{-3}ore

Estimation of molecular CO-CO_2 diffusivity.

$D_{12} = \frac{0.00185 T^{3/2}}{P \delta^2_{12} \Omega_D} [(M_1 + M_2)/(M_1 . M_2)]^{1/2}$ (D.1)

D_{12} = Molecular diffusion coefficient for gas (1) diffusing in gas (2)

T = Absolute temperature (K)

M_1, M_2 = Molecular masses of the two gases.

$P =$ Total pressure in atmospheres

Ω_D = Collision integral

$\delta_{12} =$ Force constant.

Above equation was evaluated for CO diffusing in CO/CO_2 mixtures using data listed.

In Satterfield and Sherwood [101] as follows:

M_1 = 28g CO $mole^{-1}$
M_2 =44g $CO_2 mole^{-1}$
P= 1 atm.
From data in Scatterfield and Sherwood [101]
For CO, $\delta_1 = 3.590$ A
For CO_2 δ_2 = 3.996 A
$\Omega_D = f(\frac{kT}{\epsilon})$
Where $\epsilon =$ Force constant in lennard –Jones potential function.
k = Boltzmann constant.
For CO, $\frac{\epsilon_1}{k} = 110\ K$
For CO_2 $\frac{\epsilon_2}{k} = 190\ K$
For diffusion in binary systems,
$\delta_{12} = (\delta_1 + \delta_2)\ (\frac{1}{2})$ (D.2)
Hence, δ_{12} = 3.59 +3.99 /2 = 3.79 A.

The molecular diffusivity of H_2 in H_2/H_2O mixtures, determined by Nabi and Lu[84] was extrapolated to higher temperatures and converted to the CO diffusivity in CO/CO_2 mixtures using equation (D.1), which in rewritten in the form below:

$$D_{12} = \frac{ZT^{1/2}}{\delta^2{}_{12}}(\frac{\epsilon}{kT})[\ (M_1 + M_2)/\ (M_1.M_2)]^{1/2} \quad \text{(D.3)}$$

Where, $Z = 0.00185kT/P\ \Omega_D\epsilon$ (D.4)

For H_2 diffusing in H_2/H_2O mixtures at 1284 K, equation (D.3) becomes:

D_{H_2/H_2O} = Z $(1284)^{1/2}$ * 33.3 / $(2.97)^2$ $[20/36]^{1/2}$ =100.83 (Z) (D.5)

For CO diffusivity in CO/CO_2 mixtures:

D_{CO/co_2}= $T^{1/2}$ (Z) 110/$(3.79)^2$ [28+40/28*40] = 1.88 $ZT^{1/2}$. (D.6)

The porosity of magnetite sample used by Nabi and Lu [84] was 0.19.

P_f = Total area of micropores/ (Total area of solid) + (Total area of micropores) (D.7)

From the above equation porosity was calculated as 0.204

As diffusivity is directly proportional to porosity.

$D_{H_{2/H_2O}}/D_{CO/co_2}$ = 0.19 (100.83)/P_f (1.88) $T^{½}$ (D.8)

With $D_{H_{2/H_2O}}$ =0.087 cm^2sec^{-1}

D_{CO/co_2} = (1.88) $T^{1/2}$ P_f *0.087/0.19*100.83 (D.9)
= 0.0017501998 $T^{1/2}$

Table D1: Molecular diffusivity of CO in CO/CO_2

Temperature (K)	D_{12} (cm^2 sec^{-1})
1323	0.06366
1373	0.06485
1473	0.067172
1523	0.068302

On the other hand, for an ordinary diffusion in a porous solid an effective diffusion coefficient, D_{12ef}, can be estimated by assuming an ideal model consisting of straight pores which intersect the face of a porous slab at some average angle.
In the model used by Wheeler[128], the pores are visualized as randomly oriented cylinders of fixed diameter which intersect any plane at an average of 45 ^{o} for which
$D_{12ef} = D_{12} P_f / \tau$ (D.10)
Where, τ = tortuosity factor.
From the review of Scattefield and Sherwood[101], it appeared that common value of the tortuosity of microporous ore bodies are of the order of 2.
Based on this figure, the calculated effective $CO\text{-}CO_2$ Molecular diffusivity values are given in the following table (Table D2)

Table D2: The calculated effective CO-CO_2 Molecular Diffusivity

Temperature (K)	D_{12ef} (cm^2 sec^{-1})
1323	$6.52515 * 10^{-3}$
1373	$6.647125* 10^{-3}$
1473	$6.88513 * 10^{-3}$
1523	$7.000955 * 10^{-3}$

Evalution of term in equation (5.39)

(a) M_f is measured slopes of straight line portion of corresponding metallization versus time curves, (% per minute).
(b) P, Total pressure ($1.013 * 10^5$ Nm^{-2})
(c) R , Universal gas constant (8.314 $Nm.K^{-1}$ $mole^{-1}$)
(d) T, Absolute temperature (K)
(e) C_{oxy}, total oxygen concentration for reduction calculated in Appendix D.
(f) A_s, surface area of one cubic meter of ore.

A_s can be calculated as follows:

Assume the ore particles are spheres and the mean particle sizes of the ore s were determined as -106+150/2= 128 μm for Mamatwan ore

The volume of a particle is

$$V_p = (4/3)\pi(\frac{D}{2})^3 \quad \text{(D.11)}$$

Where D is diameter of particle

$$V_p = \left(\frac{4}{3}\right) * 3.14 * \left(\frac{128}{2}\right)^3 * 10^{-18}$$

$=1.098* 10^{-12}$

The number of particles per m^3 of ore, N can be calculated as:

$N= 1/ (1.098 *10^{-12})$

$= 9.1074 * 10^{11}$

Surface Area of one particle = πD^2

$= 3.14 * (128)^2 *10^{-12}$

$= 5.144576 *10^{-8}$.

Therefore, total surface area per m^3 of ore can be found as

$A_s = (9.1074 * 10^{11}) * (5.144576 * 10^{-8})$

$A_s = 4.685 * 10^4 m^2$

Therefore, the only unknown in equation (58b) is $D_{ef}\ \sqrt{\tau}$

Which can be calculated easily from the rate equation of model by plugging the known values into the equation.

Thereafter , D_{ef} values generated by the model can be calculated by utilizing the time to complete the first stage of the metallization , t_f , which is the time determined from X-rd and EDAX studies as the time taken before metallization starts which is taken as about 30 minutes. The calculated effective diffusivity values are shown in Table D3 and Table D4

Table D3: Effective Diffusivity Values for Mn metallization with 10 % CH_4 in Ar and H_2

$D_{ef} * 10^6$, cm^2sec^{-1}				
	1050°C	1100°C	1200°C	1250°C
10 % CH_4 in Ar	0.06827	1.45235	8.427	7.1370
10 % CH_4 in H_2	0.00389	3.2549	5.19889	2.86115

Table D4: Effective Diffusivity Values for Mn metallization with 30 % CH_4 in Ar and H_2

$D_{ef} * 10^6$, cm^2sec^{-1}				
	1050°C	1100°C	1200°C	1250°C
30 % CH_4 in Ar	0.9669	6.375	7.516	6.4697
30 % CH_4 in H_2	4.184	4.857	3.1879	2.733.

Calculations of CO-CO_2 knudsen Diffusivity

In the present study ,the effective diffusivities of CO and CO_2 are assumed to be equal ,and the value of the effective diffusivity which satisfied the kinetic model was found to be $1.45*10^{-6}$ $cm^2sec^{-1}$and $7.1370*10^{-6}$ $cm^2sec^{-1}$for temp 1100°C to 1250°C .

The relationship between the effective diffusivity the Knudsen components and molecular component is given in Scatterfield and Sherwood[101] as

$1/D_{ef} = 1/D_{kef} + 1 / D_{12ef}$ (D.12)

Using the calculated value of D_{ef} , and the effective molecular diffusivity values the effective Knudsen diffusivity at 1100°C can be calculated by rearranging term in above equation

$1/D_{kef} = 1/D_{ef} -1 / D_{12ef}$ (D.13)

$= 1/ (1.45*10^{-6}) – 1/ (6.647 *10^{-3})$

$D_{kef} = 1.45 * 10^{-6}$ cm^2 sec^{-1}

From this value, it can be deduced that the present study, Knudsen diffusion is the predominant mode of diffusion, because calculated D_{12ef} values are much larger than D_{kef} values generated by the rate equation of the model.

Total gas Concentration (C_g)

$C_g = N/V = P/RT$ (D.14)

Where $P = 1.013 * 10^5 Nm^{-2}$

$R = 8.314 NmK^{-1}mole^{-1}$

C_g = moles m^{-3} ore

Table D5: Total gas concentration against Temperature

Temperature (K)	Cg (moles m^{-3} ore)
1323	9.2
1373	8.87
1473	8.27
1523	8.06

APPENDIX E

WORK PROCEDURE FOR MANGANESE AND FERROUS ION IN REDUCED ORE

Work Procedure for Manganese in Reduced Ore

SOLUTION: 5ml Bromine + 95 ml Methanol.
Prepare fresh.

APPARATUS: Magnet stirrer + 25mm Teflon follower.
250ml Erlenmeyer flask with fitted cooling condenser.

METHOD: Pulverise sample to less than 140µm.

0.4g sample are transferred to a dry 250ml Erlenmeyer flask suitable to fit a Liebert condenser.

Add Teflon stirrer.

Close flask with condenser.

Stir solution (evenly for all samples) for 1 hour at ± 20°C. (Use a cooling bath if necessary)

Use a clean and dry filtrate flask.

Filter the solution through a ± 8µm Sartorius disc filter using vacuum. Wash the filter with methanol 3 times, and then with H_2O_3 times (keep volume low).

Pour the filtrate into a 400ml beaker. Rinse flask.

Treat the filtrate with 25mls of H_2SO_4, 1:4, and evaporate to ± 5mls, just before fuming. Cool, and then add 10mls of 30 volumes H_2O_2 and heat to fumes of H_2SO_4. Cool. Add 10mls HCl and 5mls 1:1 Nitric acid. Transfer to a 250ml (or 100ml) volumetric flask and make to the mark.

Read on the ICP (0.4g/100mls) dilute if necessary.

Work Procedure for Ferrous ion

Weigh 1g sample and transfer to a 500ml comical flask with a narrow neck, and fitted with a rubber bung carrying either a Bunsen valve or a delivery tube. Add 1g sodium carbonate, 20ml hydrochloric acid and two to three drops hydrofluoric acid and quickly insert the bung. Heat gently until the sample is completely decomposed and then cools to room temperature. If a delivery tube is used, immerse the free end, during heating and cooling, in freshly prepared sodium bicarbonate solution (10 percent) contained in a 200ml beaker, allowing the bicarbonate solution to suck back during cooling. When cold, ad 200ml cold distilled water, which has been previously boiled and cooled, and titrate with N/10 potassium dichromate.

Calculation 1ml N/10 potassium dichromate = 0.005584 gm Fe^{2+}